The application of thiazole orange and artificial backbone modifications in the synthesis of fluorescent nucleic acids probes

A thesis submitted to the

Board of the Faculty of Physical Sciences

in partial fulfilment of the requirements for the degree of

Doctor of Philosophy

Piotr Klimkowski

Merton college, University of Oxford, Trinity term 2019

Supervisor: Professor Tom Brown



The application of thiazole orange and artificial backbone modifications in the synthesis of fluorescent nucleic acids probes

Wubba lubba dub dub…

Rick Sanchez

Declaration

I, Piotr Klimkowski, declare that the thesis entitled '' The application of thiazole orange and artificial backbone modifications in the synthesis of fluorescent nucleic acids probes" and the work presented in this thesis was carried out under the supervision of Professor Tom Brown. All the work presented is my own, expect where otherwise stated, and has not been submitted in full or in part for any other degree at this or any other university.

Work presented in Chapter 2, was recently published:

Klimkowski, P.; Ornellas, S. De; Singleton, D.; El-sagheer, A. H.; Brown, T. Design of Thiazole Orange Oligonucleotide Probes for Detection of DNA and RNA by Fluorescence and Duplex Melting. *Org. Biomol. Chem.* **2019**, *17*, 5943–5950.

Piotr Klimkowski

December 2019

Abstract

Thiazole orange (TO) is an asymmetric cyanine dye used in nucleic acid detection. It has wide applications due to its DNA-intercalating properties, resulting in an “on-off” fluorescent response upon binding to complementary nucleic acids. This thesis describes the use of TO in various fluorescent probe systems.

Incorporation of TO as a nucleobase surrogate into a modified FIT (forced intercalation) probe design *via* an L-threoninol acyclic backbone by amide bond formation was unsuccessful even after extensive synthetic effort. This issue was solved by introduction an azide functional group into probe sequence and efficient CuAAC labelling. The fluorogenic properties of these probes were not suitable to justify further development of the L-threoninol backbone, although this convenient synthetic route could be applied for new acyclic scaffold for FIT design.

New thymine nucleobase alkyne-amine modifications with various lengths of amine linker (AP-C_3 and AP-C_6 as phosphoramidites) were developed for the orthogonal labelling of DNA at single thymine sites using amide bond formation and CuAAC click chemistry in a single tube labelling protocol. These novel monomers were investigated in fluorescence resonance energy transfer (FRET) oligonucleotide probes with TO as the FRET donor dye, and thermal duplex melting studies were carried out showing beneficial increase of T_m with TO, where chosen reporter dye caused destabilisation . These new modifications provide an effective platform for highly efficient transfer of energy between donor and receptor fluorophore. However, undesirably high fluorescence was observed in the single stranded probe which could be improved by double incorporation of the AP-C_3modification and careful choice of a

reporter dye. Thermal melting studies showed modest increase of T_m for unlabelled modification and addition of TO did not results in high additional stabilizing effect. Additionally, this modification could be used as a simple building block for incorporation of a TO intercalator and an additional non-fluorescent label into oligonucleotides.

Investigation of the mode of attachment of thiazole orange to oligonucleotides (*via* its benzothiazole or quinoline moiety), and its point of attachment (nucleobase (major groove) or sugar (minor groove) were explored in several sequence contexts. Obtained results clearly shows preference of major grove (C6, PA) with TO attached *via* benzothiazole and minor groove (AE) with quinoline attached TO, where best fluorescence properties were achieved for pyrimidines (T and C) as a surrounding bases where purines, especially guanine gives unfavourable fluorescence enhancements. In addition, 2'-OMe sugar modification of thiazole orange probes resulted in a particularly high fluorescent enhancement and very favourable quantum yields on duplex formation. This provides a simple and effective system for detection of DNA and RNA and puts our design on par with more complex systems involving TO, including ECHO probes (exciton-controlled hybridization-sensitive fluorescent oligonucleotide probes, Okamoto); and FIT probes (forced intercalation probes, Seitz). Interestingly, the labelling of amino-modified oligonucleotides with TO-NHS ester is rapid (10 minutes at room temperature), and we were able to label oligonucleotide probes with multiple TO units in almost quantitative yields.

Table of contents

Declaration ..... **IV**
Abstract ..... **V**
Acknowledgments ..... **IX**
List of abbreviations ..... **XI**
1. Chapter 1 - Introduction **3**
1.1. Nucleic acids 3
1.1.1. Primary structure of nucleic acids 3
1.1.2. Secondary structure of nucleic acids 5
1.2. Solid phase synthesis of oligonucleotides 7
1.3. 'Click' chemistry 11
1.4. Nucleic acids labelling 14
1.4.1. Phosphoramidite approach 14
1.4.1.1. Post synthetic labelling by amide bond formation 15
1.4.1.2. Post synthetic labelling by the CuAAC reaction 17
1.4.1.2.1. Alkyne modified oligonucleotides 17
1.4.1.2.2. Azide modified oligonucleotides 18
1.5. Fluorescence 21
1.5.1. Fluorescence theory 21
1.5.2. Förster fluorescence resonance energy transfer (FRET) 21
1.6. Fluorescent hybridization probes for nucleic acid detection 24
1.7. Cyanine dyes 25
1.7.1. Thiazole orange 25
1.7.2. Incorporation of TO into nucleic acids 29
1.8. Molecule design 33
1.9. Research chaims 36
2. Chapter 2 - Thiazole orange (TO) nucleoside modification and its applications **39**
2.1. Introduction 39
2.2. Backbone modification and sequence context 40
2.3. Synthesis of thiazole orange derivatives 41
2.4. Oligonucleotide probe design and labelling with TO derivatives 45
2.4.1. DNA Duplex stabilisation by TO-ODN probes against DNA targets. 47
2.4.2. Thermal discrimination of TO-modified oligonucleotides with a mismatched base opposite the TO modification. 51
2.4.3. Fluorescence properties of TO-ODN probes with DNA targets 53
2.4.4. Fluorescence and duplex stability evaluation of ODN4 with guanine and inosine as neighbouring bases 58
2.4.5. Duplex stabilisation by 2'-*O*-methyl–RNA TO (2'-OMe–(ORNs)) probes with DNA and RNA targets 61
2.4.6. Mismatch discrimination by 2'-*O*-methyl–RNA TO probes at positions at various positions. 65
2.4.7. Duplex stabilisation by 2'-*O*-methyl–RNA probes (2'-OMe–ORN) with double AE-TO against DNA and RNA targets 66
2.4.8. Fluorescence properties of 2'-OMe–ORN probes against DNA and RNA targets 68
2.4.9. Quantum yield measurement of 2'-OMe–ORN probes against DNA and RNA targets 72

2.4.10. Effect of linker length on the properties of 2′-OMe–ORN1 AE-TO probes 75
2.5. CD spectroscopy of TO probes with DNA and RNA targets. 78
2.6. Conclusions 82
Chapter 3 - Thiazole orange and acyclic DNA backbone modifications 86
3. Chapter 3 - Thiazole orange and acyclic DNA backbone modifications 87
3.1. Introduction 87
3.2. Synthesis of Thiazole orange derivatives and L-threoninol phosphoramidite 89
3.3. Results and discussion 93
3.3.1. Amide linkage approach for FIT probe synthesis 93
3.3.2. Triazole linkage approach for synthesis of FIT probes 94
3.4. Conclusions 97
4. Chapter 4 - Orthogonal combination probes with thiazole orange 99
4.1. Introduction 99
4.2. Materials and methods 101
4.3. Synthesis of amino-propargyl ($C_{3/6}$) dT monomers 101
4.4. Synthesis of new combination dT monomer 102
4.5. Probe design and labelling of Amino-Propargyl-$C_{3/6}$ monomers 103
4.6. Fluorescence properties of AP-C_3 in combination probes. 104
4.7. Fluorescence studies of AP-C_3 and AP-C_6 modification in the 2′-OMe–ORN3 sequence context 108
4.8. UV melting studies of AP-C_3 and AP-C_6 modification in a 2′-OMe–(5′-ORN3) sequence context against DNA and RNA targets. 111
4.9. Conclusions 114
5. Conclusions and future work 115
6. Chapter 6 - Experimental 121
6.1. General synthetic procedures 121
6.2. Synthesised compounds 122
6.3. Synthesis and purification of oligonucleotides 163
6.3.1. Synthesis of DNA oligonucleotides 163
6.3.2. Synthesis of RNA oligonucleotides 164
6.3.3. Removal of 2′-TBDMS of RNA oligonucleotides 164
6.3.4. Synthesis of 2′-OMe–RNA oligonucleotides 164
6.4. Labelling of oligonucleotides 165
6.4.1. NHS ester labelling 165
6.4.1.1. TO-NHS ester labelling (Method 1) 165
6.4.1.2. TO-NHS ester labelling (Method 2) 165
6.4.2. General procedure for labelling of $TO_{B/Q2}$ on solid support 167
6.4.3. General procedure for amine to azide conversion on the oligonucleotides 170
6.4.4. General procedure Copper-Click 1,3-dipolar cycloaddition (CuAAC) 170
6.5. Steady state fluorescence measurements 172
6.6. UV melting studies 173
6.7. Quantum yield measurements 173
6.8. CD spectroscopy 174
6.9. Oligonucleotide duplex melting temperatures 175
6.10. Fluorescence data 181
6.11. Graphical representation of fluorescence and thermal melting data 193
6.12. Examples of fluorescence and UV melting curves 200
7. NMR spectra 205
References 228

Acknowledgments

I would like to thank my supervisor, Professor Tom Brown for ongoing support and wonderful scientific journey. In those four years, throughout countless meetings, discussions and great advices form you gave rise to this thesis, it wouldn't be possible without you. Also thank you for always being positive in tough moments it was truly a pleasure to work with you.

I would like to thank Dr. Afaf El-Sagheer, always being there when there was an issue that needed to be solved, countless oligonucleotide sequences, great advices and continuous questions that resulted in who I am now.

I could not do all of this if not for the Tom Brown group, working with you guys was quite an adventure. Both during everyday work time and social part. I would like to give special thanks to Dr. Sara De Ornellas and Dr. Ysobel Baker for huge help during my time in Oxford as well as unmeasurable help and advice regarding my thesis and resaearch. To Sarah Walsh, those breaks would not be as fruitful without you. I could not forget about brownies, Adam, Agnes, Anna, Arthur, Ashley, Cameron, Carolyn, Chunsen, Daniel, Ellia, Jack C, Jack H., Jo, Lynda, Marcin, Mei, Michael, Pawan, Pietro, Pui, Sven and Yutong it was really a great time thanks to you all.I would like to thank ATDBio, especially Dr. Daniel Singleton and Dr. Dorcas Brown for the time and advice during my time in Southampton. To Clickgene cohort, it was truly a pleasure to get to know you all. To Italian crowd, Marco, Luca, Alessandro and Giulio for all the great times together miniverse wouldn't be the same without you.

I could not forget my friends for all the great times we spend in queens land, Aleks, Diana, Natalia, Emilia, Rafal B., Rafal U., Marta, Marcin. Finally, I would like to give my special thanks to Romuald and Malgorzata for all the support my parents gave me during this time far away from home.

Acknowledgments

List of abbreviations

°C	degree Celsius
A	adenosine/adenine
Å	Angstrom
Ac	Acetyl
AAC	Huisgen [3+2] azide-alkyne cycloaddition
app.	Apparent
AU	arbitrary units
BO	benzothiazole orange
br	broad (NMR)
BTT	5-(benzylmercapto)-1H-tetrazole
C	cytosine/cytidine
calc.	Calculated
CD	circular dichroism spectroscopy
COSY	^{1}H-^{1}H correlation spectroscopy
CPG	controlled pore glass (solid support)
CuAAC	copper(I)-catalysed azide-alkyne 1,3-dipolar-cycloaddition
Cy3	trimethine cyanine dye
d	doublet (NMR)
DCC	*N,N*'-Dicyclohexylcarbodiimide
dd	doublet of doublets (NMR)
ddd	doublet of doublet of doublets (NMR)
DIPEA	N,N-diisopropylethylamine
DMAP	4-dimethylaminopyridine
DMF	dimethylformamide
DMSO	dimethyl sulfoxide
DMTr	4,4'-dimethoxytrityl
DNA	deoxyribonucleic acid
ds	double-stranded
DSC	*N,N*'-disuccinimidyl carbonate
dt	doublet of triplets (NMR)
ECHO	exciton-controlled hybridization-sensitive fluorescent oligonucleotide
e.g.	example
em	emission
eq	equivalent
ex	excitation
F_{ds}	area under fluorescence emission spectra of fluorescent probe-target complex
FIT	Forced Intercalation probes
Fmoc	fuorenylmethyloxycarbonyl (protective group)
FRET	Förster fluorescence resonance energy transfer
F_{ss}	area under fluorescence emission spectra of double stranded complex of fluorescent probe
g	gram
G	guanine/guanosine
h	hour
HATU	*N*-[(Dimethylamino)-1*H*-1,2,3-triazolo-[4,5-*b*]pyridin-1-ylmethylene]-*N*-methylmethanaminium hexafluorophosphate *N*-oxide
HMBC	heteronuclear multiple-bond correlation ^{1}H-^{13}C
HPLC	High Performance Liquid Chromatography

HRMS	high resolution mass spectroscopy
HSQC	Heteronuclear single-quantum correlation ^{1}H-^{13}C
Hz	Hertz
I	inosine/hypoxanthine
I	Maximum intensity of fluorescence at $\lambda_{em\ max}$
IC	internal conversion
ISAHC	imidazole-1-sulfonyl azide hydrochloride
ISC	intersystem crossing
J	coupling constant in Hz (NMR)
JO	oxazolopyridine
LRMS	low resolution mass spectroscopy
m	multiplet (NMR)
M	molar (concentration)
m/z	mass to charge ratio
m°	millidegrees
MB	molecular beacons
mg	milligram
ml	millilitre
mM	Millimolar (concentration)
MS	mass spectroscopy
NAP	nucleic acid purification
NHS	N-hydroxysuccinimide
nm	nanometer
NMM	*N*-methylmorpholine
nmol	nanomol
NMR	nuclear magnetic resonance
OD	optical density
ODN	Oligodeoxyribonucleotide
ORN	oligoribonucleotide
OTf	trifluoromethanesulfonate
p	pentet (NMR)
PCR	polymerase chain reaction
PEG	polyethylene glycol
pH	potential of hydrogen (negative logarithm of the positive hydrogen ion concentration)
PNA	peptide nucleic acid
PyBOP	(benzotriazol-1-yloxy)tripyrrolidinophosphonium hexafluorophosphate
q	quartet (NMR)
QB	quinoline blue
qPCR	quantitative polymerase chain reaction
R_0	Förster distance
R_f	retention factor
RNA	ribonucleic acid
RT	room temperature
s	singlet (NMR)
s	second
S_n	vibrational state
SNP	single nucleotide polymorphism
ss	single-stranded
SW	Single wavelength calculation of fluorescence enhancement upon binding to target oligonuclotide

t	triplet (NMR)
T	thymine/thymidine
TBDMS	tert-butyldimethylsilyl
TBTA	tris(benzyltriazolylmethyl)amine
TC	thionocarbamate
TCA	trichloroaceticacid
TEA	triethylamine
TEAA	triethylammonium acetate (HPLC buffer)
TEAB	triethylammonium bicarbonate (HPLC buffer)
TFA	trifluoroacetic acid or trifluoroacetyl protecting group
THF	tetrahydrofuran
THPTA	tris(3-hydroxypropyltriazolylmethyl)amine
TLC	thin layer chromatography
T_m	DNA melting temperature
TO	thiazole orange
TR	thiazole red
TSTU	*N*'-tetramethyl-*O*-(*N*-succinimidyl) uronium tetrafluoroborate
U	uracil/uridine
UV	ultraviolet
YO	oxazole yellow
δ	chemical shift in parts per million
Δ	delta
κ^2	acceptor absorption dipole
λ	lambda/ wavelength
µL	microliter
µm	micrometre
µM	micromolar
ν	frequency
ϕ	quantum yield
θ	theta/value (degrees)

List of abbreviations

Chapter 1 - Introduction

1. Chapter 1 - Introduction

1.1. Nucleic acids

1.1.1. Primary structure of nucleic acids

DNA (2'-deoxyribonucleic acid) is a large polymeric molecule that carries the essential genetic information in most living systems (some viruses use RNA for this purpose). DNA is composed of pentose sugars connected by phosphate groups, each pentose sugar having an attached heterocyclic base, which when taken together are referred as a nucleotide. The bases (nucleobases) present are the purines: adenine (A) and guanine (G) and the pyrimidines: cytosine (C) and thymine (T) (Figure 1.1).

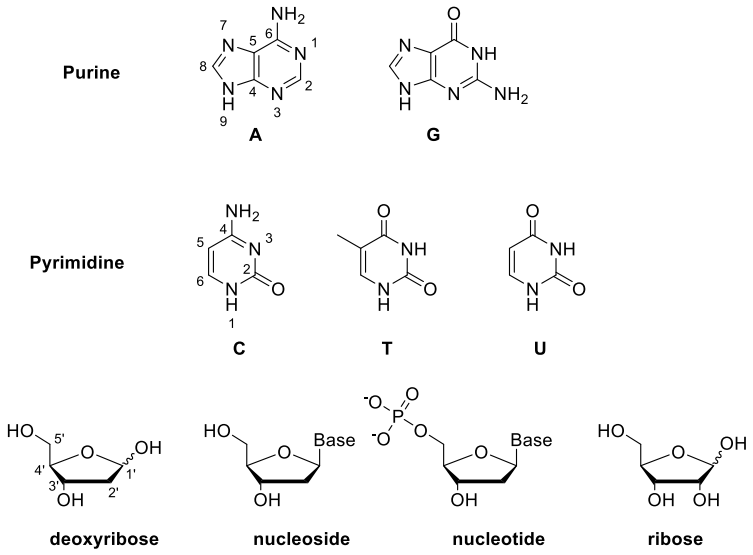


Figure 1.1 Structures of the heterocyclic bases; purines (A and G) and pyrimidines (C, T and U) present in nucleic acids, as well as the ribose and deoxyribose sugars to which nucleobases are attached, creating nucleosides and nucleotides.

The heterocyclic bases are attached to the 1' carbon of the sugar by the N(9) atom of purines and N(1) of pyrimidines, creating a nucleoside. Attachment of a heterocyclic base (nucleobase) to the sugar by a glycosidic bond allows for relatively free rotation, with *anti* and *syn* being at

the extreme conformations (Figure 1.2). The *anti*-conformation is predominant in a natural double stranded (ds) DNA when base pairs are formed.[1]

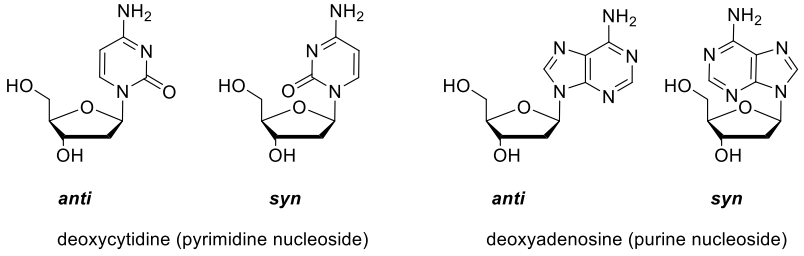


Figure 1.2 Representation of *anti* and *syn* conformations of a pyrimidine (C) and purine (A) nucleoside.

The 1' position of the deoxyribose sugar is the anomeric centre. The heterocyclic base (or other substituent) can be placed on the same face of the sugar ring as the 5'-hydroxyl group or on the opposite side. These two anomers are called β - and α-anomers respectively, in DNA all nucleosides are in the β-configuration (Figure 1.3).

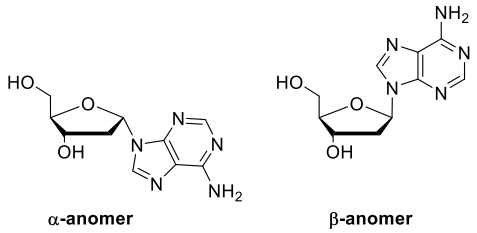


Figure 1.3 Structures of α- and β-anomers of purine (A) nucleoside.

The primary structure of DNA is by convention written from 5'-hydroxyl to the 3'-hydroxyl (Figure 1.4). The pentose sugar in DNA is a deoxy version of D-ribose which acts as a template for RNA synthesis. In turn RNA transports its encoded genetic information outside of the nucleus to the ribosome in order for proteins to be synthesized. The purines bases (A and G) and pyrimidine base (C) are found in DNA and RNA, whereas the pyrimidine base (T) is replaced by uracil (U) in RNA (Figure 1.1).

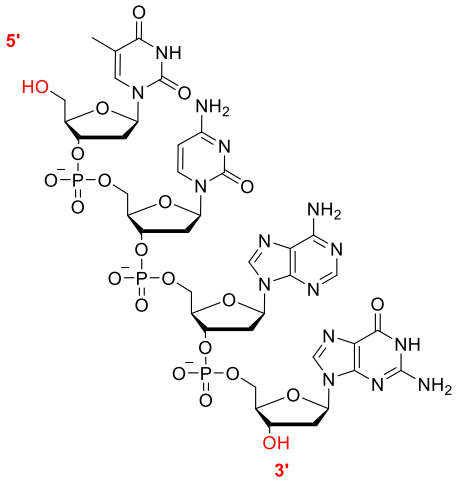


Figure 1.4 DNA primary structure. The example here is the oligonucleotide of sequence 5'-TCAG-3'.

1.1.2. Secondary structure of nucleic acids

Two nucleic acid strands can combine to form a DNA double helix. The structure of the DNA double helix was elucidated by James Watson and Francis Crick[2] largely from the combined research of Erwin Chargaff,[3,4] Rosalind Franklin,[5,6] and Maurice Wilkins[7]. The B-form of the DNA duplex is a "right-handed" helical structure (Figure 1.5A) where the two strands are oriented in antiparallel orientation, the 5' end of one strand opposite to the 3' end of the second strand. The phosphodiester groups are at the exterior of the structure creating an anionic backbone at neutral pH; its hydrophilic character allows for good aqueous solubility under physiological conditions. The hydrophobic interior of the structure is formed by interactions between nucleobases where A pairs with T *via* two hydrogen bonds and where C pairs with G *via* three hydrogen bonds (Figure 1.5B), resulting in equal ratio in DNA between pyrimidines and purines.[3,4] These interactions with the dominating stabilisation effect of π-stacking between base pairs gives this helical structure high stability.[8] This can be disrupted under alkaline or acidic conditions, or high temperature, resulting in the separation of the two strands.[9]

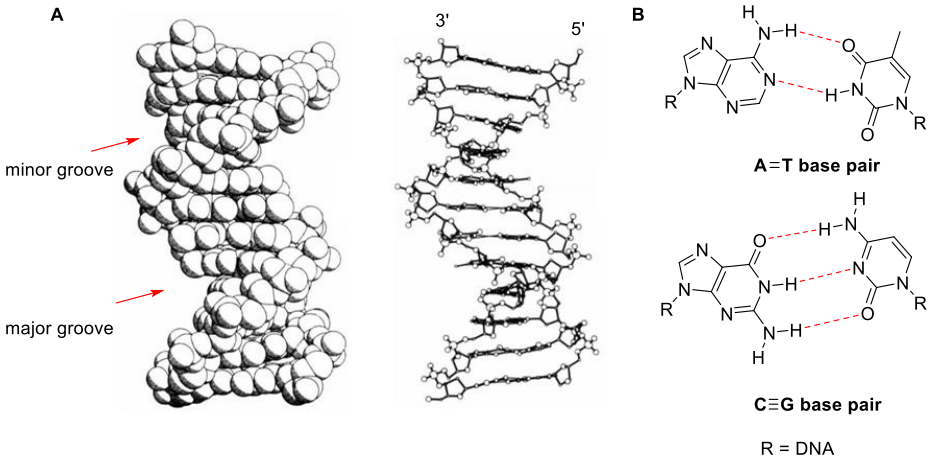


Figure 1.5 A) Crystal structure of B-type DNA helix of 5'-CGCGAATTCGCG.[10] B) Graphical representation of A:T and C:G base pairs with hydrogen bonding.

The B-type helical DNA structure has 10 to 11 base pairs per helical turn, is 2 nm wide and the separation of base pairs along the helix axis is around 0.34 nm with both major and minor groove of similar depth but different width. The second main helical structure of DNA and RNA is the A-form. This is a right-handed structure which is preferred for dsRNA[11,12] The A-helix differs from the B-helix; it is a wider and more compact structure with a more narrow and deep major groove and shallower minor groove (Figure 1.6).[13]

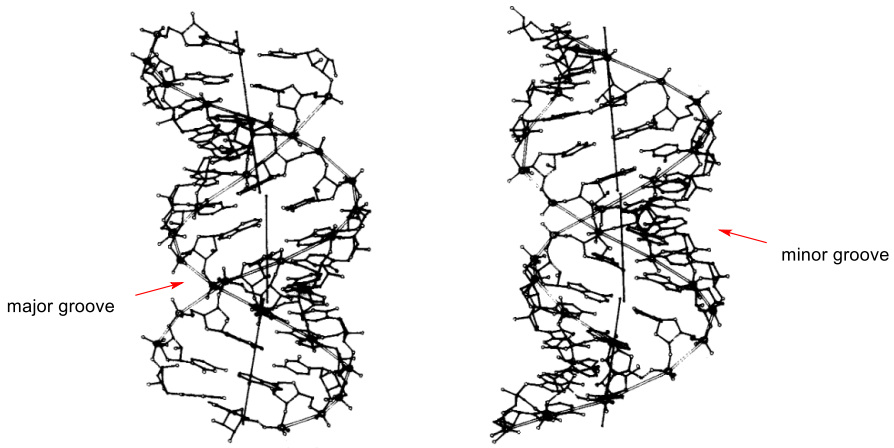


Figure 1.6 Crystal structure of the A-type RNA helix of $[U(UA)_6U]_2$.[13]

1.2. Solid phase synthesis of oligonucleotides

Nucleic acids are enzymatically produced *in vivo*. In order to study their properties *in vitro*, chemical methods for their sequence-specific synthesis have been developed. Solid phase techniques have many advantages over conventional solution phase chemical methods, overcoming the issues of incomplete reaction, poor solubility and difficulties in the purification of complex mixtures of products and reagents. Building up oligomers covalently attached to the solid support allows for easy removal of excess and unreacted reactants by filtration.[14] This method allows oligomers to be built step by step with precise control *via* computer controlled automated synthesis.[15] Upon completion of the synthesis cycle, the product can be cleaved from the solid support. This revolutionary solid phase technology was first reported by Merrifield in 1963 for the synthesis of peptides.[16–18] The range of application of solid phase synthesis was later expanded and applied to the efficient synthesis of oligonucleotides, and currently is the standard technique for obtaining oligonuclotides.[19,20]

The initially reported solid supports used by Merrifield[15] and further optimised by Letsinger *et al.*[21] were organic polymers. These resins swelling and shrink in the presence of different solvents, a problem which can cause a physical barrier to efficient reactions. For this reason Caruthers *et al.*[22] introduced inorganic matrices based on controlled pore glass (CPG) and silica gel. CPG, with the addition of macroporous polystyrene (MPPS) supports have been found to be ideal for oligonucleotide synthesis,[22] due to their rigidity and negligible degree of swelling in common solvents. The size of the pores in the CPG can be adjusted to the length of the oligonucleotide being synthesized (e.g. 500, 1000, 1500, 2000 or 3000 Å) with the large pores typically used for very long 100-200-mer oligonucleotides. Highly cross linked polystyrene bead (MPPS) are often used for small scale synthesis (10 nmol) due to improved moisture exclusion. The solid supports are functionalised in order to introduce reactive sites, a long

chain alkylamine linker (LCAA) is commonly used in derivatisation of CPG support by silylation. The nucleoside is attached to CPG *via* a succinyl ester and the other carboxylic acid of the succinyl linker is joined to the resin by an amide bond. Resin loadings of 30-80 μmol g^{-1} of nucleoside are readily achievable, higher loadings are generally not desirable as they lead to the growing DNA chains interfering with each other due to steric hindrance, inhibiting oligonucleotide chain growth.[1]

Oligonucleotide synthesis is normally achieved *via* the phosphoramidite approach, first reported by Beaucage and Caruthers in 1981.[20] It was later modified by the introduction of user friendly 2-cyanoethyl phosphoramidite monomers[23] instead of methyl phosphoramidites.[24] This approach found widespread application and dominates oligonucleotide synthesis even today (Figure 1.7). In the phosphoramidite method the oligonucleotide is synthesized in the 3' to 5' direction,[25,26] opposite to enzymatic synthesis. In order to prevent uncontrolled polymerisation, the 5'-hydroxy position of the sugar is protected with an acid labile DMTr group (4,4'-dimethoxytritryl, Figure 1.7). To protect the reactive groups of nucleobases from undesired side reactions their exocyclic amines require protection.[27] In the case of Guanine (G) in particular this also improves the solubility of the phosphoramidite monomer. [27] Standard amide-based protecting groups (Figure 1.7) allow for versatile synthesis and deprotection in aqueous ammonia, although some chemical labels used in modified oligonucleotides (e.g. fluorescence dyes) are sensitive to aqueous ammonia and require milder conditions and therefore different nucleobase protecting groups.[28]

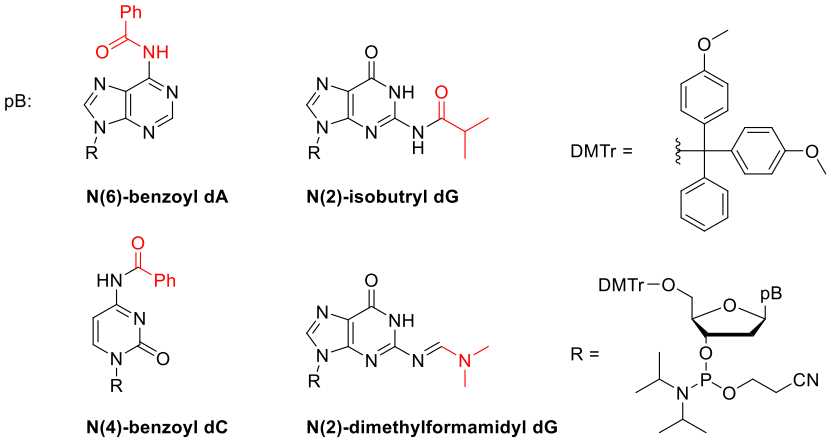


Figure 1.7 DNA monomers with common base protecting groups for adenine, guanine and cytosine used in solid phase synthesis.

The solid phase synthesis cycle starts with solid support (CPG or polystyrene) containing the first nucleoside, normally A, G, C or T. The cycle of oligonucleotide synthesis consists of four steps (Figure 1.8)[29]: first deprotection of the 5'-DMTr group with TCA (trichloroacetic acid) secondly the coupling of the next phosphoramidite monomer with tetrazole (or a derivative of tetrazole) as an activator, then capping of unreacted hydroxyl residues with Ac_2O (acetic anhydride) and finally oxidation of the newly formed P(III) linkage to P(V) with iodine and water. The synthesis is continued through multiple cycles until the desired oligomer is obtained. It is important to achieve high yields in each cycle in order to obtain reasonable yields of long oligonucleotides. The efficiency of oligonucleotide assembly is monitored by measuring the intensity of colour or the conductivity of the liberated DMTr cation; typically yield of 99.5% per step is achievable in a single cycle. Upon completion of the assembly process the oligonucleotide is cleaved from the solid support and deprotected in aqueous ammonia. This is followed by purification by one of a variety of methods including gel-filtration (desalting) or reversed-phase HPLC.

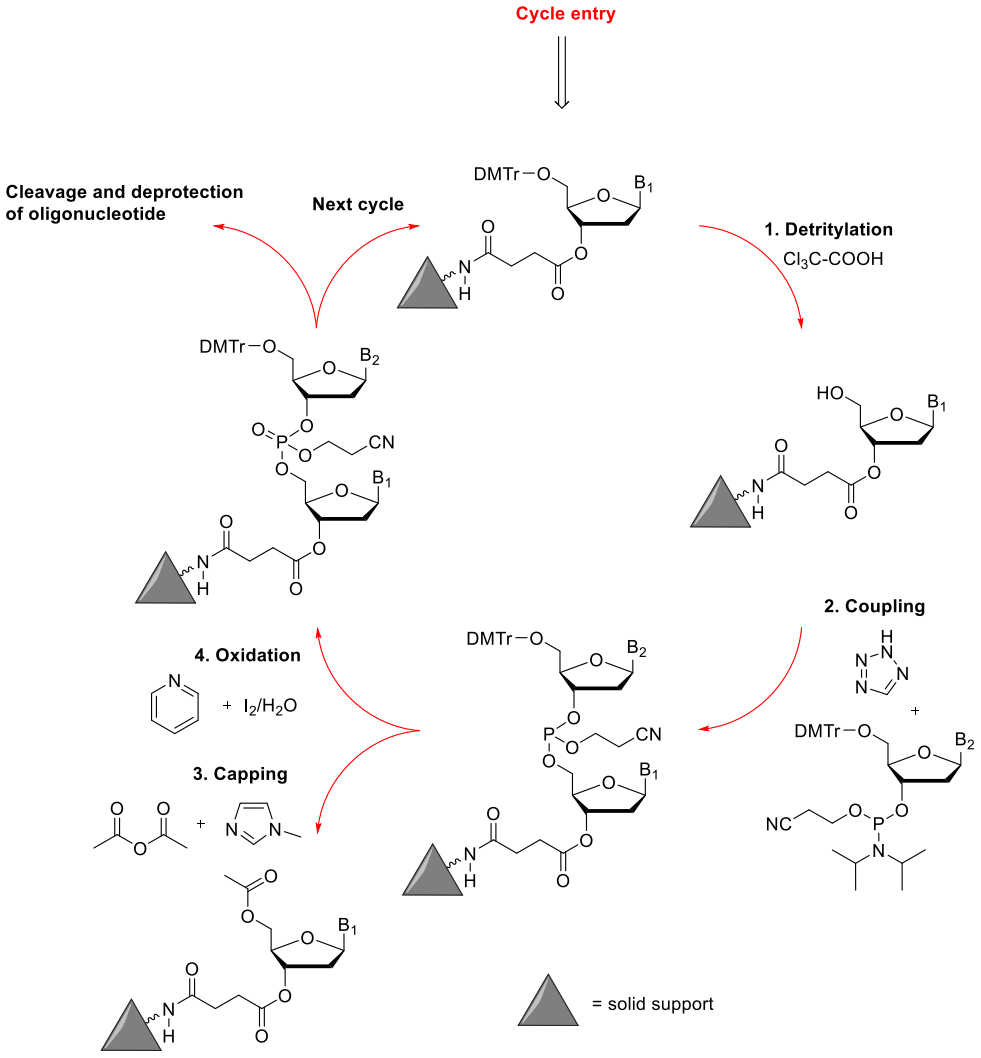


Figure 1.8 Solid phase synthesis cycle for the phosphoramidite method of oligonucleotide synthesis.

Synthesis of RNA oligonucleotides can be performed similarly, using an adaptation of the DNA solid phase cycle. The main difference is that the phosphoramidite monomers contain a 2'-hydroxyl moiety which needs to be protected. A common approach to this is to use the TBDMS (tert-butyldimethylsilyl) protecting group (Figure 1.9).[30] Similarly to DNA synthesis, the uridine nucleotide (corresponding to T in DNA) does not need to be protected. The protecting group for A, G and C in RNA is commonly tert-butylphenoxyacetyl which allows for milder deprotection and higher solubility of the monomers (Figure 1.9).[31] RNA synthesis requires a different activator than 1H-tetrazole; 5-(benzylmercapto)-1H-tetrazole (BTT) is a standard choice. The choice is dictated by the additional steric hindrance of the RNA monomers which

have bulky 2´-OH protecting groups adjacent to the phosphoramidite moiety. BTT allows for faster coupling times and higher yields of the final product than 1H-tetrazole.[32] Upon completion of RNA synthesis standard deprotection in ammonia is performed and finally removal of 2´-TBDMS is carried out using a source of F^- anion (e.g. triethylamine trihydrofluoride).[31]

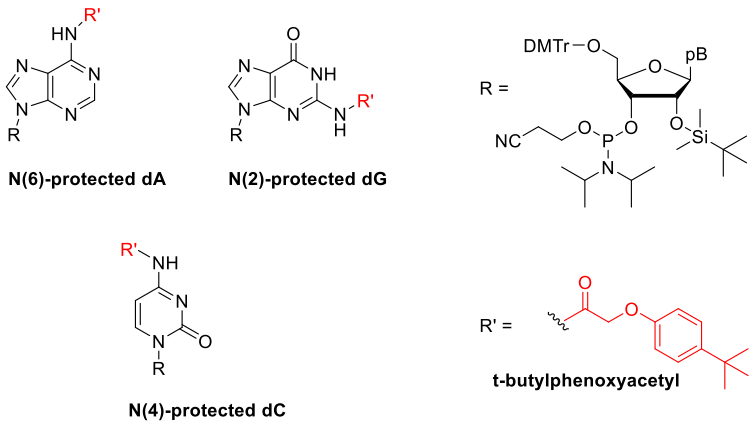


Figure 1.9 2'-*O*-TBDMS RNA monomers with the nucleobase protecting group for adenine, guanine and cytosine that are used in solid phase synthesis.

The TC (thionocarbamate) protecting group is now used increasingly to protect the 2'-hydroxyl group for RNA synthesis. Deprotection conditions (ethylene diamine) are simpler in comparison to the TBDMS chemistry.[33]

1.3.'Click' chemistry

'Click' chemistry is a concept that has become an important tool for biophysical, biochemical and biological studies. Click chemistry results in the formation of covalent bond between two molecules with high selectivity and efficiency under mild conditions.[34] The prime example is the copper(I) catalysed azide-alkyne cycloaddition (CuAAC) which, due to Cu(I) catalysis, results in highly efficient and stereospecific formation of a 1,4-triazole. It was first introduced by Meldal[35] and Sharpless independently.[36] This is in contrast to the uncatalysed Huisgen [3+2]

azide-alkyne cycloaddition (AAC), which proceeds at elevated temperatures to give both 1,4- and 1,5-triazole regioisomers (Figure 1.10).

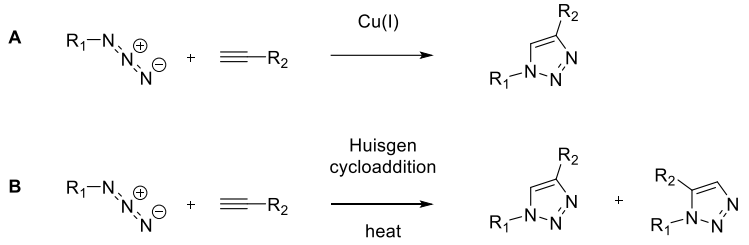


Figure 1.10 Cu(I) catalysed (A) and thermal (B) azide-alkyne cycloaddition reactions and products.

The reaction is tolerant of other functional groups,[37] side reactions are minimal and the reaction performs well in aqueous media over a broad range of temperature (0 – 160 °C) and pH (4 – 12).[38] The resultant triazole linkage is chemically stable and inert to hydrolytic, oxidizing and reducing conditions. These favourable properties have resulted in the widespread application of CuAAC in many areas including conventional synthesis,[39] metal ligand studies,[40] microwave synthesis, medicinal chemistry, advances in room temperature ionic liquids,[41] labelling and ligation of oligonucleotides[38] and protein modifications.[42]

Determination of the role of Cu(I) by mechanistic studies initially performed by Sharpless *et. al*[38] followed by Fokin *et al.*[43] showed that two different copper atoms are involved in the catalytic cycle (Figure 1.11). A problem in the CuAAC reaction is the instability of free Cu(I) due to its disproportionation in aqueous media into Cu(0) and Cu(II) as well as oxidation. The organic ligands (tris(benzyltriazolylmethyl)amine, TBTA)[44] and water soluble (tris(3-hydroxypropyltriazolylmethylamine, THPTA)[45] are used to stabilise the Cu(I) ion (Figure 1.12). In aqueous reactions, to obtain Cu(I) from Cu(II) source (e.g. $CuSO_4$) a reducing agent is added such as sodium ascorbate. Alternatively source of Cu(I) such as CuBr can be used. It is worth mentioning that the strain promoted alkyne-azide [3+2] cycloaddition (SPAAC) does not

require a metal catalyst, which makes it an important reaction for *in vivo* labelling procedures in live cells.[46]

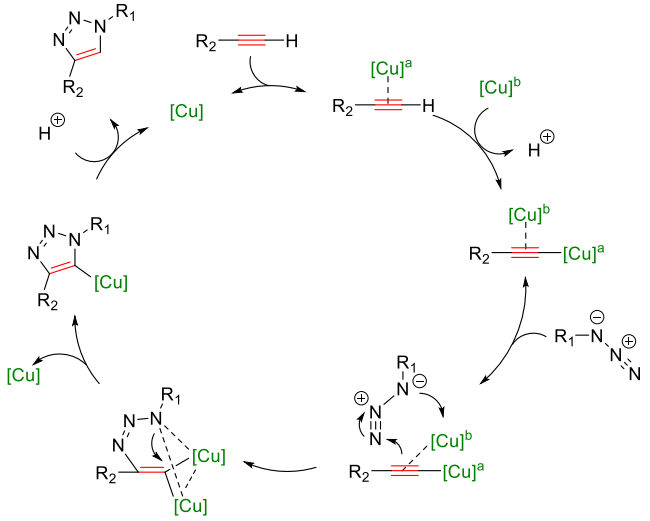
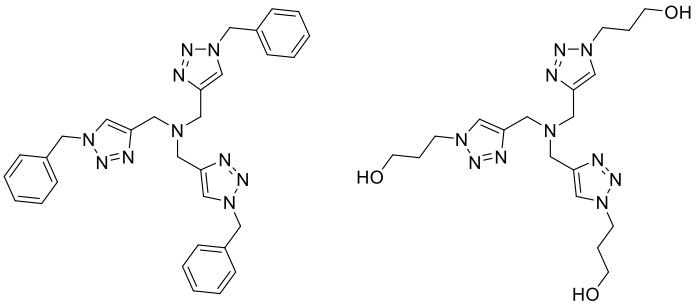


Figure 1.11 Proposed catalytic cycle of the CuAAC reaction.[43]



TBTA **THPTA**

Figure 1.12 Structures of tris-triazole ligands for Cu(I) binding in the CuAAC reaction.

1.4. Nucleic acids labelling

In order to detect DNA and RNA in diagnostic applications, labelling methods are essential. Many techniques have been developed in order to achieve this goal such as detection by hybridization with a radiolabelled complementary strand in the case of Southern blotting for DNA detection, or Northern blotting for RNA detection. Detection of small amounts of DNA or RNA can be achieved after PCR amplification or reverse-transcription followed by PCR amplification. One of the most common approaches is the use of fluorescent dyes that, upon binding to nucleic acids, emit a fluorescent signal. Nucleic acid detection can be achieved by staining with a specific dye such as ethidium bromide, SYBR® Gold or PicoGreen such that the target DNA (or RNA) can be easily detected. This approach is usually used in detection of nucleic acids in gels, where the gel is soaked in a solution of the dye and then the excess is washed away.[47] Approaches where the fluorescent dye is covalently attached to the modified oligonucleotide probe in hybridization assays is one of the most important techniques in nucleic acid imaging of fixed and live cells.[48–50] There are two main methods of synthesising the required probes, either incorporation of a fluorophore phosphoramidite during solid phase synthesis of the oligonucleotide or post synthetic labelling of the oligonucleotide. Both are discussed below.

1.4.1. Phosphoramidite approach

This approach requires monomers (with attached fluorophores) to be compatible to all the steps in the oligonucleotide synthesis cycle and the subsequent deprotection. Depending on their structures phosphoramidites can be attached at internal or terminal positions in oligonucleotides (Figure 1.13). They allow for easy incorporation of multiple fluorophores in a probe strand, the drawback is that the synthesis of those monomers can be challenging and

expensive. For fluorophores that are not stable during the solid phase synthesis cycle and/or deprotection (e.g. TAMRA[51]), post synthetic labelling methods are required.

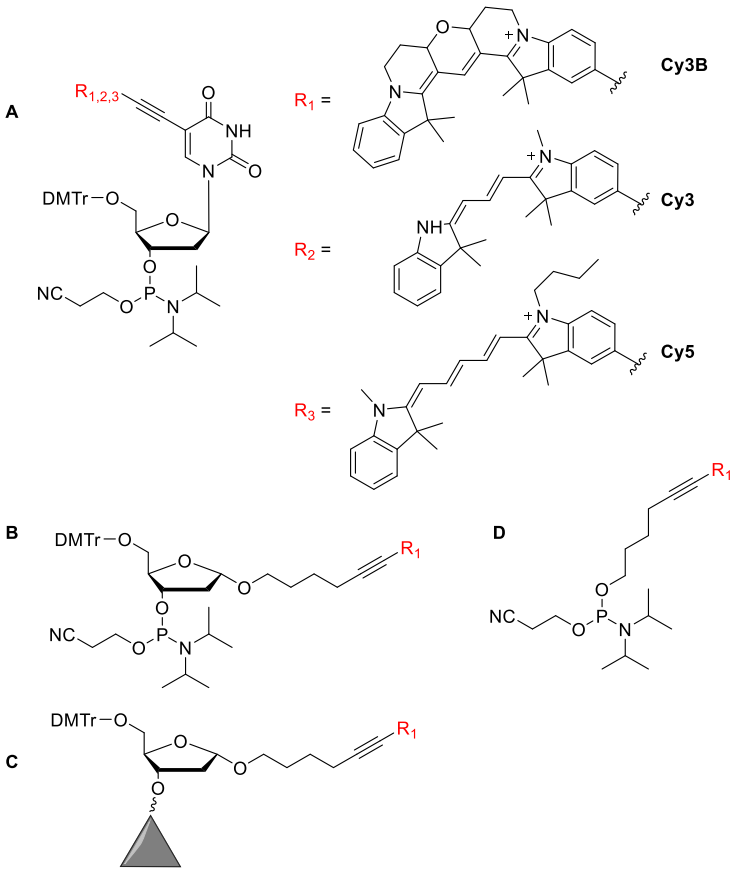


Figure 1.13 Examples of phosphoramidites of fluorescent dyes for A : internal nucleobase, B : internal sugar, C : 3'-terminal sugar, D : 5'-terminal position.[52]

1.4.1.1. Post synthetic labelling by amide bond formation

One of the most common methods to label oligonucleotides with fluorescent dyes is by formation of an amide bond between the dye and an amino modified monomer in the oligonucleotide. A broad range of primary amine modifications can be incorporated into a DNA sequence in standard solid phase synthesis (as phosphoramidites) at nucleobases, sugars or 3' or 5' termini (Figure 1.14). Some of these monomers are commercially available (A : C2-dT, C6-dT; B : 3'-amino C7 CPG; D : 5'-amino C6) where others can be easily synthesized (C :

AE-dT, E: PA-dT).[53,54,55] Amino groups can be protected by trifluoroacetyl (TFA) or fluorenylmethyloxycarbonyl (Fmoc) groups, both of which are stable during solid phase synthesis conditions. Fmoc protection allows for selective deprotection of the primary amine on resin without unwanted cleavage of the oligonucleotide from the solid support.[56]

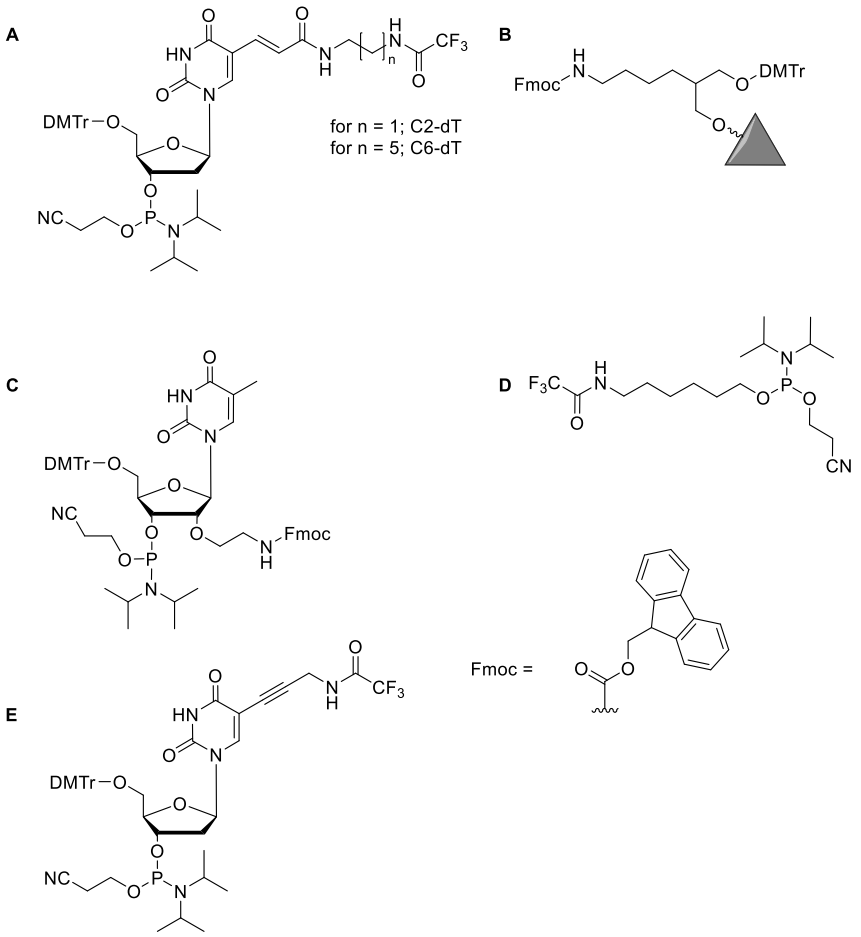


Figure 1.14 Examples of amino modified monomers for use in solid phase synthesis of DNA.

Labelling of amino modified oligonucleotide is commonly performed by using N-hydroxysuccinimide (NHS) activated ester of the fluorescent dye (Figure 1.15). Several of these are readily available form commercial sources. Alternatively, coupling of carboxylic acid derivatives of fluorescent labels can be added to amino-modified oligonucleotides using a suitable coupling reagent for *in situ* generation of their activated esters. Typical coupling agents are carbodiimides (e.g. DCC),[57] uronium reagents (e.g. HATU)[58] or phosphonium

reagents (e.g. PyBOP, Figure 1.15).[59] Alternative labelling methods using isothiocyanate[60] or thiol[61] moieties are also used in oligonucleotide labelling.

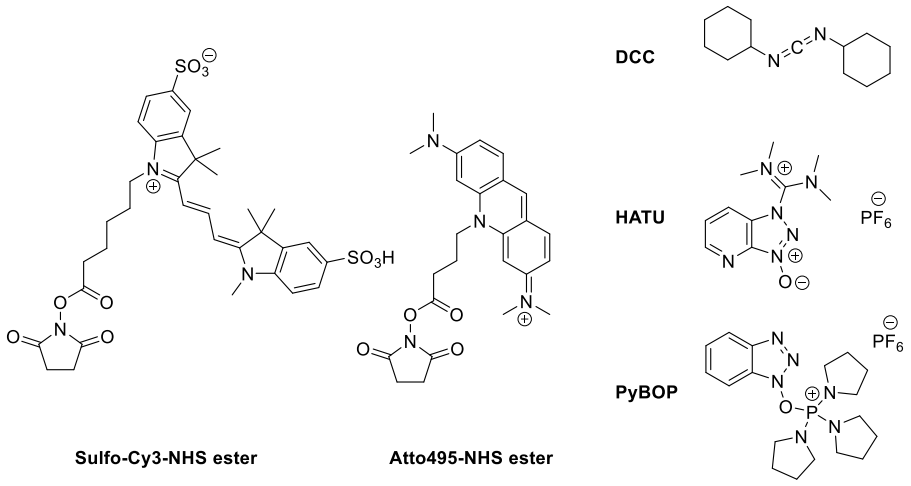


Figure 1.15 Examples of NHS esters of fluorescent dyes and coupling reagents for carboxylic modified labels.

1.4.1.2. Post synthetic labelling by the CuAAC reaction

1.4.1.2.1. Alkyne modified oligonucleotides

The CuAAC 'click' reaction is one of the most efficient methods of labelling biomolecules and since its discovery has been extensively applied to oligonucleotide labelling. Several phosphoramidite monomers with alkynyl moieties attached to the nucleobases can be added to oligonucleotides during solid phase synthesis (Figure 1.16A)[62] and reacted with a number of azide modified molecules including fluorescent dyes like fluorescein, Figure 1.16 D (ii). In the case of coumarin azide, the conjugate provides fluorescent properties only upon introduction of the triazole linkage.[63] Other methods of alkyne labelling include modification of the sugar of the nucleoside (2'-position, Figure 1.16 B) and the non-nucleosidic ((S)-(-)-3-amino-1,2-propanodiol, Figure 1.16 C).

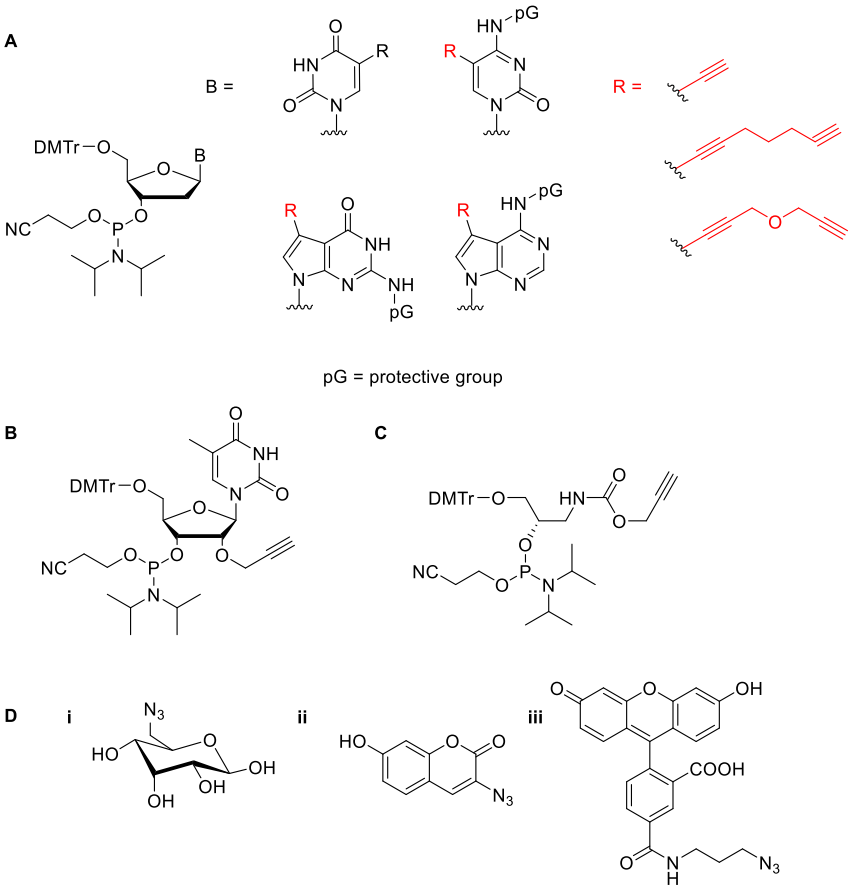


Figure 1.16 Structures of alkyne modified phosphoramidites for incorporation into DNA by solid phase synthesis (A-C) and azide functionalised molecules for labelling oligonucleotides by CuAAC.

1.4.1.2.2. Azide modified oligonucleotides

As previously shown a wide range of alkyne modified phosphoramidite monomers are available. However, introduction of azide-containing phosphoramidite monomers into oligonucleotides during solid phase synthesis is troublesome. The reason is that the Staudinger reaction[64–66] occurs between P(III) of the phosphoramidite and azide moiety, resulting in reduction of the latter, and conversion into an amine group *via* an aza-ylide intermediate (Figure 1.17).

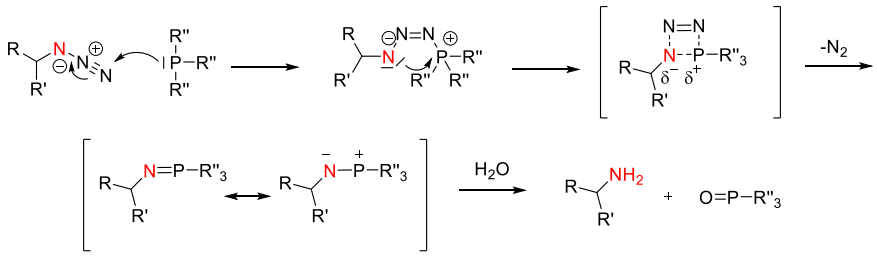


Figure 1.17 Mechanism of Staudinger reaction.[67]

Therefore alternative methods for incorporation of azide groups into oligonucleotides, to avoid the use of P(III), have been developed. These have higher phosphorus oxidation states (phosphotriesters[68,69] and H-phosphonates)[70,71] (Figure 1.18 A and B). There is a recent report of successful incorporation of non-nucleoside phosphoramidite monomer containing both P(III) and azido groups into oligonucleotides in standard solid phase synthesis (Figure 1.18 C). The drawback is the need to keep the monomer in solution, and the instability of the monomer.[72]

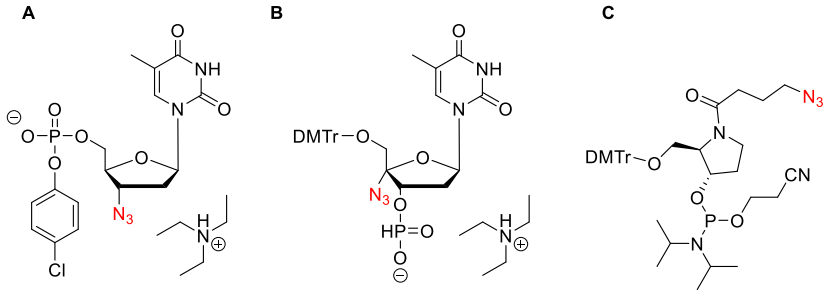


Figure 1.18 Examples of phosphotriester (A), H-phosphonate (B) and phosphoramidite (C) monomers used in synthesis of azide-containing oligonucleotides.

Due to the above drawbacks introduction of the azide group into oligonucleotides is best achieved by post-synthetic labelling of amino modified oligonucleotides with (for example) 4-azidobutyric and 6-azidohenxanoic NHS esters (Figure 1.19 A)[73] or by introduction of alkyl halide (Figure 1.19 B and C) phosphoramidite monomers and later conversion into azide by reaction with NaN_3.[74,75] Enzymatic methods based on azide functionalized triphosphates allow for incorporation of azides into oligonucleotides, although this can be time consuming and

requires the use of template oligonucleotides, limiting their application.[76] Interestingly commercially available amino modified monomers for solid phase synthesis (Paragraph 1.4.1.1) can be directly used to generate the azide functional group by reaction with the DZT (diazo-transfer) reagent imidazole-1-sulfonyl azide hydrochloride (ISAHC, Figure 1.20)[77] without loss of stereochemistry, as shown by ^{15}N NMR labelling experiments (Figure 1.20).[78] Application of this reagent with Cu(II) catalyst, allowed for both solid and aqueous phase conversion of aliphatic amine groups on DNA into azides at both 5' and internal positions.[79]

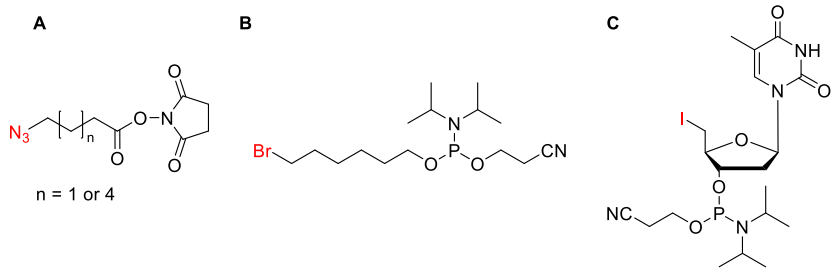


Figure 1.19 Modifications allowing introduction of the azide group into oligonucleotide sequences in a post synthetic manner.

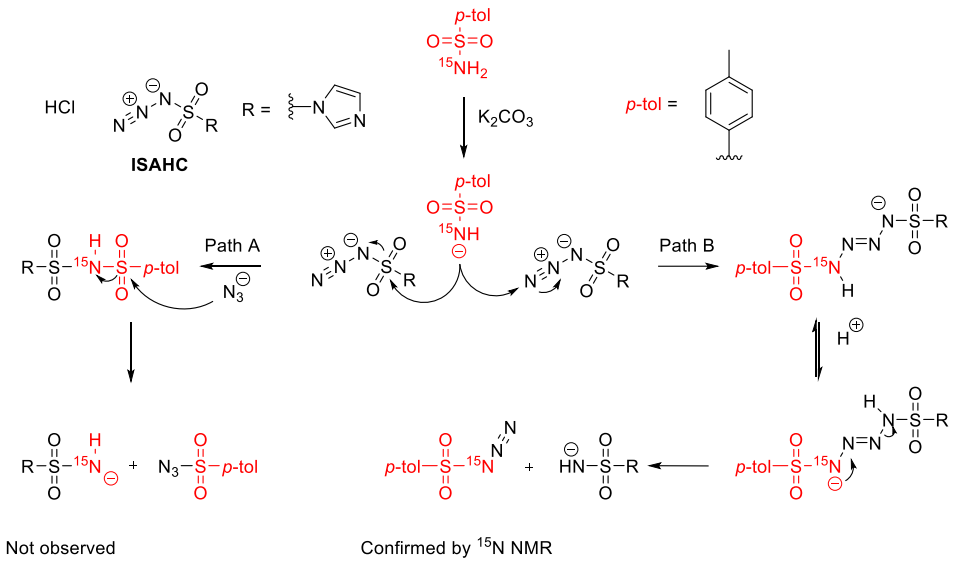


Figure 1.20 Structure of diazotransfer reagent (ISAHC) and proposed mechanism supported by ^{15}N NMR studies.[78]

1.5.Fluorescence

1.5.1. Fluorescence theory

Fluorescence is the emission of light from a substance (fluorophore) which occurs from electronic excited states. This phenomenon is initiated by absorption of a photon ($h\nu_a$, Figure 1.21 Green) which is excited from the ground state (S_0) to a higher vibrational state S_1 or S_2 (singlet state). This process occurs in a time scale of $t < 10^{-15}$ s, from this state the molecule relaxes to a first (S_1) state by non-radiative internal conversion (IC) like collision with other molecules or heat (within 10^{-11} to 10^{-14} s). Only from this lowest energy level (S_1) fluorescence can occur by emission of a photon ($h\nu_F$, Figure 1.21 Red) and it is independent of the excitation wavelength based on Kasha's rule.[80] Due to IC the emitted photon has lower energy than absorbed one and therefore a longer wavelength of emission can be observed, this is known as the Stokes shift.[81]

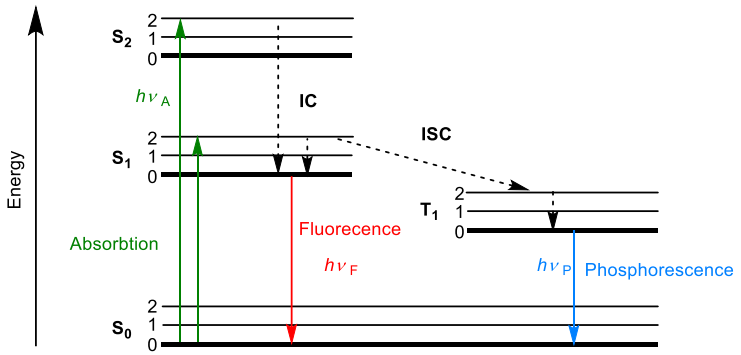


Figure 1.21 Jabłoński energy level diagram illustrating the pathway of an excited electron. $h\nu_A$: photon absorption; $h\nu_F$: photon emitted in a fluorescence phenomenon; $h\nu_P$: phosphorescence photon; S_0:ground state; S_1 and S_2: excited singlet states; T_1: excited triplet state; 0, 1, 2 : vibrational levels; IC: internal conversion; ISC: intersystem crossing.

1.5.2. Förster fluorescence resonance energy transfer (FRET)

Förster (Fluorescence) resonance energy transfer (FRET)[81] is the transmission of energy from a donor fluorophore to an acceptor molecule by dipole-dipole interactions without emission

of a photon. For FRET to occur the emission spectrum of donor fluorophore must overlap with the absorbance spectrum of the acceptor (Figure 1.22 B). The acceptor can be either a quencher or fluorophore (Figure 1.22 A). A quencher can be defined as a molecule for which absorption of a photon does not result in emission of electromagnetic radiation upon relaxation. Many mechanisms of quenching can be defined. Static quenching is where a fluorophore-quencher interact by proton-coupled electron transfer *via* weak bonds. The main controls over this process involve electrostatic, steric and hydrophobic interactions.[82] Another mechanism is collisional quenching in which intensity of the fluorescence is reduced by collisions with the quencher. The ruling principle of the FRET phenomenon is based on the spatial overlap of donor and acceptor molecular orbitals, which requires both molecules to be in close proximity. If the acceptor is a fluorophore the energy from the donor is transferred and emitted by electromagnetic radiation (photon).

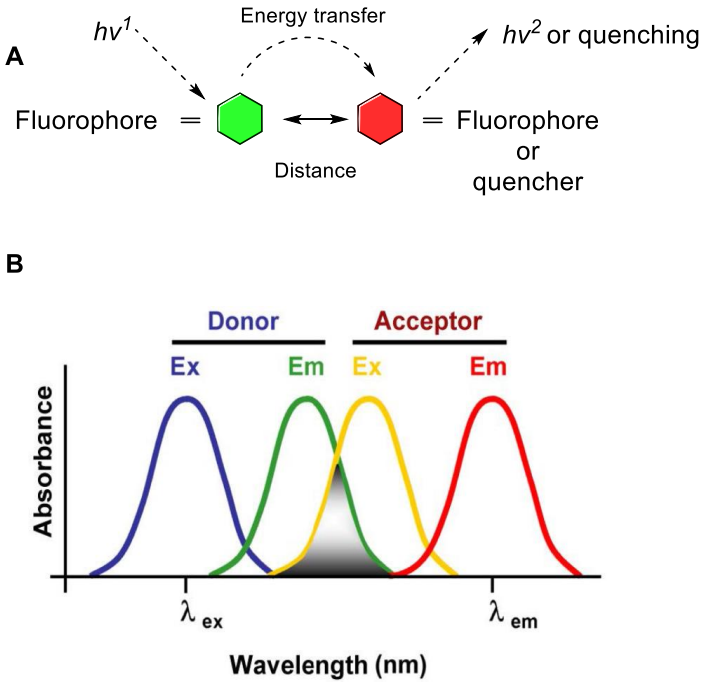


Figure 1.22 Representation of A: fluorescence resonance energy transfer (FRET); B: Spectral overlap.

The efficiency of this process strongly depends on the donor-to-acceptor separation distance and is proportional to the inverse sixth-power and the Foster distance (R_0) of the donor acceptor pair (Figure 1.23 A).[83] The efficiency of the process is 50% when the distance between molecules is equal to the Foster distance (typically 40-60 Å, Figure 1.23 B),[81] which allows for distance measurements in and between molecules, and is important for biomolecules. FRET efficiency also depends on the relative orientation of the donor emission and acceptor absorption dipole (κ^2). If the molecules are subjected to isotropic reorientation in a time shorter than the excited lifetime of the donor the average value for κ^2 is assumed to be equal to 2/3. This is in the range that allows the measurement of distances in double stranded DNA.[84–86]

A)[85] $$E = \frac{{R_0}^6}{{R_0}^6 + r^6}$$

B)[85] $$R_0 = 0.211\ (\kappa^2 n^{-4} \Phi_D\, J(\lambda))^{1/6} [\text{Å}]$$

C)[86] $$\kappa^2 = (cos\theta_A - 3cos\theta_B cos\theta_C)^2$$

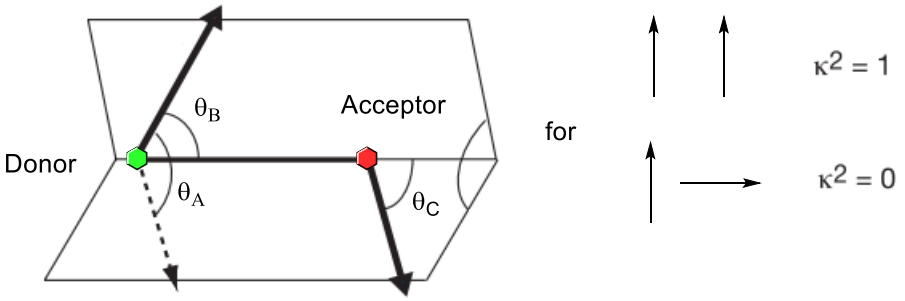


Figure 1.23 Schematic of the dipole orientation angles in FRET between a donor and an acceptor. E: the efficiency of FRET (**A**). Φ_D is the fluorescence quantum yield of the donor in the absence of the acceptor, κ^2 is the dipole orientation factor, n is the refractive index of the medium and $J(\lambda)$ is the overlap integral of the donor emission and acceptor absorbance spectra (**B**). The orientation factor κ^2 (**C**), θ_A is the angle between the emission transition dipole of the donor and the transition absorption dipole of the acceptor.

1.6. Fluorescent hybridization probes for nucleic acid detection

Fluorophores are extremely important tools for the detection processes in DNA sequencing, genetic analysis, imaging and DNA diagnostics.[87–89] Fluorophores have been widely used in biological studies of proteins and nucleic acids both *in vivo* and *in vitro* due to the high sensitivity and ease of incorporation.

Fluorescently labelled oligonucleotides have been used to detect genetic variations in DNA and to identify single nucleotide polymorphisms (SNPs) and point mutations.[88] SNPs and point mutations can be detected using fluorescent hybridization probes in conjunction with fluorescence melting analysis and/or the real-time polymerase chain reaction (rtPCR).

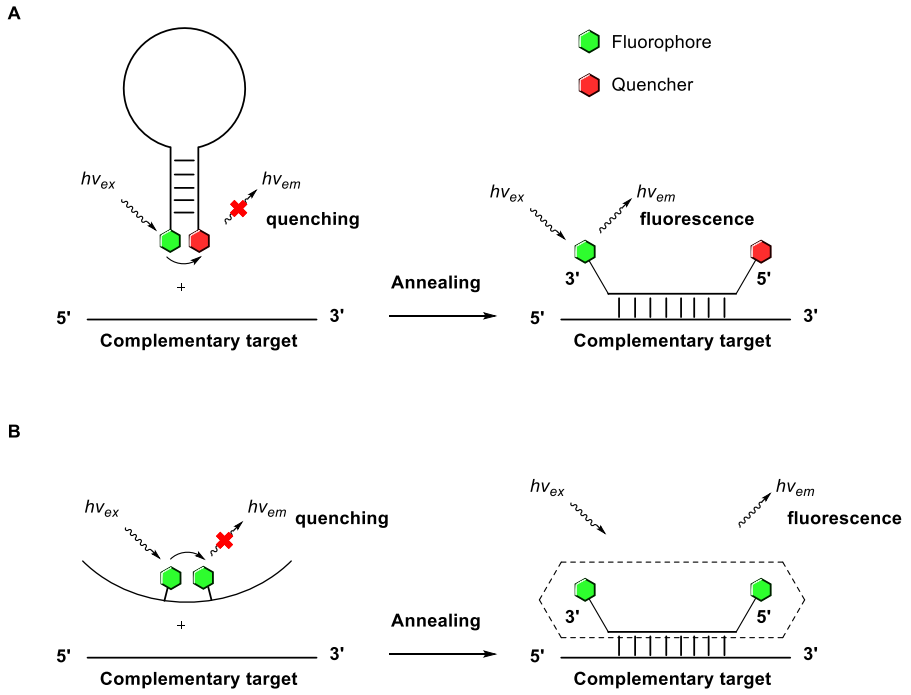


Figure 1.24 A) Molecular Beacon probe interacting with the target. Before annealing close proximity of fluorophore and quencher quenches fluorescence, upon binding to the target the newly formed duplex separates fluorophore-quencher pair allowing for emission of a fluorescent signal. B) HyBeacon probe interacting with the target sequence. Before annealing close proximity of two fluorophores quenches the fluorescence signal internally, upon binding to the target the newly formed duplex separates fluorophores allowing for emission of the fluorescent signal.

Detection of RNA in live cells is also feasible with fluorescent probes.[90] Most of these oligonucleotide probe designs involve a fluorophore and a quencher in close proximity, resulting in quenching of the fluorescence signal of the fluorophore by collisional or FRET mechanisms which are deactivated upon binding to the target (e.g. Molecular beacons (MBs)[82,91,92] and HyBeacons,[55,93,94] Figure 1.24).

1.7.Cyanine dyes

Symmetric cyanine dyes are widely used in fluorescent probes that are used in biophysical studies.[52,55] A fundamental problem of their design is that labelled oligonucleotide probes can have a strong fluorescent background due to failed hybridisation, non-specific binding or degradation of the probe sequence.[95] It is of the utmost importance to reduce the excess of fluorescence which can lead to a false-positive signal during highly sensitive measurements in live cell imaging of RNA or DNA. Therefore, the need for new nucleic acid probes that are more sensitive and selective is high. Cyanine dyes (e.g. Cy3 or Cy5) are routinely used in many fluorescent probe systems for fluorescence *in situ* hybridization (FISH) experiments for nucleic acid visualisation in fixed and live cells.[47,96–98] A promising candidate from the asymmetric cyanine dye family is thiazole orange (TO) and its derivatives, which have been intensively studied and used in various applications including detection of complementary DNA, RNA[99–102] and G-quadruplexes.[103,104]

1.7.1. Thiazole orange

Asymmetric cyanine dyes are an important family of fluorophores they are composed of two different heterocyclic moieties conjugated by a methine chain of variable length which allows for tuning their photophysical properties.[105] An example of these dyes is thiazole orange (TO, Figure 1.25A). It is composed of a benzothiazole and quinoline moiety joined by a mono-

methine bridge. TO becomes highly fluorescent upon binding (intercalating) to nucleic acids due to restriction of rotation about the methine bridge, forcing a planar conformation and conjugation between the two heterocycles in which energy is not emitted in non-radiative decay like in the unbound state.[106] This results in an increase of fluorescence up to 18900 times upon intercalation to the DNA.[107]

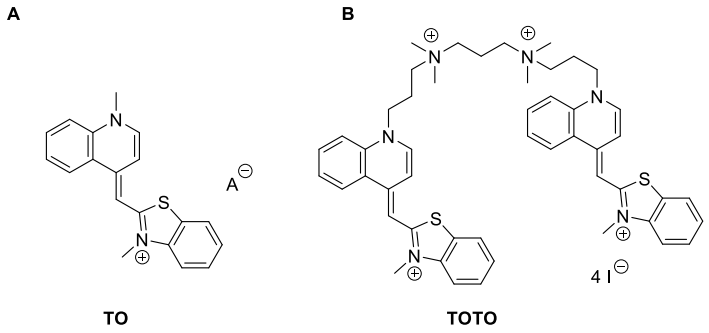


Figure 1.25 A: Structure of thiazole orange with a counterion A-; B: Structure of TOTO.

The interactions of TO with nucleic acids was reported by Nygren *et al*.[106] The highest affinity occurs when the TO is bound to double-stranded DNA duplexes. The values of log(K), where K is the binding constant of the TO dye, were equal to 4.8 for the single stranded polypurines and for polypyrimidines were equal to 3.4 and 2.3 for poly(dC) and TO-poly(dT) respectively. This values changes upon binding to double stranded DNA, log(K) for p(dA)-p(dT) and p(dG)-p(dC) was equal to 5.5 for both combinations showing the preference for dsDNA over ss. This results in 5–10 fold weaker binding to ss polypurines and a further 10–1000 fold weaker binding to ss polypyrimidines.[106] NMR studies of TOTO dimer (Figure 1.25B), where two TO moieties were linked by the endocyclic nitrogens from quinoline moieties showed how TO can intercalate as a dimer into the dsDNA helix (Figure 1.26).[108] The TOTO dimer intercalates through the minor groove and the positively charged linker is aligned with the phosphodiester backbones. The quinoline moiety from each TO is stacked between the purine nucleobases whereas the benzothiazole moiety is stacked between pyrimidine nucleobases. In the case of

a single TO moiety molecular modelling suggests intercalation is very similar to TOTO, both in terms of base stacking and the preference of the benzothiazole and quinoline moieties for pyrimidines and purines respectively.[109]

Favourable properties of the TOTO and TO-PRO1 dimer are utilised as a nucleic acid stain in gel electrophoresis with enhancement of fluorescence >3000-fold when TOTO or 2500-fold TO-PRO1 is bound to the double stranded DNA relative to the single strands.[108,109] The TOTO dimer gives 10 times higher detection sensitivity than the ethidium homodimer (EthD) and is 500 times higher than conventional ethidium bromide.[107] Choice of this molecule (TO) over other common DNA fluorophores was further supported by far superior differences of F_{ds}/F_{ss}. In the cases of Acridine Orange (F_{ds}/F_{ss} = 2.2), Hoechst 33343 (F_{ds}/F_{ss} = 30), Hoechst 33258 (F_{ds}/F_{ss} = 58) and DAPI (F_{ds}/F_{ss} = 20) this is marginal in comparison to TO-PRO1 ((F_{ds}/F_{ss} = 2500) or TO (F_{ds}/F_{ss} = 18900).[109,110]

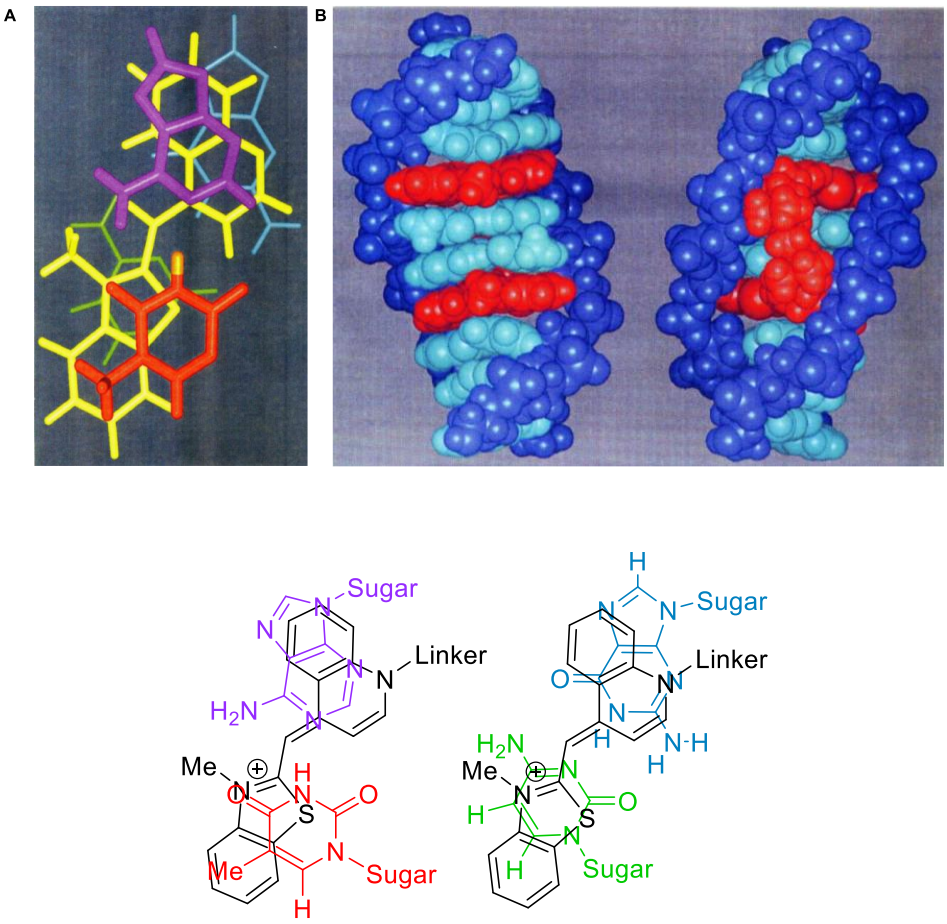


Figure 1.26 NMR resolved stacking of the TOTO chromophore in the CpT/GpA binding site, yellow: TOTO; green: cytosine base; red: thymine base; light blue: guanine base; magenta: adenine base, (A) and structure of TOTO-dsDNA complex where the helix is composed of the self-complementary sequences 5'-CGCTAGCG: blue and light blue: ss DNA strands; red: TOTO (B), schematic of intercalation site for single TO moiety from A (C)[108]

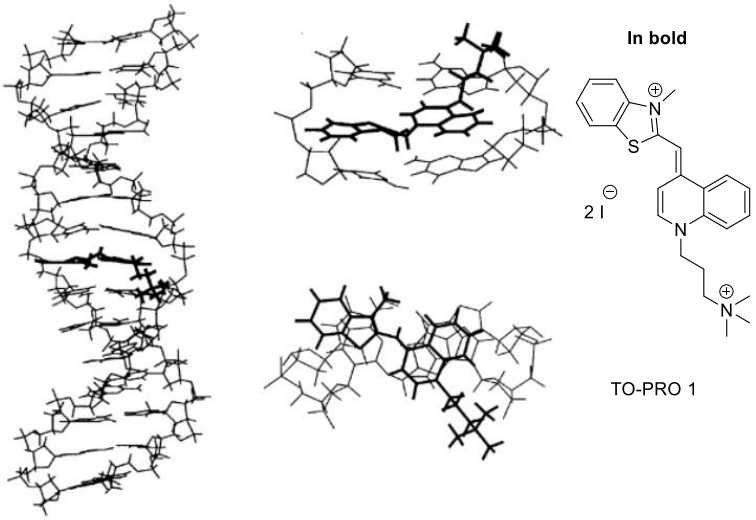


Figure 1.27 Molecular modelling of TO-PRO1 intercalation into 5'-TTCTCCCCCGCTTA 3'-AAGAGGGGGCGAAT duplex, using CHARm issue 22 program.[109]

1.7.2. Incorporation of TO into nucleic acids

Thiazole orange can be covalently attached to nucleic acid probes by either the endocyclic nitrogen of quinoline (TO_Q) or by the benzothiazole moiety (TO_B). Studies on the relationship between attachment and binding to the phosphodiester backbone showed a higher fluorescence signal and greater increase of T_m (duplex melting temperature) when TO_B was directed into the major groove and when TO_Q was directed into minor groove,[111–113] which is in agreement with TOTO dimer studies.[108] This could be linked to the dihedral angle between the methine bridge and the linker, TO_B with a smaller angle (θ_B = 69.0°) than TO_Q (θ_Q = 170.7°) (Figure 1.28) which according to the study provides better stacking between base pairs.[111]

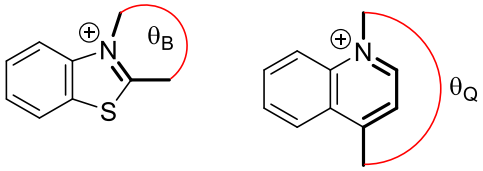


Figure 1.28 The dihedral angles of TO derivatives.[111]

TO and its derivatives can be attached to the nucleobase, sugar or phosphodiester backbone of oligonucleotide probes post-synthetically or during solid phase synthesis. Interestingly the modified nucleobase developed by Okamoto *et al.* (Figure 1.29 A) involves two TO dyes. This TO-pair forms an H-aggregate which decreases the fluorescence signal in the unbound state. Upon binding to the target this aggregate is disrupted, resulting in a strong fluorescence signal. These probes are named 'Exciton-Controlled Hybridization-sensitive fluorescent Oligonucleotide' (ECHO) probes. The resulting F_{ds}/F_{ss} is around 30-fold and in some extreme cases up to 121-fold and has applications in monitoring levels of intracellular RNA.[114–117] A different approach was developed by Qiu *et al.* where TO is incorporated on the thymidine base along with a second reporter dye. The resulting FRET (Figure 1.29 B) gave the advantage of shifting the fluorescence emission to the second dye as well utilising the intercalating

properties of TO. Fluorescence responses up to 19.5 fold upon binding to the DNA targets were achieved.[118] Modification of the sugar to give a 'TO nucleotide' (Figure 1.29 C)[95] and CuAAC-mediated attachment of TO to the 2´-position of the sugar of thymidine *via* the quinoline moiety (Figure 1.29 D)[119] gave promising fluorescent properties in terms of sensing small interfering RNAs. Modification of the phosphodiester backbone by Privat *et al.*[112] gave moderate fluorescence responses. In another study in which TO was linked to the DNA phosphodiester backbone (Figure 1.29 E) *via* its quinoline moiety, differences in fluorescence (F_{ds}/F_{ss}) were moderate; 2.4-fold for the TO-minor groove isomer and 0.8-fold for the major groove isomer (Figure 1.29 E S_p). Attachment of TO *via* its benzothiazole moiety in the major groove of DNA gave a 2.7-fold increase in fluorescence upon duplex formation and 1.3-fold increase when TO was directed into minor groove (Figure 1.29 E R_p).[111] Modifications at the 5'-phosphate of an oligonucleotide probe with TO and covalent attachment of the probe to the surface of a biosensor (Figure 1.29 F) allowed applications in surface based detection.[120]

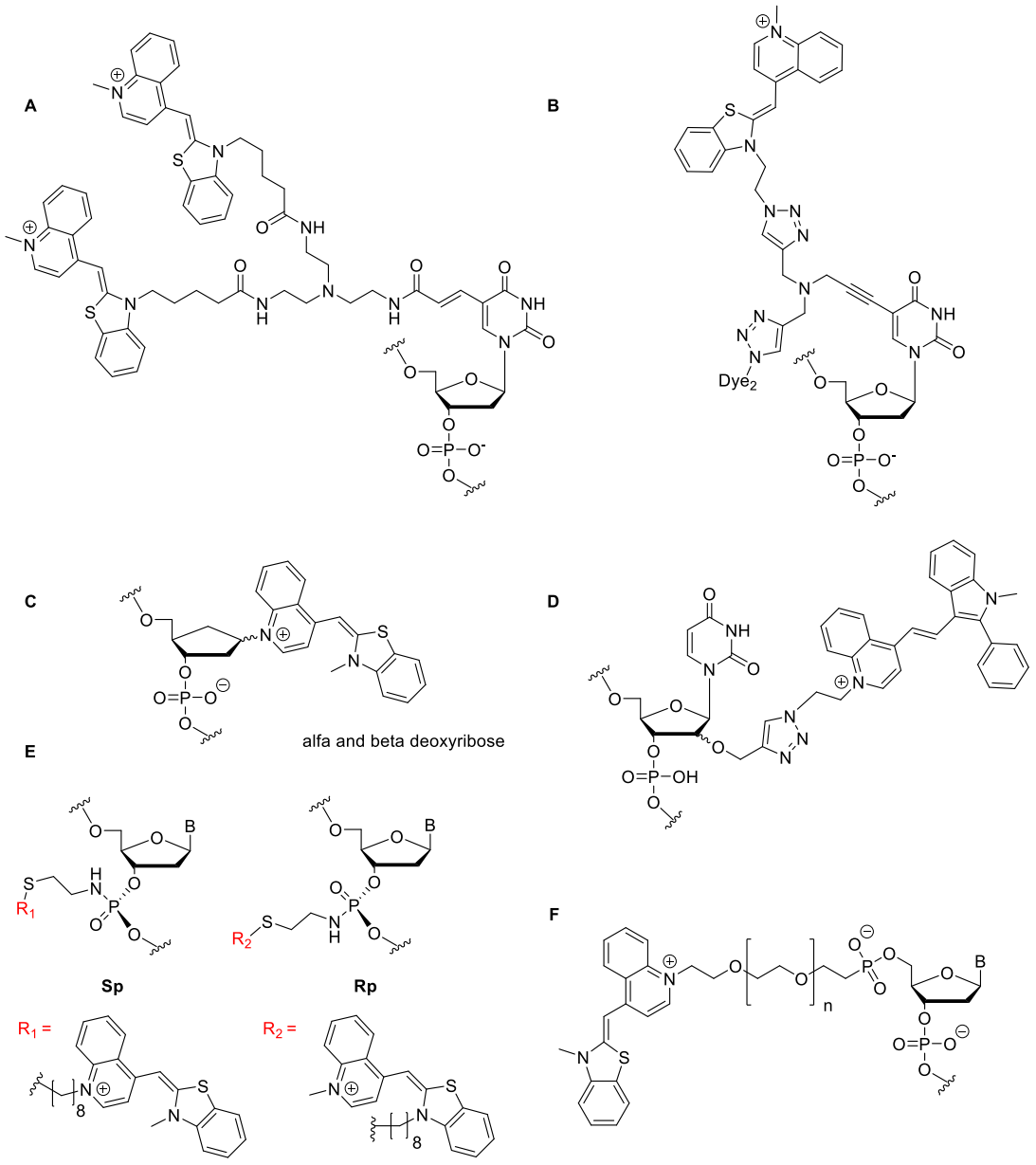


Figure 1.29 Examples of TO modified oligonucleotide-based probes. A: Double attachment of TO to the T-nucleobase (ECHO probes) [109,111,112,122]; B: incorporation of TO with a reporter dye on a thymidine[118]; C: modified sugar with attached TO[95]; D: modified nucleobase with TO attached to the sugar[119]; E: internal modification of phosphodiester backbone[123]; F: modification of 5' phosphate with TO.[120]

Thiazole orange was also incorporated into artificial DNA backbones such as (R)-glycerol[124,125] (Figure 1.31 A) as part of a FRET system. A different concept was developed by Kohler *et al.* where TO was attached by a short carboxylic linker *via* the quinoline moiety to peptide nucleic acid (PNA).[126] In this design TO functioned as an artificial nucleobase, and the resultant probes

were named PNA Forced Intercalation Probes (PNA-FIT, Figure 1.30 B).[127] These were based on "light-up" probes developed by Svanvik *et al*. (Figure 1.30 A).[99] This concept provided good duplex stability and gave fluorescence increases upon duplex formation up to 26-fold, allowing for detection of mRNA in live cells.[127,128] This idea was then applied in a DNA-FIT design with TO and its derivatives attached to an L-serinol acyclic DNA backbone (Figure 1.31 B, n = 1) for detection of complementary DNA and RNA.[129,130] Further development of this idea utilised a D-threoninol backbone along with a fluorescence quencher to give highly sensitive (F_{ds}/F_{ss} = 70) MBs (Figure 1.31 C).[131]

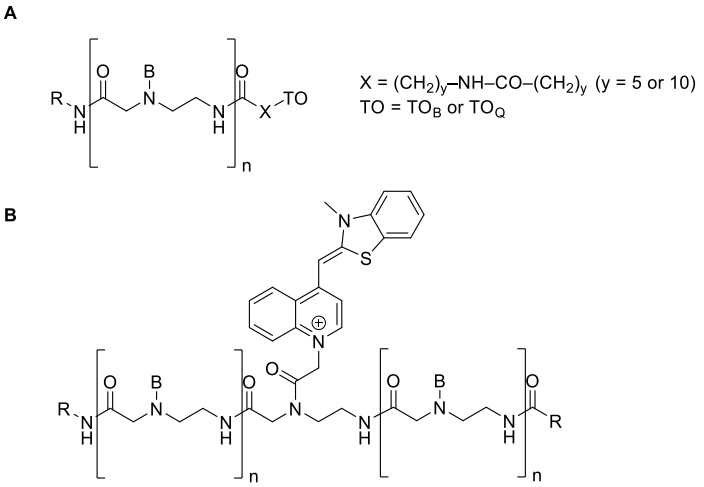


Figure 1.30 Examples of PNA based probes with TO. A: Light-up probes[99]; B: PNA-FIT probes.[132,127] Where B is a nucleobase: A, T, C or G.

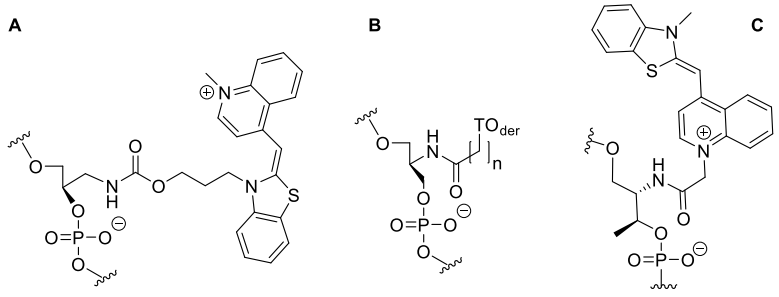


Figure 1.31 Examples of artificial modifications incorporated into oligonucleotide probes with TO. A: (R)-glycerol[124,125]; B: L-serinol[133,134]; C: D-threoninol.[131]

Various modifications to thiazole orange such as increasing the length of methine bridge or exchanging the sulphur atom in the benzothiazole moiety for oxygen allow for fine tuning of fluorescence properties. This gives the range of fluorophores for multicolour (multiplex) assays which were used in the ECHO probe system (Figure 1.32 A1-4).[115] Modification of the quinoline (Figure 1.32 B1), the benzothiazole (Figure 1.32 B3) or exchange the benzothiazole for the quinoline moiety have also been carried out to alter the fluorescence properties of the DNA-FIT system(Figure 1.32 B4).[135,136]

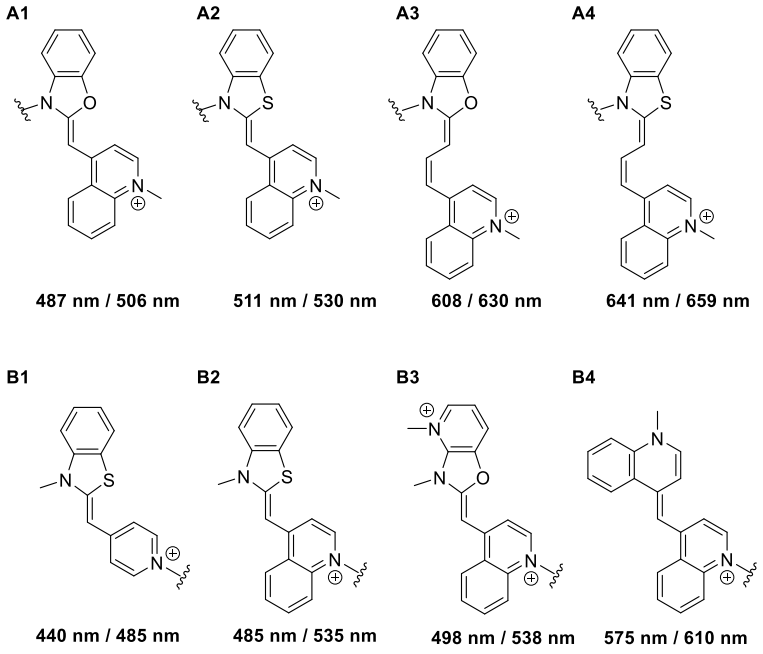


Figure 1.32 Examples of TO and its derivatives with varying $\lambda_{ex,\,max}$/ $\lambda_{em,\,max}$ values used in ECHO probes (A); A1: YO; A2: TO; A3: TO-3; A4: YO-3[115] and DNA-FIT probes (B); B1: BO; B2: TO[135]; B3: JO[136]; B4: QB.[135]

1.8. Molecule design

As previously mentioned (Paragraph 1.7.1) thiazole orange is 'go to' molecule for the fluorescence determination between ss and ds of the oligonucleotide, derived from superior fluorescence 'on-off' properties.

Molecule design

Important factor is the desired target at with probe will be directed towards, as in cells other structures of oligonucleotides can be present such as triplexes and G-quadruplexes.[137–139] This issues will not be covered in this thesis, although worth noting are studies performed in this area with TO. Thiazole orange as free dye against ds DNA and telomeric G-quadruplexes shows no preference in terms of fluorescence responses, only modified TO a position 2 of quinoline moiety with p-(dimethylamino)styryl substituent exhibits 10-fold preference towards G-quadruplexes.[103] Additionally in the same study Triplex AT*T as a target with modified TO showed highly comparable fluorescence enhancement results for the G-quadruplex (telo21, information in SI[103]). TO can be also used in displacement assay for determination between ds and G-quadruplex with putative ligands.[140]

In terms of triples forming oligonucleotides (TFO), TO show high stability when TO is used as a stain in gel electrophoresis, showing that complexes with TFO and G-quadruplexes are more stable that in case of dsDNA when loaded with TO.[104] Interestingly when TOTO was used as an additive in loading, complex with all three types of structures could be visualised without additional staining, showing importance of molecule design for appropriate targets. Recent reports on TO covalently linked to the TFO showed promising results, both with PNA against dsRNA target at pH = 5.5[102] and more promising DNA backbone showing formation of triplexes at higher pH = 7.0,[141] developed in our group. In case of DNA backbone TFO apart from high increases of Tm values (up to +43.6 °C for triple addition of TO) high F_{ds}/F_{ss} (up to 35.7-fold for triple addition of TO and up to 26.3 for single addition) which in comparison to probes developed in Chapter 2 shows up to 6.6-fold increase for same structure for modification and TO and +14.6 °C in terms of thermal stabilisation. This design was later improved to obtained up to 50-fold increase of fluorescence and increases of Tm up to 19.3 °C per single incorporation showing promising evaluation for TFOs.

Molecule design

This work is focused on the ss oligonucleotide target, in case of RNA methods such as *in situ* staining in animal embryos,[142] molecular beacons for fluorescence in fixed[143] and live cells[144] or fluorescence in situ hybridization (FISH) protocols.[145] In case of DNA the main problem is that genetic information encoded in DNA is present in the nucleus which causes problem with efficient delivery. Secondly that it normally requires denaturation of dsDNA in order to access ss target followed by FISH[146] or PCR amplification[147] is not compatible with live cell imagining.

Additional problem is limit of detection of fluorescent as abundant RNA targets or repetitive DNA sequences are possible to detect pushing new designs to be more specific, as there is a growing need for nucleic acid probes with low background fluorescence properties, and are more responsive (fold increase upon binding to target). Additionally probe systems that are easy to synthesize are more than needed. Thiazole orange as a 'smart' probe is a highly promising solution to this problem as has been previously demonstrated.[100] However, there is a need for efficient methods of TO-oligonucleotide synthesis probes and efficient labelling procedures to achieve readily obtainable TO probes with favourable fluorescence response and high thermal duplex stability.

1.9.Research aims

For these reasons TO with selective groove binders modifications (PA, C6 and AE) with different lengths of linkage to two moieties (benzothiazole or quinoline) requires detailed evaluation. Two main biophysical techniques used in this work are fluorescence change upon binding to the target oligonucleotide and thermal stability with relation to the sequence dependence of TO properties. Additional modification to the sequence probe (2'−OMe) needs to be answered in easily comparable conditions and sequence context. This topic is covered in the Chapter 2 and findings were recently published.[148]

Discussion in Chapter 2 is focused on the nucleoside modifications with TO, different approach is shown when TO is used as a surrogate base (FIT probes).[101]This promising approach design is based on the acyclic (L-serinol) modification conjugated with TO. Here we have evaluated a new DNA backbone (L-threoninol) in order to improve biophysical properties. In this context L-threoninol as scaffold only modification shows preferential binding affinities to complementary DNA and RNA when compared to L-serinol. Novel approach to this topic and is discussed in Chapter 3.

Thiazole orange can be incorporated into oligonucleotide probe systems along with a reporter dye, allowing for FRET based multicolour detection of RNA. Such a system (combinations probes) was recently reported as a work from our group.[149] Using reporter dye gives the advantage of multicolour readout, although combinational probes are hard to synthetize reducing ease of screening process. Development of new nucleobase modifications for orthogonal labelling of these probes, involving CuAAC chemistry and amide bond formation is presented in Chapter 4.

Chapter 2 - Thiazole orange (TO) nucleoside modification and its applications

2. Chapter 2 - Thiazole orange (TO) nucleoside modification and its applications

2.1. Introduction

Fluorescent nucleic acid probes are used in the growing field of clinical diagnostic and gene expression studies,[97] allowing for the detection of biomolecules and monitoring their activities in living cells.[150] Unfortunately fluorophore-labelled nucleic acid probes often have a strong fluorescence background, due to failed hybridisation or non-specific binding of excess probe. False positive signals due to non-specific interactions and nuclease degradation in some fluorescent probe systems (e.g. Molecular Beacons)[151] is also a problem which needs to be addressed. Removal of the background fluorescence is challenging, especially in live cell imaging due to unspecific binding, off-target false positive signal of the probe or in case of MB digestion of probe sequence. For these reasons, designing new nucleic acid probes with a strong fluorescence response upon binding to the desired nucleic acid target with a low unbounded fluorescence signal is necessary, as 'on-off' properties of TO allow for specific generation of fluorescence signal upon binding to the target shows great potential.[135,149,152]

The numerous diagnostic applications highlight the importance of evaluating the properties of thiazole orange oligonucleotide conjugates. With this in mind we explored the conjugation of thiazole orange to oligonucleotides *via* the quinoline and benzothiazole moieties and also investigated placement of TO in the major and minor grooves of the duplex (PA, C6 and AE, Figure 2.1).

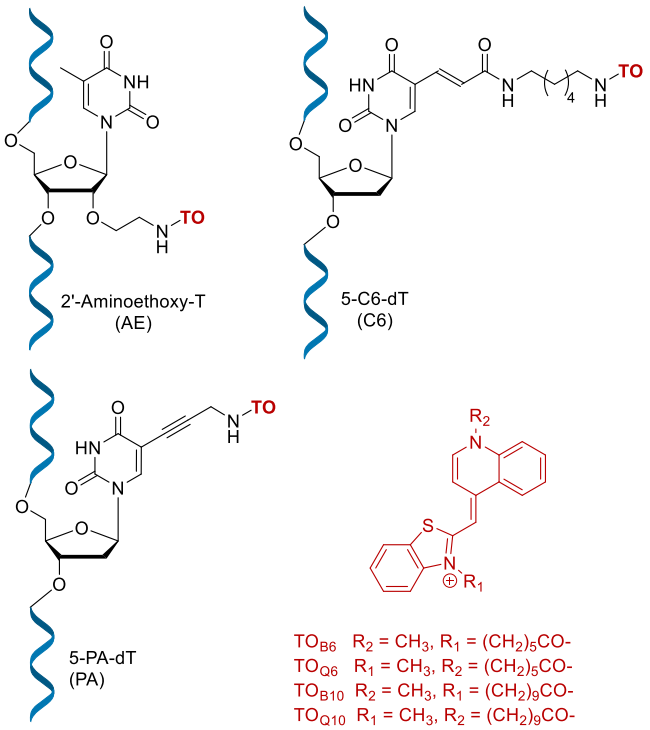


Figure 2.1 Structures of TO-modified nucleotides AE, C6, PA and the TO moieties used as carboxylic acids or NHS esters for oligonucleotide labelling.

2.2. Backbone modification and sequence context

Choice of modifications used in this study (PA, C6 and AE) was derived from groove directing effects. PA[153] and C6 modification (amine linker) in vicinity of the major groove, PA provide additional stabilising effect upon formation of duplex based on the effect of the propynyl grup.[154] Although main approach was to allow the variable length of the linker for $TO_{B/Q6}$, where constant length of TO linkage was varied by modification at two extremes with C6 modification allowing for higher degree of freedom(Figure 2.2 A and B). Additionally this monomer is commercially available allowing for simple extension of the linker without unnecessary synthetic effort. Arguably C6 modification could allow for TO to stack on the end of the duplex, although mismatch experiments at position -2 to +2 (thermal melting and fluorescence) support intercalation of the dye.

In case of AE (Figure 2.2 C) length of modification was not extended, only different TO derivative with longer linker was applied ($TO_{B/Q10}$). In most cases length of the linker (6 carbon atoms) should provide favourable position of TO for intercalation.

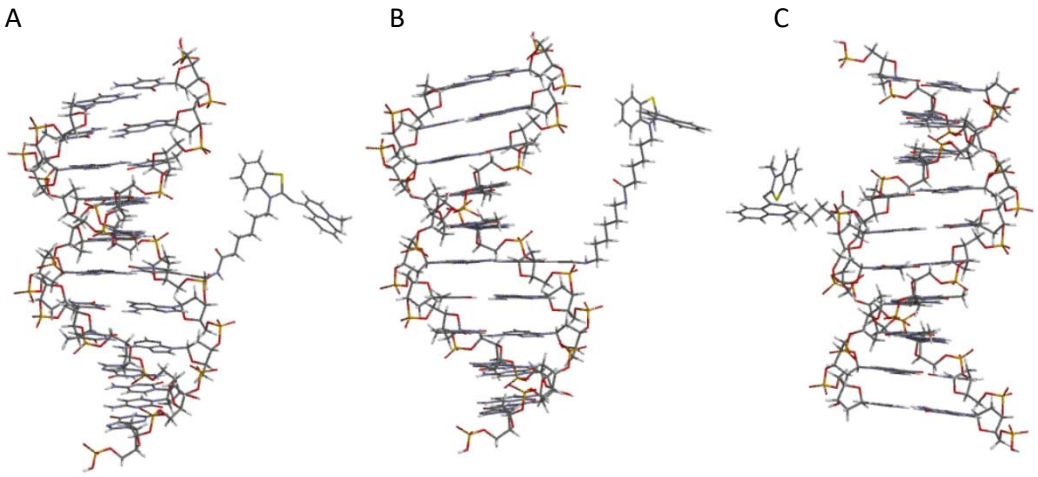


Figure 2.2 Visual representation of linker length (modification-$TO_{B/Q6}$) of sequence 5′-GCAA**X**ATACG with complementary DNA target where X for A: PA-TO_{B6}, B: C6-TO_{B6} C: AE-TO_{Q6}. Supported by data for PA[153] and AE,[155] software used for visualisation: SPARTAN. Calculations were not performed on any of those structures.

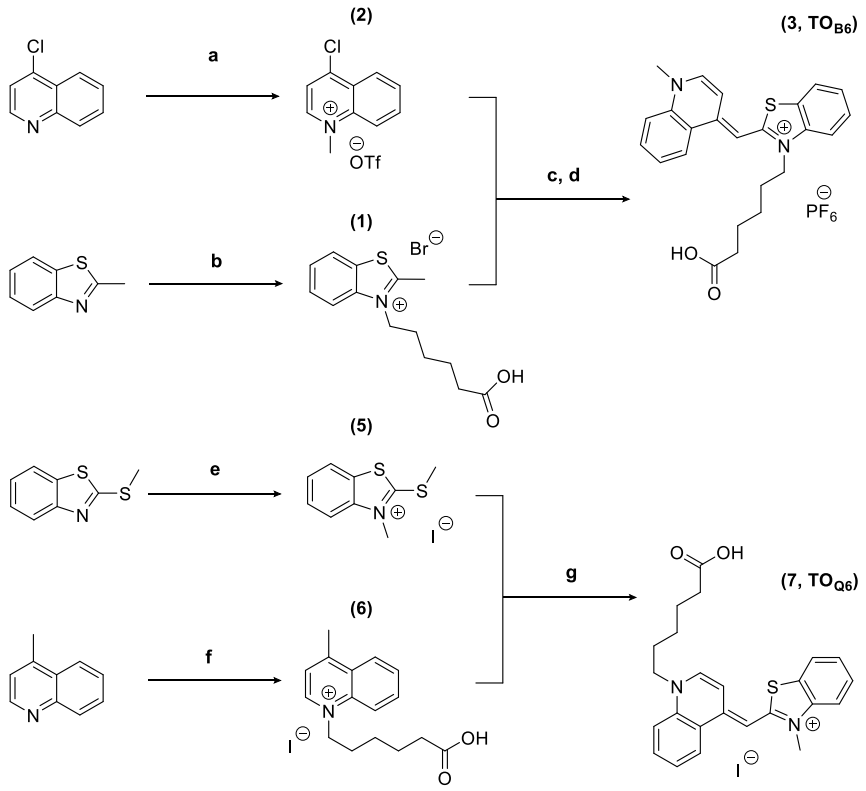
The specific base sequence for the decamer used in this study, 5'-GCAYXYTCAG-3' (where X = T or artificial backbone and Y = A, C, T or G), was selected for several reasons. First, an decameric length produced a stable duplex, with a convenient T_m. Additionally, guanosine/cytidine pairs were positioned at the duplex ends to prevent fraying,[156] while thymidine base was positioned near the centre to allow labelling. Surrounding positions of various bases allows for sequence dependence study.

2.3. Synthesis of thiazole orange derivatives

Thiazole orange is an asymmetric cyanine dye that can be covalently attached by the quinolone (TO_Q) or benzothiazole (TO_B) endocyclic nitrogen to the oligonucleotide probe sequence *via* amide bond formation. As described previously, the acyclic serinol backbone

modification used with PNA/DNA FIT probes requires usage of quinoline attached TO for good fluorescence properties.[127,130] In the case of ECHO probes[122] and combinational probes[118] benzothiazole linked TO is attached to the modified thymidine.

Therefore our investigations required both types of thiazole orange derivatives, with linkers on benzothiazole (TO_B) and quinoline (TO_Q) nitrogens. Four derivatives with various length of the linker were synthesized: TO_{B6} and TO_{B10} as well as TO_{Q6} and TO_{Q10}. All thiazole orange derivatives contained carboxylic acid groups for labelling of amine containing oligonucleotides. This labelling method was chosen due to abundance efficient of amide coupling methods. [122,127]

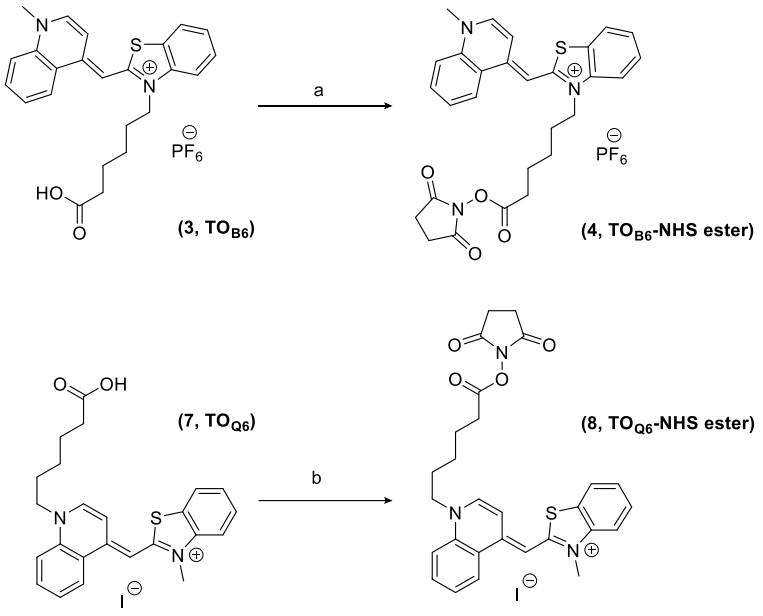


Scheme 2.1. Synthetic route for TO_{B6} and TO_{Q6}. Reagents and conditions: (a) MeCN, MeOTf, 3 h, RT, 90%; (b) MeCN, 6-bromohexanoic acid, 48 h, reflux, 41%; (c) CH_2Cl_2:MeOH, Et_3N, 15 min, RT; (d) H_2O:2-propanol, $NaPF_6$, RT, 41% over two steps; (e) MeCN, MeI, 24 h, 50 °C, 46%; (f) 6-bromohexanoic acid, 20 h, 130 °C, 61%; (g) DMF, Et_3N, RT, 0.5 h, 79%.

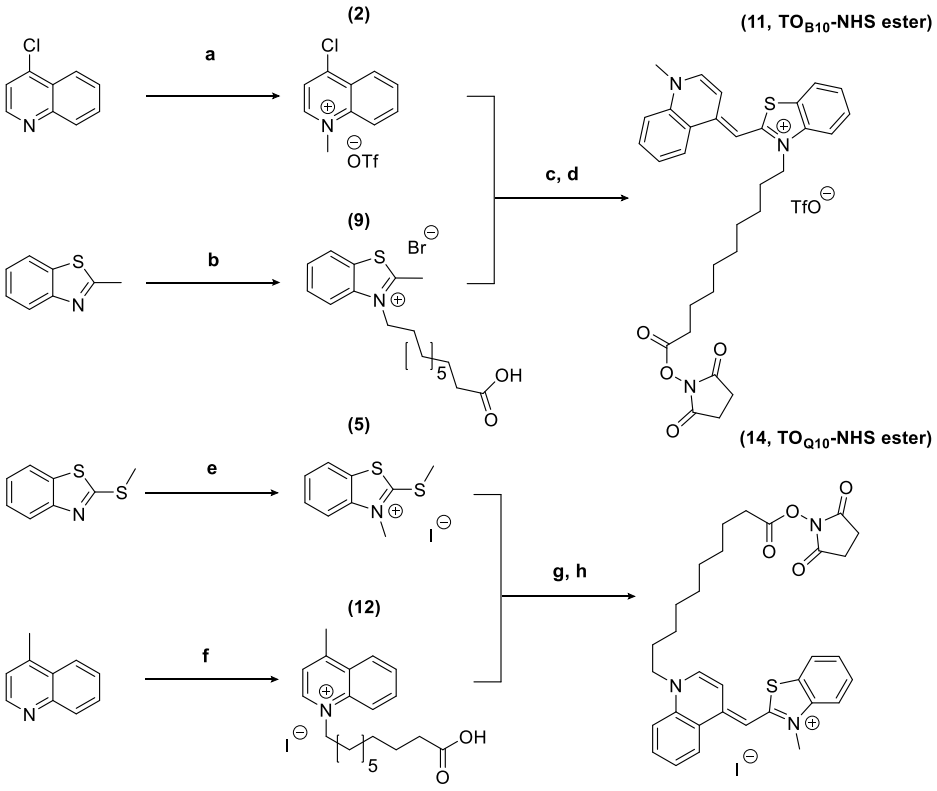
TO attached by the benzothiazole linker was obtained by synthesis of building block (**2**) which allows for faster couplings (minutes vs hours) than the N-methylquinoline commonly used in the literature.[114,157,158] This building block was conjugated with benzothiazole modified with an appropriate carboxylic linker (compound **1** or **9**, Scheme 2.1 and Scheme 2.2) in order to obtain TO. These carboxylic derivatives of TO (TO_{B6} and TO_{B10}) were then successfully converted and isolated as NHS esters by reaction with TSTU (Scheme 2.2 and Scheme 2.3). Isolation of TO active esters allows for convenient labelling method (Experimental 6.4.1.2) with no requirement of a preactivation step (Experimental 6.4.1.1), shortening the time and effort needed to obtain TO-modified oligonucleotides probes.

Thiazole orange derivatives attached by the quinoline nitrogen (TO_{Q6}, TO_{Q10}) were obtained by adopting literature procedures[157,99] involving conjugation of building block (**5**) with the appropriate 4-methylquinoline derivatized with a carboxylic acid linker (compound **6** or **12**). These thiazole orange derivatives were converted to NHS esters and isolated similarly to the benzothiazole modified TO (Scheme 2.2 and Scheme 2.3).

This versatile synthetic scheme allows for easy and convenient modification of position, type and length of the linker. This approach was also used for shorter carboxylic acid linker derivatives and propargyl functionalised TO derivatives for evaluation of FIT probes (described in Chapter 3).



Scheme 2.2 Synthetic route to NHS esters of TO derivatives. Reagents and conditions: (a) DMF, TSTU, DIPEA, 0.5 h, RT 47%; (b) DMF, TSTU, DIPEA, 0.5 h, RT, 80%.



Scheme 2.3 Synthetic route to $TO_{B/Q10}$ NHS esters. Reagents and conditions: (a) MeCN, MeOTf, 3 h, RT, 90%; (b) 10-bromodecanoic acid, 5 h, 110 °C, 18%; (c) CH_2Cl_2:MeCN, Et_3N, 0.5 h, RT, 63%; (d) DMF, TSTU, DIPEA, RT, 77%; (e) MeCN, MeI, 24 h, 50 °C, 46%; (f) 10-bromodecanoic acid, 3 h, 110 °C, 18%; (g) DMF, Et_3N, RT, 0.5 h, 51%; (h) DMF, TSTU, DIPEA, RT, 87%.

2.4. Oligonucleotide probe design and labelling with TO derivatives

The effects of dye location on duplex stabilisation and fluorogenic properties of TO-ON probes are not yet fully understood despite the fact that detection and imaging of cellular DNA and RNA is an increasingly important fields of study.[159,160] Hence the field requires further investigation.

In this study, for synthetic convenience, our focus was on attachment of TO to the thymidine nucleotide, but linking thiazole orange to other nucleotides should also be feasible. Indeed in ECHO probes two TO moieties have been attached to cytidine.[117] The other key variable is the position of linker attached to the thiazole orange. It can be linked to the probe either *via* its benzothiazole or quinoline nitrogen.[111,161] In order to investigate the effects of these alternative modes of attachment on fluorescence and duplex stability, three nucleoside monomers, 5-propargylamino-dT (PA), amino-C6-dT (C6) and 2'-aminoethoxy-T (AE) were used to introduce TO into oligonucleotides by labelling their aliphatic amino groups (Figure 2.1). To achieve this, thiazole orange was functionalised with a hexanoic or decanoic acid linker on either the benzothiazole (TO_{B6}/ TO_{B10}) or the quinoline moiety (TO_{Q6}/ TO_{Q10}) (Scheme 2.1 − Scheme 2.3). In the nucleic acid duplexes PA and C6 locate the TO dye in the vicinity of the major groove,[153] which should promote good fluorescence properties with benzothiazole attached TO, while AE modification positions the dye in the minor groove region,[162] which should allow the best performance for quinoline-attached TO. These three modifications along with TO derivatives attached by various linker lengths (C6 or C10) and attachment positions (TO_Q or TO_B) provide structural diversity, allowing for an in-depth photophysical evaluation.

The phosphoramidite monomers of PA and AE, were synthesized according to the published procedures,[53,162,163] and C6 phosphoramidite (amino-C6-dT) was purchased from Glen

Research. All three monomers were incorporated into a series of 10-mer oligonucleotides (ONs), which were post-synthetically labelled with TO_{B6} or TO_{Q6} in high yield using (benzotriazol-1-yloxy)tripyrrolidinophosphonium hexafluorophosphate (PyBOP) and *N*-methylmorpholine (NMM) in DMF.[164] PyBOP was found to give better yields and conversion to previously reported coupling methods with *N,N*'-disuccinimidyl carbonate (DSC) (Experimental 6.4.1.1, Figure 2.3).[165,166] An optimised labelling procedure using the NHS esters of TO_{B6} or TO_{Q6} remarkably gave almost 100% conversion to the product in just 5 minutes (Figure 2.4, Experimental 6.4.1.2). These efficient coupling strategies were also applied in a more demanding system, the synthesis of probes with double incorporation of TO (Figure 2.4) where coupling with DSC gave a mixture of products. The obtained TO-ODN labelled oligonucleotides are shown in Table 6.1.

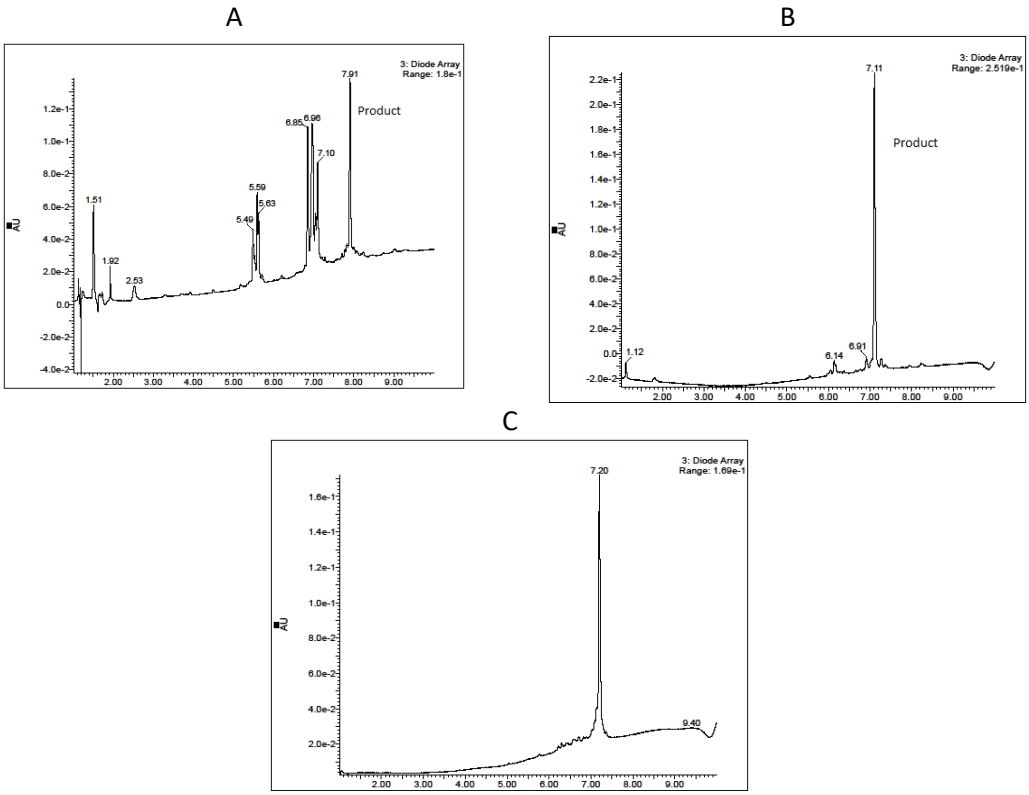


Figure 2.3 Examples of HPLC chromatograms at 260 nm showing labelling reactions of 5'-C**PA**GAA**PA**ATGC with TO_{B6} before HPLC purification **A**. Method 1, using DSC as the coupling reagent; **B**. Method 1, using PyBOP as the coupling reagent; **C**. HPLC purified oligonucleotide 5'-C**PA-**$\mathbf{TO_{B6}}$GAA**PA-**$\mathbf{TO_{B6}}$ATGC generated using DSC. Sequence was chosen as an example of more challenging double incorporation of TO and as representative case of optimised conditions for labelling. Sequence 5'-C**PA**GAA**PA**ATGC mass calculated: 3105 mass found: 3106; sequence 5'-C**PA-**$\mathbf{TO_{B6}}$GAA**PA-**$\mathbf{TO_{B6}}$ATGC mass calculated: 3879 mass found: 3879.

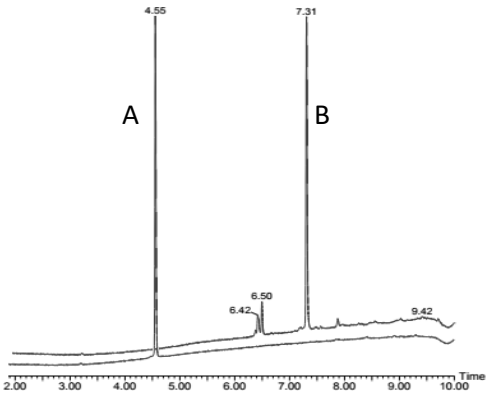


Figure 2.4 HPLC chromatograms at 260 nm showing efficient (5 min coupling time) labelling reaction of 2'-OMe–(ORN1) (5'-GCA**AE**UU**AE**ACG) with TO_{Q6}-NHS using Method 2 as described above. A – Unlabelled oligonucleotide: starting material, B – crude labelled product before HPLC purification.

2.4.1. DNA Duplex stabilisation by TO-ODN probes against DNA targets.

For biological applications of TO-probes it is important to understand the properties of the modified duplexes. Good thermal stability is essential, the higher the T_m of the duplex the higher the affinity of probe to the desired target. PNA-FIT probes show slight destabilisation, the T_m of DNA-PNA duplexes being -1 to -3 °C relative to DNA duplexes,[167] and for DNA-FIT probes ΔT_m is similar to the T_m of unmodified control DNA duplexes (from -4 to +2 °C depending on the position of TO modification).[130] Internal phosphodiester backbone modifications in DNA give T_m's of +4.0 and +6.5 °C respectively for TO_B and TO_Q, whereas incorporation of TO at 5' end gives +4.5 to +7.5 °C increase in thermal stability.[123] ECHO probes give an increase in T_m (to a varying degree) depending of the sequence context (on average their T_m is +11.3 °C).[168] These strong effects can be attributed to the intercalation of TO, and in the case of FIT probes thiazole orange functions as a base surrogate, reducing the natural H-bonding and pi stacking of base pairs, but restoring duplex stability to the natural level due to the intercalating properties of TO.

UV melting studies were performed in order to investigate the effects of base stacking on fluorescence and duplex stability of our TO-probes, four different oligonucleotide sequences were synthesized with varied base sequence around the TO-modified nucleotide (Table 2.1A, Table 6.7, Figure 2.5) incorporated into the sequence 5'-GCAY**X**YUACG were X is the modification (PA, C6 or AE) with TO_{B6} or TO_{Q6} attached and Y is one of the four natural nucleobases.

There are some strong sequence-dependent effects, addition of TO increased duplex stability (melting temperature, T_m, with statistical error no higher than 1.1 °C based on Gauss method[169]) to quite varying degrees when the ODNs were hybridised to fully complementary DNA strands (ΔT_m = +1.3 to 14.6 °C). Most notably, in fully matched DNA duplexes, placing the TO-modified nucleotide in the sequence context CXC and GXG (ODN3 and ODN4), give the highest T_m values (56.8 and 57.7 °C respectively) whereas lower T_m values were obtained for TXT and AXA sequence contexts (ODN1 and ODN2, T_m = 47.0 and 48.9 °C respectively).

Across all sequences, in the major groove (the 5-position of the thymine nucleobase), the TO_{B6} modification is more stabilising than TO_{Q6}, and the short linker (PA) is more effective than the long linker (C6) (ΔT_m = +5.2 °C for TO_{Q6} and ΔT_m = +11.6 °C for TO_{B6} for the PA modification and ΔT_m = +4.0 °C for TO_Q and ΔT_m = +10.0 °C for TO_{B6} in the case of the C6 modification). Evaluation of sequence dependence showed that PA modified ODN1 with TO_{B6} (TXT) gave a smaller increase in T_m (ΔT_m = +6.6 °C) whereas for the PA monomer with other sequences gave higher and similar levels of stabilisation (AXA, ΔT_m = +12.8 °C; CXC, ΔT_m = +14.6 °C; GXG, ΔT_m = +12.3 °C). The highest increase was observed for the combination of PA with TO_{B6} (ΔT_m = 14.6 °C) in the ODN3 sequence context.

In the minor groove (2'-position of the sugar, AE), TO_{B6} and TO_{Q6} have similar stabilising effects (ΔT_m = +9.3 °C and +8.6 °C for TO_{Q6} and TO_{B6} respectively), which is slightly lower than for TO

located in the major groove (PA and C6) and for the TO_{B6} combination. The sequence dependence of stabilisation was in the following order: ODN2 (AXA) > ODN3 (CXC) > ODN4 (GXG) > ODN1 (TXT), with AXA, ΔT_m = +11.1 °C; GXG, ΔT_m = +9.2 °C; CXC, ΔT_m = +8.6 °C; TXT ΔT_m = +7.0 °C for both TO derivatives.

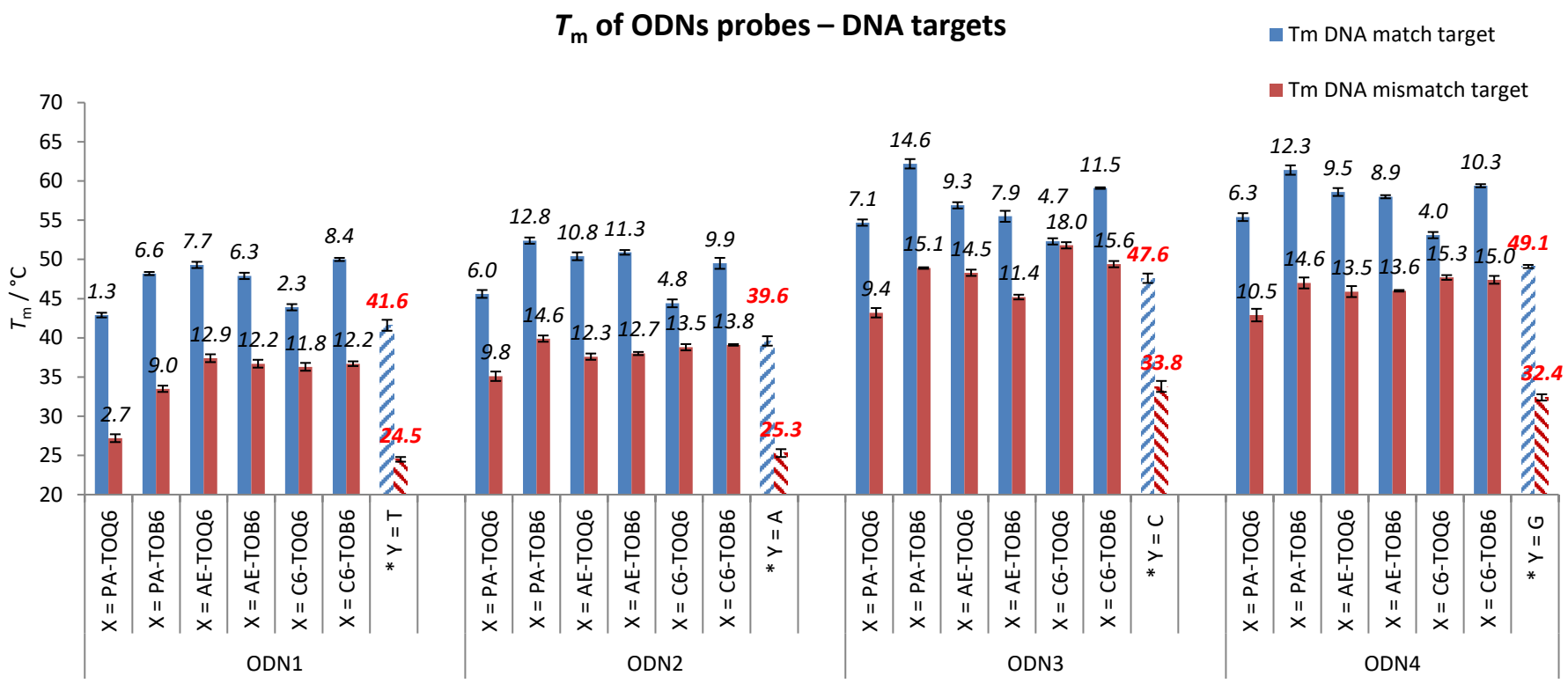


Figure 2.5 UV melting data for ODNs (ODN1 (5'-GCATXTTACG), ODN2 (5'-GCAAXATACG), ODN3 (5'-GCACXCTACG), ODN4 (5'-GCAGXGTACG)) probes against DNA targets. The base opposite the TO is either A – match or T – mismatch, number above bar = ΔT_m to unmodified target, * = T_m value of unmodified matched and mismatched duplexes. Detailed values: see Table 6.7.

2.4.2. Thermal discrimination of TO-modified oligonucleotides with a mismatched base opposite the TO modification.

The TO-modified ODNs were also evaluated in mismatched duplexes by replacing the adenine base opposite to the TO-modified T with thymine to create a T:T mismatch directly opposite to TO-Thymidine labelled nucleotide. As expected, melting temperatures were significantly lower than those with the fully complementary strands, PA-TO_{B6} showing the greatest mismatch discrimination of the series (ΔT_m between match and mismatch target = 13.7 °C for PA-TO_{B6}; 11.4 °C for C6-TO_{B6}; 11.5 °C for AE-TO_{Q6}; 11.6 °C for AE-TO_{B6}) across all sequences. The TXT sequence (ODN1) was the most sensitive to the mismatch (TXT ΔT_m between match and mismatch target = 12.4 °C; AXA ΔT_m = 10.8 °C; CXC ΔT_m = 9.0 °C; GXG ΔT_m = 11.5 °C).

Interestingly differences between TO_{Q6} and TO_{B6} for PA and AE modifications across all sequences were comparable (Table 2.1A, ΔT_m between matched and mismatch targets for PA modification were equal to 12.6 °C and 13.7 °C for TO_{Q6} and TO_{B6} respectively; ΔT_m between match and mismatch for the AE modification = 11.5 °C and 11.6 °C for TO_{Q6} and TO_{B6} respectively) whereas the C6 modification showed a clear preference for TO_{B6} (ΔT_m between matched and mismatch for the C6 modification 11.4 °C for TO_{B6} and 4.8 °C for TO_{Q6}).

This data indicates that when thiazole orange is opposite a mispaired base it does not prevent thermal mismatch discrimination, although it does reduce it relative to unmodified mismatched duplexes. Mismatch discrimination is in the following order: ODN4 (GXG) > ODN3 (CXC) > ODN1 (TXT) > ODN2 (AXA) (averaged values across all sequence contexts). The ΔT_m between match and mismatch for (natural duplex) – (TO-modified duplex) = 5.2 °C, 4.8 °C, 4.7 °C and 3.5 °C respectively. However, locating the mispaired base pair directly opposite thiazole orange is not the optimum strategy for detection of point mutations or single nucleotide

polymorphisms (SNPs). A more sensitive detection approach to this problem is discussed later (Paragraph 2.4.6).

Table 2.1 Changes in melting temperature (ΔT_m) for DNA duplexes formed by TO-labelled ODN1-4 (A) and changes in fluorescence emission (F_{ds}/F_{ss}) before and after formation of matched and mismatched DNA duplexes (B). T_m, F_{ss}, F_{ds} were obtained in a buffer containing 10 mM phosphate 200 mM NaCl at pH 7.0. DNA concentrations for T_m studies were 3.0 µM of ODN1-4 and 3.3 µM of target strand. For F_{ds}/F_{ss} 0.25 µM of ODN1-4 and 0.28 µM of target were used. T_m values are an average of 4 measurements, fluorescence data were measured at least as a duplicate. $TO_{Q/B6}$: λ_{ex} = 484 nm, λ_{em} = 510 nm, slit ex = 7 nm, slit em = 7 nm at 20 °C.

A	Sequence	**ODN1** dGCAT**X**TTACG		**ODN2** dGCAA**X**ATACG		**ODN3** dGCAC**X**CTACG		**ODN4** dGCAG**X**GTACG		Average ΔT_m	Average ΔTm *m-mm*[c]
X =	duplex	ΔT_m	ΔTm *m-mm*[c]	ΔT_m	ΔTm *m-mm*[c]	ΔT_m	ΔTm *m-mm*[c]	ΔT_m	ΔTm *m-mm*[c]		
PA-TO_{Q6}	match[a]	1.3	15.7	6.0	10.5	7.1	11.5	6.3	12.5	5.2	12.6
	mismatch[b]	2.7		9.8		9.4		10.5		8.1	
PA-TO_{B6}	match[a]	6.6	14.7	12.8	12.5	14.6	13.3	12.3	14.4	11.6	13.7
	mismatch[b]	9.0		14.6		15.1		14.6		13.3	
AE-TO_{Q6}	match[a]	7.7	11.9	10.8	12.8	9.3	8.6	9.5	12.7	9.3	11.5
	mismatch[b]	12.9		12.3		14.5		13.5		13.3	
AE-TO_{B6}	match[a]	6.3	11.2	11.3	12.9	7.9	10.3	8.9	12.0	8.6	11.6
	mismatch[b]	12.2		12.7		11.4		13.6		12.5	
C6-TO_{Q6}	match[a]	2.3	7.6	4.8	5.6	4.7	0.5	4.0	5.4	4.0	4.8
	mismatch[b]	11.8		13.5		18.0		15.3		14.7	
C6-TO_{B6}	match[a]	8.4	13.3	9.9	10.4	11.5	9.7	10.3	12.0	10.0	11.4
	mismatch[b]	12.2		13.8		15.6		15.0		14.2	
Average values	match	5.4	12.4	9.3	10.8	9.2	9.0	8.6	11.5		
	mismatch	10.1		12.8		14.0		13.8			
T_m of T*	match	41.6	17.1	39.6	14.3	47.6	13.8	49.1	16.7		
	mismatch	24.5		25.3		33.8		32.4			

[a] in comparison to the matched unmodified duplex, [b] in comparison to the mismatched unmodified duplex, [c] difference between T_m of matched (m) and mismatched (mm) target in °C, * = T_m value of unmodified matched and mismatched duplexes.

B	Sequence	**ODN1** dGCAT**X**TTACG		**ODN2** dGCAA**X**ATACG		**ODN3** dGCAC**X**CTACG		**ODN4** dGCAG**X**GTACG		Average F_{ds}/F_{ss}	Average I_m/I_{mm}
X =	duplex	F_{ds}/F_{ss}[a]	I_m/I_{mm}[b]	F_{ds}/F_{ss}	I_m/I_{mm}[b]	F_{ds}/F_{ss}	I_m/I_{mm}[B]	F_{ds}/F_{ss}	I_m/I_{mm}[b]		
PA-TO_{Q6}	match	1.0 / **1.0**	1.1	1.4 / **1.4**	1.2	1.5 / **1.5**	0.7	0.9 / **0.9**	0.9	1.2 / **1.2**	1.0
	mismatch	0.9 / **0.9**		1.3 / **1.2**		2.6 / **2.1**		1.3 / **1.1**		1.5 / **1.3**	
PA-TO_{B6}	match	3.7 / **4.4**	3.4	5.5 / **6.3**	1.8	5.3 / **6.0**	1.3	2.7 / **3.4**	2.1	4.3 / **5.0**	2.1
	mismatch	1.1 / **1.2**		3.8 / **4.0**		3.3 / **4.1**		1.3 / **1.5**		2.4 / **2.7**	
AE-TO_{Q6}	match	2.8 / **3.8**	2.0	7.4 / **8.3**	2.7	4.1 / **4.6**	3.5	1.3 / **1.3**	2.1	3.9 / **4.5**	2.6
	mismatch	1.5 / **1.6**		3.2 / **3.1**		1.5 / **1.2**		0.6 / **0.6**		1.7 / **1.6**	
AE-TO_{B6}	match	0.8 / **0.8**	0.9	1.0 / **1.4**	0.8	1.9 / **3.1**	1.4	0.8 / **1.0**	1.5	1.1 / **1.6**	1.1
	mismatch	0.9 / **0.8**		1.2 / **1.1**		1.3 / **2.1**		0.6 / **0.6**		1.0 / **1.2**	
C6-TO_{Q6}	match	1.0 / **0.8**	1.5	3.7 / **4.0**	1.3	3.1 / **3.1**	3.4	1.4 / **2.0**	2.1	2.3 / **2.5**	2.1
	mismatch	0.5 / **0.6**		2.5 / **1.1**		0.9 / **0.9**		0.6 / **0.9**		1.1 / **0.9**	
C6-TO_{B6}	match	6.6 / **9.4**	3.3	8.6/**11.1**	1.9	6.9 / **8.1**	2.8	3.0 / **5.9**	3.8	6.3 / **8.6**	3.0
	mismatch	2.3 / **2.7**		5.5 / **6.6**		2.6 / **2.6**		1.1 / **1.5**		2.9 / **3.4**	
Average values	match	2.7 / **3.4**	2.0	4.6 / **5.4**	1.6	3.8 / **4.4**	2.2	1.7 / **2.4**	2.1		
	mismatch	1.2 / **1.3**		2.9 / **2.9**		2.0 / **2.2**		0.9 / **1.0**			

[a] Ratio of integrated fluorescence intensity for F_{ds} and F_{ss} of ODN probes with matched or mismatched targets where bold number is calculated accordingly to the ECHO probes[122] and first is calculated by surface area under the curve, [b] Ratio of fluorescence intensity of matched (I_m) and mismatched (I_{mm}) intensity of probes-targets duplexes at $\lambda_{em, max}$.

2.4.3. Fluorescence properties of TO-ODN probes with DNA targets

The varying fluorescence properties of TO are due to rotation around the methine bridge. A lack of intercalation sites in the single strand results in a dark state, whereas in a double stranded helix TO becomes highly fluorescent. This property makes it a great analytical tool for investigation of biophysical processes.

At this point clarification is needed on how the fold increase of fluorescence emission between ss and ds (F_{ds}/F_{ss}) can be calculated. In this work two approaches were used, first calculation by the area under the fluorescence emission spectra (S_{ds}/S_{ss}, Figure 2.6 A) or by intensity at $\lambda_{em,\,max}$ of ds compared to λ_{em} of ss at $\lambda_{em,\,max}$ of ds (I_{ds}/I_{ss}, Figure 2.6 B). Both methods are valid although the second one results in higher values of F_{ds}/F_{ss}. The main difference is that the surface area calculation gives more similar results between samples, whereas the single peak method can give higher differences, secondly values obtained by I_{ds}/I_{ss} are higher than by S_{ds}/S_{ss}. In the literature single wavelength calculations for obtaining F_{ds}/F_{ss} values are performed,[122,127] so throughout discussions both methods will be listed for comparison reasons, where the single wavelength is referred as SW.

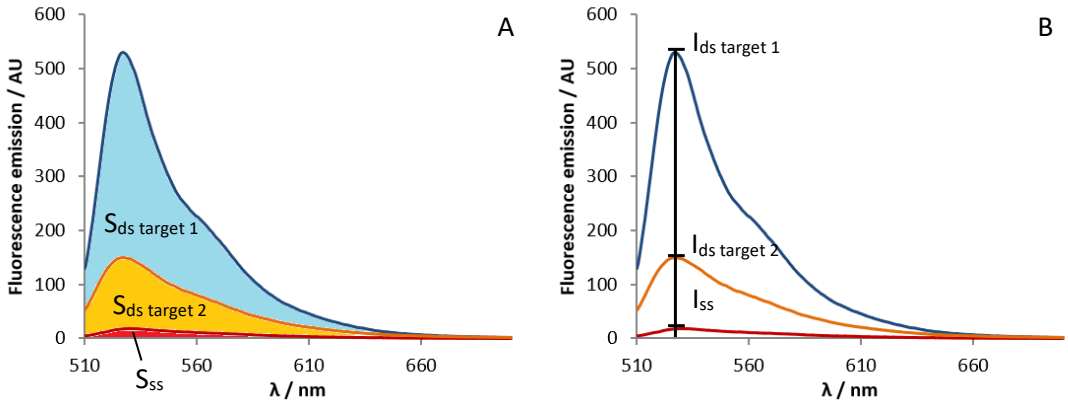


Figure 2.6 Graphical representation of two possible calculation methods for F_{ds}/F_{ss} for two different examples of targets.

Fluorescence emission spectroscopy of the TO-modified ODNs both as single stranded probes, and when paired with their matched and mismatched complementary DNA strands showed clear trends (Table 2.1B, Figure 2.7). Both the position and mode of attachment of the dye strongly influence the fluorescence properties.

In the case of attachment of thiazole orange in the major groove, C6-TO_{B6} and PA-TO_{B6} probes provided good fluorescence increases upon duplex formation, and C6 showed superior properties relative to PA with an average 6.3-fold (SW 8.6) increase in fluorescence upon duplex formation in comparison to 4.3 (SW 5.0) for PA. Attachment *via* the quinoline nitrogen gave small changes of fluorescence when hybridised with matched DNA targets (1.2-fold (SW 1.2) for PA and 2.3-fold (SW 2.5) for the C6 modification). Similarly, fluorescence-based mismatch discrimination of TO-ODNs (1-4) against DNA targets was best achieved by PA and C6 attached to TO_{B6} rather than TO_{Q6} (Table 2.1B). In terms of sequence specificity, the best fluorescence responses were observed for C6-TO_{B6} with matched DNA targets in the order ODN2 (AXA) > ODN3 (CXC) > ODN1 (TXT) > ODN4 (GXG) (8.6, 6.9, 6.6 and 3.0 fold increase respectively, SW 11.1, 8.1, 9.4, 5.9; Figure 2.7). This example shows the differences between calculations, although the change is between pyrimidine bases leaving the general trend consistent.

In contrast, for the AE modification in which the dye is situated in the minor groove, the greatest changes in fluorescence occur for attachment *via* the quinoline moiety (TO_{Q6}), (3.9 fold; SW 4.5), whereas for benzothiazole (TO_{B6}) attachment, the increase was 1.1 fold (SW 1.6) among all sequences. In terms of sequence specificity, the best fluorescence responses for AE-TO_{Q6} with matched DNA targets were in the order ODN2 (AXA) > ODN3 (CXC) > ODN1 (TXT) > ODN4 (GXG) (7.4, 4.1, 2.8 and 1.3 fold increase respectively; SW 8.3, 4.6, 3.8 and 1.3 fold; Table 2.1B, Figure 2.7).

Comparison of the fluorescence properties of these TO-probes with ECHO probes, which gave up to 14.4-fold fluorescence increase against DNA targets when the doubly labelled thymidine modification was in the mixed sequence.[114] Improvement of fluorescence response of already comparable fold increases for obtaining higher response levels and is shown in Paragraph 2.4.8.

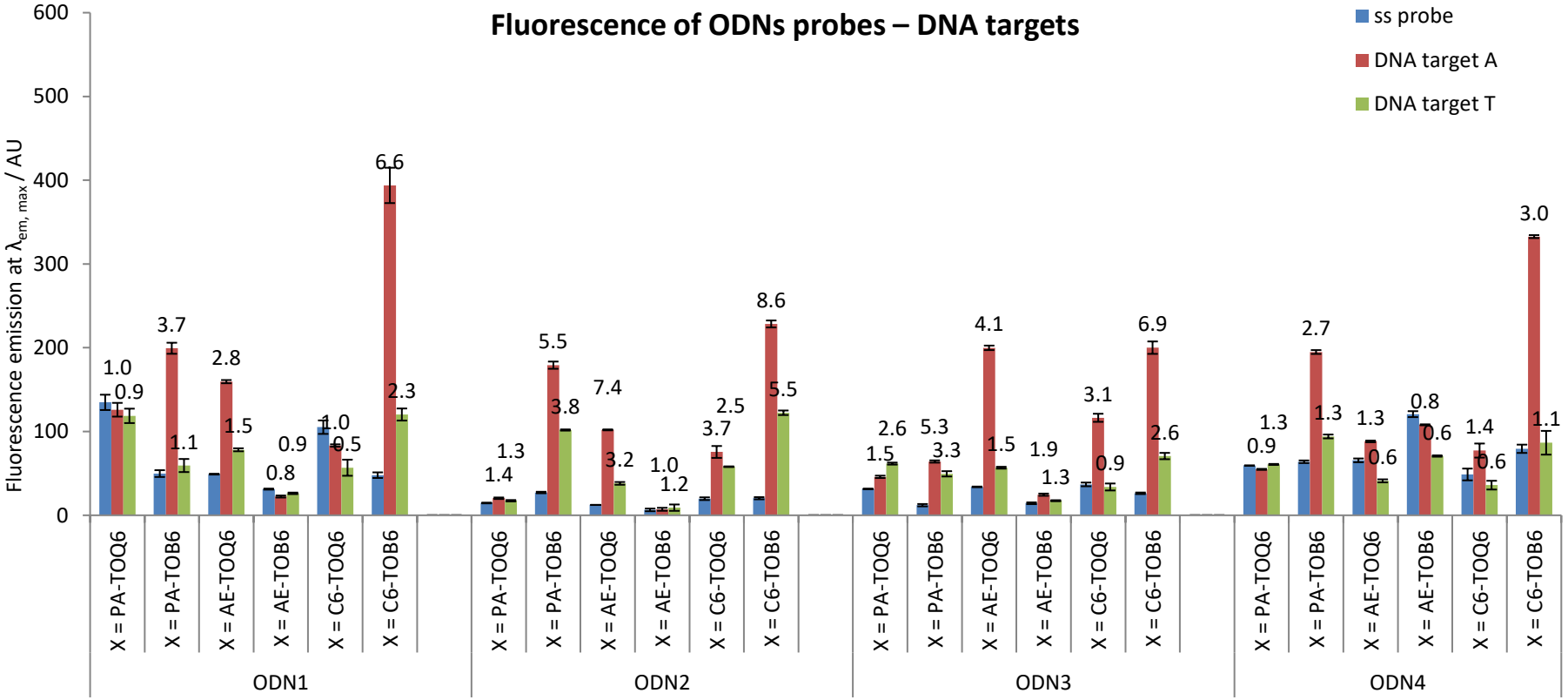


Figure 2.7 Fluorescence emssion intensity at $\lambda_{em,\,max}$ for TO-modified ODNs (ODN1 (5'-GCATXTTACG), ODN2 (5'-GCAAXATACG), ODN3 (5'-GCACXCTACG), ODN4 (5'-GCAGXGTACG)) probes against DNA targets. The base opposite the TO is either A – match or T – mismatch, ss probe – fluorescence emission intensity of single stranded probe, DNA target A/T - fluorescence emission intensity of probe-target duplex, AU - arbitrary units, number above bar = F_{ds}/F_{ss}. Detailed values: see Table 6.13.

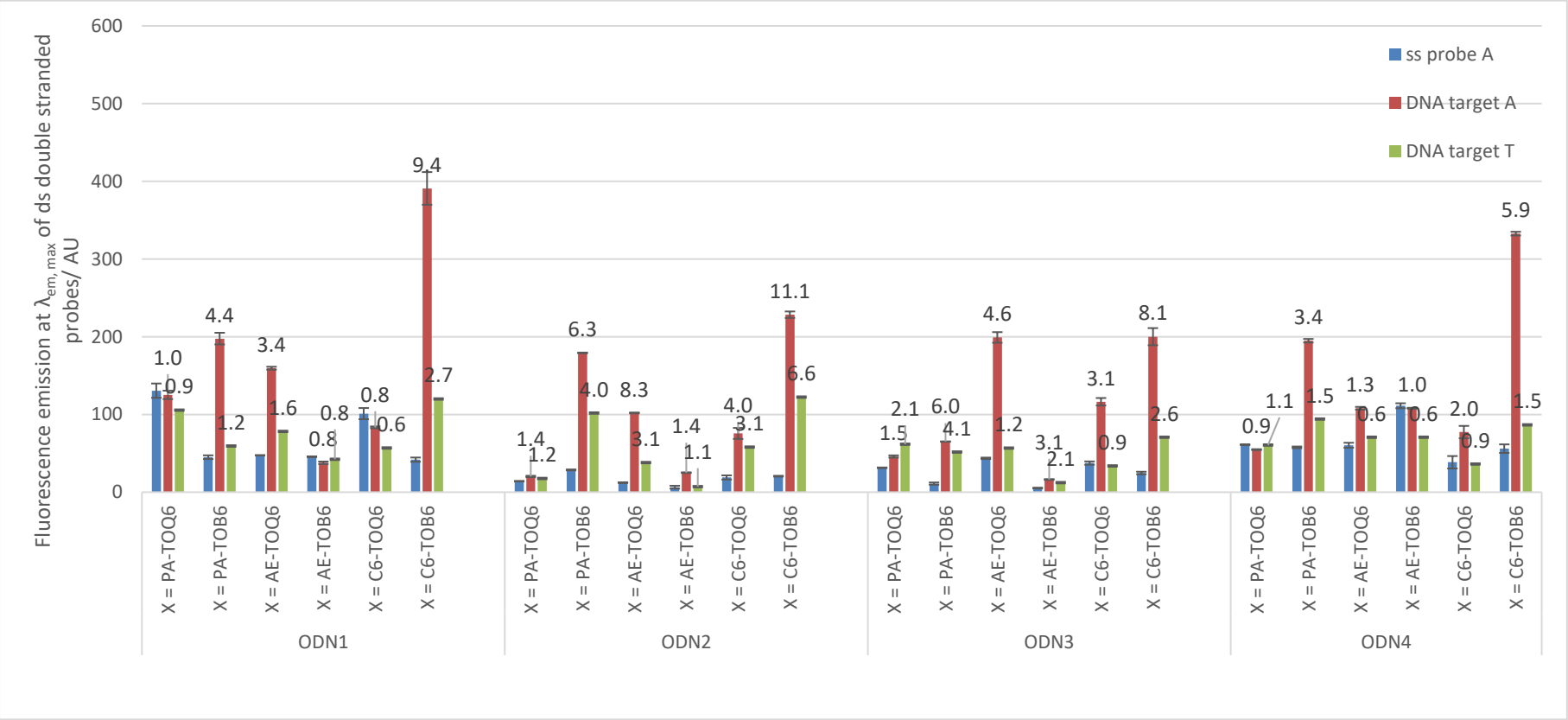


Figure 2.8 Representation of Figure 2.7 with fluorescence emssion intensity of double stranded probes at $\lambda_{em, max}$ and fluorescence emssion intensity of single stranded probe at $\lambda_{em, max}$ of double stranded probes. Detailed values: see Table 6.14. F_{ds}/F_{ss} calculated at $\lambda_{em, max}$ of double stranded probe (single wavelength), accordingly to ECHO probes studies.[122]

2.4.4. Fluorescence and duplex stability evaluation of ODN4 with guanine and inosine as neighbouring bases

In terms of base stacking environment, the weakest fluorescence enhancement was observed with TO adjacent to guanine bases (ODN4, 5'-GCAG**X**GTACG) as previously reported.[165,170] The reason for this is not because the TO moiety is less fluorescent (strongly quenched) when bounded to the target, but rather that the single stranded probe is more fluorescent (Figure 2.7, Table 6.13, Table 6.17). This could be caused by strong single stranded stacking between TO and guanine bases, or as suggested by Okamoto *et al.* due to self-dimerization of the probes.[165] Attempts to reduce single stranded fluorescence (F_{ss}) of ODN4 were previously made. Guanine was replaced by inosine (ODN4', 5'-GCA**I**X**I**TACG) which should reduce the binding strength of the natural G:C base pairs due to reduced hydrogen bonding (Figure 2.9) thus reducing unwanted interactions in a single stranded state of the probe, this gave mixed results.[171,152]

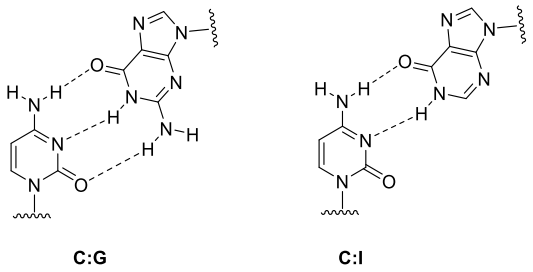


Figure 2.9 Cytosine:guanine (C:G) and cytosine-inosine (C:I) base paring motifs.

Probes with the C6-TO_{B6} modification (Table 6.1) were hybridized with DNA and RNA targets. As shown previously (previous paragraph), benzothiazole linked TO gave good fluorescence response where quinoline attached TO gave little to no response (Figure 2.10). Incorporation of inosine next to the modification in probe sequence resulted in decreased F_{ss} , at the same time increasing the F_{ds}/F_{ss} from 3.0 fold (SW 5.9) for guanine (ODN4) to 6.2 fold (SW 8.0) for inosine (ODN4') containing sequence against DNA targets. Unfortunately sequence specificity

and duplex stabilisation were compromised. ODN4' probes gave fluorescence signal against ODN1 match DNA target (Figure 2.10) indicating nonspecific binding properties of inosine modification which wasn't observed for any other sequences. Secondly general increase of thermal stability of TO-ODN probes was lost (Figure 2.12), suggesting reduction of hydrogen bonding of I:C base pair resulting in decrease of duplex stability[171] which could not be regained by incorporation of TO.

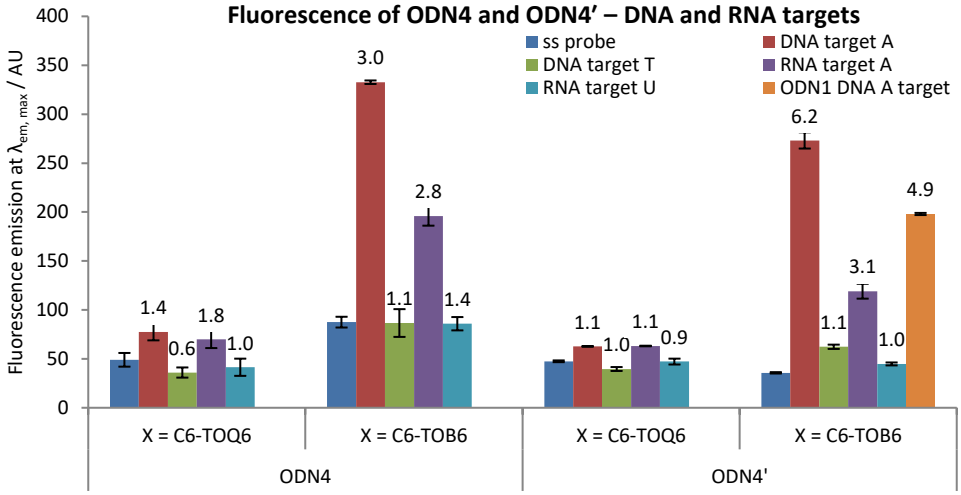


Figure 2.10 Comparison of fluorescence emssion intensity at $\lambda_{em,\,max}$ data for ODN4 (5'-GCA**G**X**G**TACG) and ODN4' (5'-GCA**I**X**I**TACG) with $TO_{B/Q6}$ probes against DNA and RNA targets. The base opposite the TO is either A – match or T/U – mismatch, ss probe – fluorescence emission intensity of single stranded probe, DNA target A/T and RNA target A/U - fluorescence emission intensity of probe-target duplex, AU - arbitrary units, number above bar = F_{ds}/F_{ss}. Detailed values: see Table 6.13 and Table 6.17.

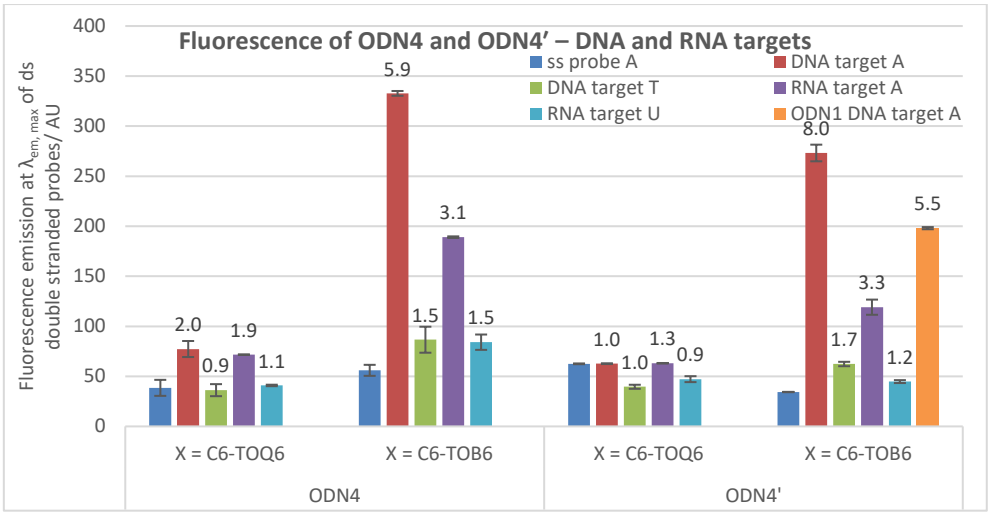


Figure 2.11 Representation of Figure 2.10 with fluorescence emssion intensity of double stranded probes at $\lambda_{em, max}$ and fluorescence emssion intensity of single stranded probe at $\lambda_{em, max}$ of double stranded probes. Detailed values: see Table 6.15 and Table 6.16. F_{ds}/F_{ss} calculated at $\lambda_{em, max}$ of double stranded probe (single wavelength), accordingly to ECHO probes studies.[122]

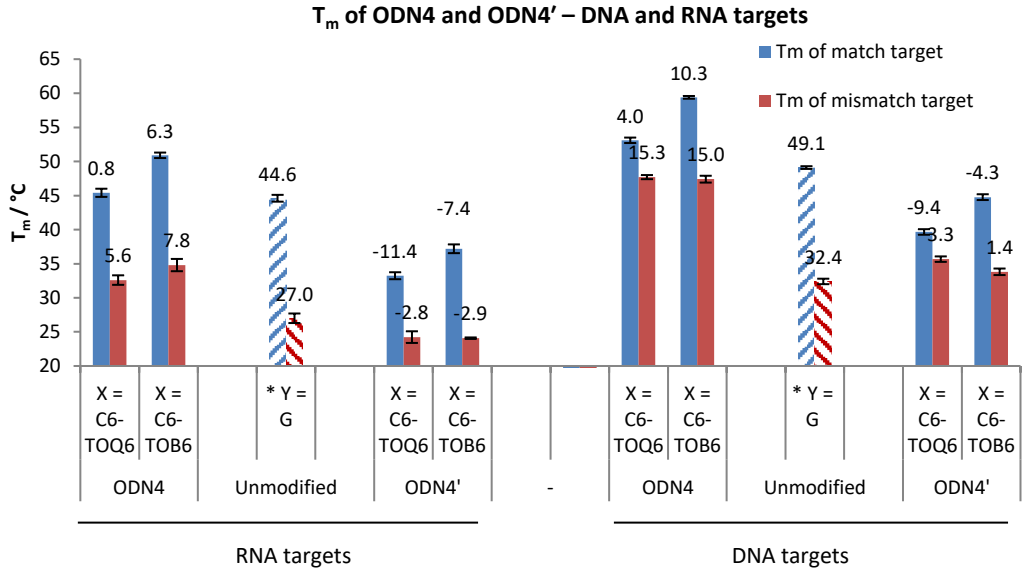


Figure 2.12 UV melting data for ODN4 (5'-GCA**G**X**G**TACG) and ODN4' (5'-GCA**I**X**I**TACG) with $TO_{B/Q6}$ probes against DNA and RNA targets. The base opposite the TO is either A – match or T/U – mismatch, number above bar = ΔT_m to unmodified target, * = T_m value of unmodified matched and mismatched duplexes. Detailed values: see Table 6.7 and Table 6.9.

2.4.5. Duplex stabilisation by 2′-*O*-methyl–RNA TO (2′-OMe–(ORNs)) probes with DNA and RNA targets

An important application of fluorogenic oligonucleotide probes is detection of DNA and RNA in both live and fixed cells.[122] A common approach is to use 2′-*O*-methyl oligoribonucleotide probes (2′-OMe-ORNs, Figure 2.13) instead of DNA probes, as the former are much more stable in live cells in presence of nucleases.[172] This concept where TO was used as a fluorogenic dye was previously used for live RNA imaging in cells[122] where 2′-*O*-methyl probes showed superior stability in comparison to DNA equivalent when exposed to the S1 endonuclease[173,174] and exonuclease I[175] (up to 12 h for both nucleases) which degrades single stranded DNA or RNA to 5′-mononuclotides. Hence there is a clear opportunity to use the 2′-OMe-RNA modification with TO probes.

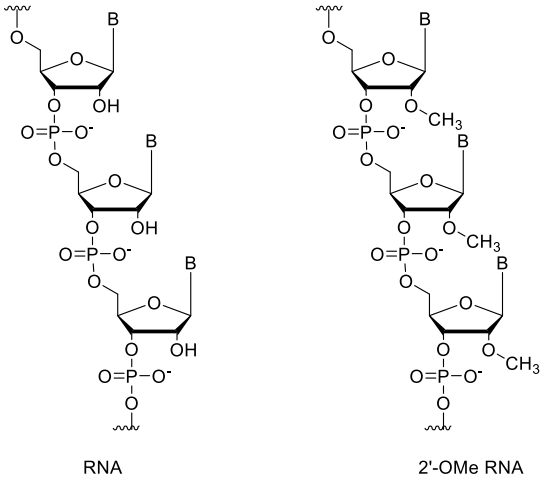


Figure 2.13 Structural differences between natural RNA and OMe modified RNA.

In order to explore the effects of the 2′-*O*-methyl modification on the properties of TO probes, 2′-OMe oligonucleotide probes (2′-OMe-(ORN1-4)) with the same sequences as ODN1-4, containing AE or C6 modifications (Figure 2.1) were synthesized and labelled with TO_{Q6} and TO_{B6}: the PA monomer wasn't used due to unfavourable fluorescence properties in comparison to the C6 modification. These probes were tested against both DNA and RNA targets (Table 2.2).

Increases in melting temperature were greater against DNA than RNA on average by 6.2 °C for all modifications and sequences. In the major groove TO_{B6} performed better than TO_{Q6} in terms of stabilisation (+10.9 °C and +6.4 °C against DNA targets and +4.2 °C and 1.5 °C against RNA targets; Table 2.2, Figure 2.17), whereas in the minor groove both TO derivatives preformed similarly (+12.0 °C and 12.9 °C for DNA targets and +6.1 °C and +5.7 °C against RNA targets for TO_{Q6} and TO_{B6} respectively). ΔT_m values were always higher for AE-TO (TO_B and TO_Q) relative to C6-TO_{Q6} with both DNA and RNA targets. Surprisingly AE-TO_{B6} gave higher or similar increases of T_m in comparison to TO_{Q6} and in all cases was superior to C6-TO_{B6}. This data shows that the minor groove (AE) modification gave better results than the major groove (C6), at the same time showing less specificity for TO derivative mode of attachment in terms of increase of T_m than was previously observed for the DNA version of those probes (Table 2.1A).

The highest increases in T_m were observed for 2'-OMe-(ORN1) with DNA targets (AE-TO_{Q6} +18.0 °C and AE-TO_{B6} +19.3 °C) followed by, in decreased order of stabilisation, by 2'-OMe-(ORN3), 2'-OMe-(ORN2) and 2'-OMe-(ORN4) (Table 2.2) for the AE modification. On average among all sequences 2'-OMe-(ORN1) gave the highest increases for both modifications against DNA (ΔT_m = 18.7 for AE and 12.0 °C for C6) and RNA targets (ΔT_m = 7.8 for AE and 6.1 °C for C6).

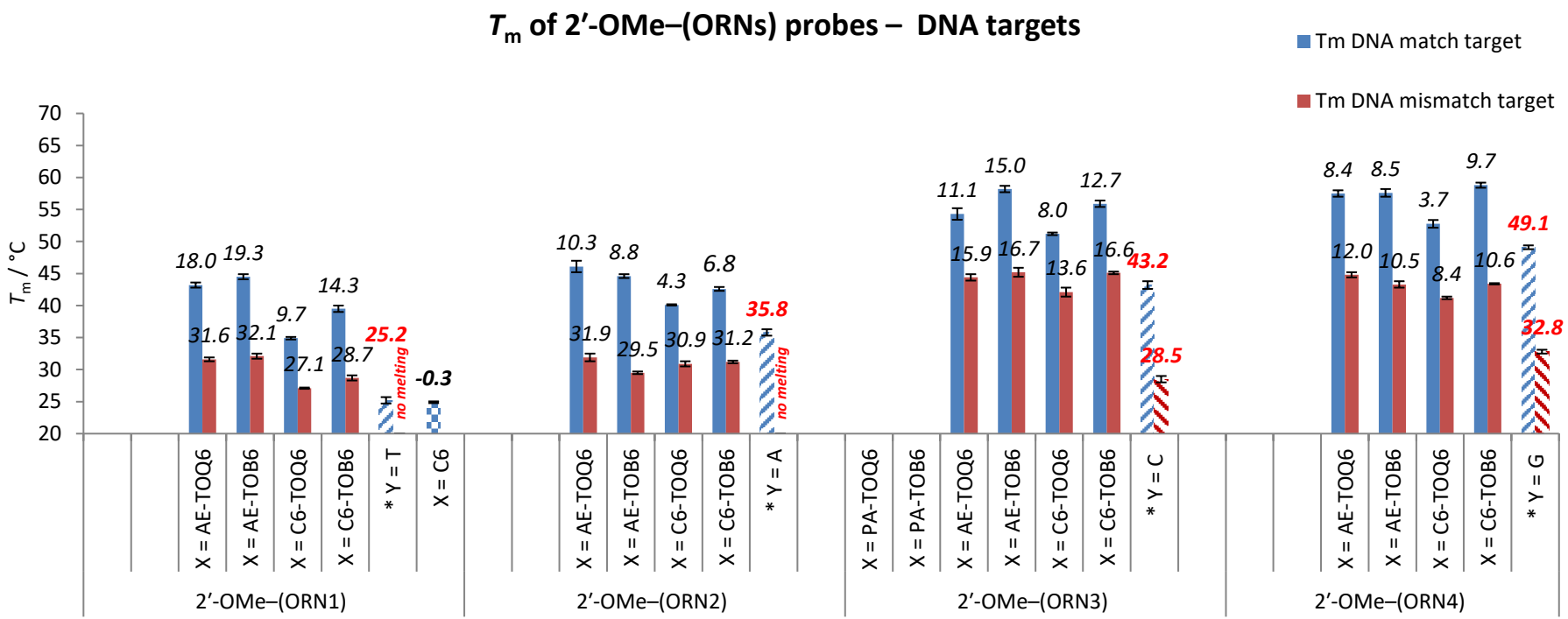


Figure 2.14 UV melting data for 2′-OMe–(ORNs) (2′-OMe–(ORN1) (5′-GCAUXUUACG), 2′-OMe–(ORN2) (5′-GCAAXAUACG), 2′-OMe–(ORN3) (5′-GCACXCUACG), 2′-OMe–(ORN4) (5′-GCAGXGUACG)) probes against DNA targets. The base opposite the TO is either A – match or T – mismatch, number above bar = ΔT_m to unmodified target, * = T_m value of unmodified matched and mismatched duplexes. Detailed values: see Table 6.8.

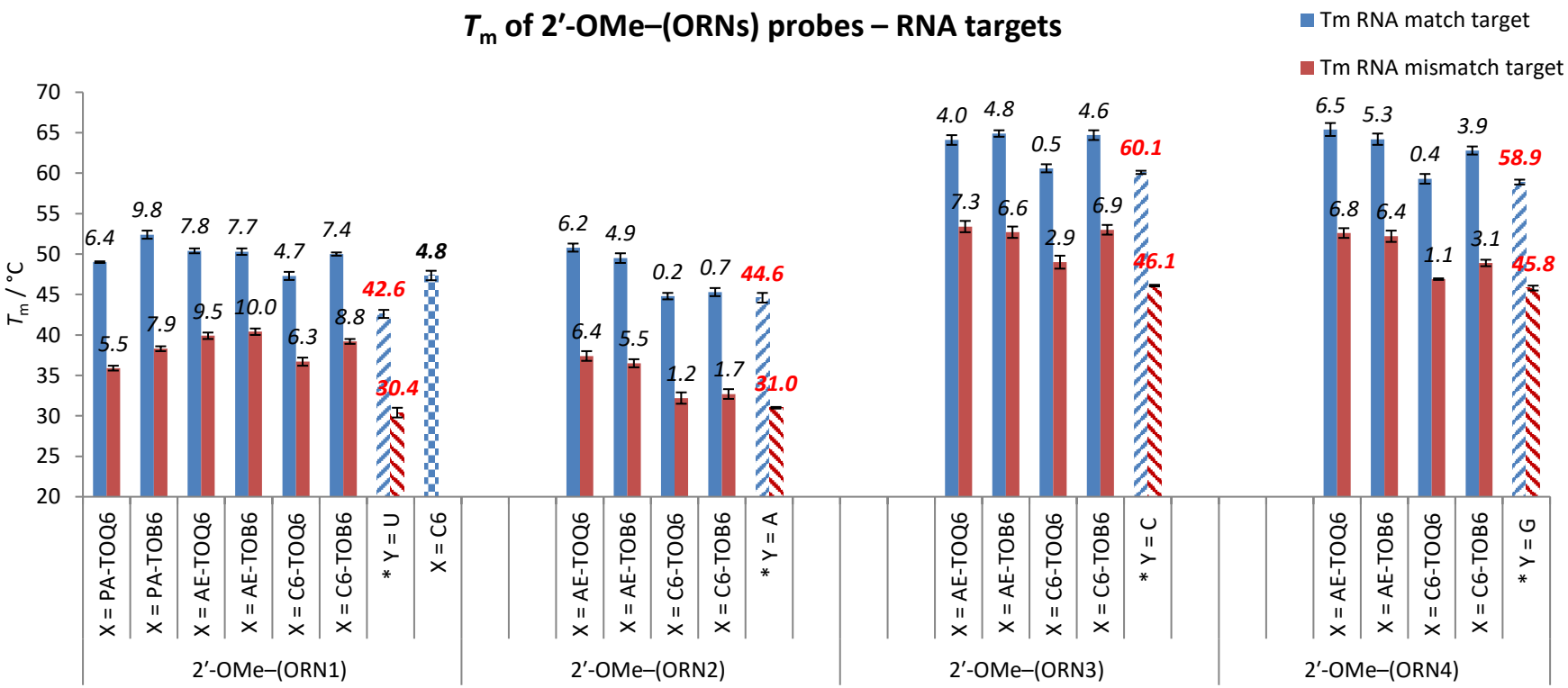


Figure 2.15 UV melting data for 2′-OMe–(ORNs) (2′-OMe–(ORN1) (5′-GCAUXUUACG), 2′-OMe–(ORN2) (5′-GCAAXAUACG), 2′-OMe–(ORN3) (5′-GCACXCUACG), 2′-OMe–(ORN4) (5′-GCAGXGUACG)) probes against RNA targets. The base opposite the TO is either A – match or U – mismatch, number above bar = ΔT_m to unmodified target, * = T_m value of unmodified matched and mismatched duplexes. Detailed values: see Table 6.10.

Interestingly, although generally lower increase of T_m for RNA targets were observed as a result of the presence of TO, the T_m values were higher than with DNA targets. This is explained by the preference of 2′-OMe modification in probes sequence resulting forming A type duplex conformation which is also preferred by pure RNA strands.[176] Attaining this favourable helical structure results in more stable duplexes.

Importantly the ability of 2′-OMe-(ORN1-4) to discriminate matched from mismatched DNA targets was preserved (mismatch positioned opposite to TO), and on average ΔT_m was improved slightly in comparison to ODNs probes.

Table 2.2 Changes in melting temperature (ΔT_m) for ODNs against RNA targets and 2′-OMe–(ORNs) against DNA and RNA targets. Conditions: see Table 2.1.

Probe	Target (matched)	X = AE		X = C6		X = T/U
		TO_{Q6}	TO_{B6}	TO_{Q6}	TO_{B6}	-
		ΔT_m[a]				T_m
ODN1	RNA	5.7	-[b]	3.3	8.2	35.9
ODN2		-[b]	-[b]	1.3	5.2	32.0
ODN3		-[b]	-[b]	0.6	5.9	48.9
ODN4		-[b]	-[b]	0.8	6.3	44.6
2′-OMe–(ORN1) 2′-OMe–(5′-GCAU**X**UUACG)	RNA	7.8	7.7	4.7	7.4	42.6
	DNA	18.0	19.3	9.7	14.3	25.2
2′-OMe–(ORN2) 2′-OMe–(5′-GCAA**X**AUACG)	RNA	6.2	4.9	0.2	0.7	44.6
	DNA	10.3	8.8	4.3	6.8	35.8
2′-OMe–(ORN3) 2′-OMe–(5′-GCAC**X**CUACG)	RNA	4.0	4.8	0.5	4.6	60.1
	DNA	11.1	15.0	8.0	12.7	43.2
2′-OMe–(ORN4) 2′-OMe–(5′-GCAG**X**GUACG)	RNA	6.5	5.3	0.4	3.9	58.9
	DNA	8.4	8.5	3.7	9.7	49.1

[a]- in comparison to the unmodified duplex, [b]- no data obtained

2.4.6. Mismatch discrimination by 2′-*O*-methyl–RNA TO probes at positions at various positions.

To evaluate the effect of mismatch position on ΔT_m five different DNA hybrids were designed to give a single mismatch against TO-2′-OMe–(ORN3) as this sequence has shown both good thermal stabilisation and good fluorescence responses (Table 2.2 and Table 2.3). Placement of mismatch was in a various positions from -2 (2 bases to the 5′-side of TO) to +2 (2 bases to the 3′-side of TO) (Figure 2.16, Table 6.11) in the target strand. For both AE-TO_{Q6} and C6-TO_{B6}

mismatch discrimination at positions -1 and +1 was excellent (ΔT_m > 20 °C) and far superior to the case when the mismatch was directly opposite TO (ΔT_m = 9-12 °C). This position-dependence of mismatch discrimination is a crucial factor when designing TO probes to detect mutations or SNPs. Is worth noting that a similar study by Okamoto *et al.* on fluorescence effects by introduction of locked nucleic acid (LNA) modification into the probe sequence for ECHO probes system. Unfavourable fluorescence enhancement was observed when LNA modification was placed in close proximity of the TO-containing modification.[177]

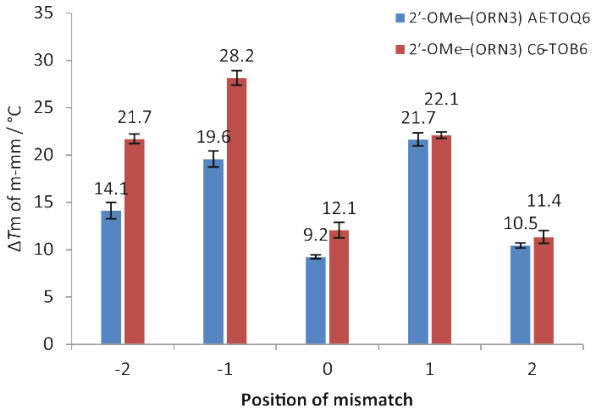


Figure 2.16 UV melting for 2′-OMe–(ORN3) (2′-OMe–(5′-GCACXCUACG)) TO-modified oligonucleotides probes against various DNA targets. Position of mismatch refers to a mismatch in the target strand counting from the TO-modified base, e.g.: position "0" is directly opposite modification and "-2" is two nucleobases towards 5′ end of the probe sequence. Number above bar = ΔT_m to match target, T_m for fully matched targets 2′-OMe–(ORN3) AE-TO_{Q6}: 51.7 °C; 2′-OMe–(ORN3) C6-TO_{B6}: 52.5 °C, all samples measured at 1.0 µM with 1.1 eq of target. Mismatch sequences see: Table 6.11, ODN3 – targets from -2 to +2.

2.4.7. Duplex stabilisation by 2′-*O*-methyl–RNA probes (2′-OMe–ORN) with double AE-TO against DNA and RNA targets

The very high increases in duplex stability resulting from the TO-AE modification against DNA and RNA targets are remarkable for a single intercalating fluorophore. To further evaluate the ability to increase duplex stability, a double labelled TO probe system was investigated in two sequences 5′-GCAXUUXACG (ODN1; 2xTO_{Q6} #1) and 5′-GCAUUXXACG-propanol (ODN1; 2xTO_{Q6} #2) where X = AE-TO_{Q6}. Against DNA targets the thermal stabilisation provided by double incorporation was better when the AE modifications were separated by two uridines (ΔT_m = +29.1 °C, Figure 2.17) than for close proximity (ΔT_m = +21.1 °C). Similarly, against RNA

targets the double-separated design gave a better increase of T_m (ΔT_m = +14.6 °C against +10.5 °C, Figure 2.17). In both cases double TO-incorporation gave higher increases than single incorporation. Mismatch discrimination was preserved but as expected differences were lower than in the case of natural duplexes. Probes of this design with multiple TO insertions have great potential in duplex stabilisation and are simple to synthesize.

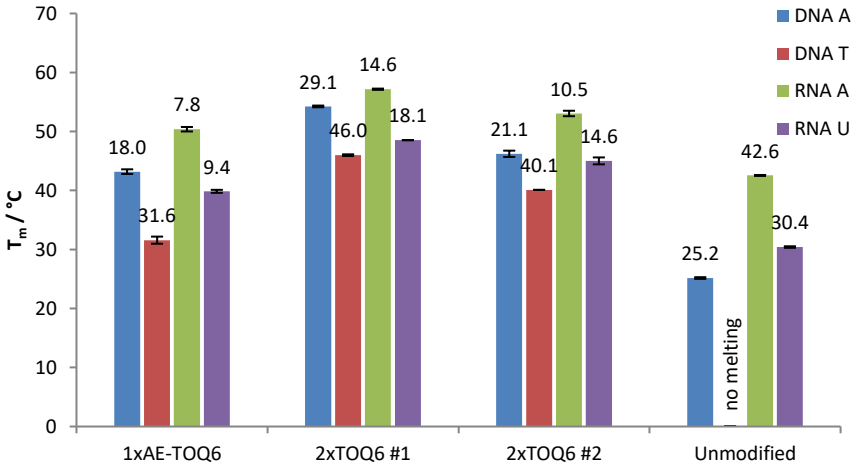


Figure 2.17 UV melting data for 2'-OMe–(ORNs) (2'-OMe–(ORN1) (5'-GCAUXUUACG)2'-OMe–(ORN1) (5'-GCAUXXUACG) #2 and 2'-OMe–(ORN1) (5'-GCAXUUXACG) #1 where X = AE-TO_{Q6}) probes against DNA and RNA targets. The base opposite the TO is either A – match or T/U – mismatch, number above bar = ΔT_m to unmodified target or in case of no reference actual melting temerature, * = T_m value of unmodified matched and mismatched duplexes. Detailed values: see Table 6.8 and Table 6.10.

2.4.8. Fluorescence properties of 2′-OMe–ORN probes against DNA and RNA targets

The 2′-OMe–(ORN1-4) series of probes show great potential as fluorogenic sensors of complementary DNA and RNA. The fluorescence enhancement upon duplex formation for AE-TO_{Q6} and C6-TO_{B6} is excellent and is far superior to the equivalent deoxyribose versions (Table 2.1A). The probes showed the same preference for the dye attachment as the DNA probes and the most impressive fluorescence enhancement (F_{ds}/F_{ss}) was observed for AE-TO_{Q6} and C6-TO_{B6} against DNA targets. Increase of duplex fluorescence was low when the dye was attached in the opposite configuration (AE-TO_{B6} or C6-TO_{Q6}, Figure 2.20, Table 2.3), following the trend for the ODNs versions of the probes.

Surprisingly in one special case (AE-TO_{B6} in 2′-OMe-ORN4) the single stranded oligonucleotide was four times as fluorescent as its duplex with complementary DNA, and twice as fluorescent as its duplex with RNA (Table 6.16 and Table 6.18). This sequence 2′-OMe–(5′-GCAGXGUACG) places the thiazole orange between guanine bases and it is possible that the stacking interactions are strong enough to allow the TO molecule to adopt a planar fluorescent

Table 2.3 Changes in fluorescence emission (F_{ds}/F_{ss}) for 2′-OMe–(ORN1-4) with DNA targets before and after formation of matched and mismatched duplexes. Conditions: see Table 2.1. In this study F_{ds}/F_{ss} was calculated on the basis of area under the fluorescence emission spectra from 510 nm to 650 nm, or (bold number) calculated accordingly to the ECHO probes.[122]

Sequence		2′-OMe–(ORN1) rGCA**U**X**U**UACG		2′-OMe–(ORN2) rGCA**A**X**A**UACG		2′-OMe–(ORN3) rGCA**C**X**C**UACG		2′-OMe–(ORN4) rGCA**G**X**G**UACG		Average F_{ds}/F_{ss}	Average I_m/I_{mm}
X =	duplex	F_{ds}/F_{ss}[a]	I_m/I_{mm}[b]	F_{ds}/F_{ss}[a]	I_m/I_{mm}[b]	F_{ds}/F_{ss}[a]	I_m/I_{mm}[b]	F_{ds}/F_{ss}[a]	I_m/I_{mm}[b]		
AE-TO_{Q6}	match	21.5 / **34.5**	2.8	7.6 / **11.1**	2.6	33.9 / **49.4**	2.2	3.1 / **4.6**	2.1	16.5 / **24.9**	2.4
	mismatch	8.9 / **11.6**		3.0 / **3.9**		17.0 / **20.5**		1.4 / **1.9**		7.6 / **9.5**	
AE-TO_{B6}	match	1.3 / **1.3**	0.8	0.9 / **0.8**	0.4	3.5 / **3.6**	1.3	0.2 / **0.2**	0.7	1.5 / **1.5**	0.8
	mismatch	1.6 / **1.5**		1.6 / **1.7**		2.6 / **2.7**		0.3/ **0.3**		1.5 / **1.6**	
C6-TO_{Q6}	match	4.2 / **4.0**	2.3	9.1/ **10.5**	3.4	6.4 / **6.4**	2.9	1.0 / **1.0**	1.3	5.2 / **5.5**	2.5
	mismatch	1.7 / **1.5**		2.8 / **3.0**		2.0 / **1.9**		0.7 / **0.8**		1.8 / **1.8**	
C6-TO_{B6}	match	14.6 / **19.8**	6.0	17.5 / **21.0**	1.9	17.2 / **20.9**	3.8	3.7 / **5.4**	3.9	13.2 / **16.8**	3.9
	mismatch	2.7 / **3.2**		8.6 /**11.4**		3.9 / **4.2**		1.2 / **1.3**		4.1 / **5.0**	
Average values	match	10.4/ **14.9**	2.4	8.8 / **10.9**	1.7	15.2/ **20.1**	2.1	2.0 / **2.8**	1.6		
	mismatch	3.7 / **4.5**		4.0 / **5.0**		6.4/ **7.3**		0.9 / **1.1**			

conformation (fixed rotation around methine bridge). The same effect is observed with the equivalent DNA probe (AE-TO_{B6} in ODN4) but in that case differences are minor (Figure 2.18).

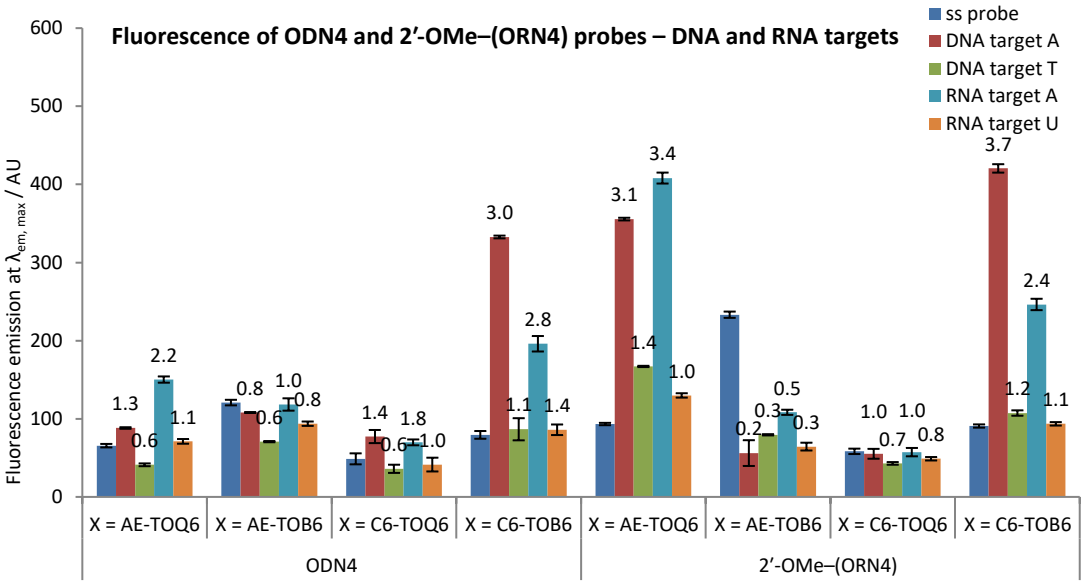


Figure 2.18 Fluorescence emssion intensity at $\lambda_{em,\ max}$ for TO-modified ODN4 (5'-GCA**G**X**G**TACG) and 2'-OMe–(ORN4) (5'-GCA**G**X**G**UACG) probes against DNA and RNA targets. The base opposite the TO is either A – match or T/U – mismatch, ss probe – fluorescence emission intensity of single stranded probe, DNA target A/T and RNA target A/U - fluorescence emission intensity of probe-target duplex, AU - arbitrary units, number above bar = F_{ds}/F_{ss}. Detailed values: see Table 6.13, Table 6.16, Table 6.17 and Table 6.18.

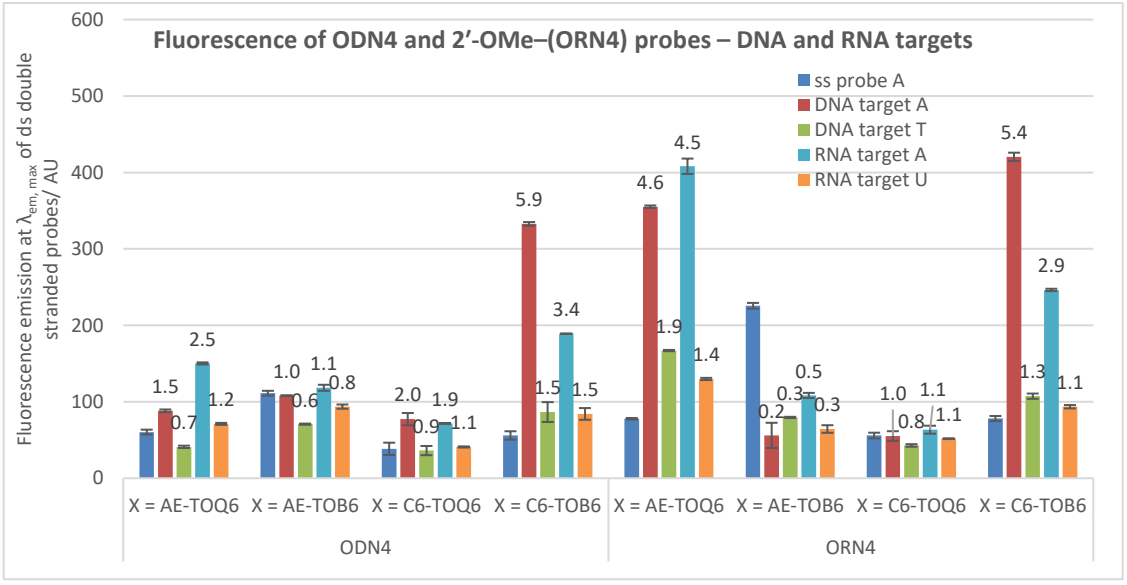


Figure 2.19 Representation of Figure 2.18 with fluorescence emssion intensity of double stranded probes at $\lambda_{em,\ max}$ and fluorescence emssion intensity of single stranded probe at $\lambda_{em,\ max}$ of double stranded probes. Detailed values: see Table 6.14, Table 6.15, Table 6.19 and

Table 6.20. F_{ds}/F_{ss} calculated at $\lambda_{em,\ max}$ of double stranded probe (single wavelength), accordingly to ECHO probes studies.[122]

It is unclear why in this specific example the 2'-*O*-methyl sugars promote fluorescence in the single strand whereas in other cases they suppress it. Nevertheless, this shows the need for careful evaluation of different modes of attachment between TO and DNA/RNA.

The C6-TO_{B6} modification in 2'-O-methyl RNA gave good F_{ds}/F_{ss} ratios with DNA targets, for example 2'-OMe–(ORN3) and 2'-OMe–(ORN1) gave fluorescence enhancements of 17-fold and 15-fold respectively (Figure 2.20 and Figure 6.9, SW 21 and 22-fold). Smaller increases were observed with RNA targets; comparing F_{ds}/F_{ss} of probes against DNA and RNA targets the AE modification gave higher value (2.5-fold, SW 3.0) than the C6 modification (1.7 fold, SW 1.7-fold). In these calculations the 2'-OMe–(ORN4) sequence was omitted as its fluorescence properties are unfavourable and need more careful evaluation. With complementary DNA targets, the AE-TO_{Q6} modification attached to 2'-OMe–(ORN3) gave an impressive 34-fold fluorescence enhancement (Figure 2.20, SW 49-fold), and when attached to 2'-OMe–(ORN1) the enhancement was 22-fold (SW 35-fold).

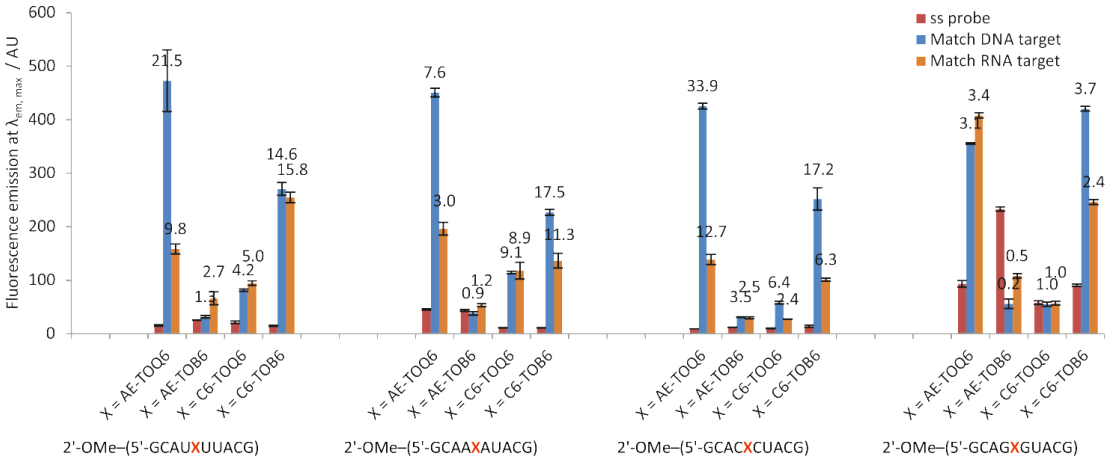


Figure 2.20 Fluorescence emission intensities at $\lambda_{em, max}$ of a single stranded 2'-OMe–(ORN1-4) probes with DNA and RNA matched targets duplexes. Conditions: see Table 2.1A

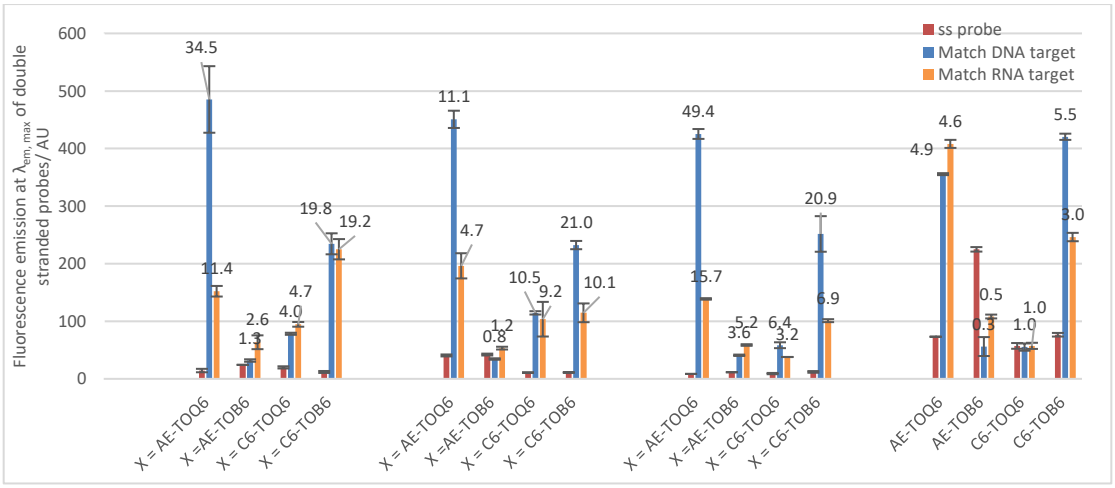


Figure 2.21 Representation of Figure 2.25 with fluorescence emssion intensity of double stranded probes at $\lambda_{em, max}$ and fluorescence emssion intensity of single stranded probe at $\lambda_{em, max}$ of double stranded probes. Detailed values: see Table 6.19 and

Table 6.20. F_{ds}/F_{ss} calculated at $\lambda_{em, max}$ of double stranded probe (single wavelength), accordingly to ECHO probes studies.[122]

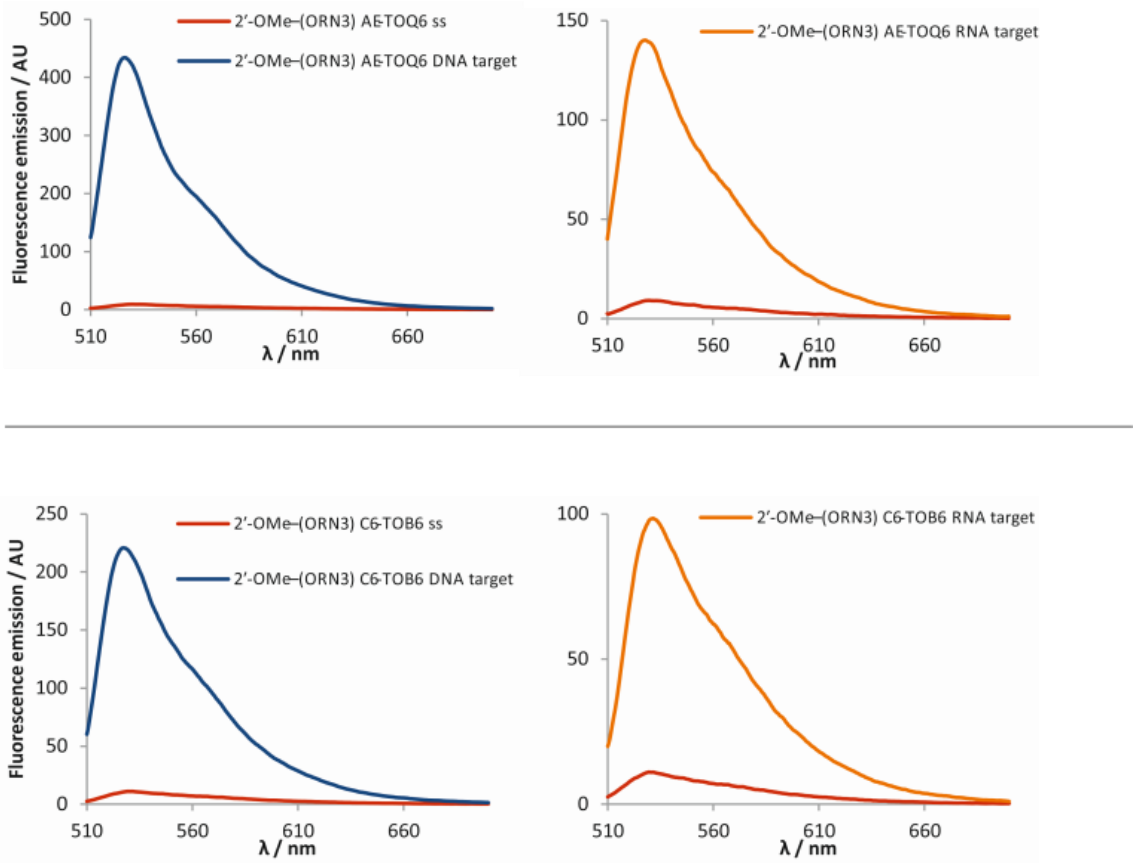


Figure 2.22 Examples of fluorescence emission spectra of single stranded (ss) probes and DNA or RNA matched target duplexes. Probes: 2′-OMe–(ORN3) (5′-GCAC**X**C**X**CUACG) were X = AE-TO_{Q6} or C6-TO_{B6} with structures of

modification and correct TO isomer for optimum fluorescence. Examples of F_{ds}/F_{ss} are calculated at $\lambda_{em,\,max}$ of ds. Conditions: see Table 2.1

Interestingly no simple correlation between increase in T_m and increase in fluorescence response could be found, best shown by 2′-OMe–(ORN1) with the AE modification. In this case the high ΔT_m for both AE-TO_{Q6} and AE-TO_{B6} against DNA targets (+18.0 and +19.3 °C) gives one of the highest fluorescence responses (21.5-fold increase, SW 34.5-fold) only for thiazole orange attached by the quinoline, where linkage of TO by benzothiazole gives a negligible fluorescence enhancement (1.6 fold). This lack of correlation can be observed in all sequences against both DNA and RNA targets.

For double TO-labelled probes, F_{ds}/F_{ss} of 2×AE-TO_{Q6} 2′-OMe–(ORN1) when TO modifications were separated by two uridines (2xTO_{Q6} #1) the fluorescence response was reduced to 14-fold (Table 6.16, or if calculated accordingly to ECHO probes 32-fold) and for close proximity modifications (2xTO_{Q6} #2) it was just 5-fold (if calculated accordingly to ECHO probes 9-fold, Table 6.19). This may be due to mutual quenching of TO dyes in the double strand.[130] However, so far only a few example of a dual-labelled TO probes have been studied, and it may be possible in the future to optimise the design to improve their fluorescence properties.

2.4.9. Quantum yield measurement of 2′-OMe–ORN probes against DNA and RNA targets

This higher fluorescence enhancement with the 2′-OMe RNA probes is in part due to the low background fluorescence observed in the single stranded 2′-OMe RNA TO-oligonucleotides (Φ = 0.013-0.022, 2′-OMe–(ORN1) and 2′-OMe–(ORN3)), in comparison to equivalent ODN probes (Φ = 0.050-0.089, Table 2.4), as well as the increased F_{ds} especially for AE modifications with DNA targets. Fluorescence quantum yields for AE-TO_{Q6} on 2′-OMe–(ORN3) and 2′-OMe–(ORN1) were 0.318 and 0.580 respectively against DNA targets (Table 2.4),[178] which places this

easy to synthesize design on par with other well established TO probe systems such FIT and ECHO probes, both in terms of fluorescence increase (F_{ds}/F_{ss}) and quantum yields.[122, 159]

Table 2.4 Fluorescence quantum yields of ODN1 (5′-GCA**T**<u>**X**</u>**T**TACG), ODN3 (5′-GCA**C**<u>**X**</u>**C**TACG), 2′-OMe–(ORN1) (2′-OMe–(5′-GCA**U**<u>**X**</u>**U**UACG)) and 2′-OMe–(ORN3) (2′-OMe–(5′-GCA**C**<u>**X**</u>**C**UACG)) oligonucleotides probes with matched DNA and RNA targets. Samples were measured at λ_{ex} = 484 nm, λ_{em} = 490 nm, slit ex slit = 3 nm, slit em = 3 nm, 20°C. Reference dye: fluorescein in 0.1 M NaOH. (6.7)

		Φ				
		ss	DNA	RNA	DNA/ss	RNA/ss
ODN1	AE-TO_{Q6}	0.089	0.279	0.278	3.1	3.1
	AE-TO_{B6}	0.054	0.067	0.172	1.2	3.2
	C6-TO_{Q6}	0.115	0.118	0.208	1.0	1.8
	C6-TO_{B6}	0.056	0.469	0.477	8.4	8.5
2′-OMe–(ORN1)	AE-TO_{Q6}	0.016	0.580	0.215	36.3	13.4
	AE-TO_{B6}	0.035	0.065	0.113	1.9	3.2
	C6-TO_{Q6}	0.023	0.152	0.147	6.6	6.4
	C6-TO_{B6}	0.019	0.493	0.477	25.9	25.1
ODN3	AE-TO_{Q6}	0.051	0.061	0.043	1.2	0.8
	AE-TO_{B6}	0.034	0.053	0.062	1.6	1.8
	C6-TO_{Q6}	0.036	0.045	0.050	1.3	1.4
	C6-TO_{B6}	0.050	0.073	0.063	1.5	1.3
2′-OMe–(ORN3)	AE-TO_{Q6}	0.013	0.318	0.162	24.6	12.5
	AE-TO_{B6}	0.013	0.086	0.035	6.9	2.7
	C6-TO_{Q6}	0.014	0.096	0.044	7.1	3.1
	C6-TO_{B6}	0.022	0.382	0.190	17.3	8.6

2.4.9.1. Mismatch discrimination by fluorescence change for 2′-OMe–ORN probes against DNA and RNA targets

If a mispaired base is positioned opposite to TO, discrimination on the basis of fluorescence intensity ($I_{matched}/I_{mismatched}$ at $\lambda_{em,\ max}$) of 2′-*O*-methyl RNA TO probes against DNA targets is significant (2′-OMe–(ORN1) and 2′-OMe–(ORN3) with C6-TO_{B6}, 6.0 and 3.8-fold differences respectively) and better than DNA equivalents (for ODN1 and ODN3 differences were 3.3 and 2.8-fold). As mentioned before varying the mismatch position relative to thiazole orange for 2′-OMe–(ORN3) in UV melting experiment gave excellent results (Paragraph 2.4.6). For this reason, fluorescence discrimination was also performed. TO probes with C6-TO_{B6} and AE-TO_{Q6}

gave significant fluorescence discrimination at positions -1 and +1 (3.4 to 3.6-fold for C_6-TO_{B6} and 2.0 to 2.4 for AE-TO_{Q6}), the same positions at which mismatch discrimination by T_m is highest (Figure 2.16 and Figure 2.23). Surprisingly fluorescence discrimination at these positions was similar to the mismatch opposite TO (3.8 for C6-TO_{B6} and 2.2 for AE-TO_{Q6}) where UV melting data showed bigger differences. In position -2 a large change in T_m (Figure 2.16) gave greater match/mismatch differences in fluorescence response for AE-TO_{Q6} and a smaller value for C6-TO_{B6}, and in position 2 a smaller change in T_m gave less decreased F_{ds}/F_{ss} to the match target, indicates no simple correlation between decrease in ΔT_m for mismatch targets. More detailed photophysical studies are needed to explain this behaviour of TO probes. Nevertheless, in summary the favourable fluorescence properties of these simple 2'-OMe TO probes may be useful in detection of DNA *in vitro*.

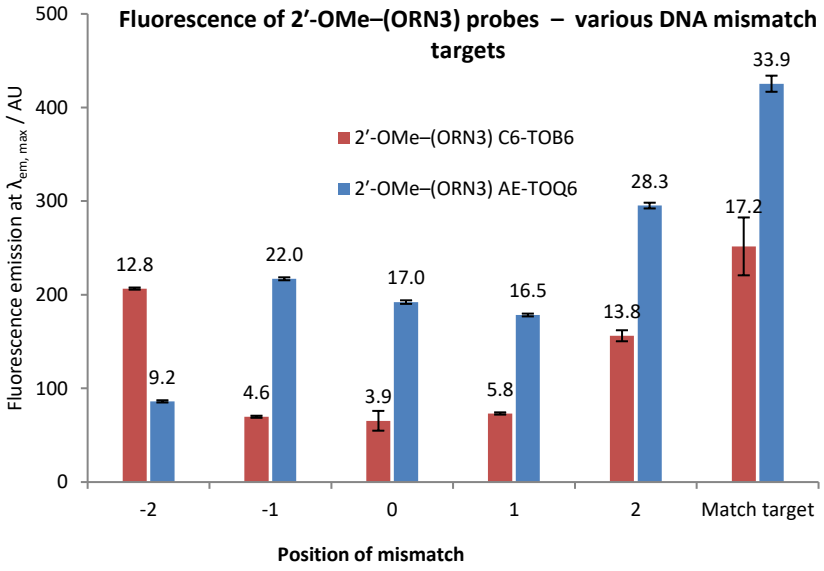


Figure 2.23 Fluorescence emssion intensity at $\lambda_{em,\ max}$ of TO-modified 2'-OMe–(ORN3) (5'-GCA**C**X**C**UACG) probes against various DNA targets with mismatches. Position of mismatch refers to a mismatch in the target strand counting from the TO-modified base, e.g.: position "0" is directly opposite modification and "-2" is two nucleobases towards 5' end of the probe sequence. Value above the bar represents F_{ds}/F_{ss} – ratio of integrated fluorescence emission of oligonucleotide probe-target duplexes to single stranded probes. Detailed values: see Table 6.16 and Table 6.21.

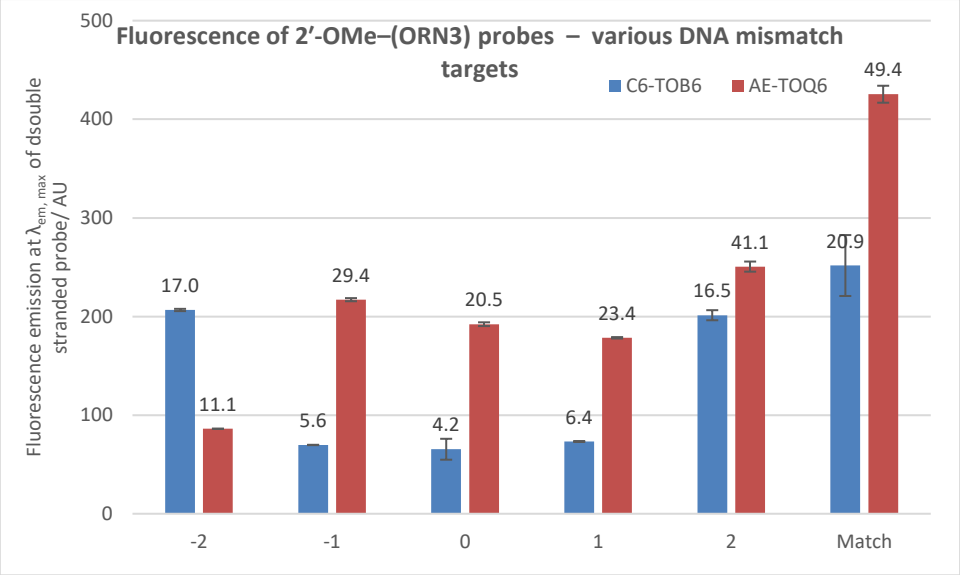


Figure 2.24 Representation of Figure 2.23 with fluorescence emssion intensity of double stranded probes at $\lambda_{em,\ max}$ and fluorescence emssion intensity of single stranded probe at $\lambda_{em,\ max}$ of double stranded probes. Detailed values: see Table 6.19 and Table 6.22 . F_{ds}/F_{ss} calculated at $\lambda_{em,\ max}$ of double stranded probe (single wavelength), accordingly to ECHO probes studies.[122]

2.4.10. Effect of linker length on the properties of 2′-OMe–ORN1 AE-TO probes

As shown in paragraph 2.4.1, the properties of the TO probes are somewhat altered when they are attached to the 5-position of the nucleobase by different linkers (C6 or PA). An important question is how those differences affect photophysical properties. For this reason TO_{B10} and TO_{Q10} NHS esters (Paragraph 2.3) were synthesized and used to label the 2′-OMe–(ORN1) AE and C6 probe (Table 6.2). UV melting studies with fully matched DNA and RNA targets showed the same trends as previously observed for AE and C6-$TO_{B6/Q6}$ with slightly lower increases in T_m (0.6 – 17.8 °C compared to 4.7 – 19.3 °C, Figure 2.25).

The fluorescence changes followed the same trends as C6 and AE labelled with $TO_{B/Q6}$ against DNA and RNA targets, but with slightly increased F_{ds}/F_{ss} (18.9 for AE-TO_{Q10} compared to 15.7 for AE-TO_{Q6}: SW 24.8 and 23.0) and decreased F_{ds}/F_{ss} (8.0 for C6-TO_{B10} compared to 15.2 for

C6-TO_{B6}; SW 9.0 and 19.5). Fluorescence intensity increased by 1.18 fold for AE-TO_{Q10} and decreased by 1.07 fold for C6-TO_{B10} on average against DNA and RNA matched targets (Figure 2.26). However, fluorescence-based mismatch discrimination was compromised. Taking those results into consideration there is no advantage of the longer linker relative to the previously studied $TO_{B/Q6}$ systems.

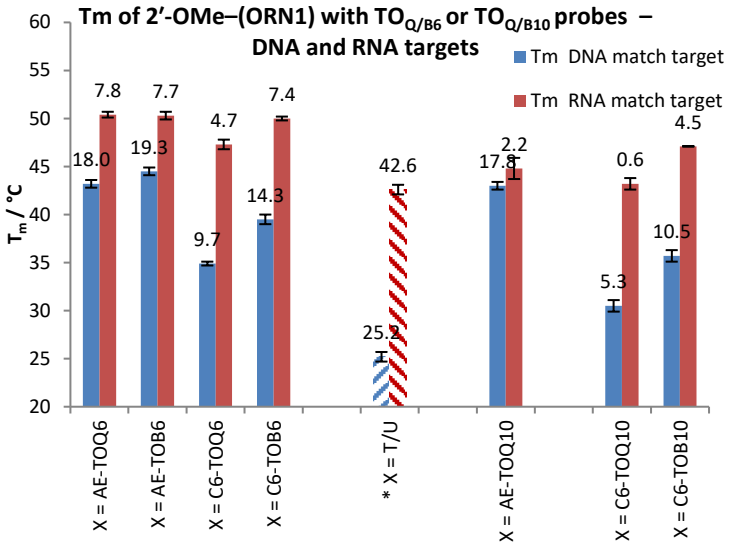


Figure 2.25 UV melting data for 2'-OMe–(ORN1) (5'-GCAU**X**UUACG) with $TO_{B/Q6}$ and $TO_{B/Q10}$ probes against DNA and RNA targets. The base opposite the TO is either A – match or T/U – mismatch, number above bar = ΔT_m to unmodified target, * = T_m value of unmodified matched and mismatched duplexes. Detailed values: see Table Table 6.8 and Table 6.10.

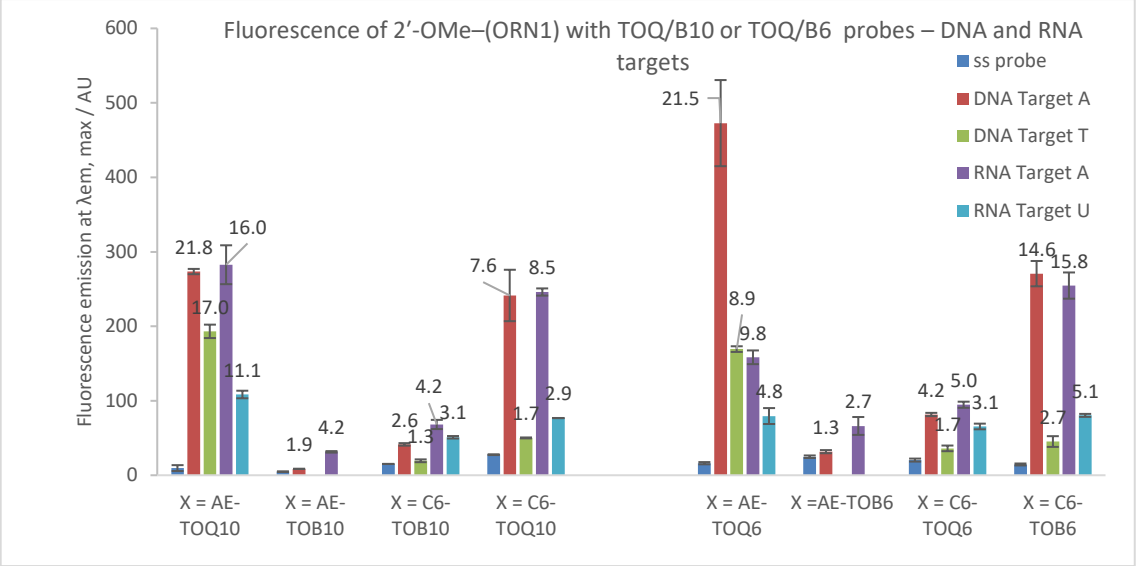


Figure 2.26. Comparison of fluorescence emssion intensity at $\lambda_{em,\ max}$ data for 2'-OMe–(ORN1) (5'-GCAUXUUACG) with $TO_{B/`Q6}$ or $TO_{B/Q10}$ probes against DNA and RNA targets. The base opposite the TO is either A – match or T/U – mismatch, ss probe – fluorescence emission intensity of single stranded probe at $\lambda_{em,\ max}$, I_{max} – fluorescence emission intensity of probe-targetduplex at $\lambda_{em,\ max}$, AU - arbitrary units, number above bar = F_{ds}/F_{ss}. Detailed values: see Table 6.16 and Table 6.18.

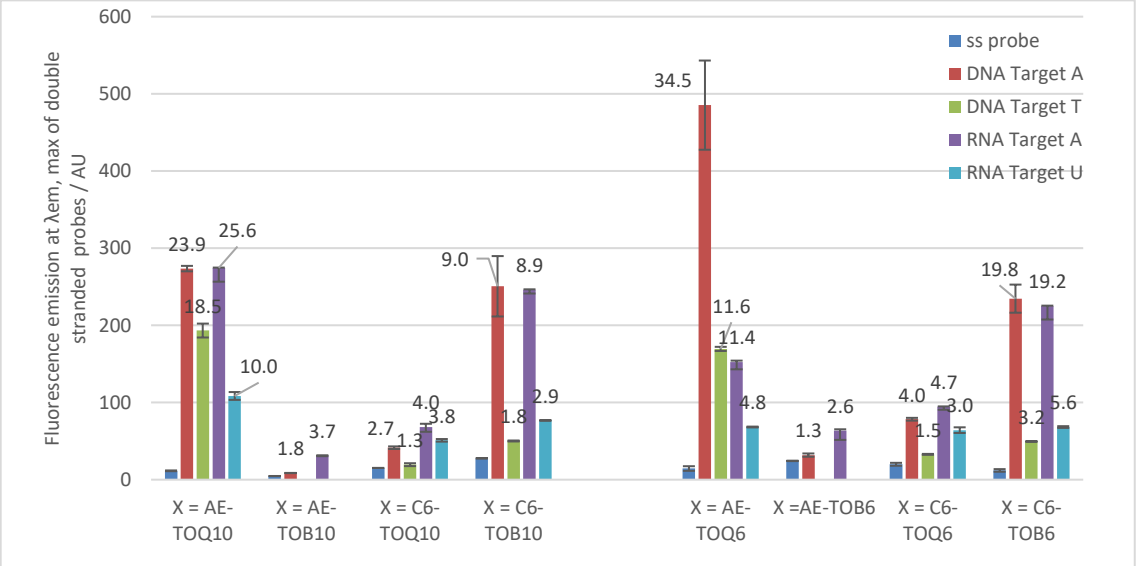


Figure 2.27. Representation of Figure 2.26 with fluorescence emssion intensity of double stranded probes at $\lambda_{em,\ max}$ and fluorescence emssion intensity of single stranded probe at $\lambda_{em,\ max}$ of double stranded probes. Detailed values: see Table 6.19 and

Table 6.20. F_{ds}/F_{ss} calculated at $\lambda_{em,\ max}$ of double stranded probe (single wavelength), accordingly to ECHO probes studies.[122]

2.5. CD spectroscopy of TO probes with DNA and RNA targets.

Circular dichroism spectroscopy of the modified TO-containing DNA duplexes (TO-ODNs) indicate in general the formation of B-like DNA with no major perturbation from the unmodified structure (Figure 2.28 and Figure 2.29). CD spectra of the 2'-OMe-(ORN) duplexes are very similar to the equivalent unmodified duplexes (Figure 2.28, and Figure 2.30) indicating that TO does not disrupt natural structure of oligonucleotide double helices.

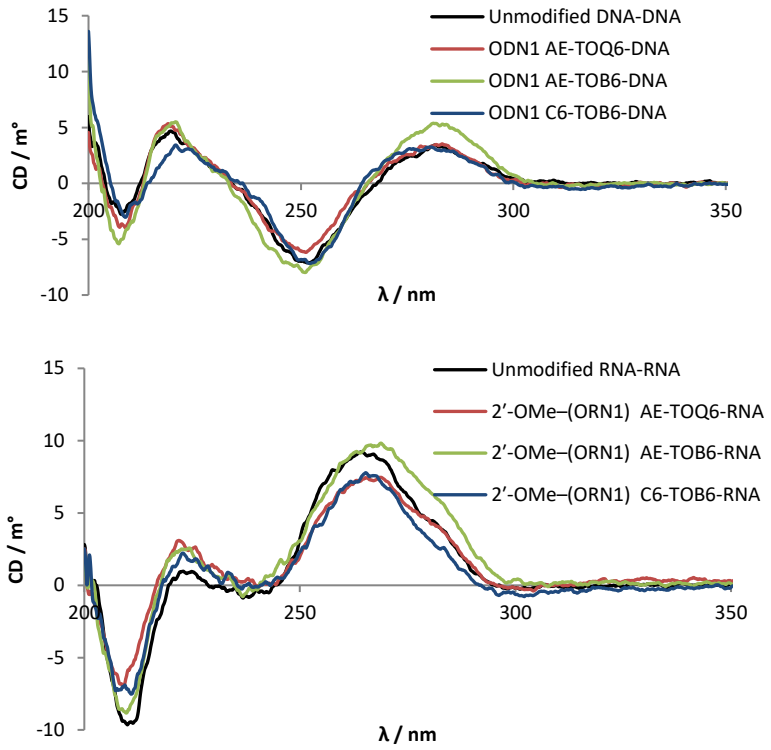


Figure 2.28. CD spectra of selected TO-labelled probes-DNA/RNA targets duplexes and unmodified DNA/RNA-DNA/RNA target duplexes. A – 2'-OMe–(ORN1) (5'-GCA**U**<u>**X**</u>**U**UACG) probes and unmodified RNA 2'-OH–(5'-GCA**U**<u>**U**</u>**U**UACG) with RNA target, B – ODN1 (5'-GCA**T**<u>**X**</u>**T**TACG) probes and unmodified DNA (5'-GCA**T**<u>**T**</u>**T**TACG) with DNA target.

Circular dichroism can also provide information about TO interaction with the double stranded helix. According to the literature the negative peak in the 450-550 nm range can be assigned to the intercalating mode of interaction between TO and the DNA helix. The positive-negative peak is presumed to be a second, possibly a groove binding, mode of interaction.[170] The data obtained in this region for ODN1 probes with DNA targets shows a small negative peak for PA and C6 modifications

with TO_{B6} as well as for PA-TO_{Q6} whereas for AE-TO_{B6}, C6 and AE-TO_{Q6} the CD spectrum was unchanged in this region (Figure 2.29). When the same probes were measured against RNA targets only C6-TO_{B6} showed a shift of signal to negative values whereas the others remained unchanged (Figure 2.31). In the case of 2'-OMe-(ORN1) probes the AE-TO_{B6} modification showed a positive peak against DNA and RNA targets whereas the other modifications showed no change in CD spectrum (Figure 2.30 and Figure 2.32). Additionally CD spectra of ss probes were measured (Figure 2.33 and Figure 2.34), in most cases showing no signal in the TO region (450-550 nm), only in case of ODN1 PA-TO_{Q6} and ORN1-AE-TO_{B6} were positive signals observed. A residual signal form 200-300 nm range is generally present as nucleic acids do not require a hydrogen-bonded double strand to maintain the helical structure.[181] This lack of consistency with the literature suggests that in our system a more in-depth investigation of the nature of the TO interactions with duplexes against DNA and RNA is required.

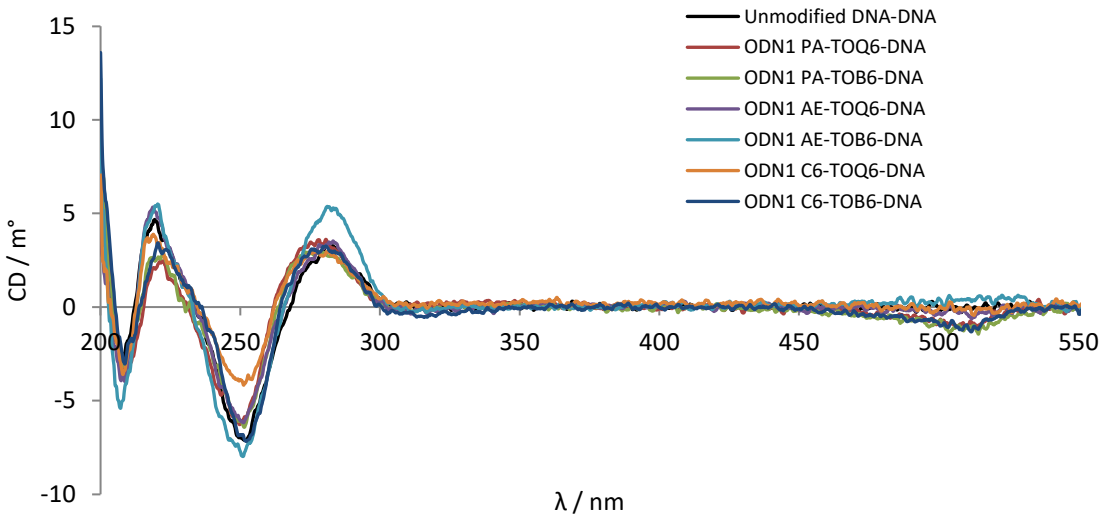


Figure 2.29 CD spectra of TO-labelled ODN1 (5′-GCAT**X**TTACG) probes-DNA target duplexes with comparison to unmodified DNA (5′-GCAT**T**TTACG) duplex with DNA target.

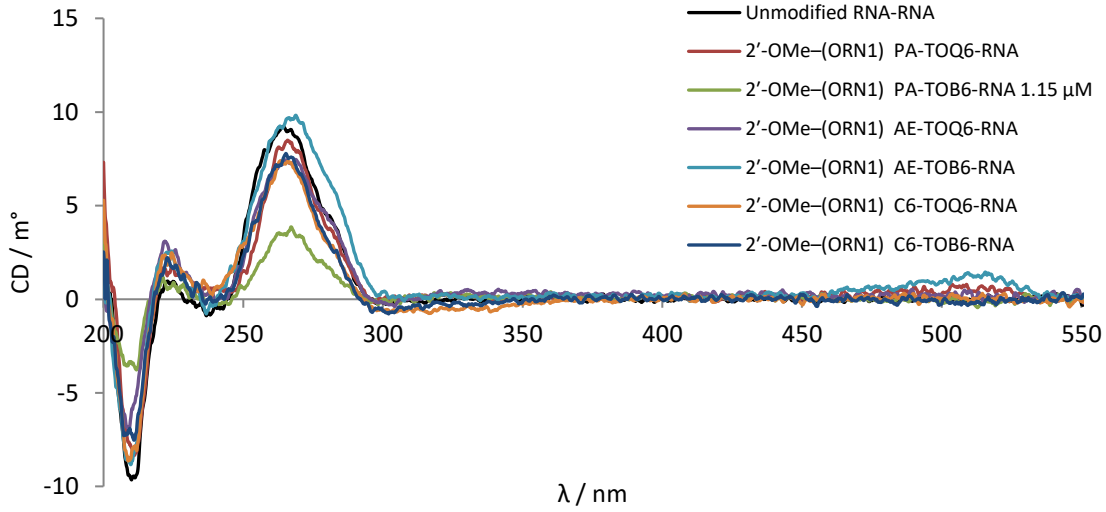


Figure 2.30 CD spectra of TO-labelled 2′-OMe–(ORN1) (5′-GCA**U**X**U**UACG) probes-RNA target duplexes with comparison to unmodified RNA 2′OH–(5′-GCU**U**UUACG) duplex with RNA target.

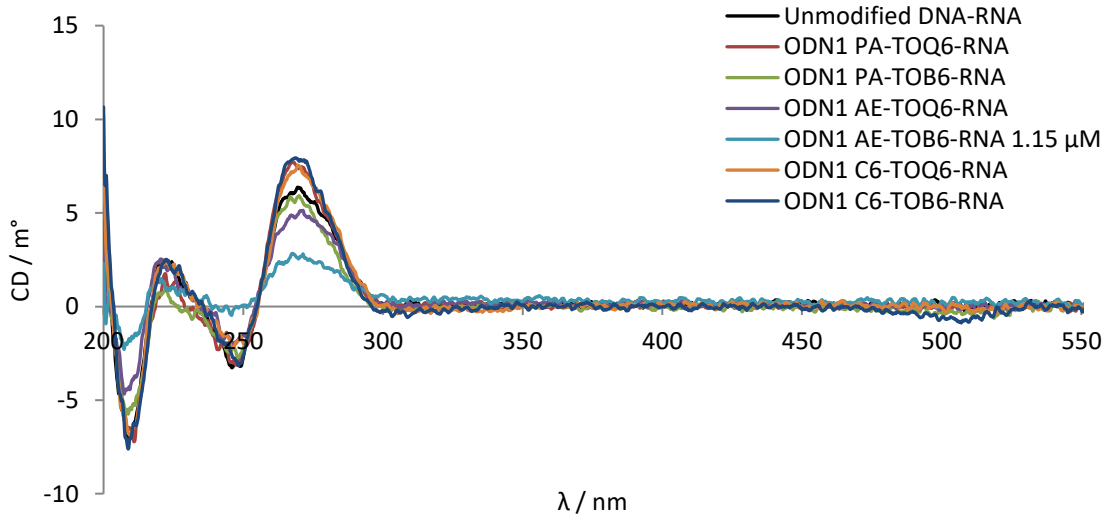


Figure 2.31 CD spectra of TO-labelled ODN1 (5′-GCA**T**X**T**TACG) probes-RNA target duplexes with comparison to unmodified DNA (5′-GC**T**T**T**TACG) duplexes with RNA target.

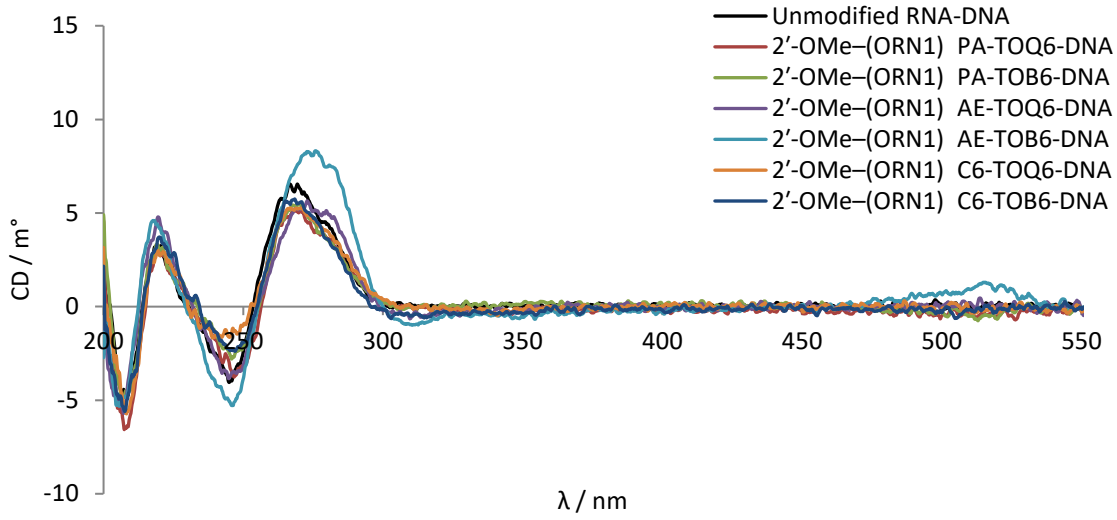


Figure 2.32 CD spectra of TO-labelled 2'-OMe–(ORN1) (5'-GCA**U**X**U**UACG) probes-DNA target duplexes with comparison to unmodified RNA 2'OH–(5'-GCU**U**UUACG) duplex with DNA target.

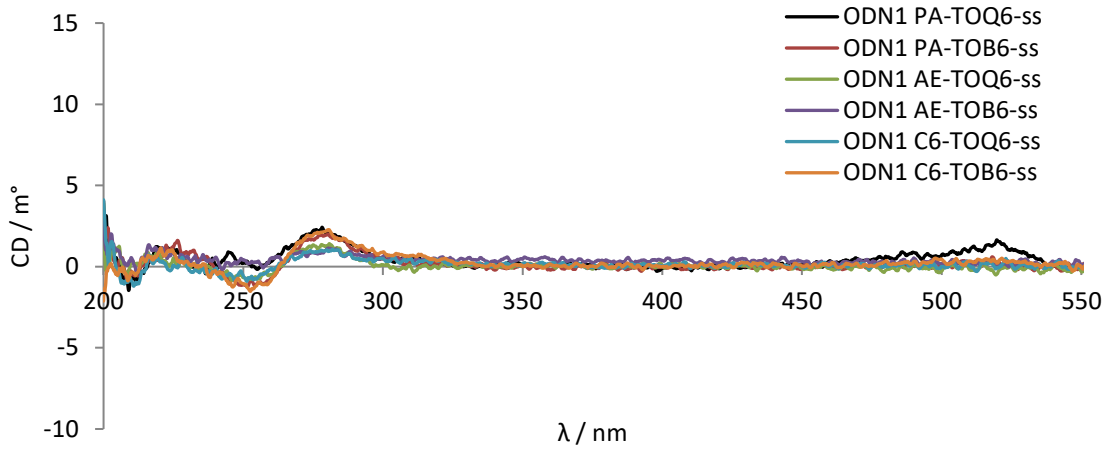


Figure 2.33 CD spectra of TO-labelled 2'-OMe–(ODN1) (5'-GCAT**X**T**T**ACG) probes without target.

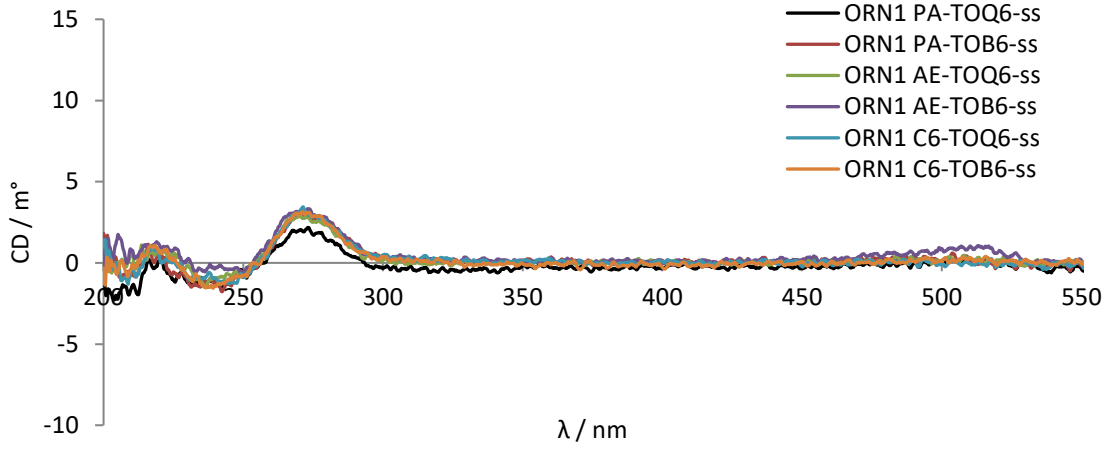


Figure 2.34 CD spectra of TO-labelled 2'-OMe–(ORN1) (5'-GCA**U**X**U**UACG) probes without target.

2.6. Conclusions

In summary, a set of thiazole orange (TO) probes was obtained with various modifications where the dye was attached either to the 5 position of a thymidine (PA and C6) nucleobase or at the 2′ position of the sugar (AE). The photophysical properties of the TO-probes upon duplex formation with DNA or RNA targets showed a dependence on the length of the linker by which TO was attached, the position of the attachment of the linker to the asymmetric dye (*via* the benzothiazole or quinoline moiety) and the nature of the nucleotide modification which places TO into the major (nucleobase) or the minor (sugar) groove. The best fluorescence properties upon duplex formation with DNA and RNA targets in the major groove were obtained when TO was attached by its benzothiazole moiety (C6-TO_{B6}) and in the minor groove *via* quinoline moiety (AE-TO_{Q6}). Thermal duplex stabilisation experiments showed higher stabilisation by C6-TO_{B6} relative to C6-TO_{Q6}, whereas for the AE modification both TO_{Q6} and TO_{B6} derivatives showed similar effects. Experiments were carried out with double incorporation of the AE modification into 2′-OMe RNA probe sequences with TO attached by its quinoline moiety (2×AE-TO_{Q6}). With complementary DNA targets a significant increase of thermal stabilisation was achieved in comparison to a single incorporation when the modification was separated by two nucleotides. Mismatch discrimination based on differences in thermal melting for both AE-TO_{Q6} and C6-TO_{B6} at positions -1 and +1 with target DNA strand was excellent and far superior in comparison to when the mismatch was placed directly opposite the modified nucleotide. In contrast fluorescence-based mismatch discrimination was similar for positions -1, 0 and +1. These properties are of great importance when designing probes for mutation and SNPs detection. The fluorogenic properties of DNA-based TO probes are compromised by residual fluorescence in the single stranded state of the probe, in which the positively charged TO presumably interacts with the negatively charged DNA phosphodiester backbone, resulting in formation of secondary structures, leading to a significant fluorescent signal in the unbound state. This problem was previously addressed by usage of PNA and ECHO probes. Our results show that use of the 2′-*O*-Me RNA modification in probe sequence reduces this problem and at the same time preserves the simplicity of probe design and ease of synthesis.

Comparison of obtained 2'-OMe probes with ECHO probe, also modified with at 2' position, system in terms of fluorescence shows highly promising results. As ECHO probes exhibit F_{ds}/F_{ss} from 7 to 30-fold, although it is important to notice that in some special sequence context (poly U probe sequence) enhancement was equal to 209-fold.[122] In case of our probe system up to 50-fold F_{ds}/F_{ss} could be observed (AE-TO_{Q6} in ORN3) or 35-fold for ORN1 sequence context. Showing dependence of fluorescence properties based on sequence factor for both approaches. Thus in order to fully compare those two systems identical sequence should be used in the future. Additionally when DNA version of ECHO system with single TO, shows F_{ds}/F_{ss} = 3.4[114] which is close to 3 times smaller (ODN1 C6-TO_{B6}, 9.4-fold) against DNA targets, showing to some extend beneficial properties of used in this work TO-artificial modification conjugates. Thermal stabilisation of ECHO system varies from +4 to +16 °C against RNA targets,[122] our system gives slightly smaller values ranging from +4 to +8 °C, worth noting is that against DNA targets stabilisation up to 19.3 °C can be achieved. Secondly system showed in this work contains single TO moiety in comparison to two in case of ECHO. Experiments with double incorporation of AE-TO_{Q6} clearly shows that close to double increase of T_m can be achieved upon addition of second modification.

Comparison with FIT probe system, in which by design TO serves as an artificial nucleobase doesn't provide any additional stability of obtained duplex, making it inferior to the modified nucleoside systems. Although comparing fluorescence properties shows that FIT probe system gives up to 13.4-fold increase of fluoresce when TO is used as an intercalator.[134,135] In comparison to our system in which one of the lowest F_{ds}/F_{ss} are at similar level. Higher fold values can be achieved by using different fluorophore (Quinoline Blue) in FIT design, unfortunately emission intensity of obtained signal is low.[135]

Out of all tested sequences in which TO was attached to the AE modification (AE-TO_{Q6}) unusual fluorogenic properties were observed when TO was placed between two guanine bases, highlighting the need for careful evaluation of the design. In conclusion, these 2'-OMe-RNA TO-probes have potential for applications in cell imaging of DNA and RNA. Some potential issues, such as the ability to

specifically detect target DNA or RNA in a genomic background (which could be compromised by non-specific interactions between TO and DNA) were not addressed in this study.

Chapter 3 - Thiazole orange and acyclic DNA backbone modifications

3. Chapter 3 - Thiazole orange and acyclic DNA backbone modifications

3.1. Introduction

Exploring new artificial backbones for the design of probes is important in order to achieve the best performing diagnostic tools. Thiazole orange, as mentioned previously has many applications in diagnostic field. In Chapter 2 attachment of TO to the thymidine nucleotide was discussed in detail. A different approach was demonstrated with FIT probes (Force Intercalation Probes)[101], where TO is used as an artificial nucleobase by linking it to the DNA backbone by short (C2) carboxylic linker. The dye is forced into stacking into the double stranded helix resulting in a fluorescence response. This probe system was utilised mainly for RNA imaging, including human lung cancer cells and targets such as kras2 mRNA and IncRNA CCAT1.[182,183] Although those examples use a peptide nucleic acid (PNA) backbone, the DNA/RNA backbone is of most interest for our work as the hydrophobic character of the PNA backbone is problematic; it can lead to aggregation, non-specific binding to incorrect target sequences and poor aqueous solubility which can be mediated by lysine modification and PEGylation.[128,184] Moreover, in contrast to oligonucleotide probes, PNA probes are expensive to make and are not widely available in chemically modified forms.

DNA backbones for FIT probe design have been studied with various artificial modifications such as α and β linked TO in carbocyclic deoxyribose,[185] or in acyclic backbones such as (*R*)-glycerol, (*L*) and (*D*)-serinol (2-amino-1,3-propanodiol, Figure 3.1)[186] where TO was attached by various lengths of linkers. Attachment by a short (acetic acid) linker to the quinoline moiety was found to be superior.[133] It was used in applications such as qPCR[185] imaging of ribonucleotide particles in developing oocytes from Drosophila melanogaster and to detect various RNA targets in cells.[101,130]

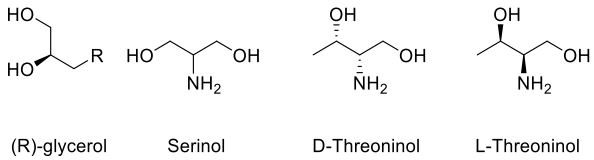


Figure 3.1 Structures of substrates for acyclic scaffold.

This work shows both the importance of the mode of TO attachment and the structure of the artificial backbone. Reports on serinol and D- and L-threoninol (2-amino-1,3-butanodiol) as artificial backbones with amine linked standard nucleobases (A, G, C and T) revealed interesting properties. Binding affinities of these artificial oligonucleotides for DNA and RNA were quite different.

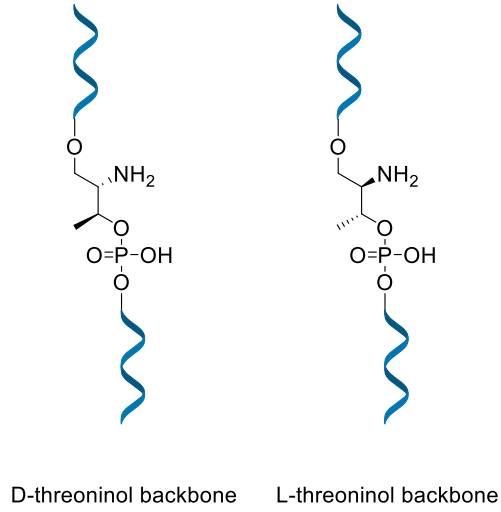


Figure 3.2 Structure comparison between D and L-threoninol backbones.

The D-threoninol backbone does not form stable hybrids with DNA or RNA. In contrast, the serinol backbone (SNA, synthesized from L-serine, Figure 3.1) which lacks a methyl group in comparison to the threoninol, forms stable hybrids with DNA and RNA (Figure 3.2).[187] Surprisingly in same study, L-threoninol showed a higher affinity for DNA and RNA than did SNA, indicating the importance of both the methyl group and the configuration of the amino group. Single incorporation of L or D-threoninol into the DNA sequence with a diazobenzene moiety showed that the D-enantiomer gives higher duplex thermal stability (Figure 3.3).[188] This modification (D-enantiomer) was later used with TO linked by its quinoline moiety as an effective probe system.[131,189] Additionally, the L-threoninol backbone provided

better thermal stabilisation of duplex in comparison to the D-threoninol against RNA targets and favourable photophysical properties when conjugated with an acridine moiety (Figure 3.3), further supporting the need to evaluate the L-enantiomer with TO.[190]

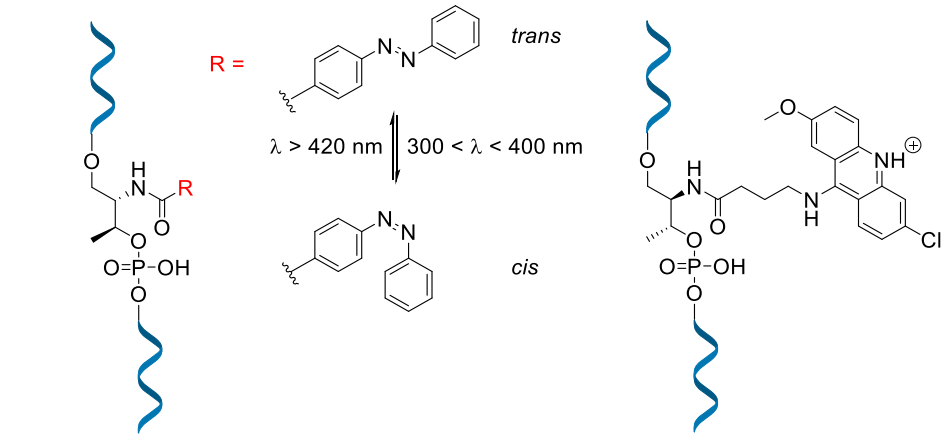


Figure 3.3 Structures of D-threoninol[188] and L-threoninol[190] conjugates with preferable photophysical properties over second isomer.

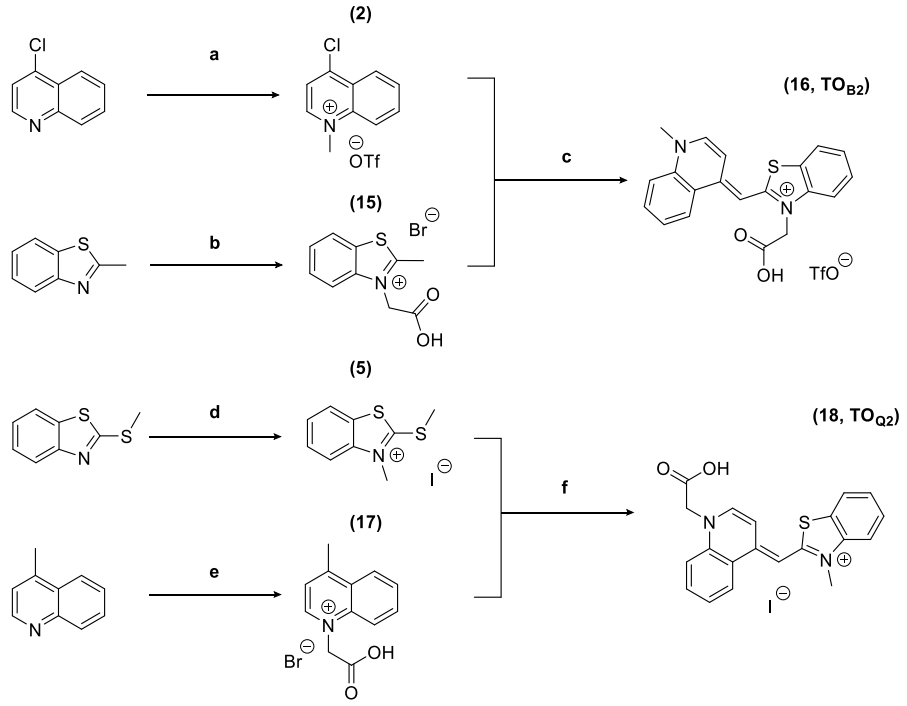
No study of the TO conjugate with L-threoninol backbone has been performed, despite the preference of the L-theroninol backbone over the D-form against DNA and RNA targets as well as better thermal stability of the L-threoninol over L-serinol backbone which is heavily used in FIT probes. For this reasons, L-threoninol should provide a good alternative for the FIT probe design.

3.2. Synthesis of Thiazole orange derivatives and L-threoninol phosphoramidite

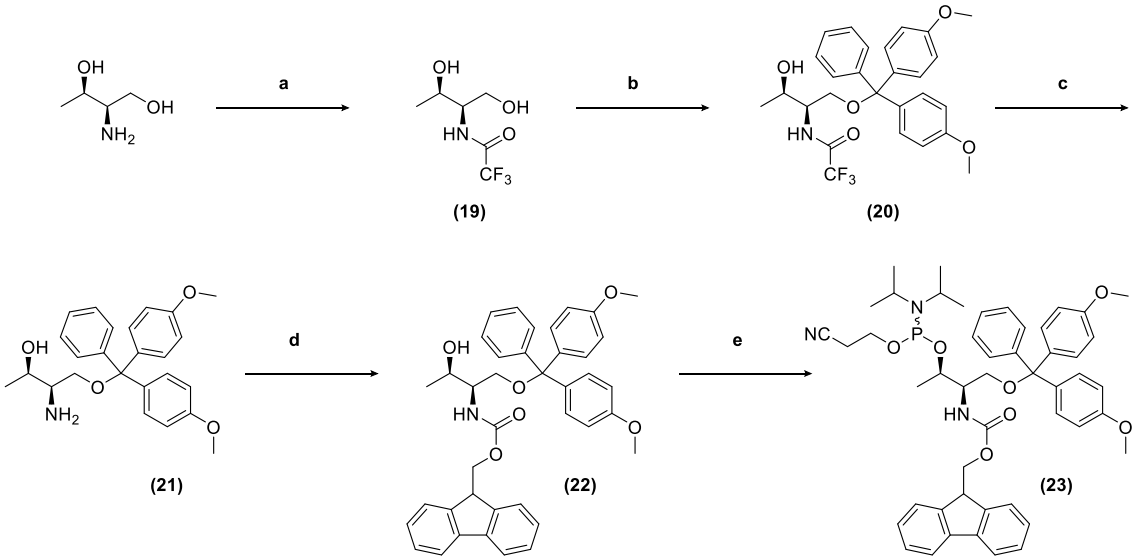
Previous work suggests that the FIT probes design requires TO attached by the quinoline moiety for good quantum yields and favourable F_{ds}/F_{ss}.[127] Nevertheless, for development of a new applications of the L-threoninol acyclic backbone, both derivatives were synthesized. As mentioned before the best fluorescence response of TO in FIT probes requires TO to be attached by a short carboxylic linker (TO-CH_2-COOH).[127]

These TO derivatives (TO_{B2} and TO_{Q2}) are not commercially available therefore synthesis of the necessary building blocks was carried out according to published procedures (compounds **5**, **15** and **17**)[191,192,193] with improved synthesis of compound **2** (shorter reaction time and higher yield) over literature procedures as mentioned in paragraph 2.3.[130,194] TO_{Q2} (**18**) was synthesized according to the literature procedure.[193] For TO_{B2} (**16**) although synthesis of the compound was previously published,[127] no spectral data or synthesis protocol is available. It was synthesized similarly to TO_{B6} (**3**) and the synthetic route is presented in Scheme 3.1. Isolation of the NHS esters of these TO derivatives was unsuccessful, unlike for $TO_{B/Q6}$ (paragraph 2.3).

Next the synthesis of N-Fmoc-1-*O*-(4,4'-dimethoxytritryl)-L-threoninol phosphoramidite was carried out based on previous work on the D-threoninol enantiomer.[131] Starting from commercially available and optically pure L-threoninol protecting the amino group with trifluoroacetamide (**19**) was followed by addition of 4,4'-dimethoxytritryl to one of the oxygen atoms attached to the primary carbon (**20**). Then the TFA-amino group was deprotected using aqueous ammonia and ethanol and re-protected with Fmoc (**22**) which can be selectively cleaved on solid phase for labelling purposes. This precursor (**22**) was then converted into the phosphoramidite (**23, TH**) that was later efficiently incorporated into oligonucleotide sequences (accordingly to Experimental 6.3).



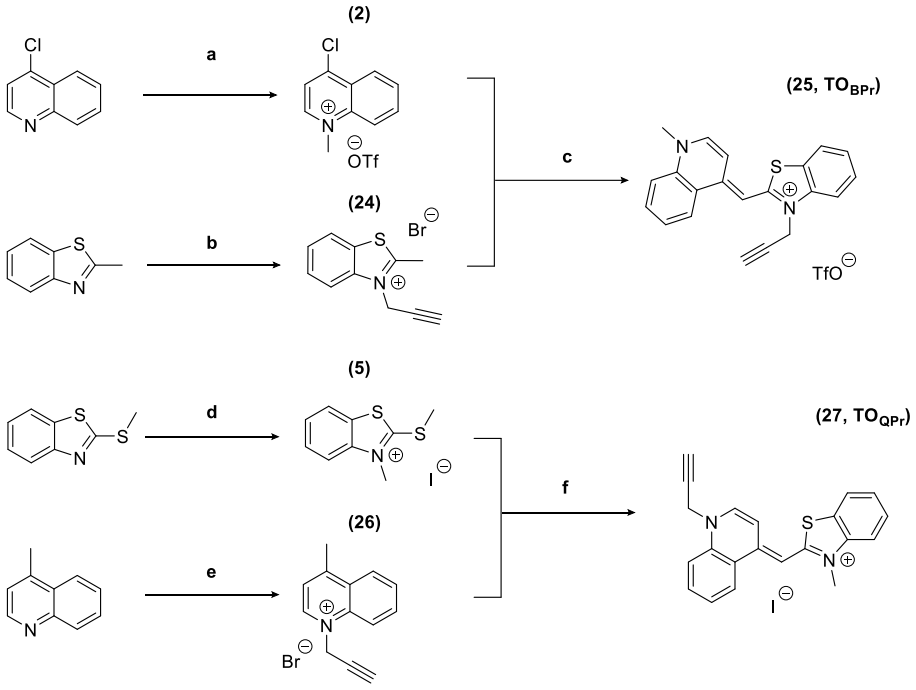
Scheme 3.1. Synthetic route to TO_{B2} and TO_{Q2}. Reagents and conditions: (a) MeCN, MeOTf, 3 h, RT, 90%; (b) MeCN, bromoacetic acid, 24 h, reflux, 57%; (c) CH_2Cl_2:MeOH, Et_3N, 3 h, RT, 39%; (d) MeCN, MeI, 24 h, 50 °C, 46%; (e) MeCN, bromoacetic acid, 12 h, reflux, 12%; (f) EtOH, Et_3N, RT, 2 h, 52%.



Scheme 3.2 Synthetic route to L-threoninol phosphoramidite (**TH**). Reagents and conditions: (a) MeOH, $EtOCOCF_3$, 2.5 h, 0 °C to RT, 93%; (B) Pyridine, CH_2Cl_2, DMTrCl, DMAP, 3 h, 0 °C to RT, 66%; (c) EtOH/$NH_{3(aq)}$, 4 days, RT, quant.; (d) CH_2Cl_2, Fmoc-OSu, DIPEA, 2 h, RT, 81%; (e) CH_2Cl_2, 2-Cyanoethyl N,N-diisopropylchlorophosphoramidite, DIPEA, 1 h, RT, 63%.

TO derivatives for CuAAC labelling were synthesized using the same building blocks that were applied for carboxylic linker derivatives (**2** and **5,** Scheme 3.3). Additionally, the synthesis of new building block **24** in a pressure vial resulted in a higher yield than reported in the literature.[195] Building block **26** was

obtained according to the literature procedure.[196] TO_{QPR} (**25**) was synthesized using a slightly modified literature procedure,[197] and novel TO_{BPr} (**27**) was also synthesized. Both derivatives are equipped with a propargyl linker for CuAAC labelling which should allow forced intercalation within a new FIT probe design.

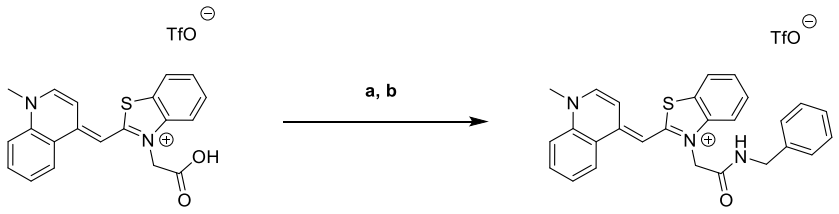


Scheme 3.3. Synthetic route to TO_{BPr} and TO_{QPr}. Reagents and conditions: (a) MeCN, MeOTf, 3 h, RT, 90%; (b) MeCN, propargyl bromide, 12 h, 100 °C, 30%; (c) EtOH, Et_3N, 0.3 h, RT, 25%; (d) MeCN, MeI, 24 h, 50 °C, 46%; (e) MeCN, propargyl bromide, 72 h, RT, 43%; (f) EtOH, Et_3N, RT, 10 min, 20%.

3.3. Results and discussion

3.3.1. Amide linkage approach for FIT probe synthesis

L-Threoninol phosphoramidite (**TH**, Scheme 3.2) was incorporated into a DNA sequence (NH_2–TH–ODN3–DNA (5′-GCAC**TH-NH_2**CTACG)). This procedure was straightforward and efficient under standard solid-phase synthesis conditions (Experimental 6.3). Next the coupling of TO_{Q2} and TO_{B2} (Scheme 3.1) under published conditions for TO_{Q2} into PNA was attempted using PyBOP, HATU and DSC as coupling reagents in DMF or DMSO as solvents with addition of PPTS as a solubilising agent.[164] Unfortunately after a large screening process exploring many (A-1 to A-24) conditions no desired labelled product could be detected. Only the positive control with TO_{B6} was successful (A-25) (Experimental 6.4.2 and Table 6.3). The same conditions in aqueous solvent also did not result in the desired labelled product. A control reaction with benzylamine (Scheme 3.4) using conditions from a published procedure were tested,[135] which resulted in the coupled product. Those conditions were applied to the oligonucleotide labelling of 5′-GCAC**TH-NH_2**CTACG with TO derivatives equipped with short carboxylic linkers but unfortunately did not give the desired labelled product. Additionally, the synthesis of a phosphoramidite where L-threoninol was linked to the TO derivative gave no positive results due to instability of the obtained phosphoramidite monomer. In conclusion this approach was abandoned in a favour of a successful CuAAC labelling method.



Scheme 3.4 Control reaction for coupling of TO_{B2} with amine. Reagents and conditions: (a) DMF, PPTS, DIC, HOSu, (b) Benzylamine, Carbonate buffer. Obtained product was confirmed by LRMS (ESI^+) *m/z* (%): 438$[M]^+$ (100), 290 (90) and TLC change R_f of TO_{B2} = 0.2, R_f of coupled product = 0.6 (MeOH : DCM 2 : 8).

3.3.2. Triazole linkage approach for synthesis of FIT probes

As mentioned in the previous paragraph, obtaining amide linked FIT probes proved to be not feasible for $TO_{B/Q2}$ and the L-threoninol backbone. An interesting alternative is CuAAC coupling (Paragraph 1.3) which is already widely used in the oligonucleotide field.[198] This high yielding, catalytic method has many advantages including easy introduction of alkyne modifications into oligonucleotide sequences,[199] large numbers of commercially available labels and a straightforward protocol. Incorporation of the azido moiety is more troublesome (Paragraph 1.4.1.2.2), due to possibility of Staudinger reaction of the azide with phosphorus(III).[70,200] Various approaches to tackle this problem have been developed, such as H-phosphonates,[70,71] phosphotriester[68,69] and various post synthetic modifications[46,201–204] or enzymatic methods.[205] Recently a phosphorus(III) monomer containing an azide moiety was successfully used in a solid phase synthesis of oligonucleotides.[72] In another approach an amino group was directly converted into azide without loss of stereochemistry,[78] both in small molecule reactions[77] and on an oligonucleotide in solid support and in solution phase. This conversion was chemoselective towards the alkylamine; the amine groups present on the nucleobases were unaffected (Paragraph 1.4.1.2.2).[79]

Designing a new approach for FIT probes required a better understanding of structural properties of the TO-linkage. To utilise the previously synthesized **TH** backbone the most efficient route would seem to be introduction of an azide moiety into the sequence. Adding an alkyne functional group into the modification would require a large synthetic effort and could possibly compromise functionality by placing TO too far away from its most efficient (Forced) intercalation site.[164] This objective was accomplished by usage of the hydrochloride salt of diazotransfer reagent (ISAHC)[79] (Figure 3.4), on the 5'-GCAT**TH-NH_2**TTACG sequence. Conversion of the amine to azide was achieved with 100% efficiency (Experimental 6.4.3, Figure 3.4 and Figure 3.5).

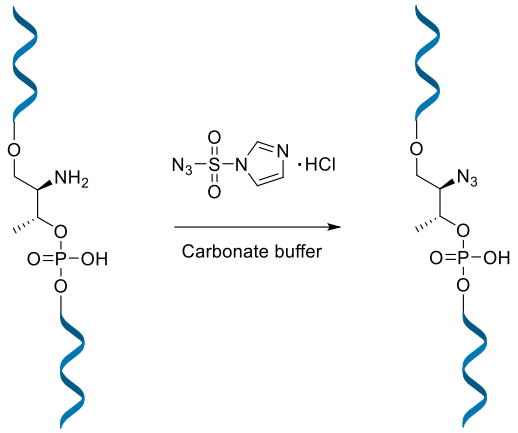


Figure 3.4 Amine to azide conversion with ISAHC DZT reagent within the oligonucleotide sequence.

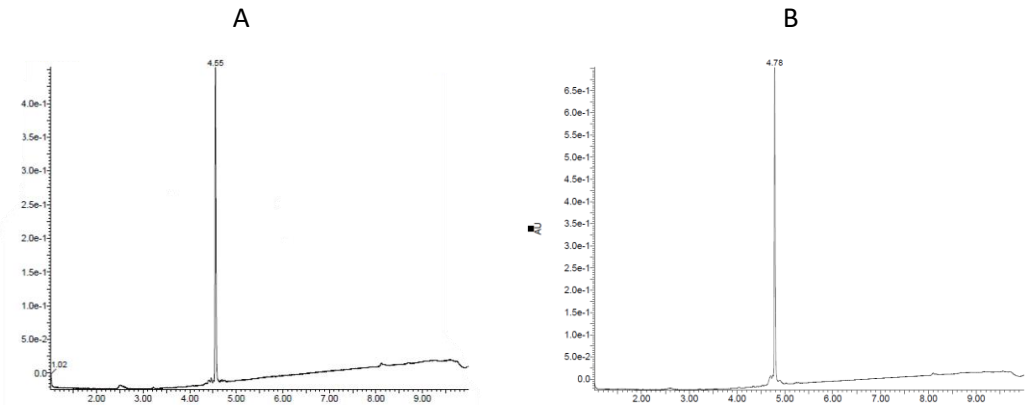


Figure 3.5 Examples of HPLC chromatograms at 260 nm of purified NH_2 oligonucleotide (A) and crude reaction (B): A: NH_2–TH–ODN3–DNA (5′-GCA**CTH-NH$_2$C**TACG); B: N_3-TH–ODN3–DNA (5′-GCA**CTH-N$_3$C**TACG); sequence 5′-GCA**CTH-NH$_2$C**TACG mass calculated: 2851 mass found: 2851, 5′-GCA**CTH-N$_3$C**TACG mass calculated: 2877 mass found: 2877.

Next, the TO derivatives with a propargyl group were synthesized (Scheme 3.3). Based on the literature thiazole orange attached by quinoline (TO_{QPr}) should provide the best fluorescence response, so TO_{BPr} was synthesized for detailed evaluation. Both dyes were successfully conjugated to ODN1-N_3 using CuAAC (Figure 3.6, Experimental 6.4.4,). Sequences are summarised in Table 6.4.

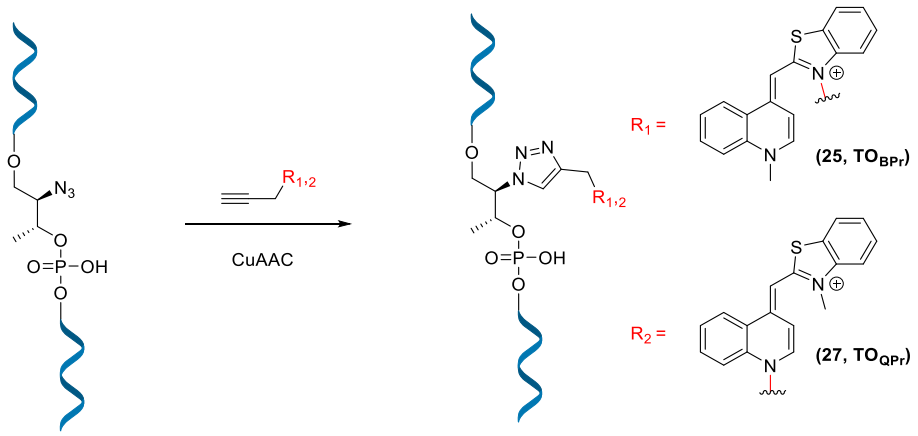


Figure 3.6 Labelling of TH-N_3 containing sequence with TO_{BPr} (**25**) and TO_{QPr} (**27**) *via* CuAAC.

The most important function of these probes is their fluorescence response upon binding to their complementary target oligonucleotide strand. These properties were tested on this new FIT probe system ($TO_{B/QPr}$-**TH**-ODN1). Neither of the TO derivatives gave good F_{ds}/F_{ss} responses with matched DNA targets (Figure 3.7).

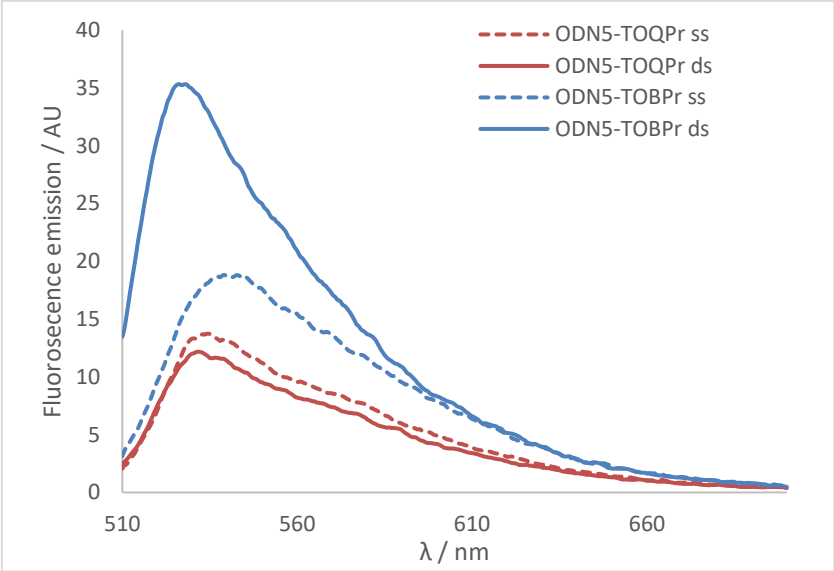


Figure 3.7 Examples of fluorescence emission spectra of ODN1 (5'GCA**T**X**T**TACG) where X = TH-TO_{BPr} and TH-TO_{QPr} probes with DNA target (ODN1 target A). Conditions: λ_{ex} = 484 nm, 200mM NaCl, 10 mM phosphate, pH = 7.0 at 20 °C, probe *concentration:* 0.25 µM, target concentration: 0.28 µM.

These results gave enough information for us not to pursue this FIT probe design. Both probe systems either gave no fluorescence difference between unbound and bound (ds) state or the increase was small. The intensity of the obtained signal is also inferior to previously studied systems (Chapter 2).

Interestingly TO_{BPr} gave fluorescence change upon binding where TO_{QPr} remained unchanged; this result is opposite to the previously reported literature on the serinol backbone but this could be due to differences in attachment (amine vs triazole).[127] Further studies on the relationship between structure of this acyclic backbone and $TO_{Q/BPr}$ derivatives needs to be performed in the future. A possible solution could be use of a D-threoninol[131] or an inverse L-threoninol monomer recently reported in the literature.[206]

3.4. Conclusions

In summary, TO derivatives with a short carboxylic linker ($TO_{B/Q2}$) were synthesized for attachment to the L-threoninol backbone in a new FIT probe design but after detailed evaluation it was discarded. Literature reports on similar structures (Paragraph 3.3.1) suggested a more complex problem. [135,164] Based on this, a new approach using CuAAC labelling was undertaken, resulting in a good synthetic route for obtaining an azido acyclic backbone by a chemoselective alkyl-amine to azide conversion utilising the amine of L-threoninol on the oligonucleotide. Straightforward and successful coupling of the azide modified scaffold with TO derivatives equipped with a propargyl linker resulted in a new probe system. Unfortunately, fluorescence properties of this system were unsatisfactory. Further studies on both the backbone modification and TO-alkyne derivatives are needed.

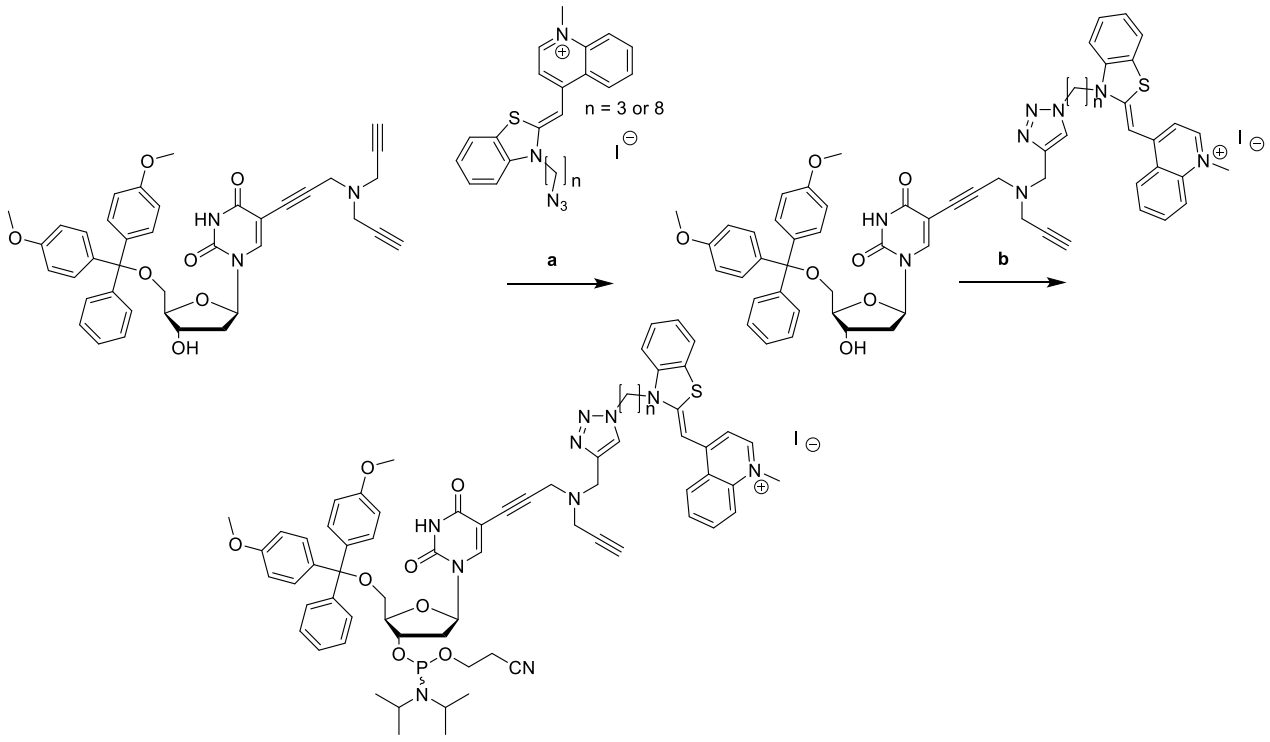
Chapter 4 - Orthogonal combination probes with thiazole orange

4. Chapter 4 - Orthogonal combination probes with thiazole orange

4.1. Introduction

As mentioned in chapter 2 obtaining fluorescence probes with low background signal for diagnostic applications is of most importance. A solution to this problem could be *via* "smart" fluorophores such as thiazole orange. A combination of the "on-off" properties of this intercalator dye with a bright reporter dye gives great advantages and has been explored in various contexts. Studies on DNA FIT probes accompanied by the reporter dye JO improves the brightness of the probe system, increasing the limit of detection for low abundance targets, at the same time maintaining favourable F_{ds}/F_{ss} ratio for TO labelled probes against RNA targets.[130] Other examples of PNA-based FIT probes with various reporter dyes have been reported. The best results were obtained with Alexa594, NIR664 and ITCC that quench the fluorescence of TO both in ss and ds state simultaneously increasing the $F_{ds}/F_{ss,}$ ratio, resulting in up to 450 fold increase of TO fluorescence, although the intensity of the FRET signal was significantly reduced. This design with addition of second reported dye was applied to cytosine vs uracil SNP detection for RNA targets *in* vitro.[207,208] Utilizing the FRET properties of TO and thiazole red in an RNA "traffic lights" system allowed for monitoring of siRNA integrity by hybridization of two probes each labelled with one of the dyes.[209] A different approach was demonstrated by the combination of ECHO probes with a Cy5 reporter dye to monitor distribution of poly(A) RNA in the nucleoplasm *in vitro* and fixed cells.[210] Recently an interesting concept from our laboratory was reported where TO was used as an intercalating anchor along with a reporter fluorophore for use in genetic analysis and RNA detection. TO gives the advantage of shorter probes thanks to the increase of thermal stability of obtained complex without loss of specificity, and an "on-off" response upon binding to the target where the reporter dyes allow for multicolour readout. This system was obtained by synthesis of a new modification that locates two dyes, TO and the reporter dye, on a single thymine nucleobase both attached *via* click chemistry (Figure 4.1 A). This probe with two incorporations of the modification with ATTO647N as the reporter dye was used to detect the R516G locus of the CFTR gene, and detection of

the G-mutant by fluorescent melting studies.[118] Its favourable properties such as good F_{ds}/F_{ss} (up to 19.5-fold) arise from the collisional quenching of the dyes in the unbounded state, which upon binding to the target, TO intercalates and an efficient FRET based signal is obtained. The main drawback of this method is the demanding synthesis of the TO-thymidine modification (Scheme 4.1) which limited wider application of this approach as well as high polarity of the monomer and need for UltraMILD protective groups on standard nucleotide monomers . The following work represents an a new design of combinational probes that allows for easy and straightforward synthesis of probe sequence with post synthetic incorporation of fluorescent dyes for further investigation of this probe system.



Scheme 4.1 Synthetic route to Combination probe monomer. Reagents and conditions: (a) DMF, H_2O, TBTA, $CuSO_4$ 5·H_2O, sodium ascorbate, RT, 2 h (n = 3, 38%; n = 8, 29%); (b) CH_2Cl_2, DIPEA, DMF, 2-cyanoethyl-N,N-diisopropyl chlorophosphoramidite, RT, 2 h (n = 3, 70%; n = 8, 66%).[118]

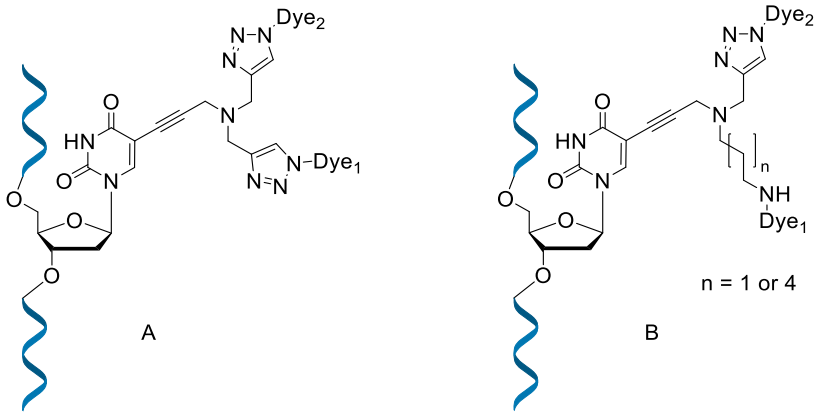
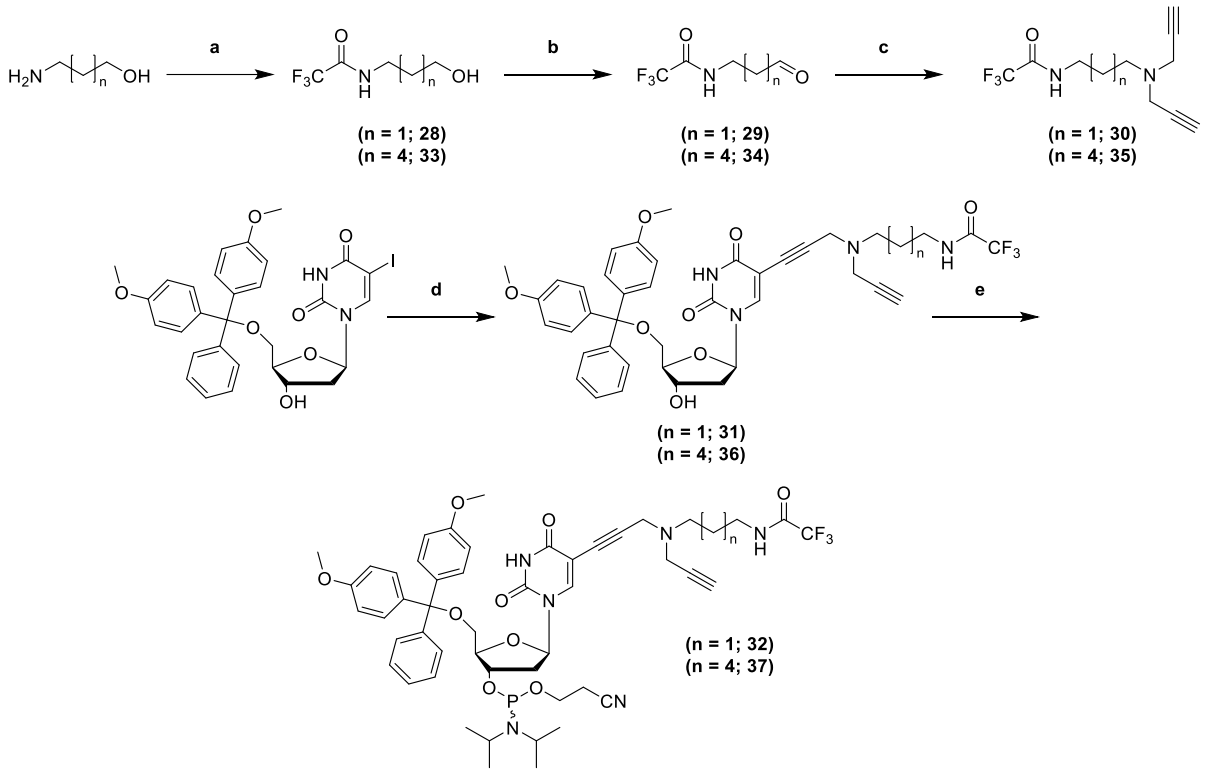


Figure 4.1 Structure of combination probe (A) and new approach (B).

4.2. Materials and methods

4.3. Synthesis of amino-propargyl ($C_{3/6}$) dT monomers

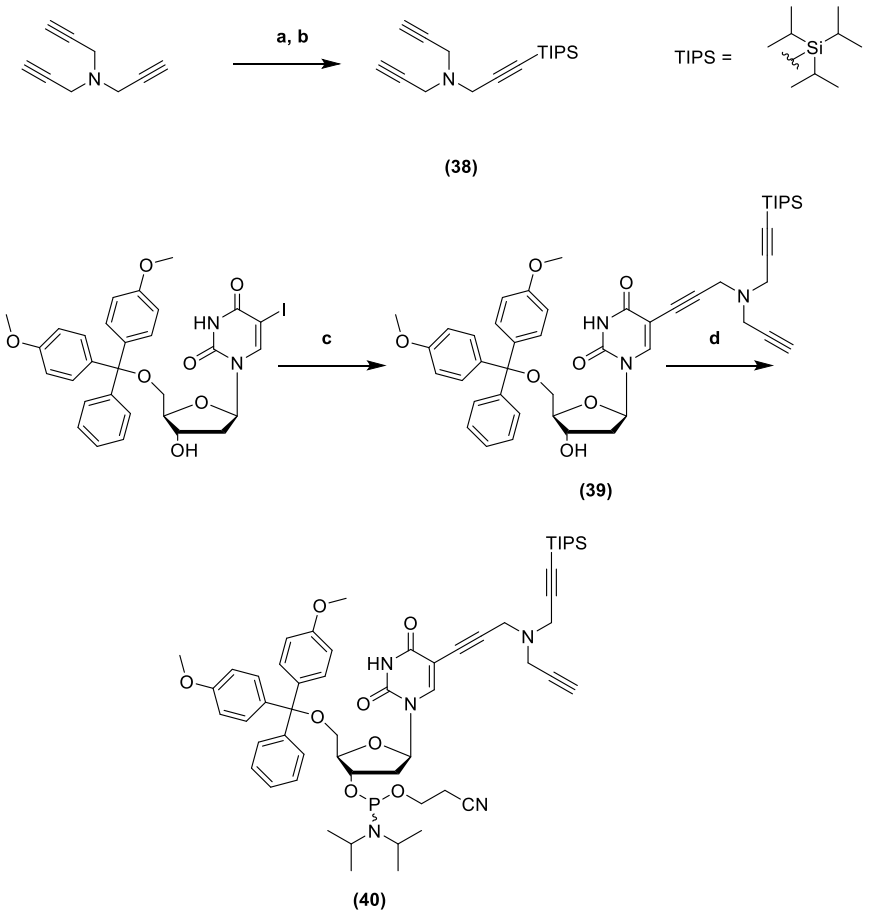
Synthesis of new amino-propargyl-C_3 (**AP-C_3 dT; 32**) and amino-propargyl-C_6 (**AP-C_6 dT; 37**) dT phosphoramidites were based on the synthetic route published in by Qiu *et. al.*[118] The main difference was employment of the orthogonal labelling groups (amine and alkyne) with various lengths of amine linkage (from 3 to 6 carbon atoms). In order to obtain the linkers to which two dyes will be attached, two amino alcohols (3-aminopropanol or 6-aminohexanol) were protected with the TFA group, followed by oxidation of hydroxyl group to the aldehyde. Obtained compounds (**29** and **34**) were subjected to reductive amination with dipropargylamine with high yields. Synthesized linkers (**30** or **35**) were attached to 2'-deoxy-5'-*O*-DMTr-5-iodothymidine (synthesized according to the literature procedure[211]) *via* Sonogashira coupling.[212] Incorporation of these monomers into oligonucleotide sequences was performed as previously described PA, C6, AE and TH modifications, shown in Experimental 6.3.



Scheme 4.2 Synthetic route to **AP-C_3 dT** (n = 1) monomer, reagents and conditions: (a) Neat, ethyl trifluoroacetate, 3 h, 0 °C – RT, 97%; (b) CH_2Cl_2, Dess-Martin periodinane, 2 h, 0 °C – RT, 51%; (c) CH_2Cl_2, dipropargylamine, $NaHB(OAc)_3$, 2 h, RT, 95%; (d) DMF, 5-iodo-5'-DMTr-deoxythymidine, (**30**), $PdCl_2(PPh_3)_2$, CuI, NEt_3, 12 h, RT, 59%; (e) CH_2Cl_2, 2-Cyanoethyl N,N-diisopropylchlorophosphoramidite, DIPEA, 1.5 h, RT, 72%.; Synthetic route to **AP-C_6 dT** (n = 4), reagents and conditions :(a) neat, ethyl trifluoroacetate, 2.5 h, RT, 68%; (b) CH_2Cl_2, Dess-Martin periodinane, 2 h, 0°C – RT, 89%; (c) CH_2Cl_2, dipropargylamine, $NaHB(OAc)_3$, 2 h, RT, 98%; (d) DMF, 5-iodo-5'-DMTr-deoxythymidine, (**35**), $PdCl_2(PPh_3)_2$, CuI, NEt_3, 24 h, RT, 54%; (e) CH_2Cl_2, 2-Cyanoethyl N,N-diisopropylchlorophosphoramidite, DIPEA, 1.5 h, RT, 61%.

4.4. Synthesis of new combination dT monomer

Synthesis of this new monomer (**40**) is based on the previously published work.[118] The only difference between this monomer to the published one is the protection of one propargyl group by TIPS for selective CuAAC labelling of the oligonucleotides. This is similar to a route previously reported by Carell *et al*.[199] Synthesis of this monomer was straightforward, protection of tripropargylamine gave a good yield (**38**) and Sonogashira coupling of obtained linker with the 2'-deoxy-5'-*O*-DMTr-5-iodothymidine followed by phosphitylation resulted in the monomer (**40**). After labelling this new monomer is structurally identical to the published one with the advantage of the ability to selectively label each alkyne.[199]



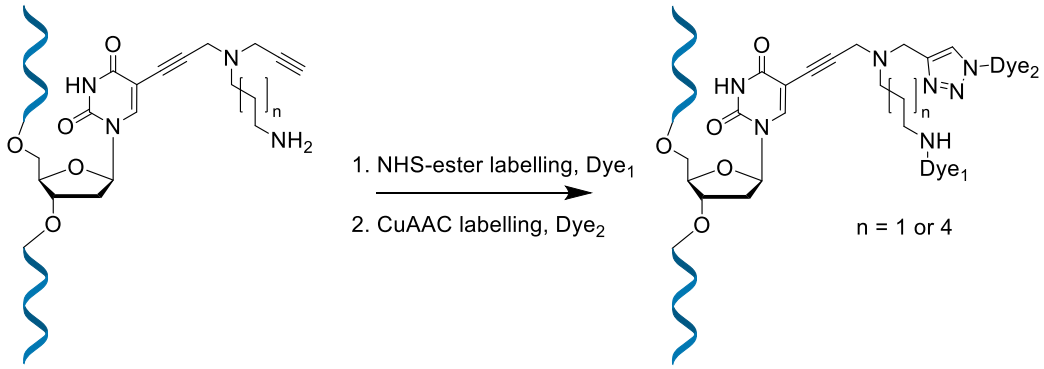
Scheme 4.3 Synthetic route to new **Combination dT** monomer. Reagents and conditions: (a) THF, lithium bis(trimethylsilyl)amide, 45 min, -78°C; (b) THF, TIPS-Cl, 2 h, -78°C, 52% over two steps; (c) DMF, 5-iodo-5'-DMTr-deoxythymidine, (**38**), $Pd(PPh_3)_4$, CuI, NEt_3, 12 h, RT, 50%; (d) CH_2Cl_2, 2-Cyanoethyl N,N-diisopropylchlorophosphoramidite, DIPEA, 1.5 h, RT, 51%.

4.5. Probe design and labelling of Amino-Propargyl-$C_{3/6}$ monomers

Development of combinational probes[118] was a very promising new strategy for a diagnostic tool allowing for versatile modification on a single nucleobase. Introduction of this monomer reduces the number of modified nucleotides that have to be incorporated into a probe sequence. The fluorescent intercalator (TO) gives the advantage of a shorter probe by increasing the duplex stability of the system as well as mismatch disrimination.[168,127] Combination of TO with different reporter dyes (e.g. ROX, HEX, ATTO647N) allows for monitoring of an intense fluorescence signal on a range of analytical devices and gives high fluorescence stability and fluorescence brightness. The synthetic route requires a statistical click (Scheme 4.1 step a) [118] which can lead to low yields. UltraMILD monomers Pac-dA, Ac-dC and iPr-

Pac-dG must be used due to incorporation of TO into the phosphoramidite monomer which is unstable to prolonged ammonia deprotection. In addition, it requires a new synthesis of the monomer for any change in the initial anchor, resulting in decreased versatility in screening for the best structure.

These drawbacks gave rise to the idea of a new monomer (Figure 4.1B, Scheme 4.4) containing two orthogonal groups that could be selectively labelled in a post-synthetic manner. These monomers are equipped with TFA protected amino group for amide coupling reaction and propargyl group for CuAAC chemistry which allows for selective incorporation of desired molecule into the oligonucleotide sequence. Synthesis of these new monomers was straightforward (Scheme 4.2) and incorporation of them into oligonucleotide sequences was carried according to standard protocols (Experimental 6.3.1). Obtained oligonucleotides were labelled with TO_{B6}-NHS ester (Experimental 6.4.1.2). Due to similarity of AP-$C_{3/6}$ to PA and C6 linkers this modification should place the intercalator in the vicinity of major groove.[153] The second dye was introduced in a single pot labelling procedure (Scheme 4.4, Experimental 6.4.4) *via* CuAAC directly and without need for purification after completion of the highly efficient NHS-ester labelling. Initial sequences obtained for this study are given in Table 6.5.



Scheme 4.4 Labelling of AP-$C_{3/6}$ dT containing oligonucleotides by NHS-ester and CuAAC protocols.

4.6. Fluorescence properties of AP-C_3 in combination probes.

To validate this new modification AP-C3 was incorporated into ODN7 5'-CGCTTC**X_1**GTATCTA**X_2**ATTCATC, where **X_1** is AP-C3 and **X_2** is AP-C3 or T. The sequence is identical to the

one published by Qiu et al.[118] (Table 6.5). Initially TO_{B6} was chosen as an intercalating anchor as the closest approximation to the published work, and ATTO647N was chosen as a reporter dye as it gave the best fluorescent response in the previous study (F_{ds}/F_{ss} = 19.5). Single incorporation of a monomer at position **X_1** was carried out as proof of concept (Figure 4.2, Table 6.5).

Initial fluorescence measurements showed no change in fluorescence before and after hybridisation of the TO_{B6}/ATTO647N probe with the DNA target (at λ_{ex} of TO, Figure 4.2). This unexpected behavior showed an interesting property, the lack of response was the result of an equally efficient FRET based fluorescence signal in *both* single and double stranded states and *not* lack of fluorescence. This indicates the possibility of an unspecific interaction of TO in the single strand, yet this unwanted fluorescence signal in the ss state should be minimalized due to collisional quenching of the two dyes.[118] In order to evaluate if this was due to unspecific binding of TO in the ss state, the probe with only TO_{B6} was synthesized. The obtained fluorescence response was not remarkable (F_{ds}/F_{ss} = 1.7) but the differences between unbound and bound state could be detected, indicating that TO combined with ATTO647N was the issue. Additionally when the probe with both dyes (TO_{B6} and ATTO647N) was excited at the λ_{ex} of the ATTO647N (647 nm) the intensity of the signal was double (Table 6.24) in comparison to the λ_{ex} of TO (484 nm), which can be explained by the non-perfect overlap of the λ_{em} of TO with the λ_{ex} of ATTO647N.

Interestingly no significant emission of TO could be observed ($\lambda_{em,\ max}$ = 530 nm) when excited at λ_{ex} of TO. The only emission that could be detected was of ATTO647N dye, suggesting highly efficient transfer of energy (FRET) between the dyes in both states.

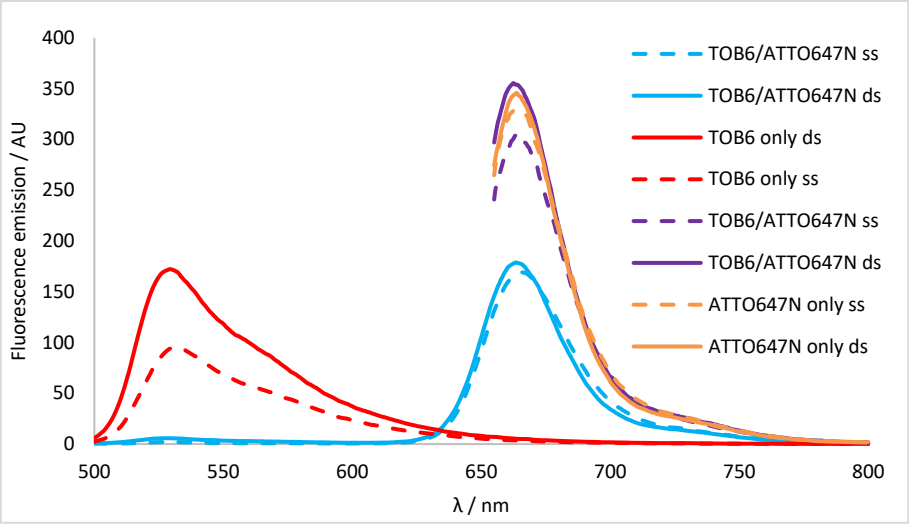


Figure 4.2 Fluorescence emission spectra of ODN7 (5'-CGCTTCXGTATCTATATTCATC) where X is AP-C3 labelled with TO_{B6}, only TO_{B6} and ATTO647N and ATTO647N only at λ_{ex} of 484 nm (TO) and 647 nm (ATTO647N) with DNA target (5'-CTATGATGAATATAGATACAGAAGCGTCAT).

This unexpected high fluorescence in the unbound probe could be attributed to the unfavourable attachment position (CuAAC vs amide) and length of the linker of the TO. To address this issue various combinations of TO (TO_{B6}, TO_{B10} as NHS esters and TO_{B3}-N_3; Figure 4.4) with the reporter dye ATTO647N (azido or NHS ester) were introduced into oligonucleotide probes (Table 6.5). The TO_{B3}-N was the same thiazole orange derivative used in the literature[118] and was obtained previously in the group by Jiegiong Qiu. These TO derivatives and the reporter dye combinations were introduced into ODN7 sequence with position X_1 modified with AP-C_3 in order to screen their fluorescence properties. The data (Figure 4.5) showed that unrelated to the type of attachment and combination of dyes no increased fluorescence (F_{ds}/F_{ss}) could be detected; intensities of fluorescence signals were higher for the TO_{B10} /ATTO647N pair which suggest that the longer linker provides more efficient energy transfer (FRET) before and after binding to the desired target. Differences in fluorescence intensities for ATTO647N dyes can be assigned to the different structures of the linkers: NHS has a short linker where azide has a PEG linker (Figure 4.3).

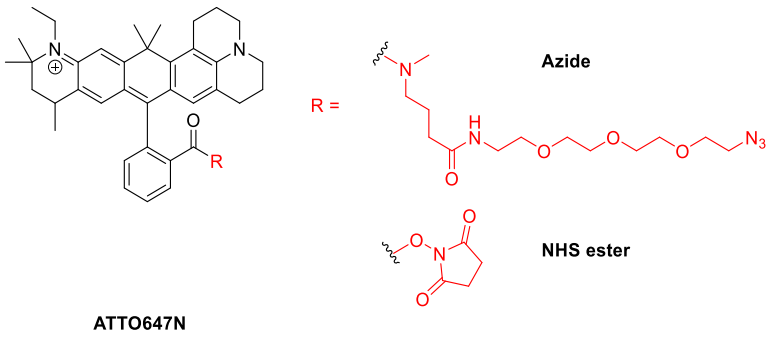


Figure 4.3 Structures of NHS ester and azide-functionalized ATTO647N dye.[213,214]

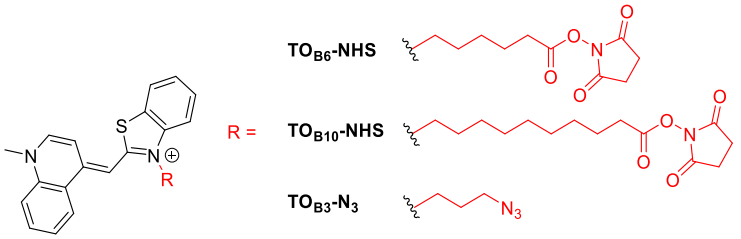


Figure 4.4 Structures of TO derivatives attached by benzothiazole moiety used in the study.

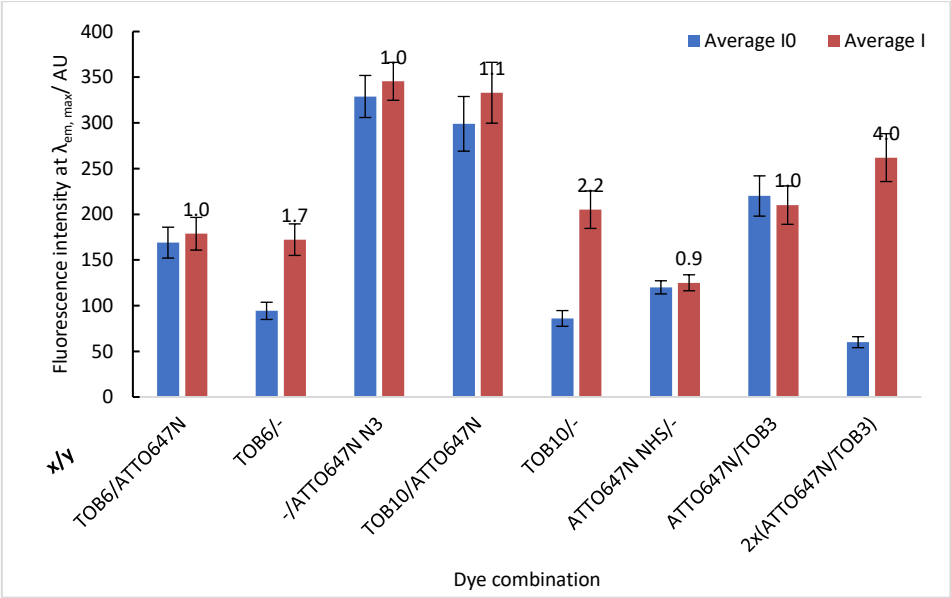


Figure 4.5 Fluorescence emssion data at λ_{ex} of 484 nm (TO), and λ_{em} of 655 nm (ATTO647N) for various TO/ATTO647N combinations in ODN7 (5'-CGCTTC**X$_1$**GTATCTA**X$_2$**ATTCATC), where **X$_1$** is AP-C3 and **X$_2$** is T apart from the double incorporation of the monomer 2x(ATTO647N/TO$_{B3}$), probe against DNA target (5'-CTATGATGAATATAGATACAGAAGCGTCAT), where in **x/y** description **x** is labelled by NHS-ester labelling and **y** by CuAAC, I_0 is intensity of fluorescence for ss probe, I_{max} is intensity of fluorescence for probe hybridized with target. **If calculation were performed similarly to ECHO probes studies,[122] values of F_{ds}/F_{ss} (at single wavelength), only probes with only TO$_{B6}$, TO$_{B10}$ and 2x(ATTO647N/TO$_{B3}$) shows worth mentioning differences and are equal to 1.8, 2.3 and 4.6 respectively. Showing no meaningful difference in this case.**

When sequence ODN7 was labelled only with TO_{B10} a slightly better response was observed in comparison to TO_{B6} (2.2 vs 1.7-fold increase respectively). In order to compare this new modification, double introduction of AP-C_3 monomer at positions X_1 and X_2 into ODN7 sequence (5'-CGCTTC**X_1**GTATCTA**X_2**ATTCATC) was carried out followed by labelling with TO_{B3}-N_3 and ATTO647N-NHS ester (2x(ATTO647N/TO_{B3}); Figure 4.5). In comparison to the study this work is based on, the only difference was the ATTO647N attachment. The obtained F_{ds}/F_{ss} ratio (4.0-fold) was inferior to the published probe system (19.5-fold). Surprisingly a single incorporation of ATTO647N-NHS and TO_{B3}-N_3 at position X_1 resulted in slightly decreased fluorescence upon binding to DNA target, indicating that the double incorporation of this monomer could be a possible solution due to more favourable collisional quenching in single stranded state.

4.7. Fluorescence studies of AP-C_3 and AP-C_6 modification in the 2′-OMe–ORN3 sequence context.

Unpublished results of Qiu showed when the monomer (Scheme 4.1) was incorporated into the 5'-TCATCCTA**X**TCT sequence and labelled with TO_{B3}-N_3/ROX or TO_{B8}-N_3/ROX-N_3, the F_{ds}/F_{ss} was 13.8 and 12.8 respectively. This indicates that the lack of fluorescence response in the case of AP-C_3 could be due to the reporter dye (there are no other examples of single incorporation apart from TO/ROX). A second possibility is that apart from structural similarities between these modifications (Figure 4.6), AP-C_3 is unable to provide a low fluorescence signal for the unbound probe by collisional quenching.

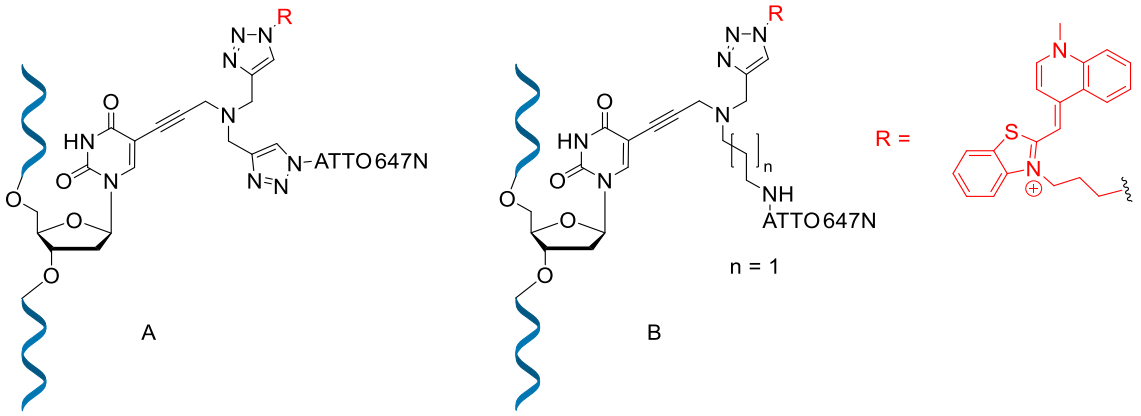


Figure 4.6 Structures of Combinational probe with attached TO_{B3}-N3, ATTO647N-N3 pair and AP-C_3 with attached TO_{B3}-N3 and ATTO647N-NHS ester.

In order to verify this idea a new AP-C_6 monomer was synthesised, in order to provide an additional structural variation, based on the improvement of fluorescence response of C6 over the PA modification (Chapter 2). Both modifications (AP-C_3 and AP-C_6) were incorporated into the previously studied sequence 2'-OMe–(5'-GCAC**X**CUACG) in which cytosine as a neighbouring bases gave one of the highest F_{ds}/F_{ss} ratios with TO_{B6} in all studied sequence contexts. Additionally, the 2'-OMe modification was used as it gave an improvement in the fluorescence response in comparison to the ODN probes. Two new reporter dyes were chosen, Alexa555 and Alexa594 to provide a wider spectral range, both containing an azido group for CuAAC labelling, along with the previously tested ATTO647N as a control. Labelling of this new sequence was carried out according as shown in Paragraph 4.5 and the obtained sequences are given (Table 6.6).

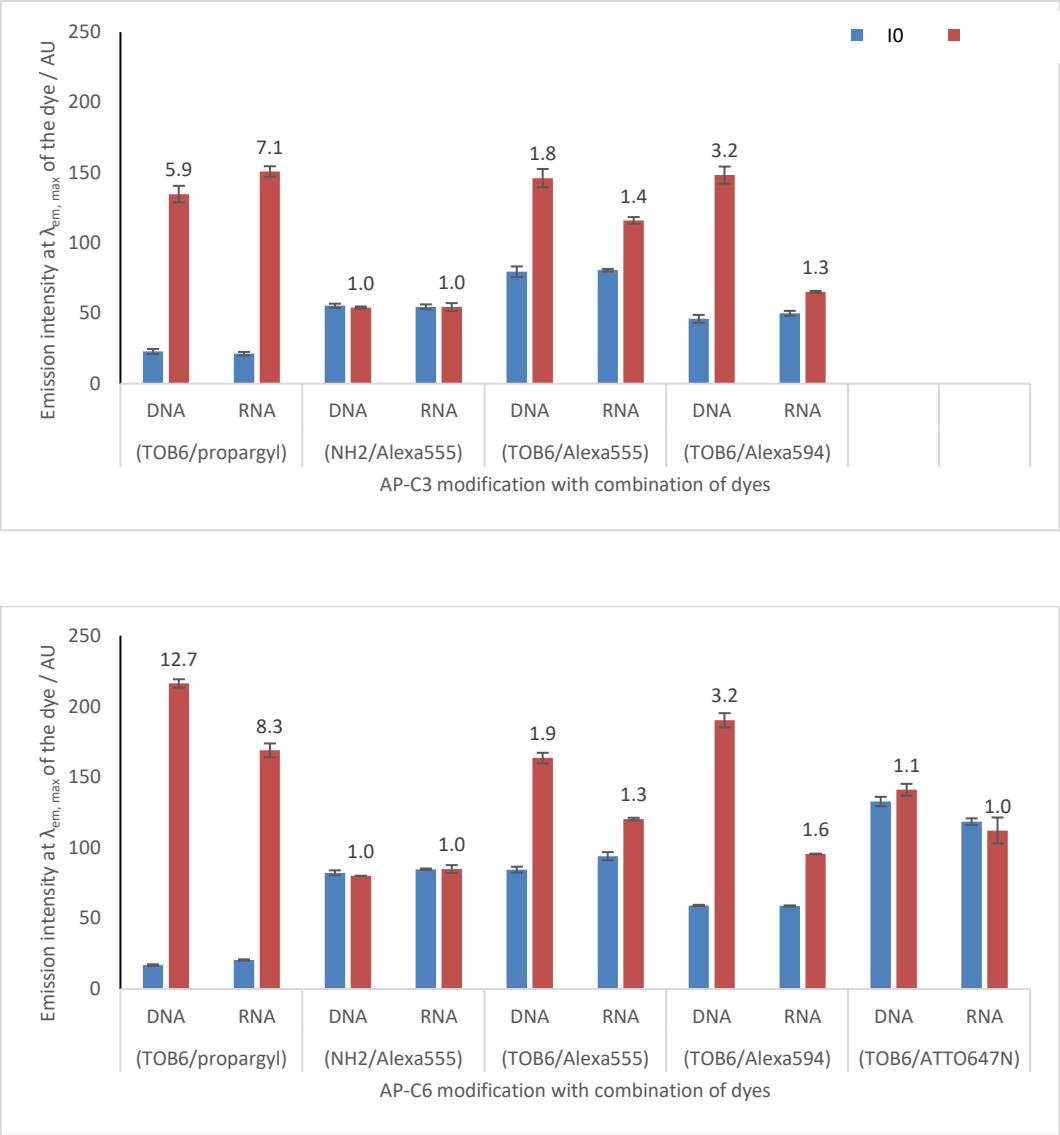


Figure 4.7 Fluorescence emssion intensity at $\lambda_{em,\,max}$ of the dye for ORN3 (2'-OMe–(5'-GCAC**X**CUACG)), where **X** is AP-C3 or AP-C6 modification, probe against matched DNA and 2'-OH–RNA targets. I_0 – fluorescence emission intensity of single stranded probe, I_{max} - fluorescence emission intensity of probe-target duplex, AU - arbitrary units, number above bar = F_{ds}/F_{ss}, for probes containing only TO $\lambda_{em,\,max} = \lambda_{em,\,max}$ of TO, for probes containing reporter dye $\lambda_{em,\,max} = \lambda_{em,\,max}$ of a reporter dye, λ_{ex} in all cases 484 nm. Detailed values: see Table 6.25. **If calculation were performed similarly to ECHO probes studies,[122] values of F_{ds}/F_{ss} (at single wavelength), only probes with only TO_{B6}, TO/Alexa555 and TO/Alexa594 shows worth mentioning differences and are equal to 5.9, 1.9, 3.5 for DNA target and 7.4, 1.5, 1.4 for RNA target (AP-C3 modification) and 12.8, 2.1, 3.8 for DNA target 8.3, 1.3,1.8 for RNA target (AP-C6 modification) respectively. Showing no meaningful difference in this case.**

Fluorescence studies on the new probes were carried out (Figure 4.7) and the results showed that the probes labelled only with TO give good F_{ds}/F_{ss} against DNA and RNA matched targets. The AP-C_6 modification gave a higher response and fluorescence intensity than AP-C_3 (AP-C_6 : 12.7 to 8.3 fold increase and 1.6 times more intense against DNA targets; AP-C_3: 8.3 to 5.9 fold increase and 1.1 more intense against RNA targets). When the new reporter dyes were introduced (Alexa555 and Alexa594)

response rates decreased and the best F_{ds}/F_{ss} was obtained for the AP-C_6 monomer with Alexa594 (F_{ds}/F_{ss} = 3.2), whereas the AP-C_3 monomer gave the same F_{ds}/F_{ss} ratio but AP-C_6 was 1.3 more intense against DNA targets. Responses against the RNA target were smaller (1.3 and 1.6 fold for AP-C3 and AP-C6 respectively) which indicates unfavourable intercalation in the probe-RNA target duplex. Introduction of Alexa555, which should have best spectral overlap with TO ($\lambda_{em\ max}$ of TO = 532 nm, $\lambda_{ex\ max}$ of Alexa555 = 555 nm) gave a moderate response, 1.8 and 1.9 fold increase against DNA targets for AP-C6 and 1.4 and 1.3 fold increase for RNA targets for AP-C3 monomer. Interestingly, the maximum intensities for both dyes were on a similar level. (The fold-increase of the probe is calculated from the difference of the surface area of the fluorescence emission spectrum of bound and unbound probe). Higher fluorescence intensity in the ss probe was observed for Alexa555 in both modifications, which could be explained by a control experiment where the probe was labelled only with Alexa555 and excited at 484 nm (λ_{ex} of TO). This resulted in a fluorescence signal as the absorption band of Alexa555 overlaps at this wavelength, and F_{ds}/F_{ss} = 1.0 as expected as this dye is not an intercalator. A control experiment where AP-C_6 was labelled with TO_{B6} and ATTO647N gave similar results as previously (Figure 4.5) showing the importance of choosing the reporter dye. In summary the AP-C_3 and AP-C_6 modifications are not allowing for effective collisional quenching between TO and the reporter dye, in contrast to the previously developed modification.[118]

4.8. UV melting studies of AP-C_3 and AP-C_6 modification in a 2′-OMe–(5′-ORN3) sequence context against DNA and RNA targets.

To further evaluate these probe systems, UV melting studies were performed (Table 6.12 and Figure 4.8) on a 2′-OMe–(ORN3) (5′-GCAC**X**CUACG) probe sequence where **X** is the new modification. In nearly all cases when the probe was labelled with *both* TO and the reporter dye a decrease in the melting temperatures against DNA targets was recorded (from -6.1 to -2.0°C) in comparison to the unlabelled probe sequence. Exception was the TO/Alexa555 combination for both modification (+2.3 °C for AP-C_3 and +3.9 °C for AP-C_6) against DNA targets in comparison to the increase of T_m achieved by the

unlabelled probe (modification without any dyes attached, AP-C_3 = +3.2 °C; AP-C_6 = +1.9 °C) compared to the unmodified duplex.

Incorporation of only TO_{B6} into AP-C6 monomer resulted in a high increase of thermal stability (ΔT_m = +9.9 °C) against the DNA target (data for AP-C3 were not obtained), and in every single case addition of the reporter dye reduced this value. This suggests non-specific interaction of the second dye with TO reducing its stabilisation abilities or entropic destabilisation of the duplex by forcing the reporter dye into a hydrophilic environment relative to the single stranded state. Interestingly the control probe design from previous studies (TO/ATTO647N) with AP-C_6 gave a slight increase of thermal stabilisation (ΔT_m = +1.5 °C).

When the same probes were tested against the RNA targets, higher T_m was observed than for the DNA targets, which is consistent with the previous results with AE and C6 modifications (Chapter2). Unfortunately, when combinations of TO/reporter dye were compared to the unlabelled probe (ΔT_m for AP-C_3 +5.0 °C; ΔT_m for AP-C_6 +5.4 °C, to the natural RNA-RNA duplex: dashed bars on far right in Figure 4.8) a decrease in T_m was observed in all cases. Even more, introduction of only TO labelled probes in both cases resulted in small or no increase of T_m (+0.1 °C and +1.5 °C).

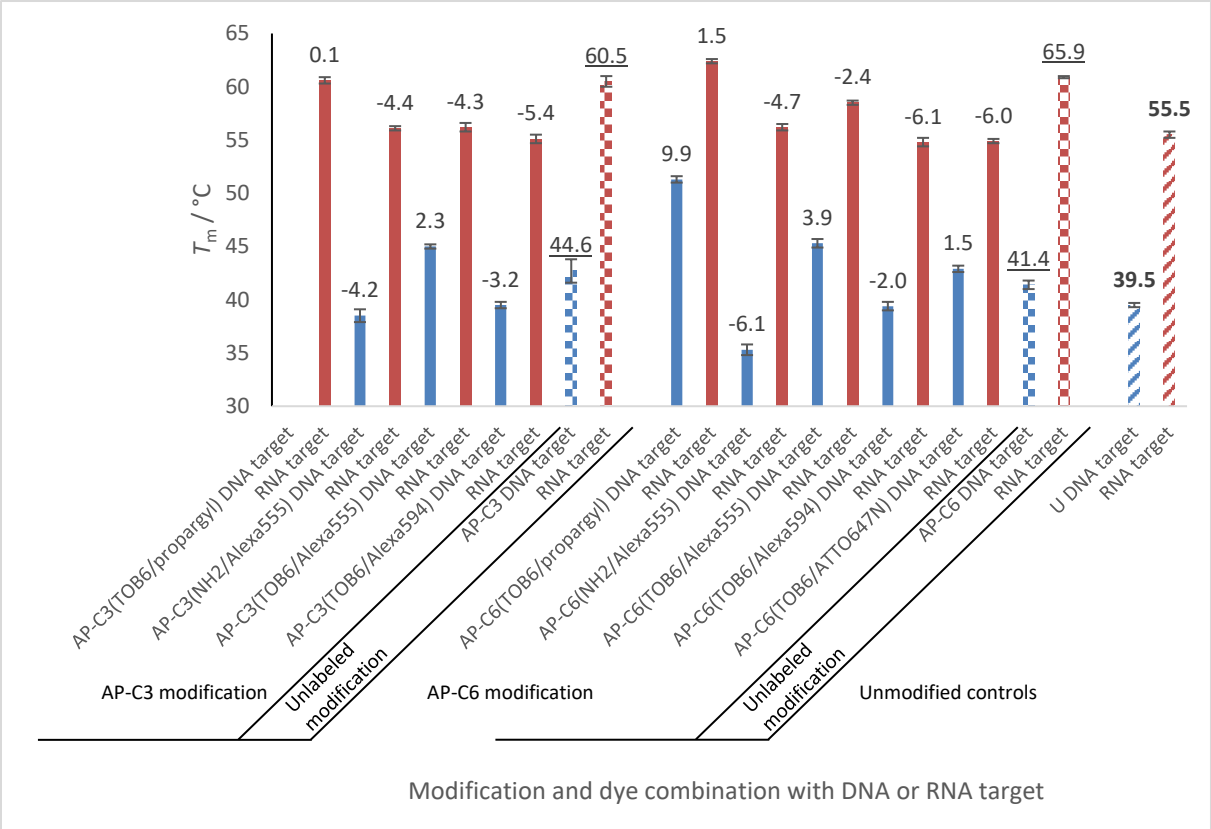


Figure 4.8 Melting temperatures for ORN3 (2'-OMe–(5'-GCA**C**X**C**UACG)), where **X** is AP-C3 or AP-C6, probe sequence labelled with TO_{B6} as NHS ester and Alexa555, Alexa594 and ATTO647N as azides duplexes with DNA and RNA matched targets (ΔT_m) in comparison to the unlabelled probes (T_m, underlined), bold number are actual values of T_m for unmodified controls. Conditions: data obtained in a buffer containing 10 mM phosphate 200 mM NaCl at pH 7.0, oligonucleotide concentrations were 1.0 µM of probe and 1.1 µM of target strand, detailed values see Table 6.12.

These decreases in T_m are caused by the introduction of a second dye. Interestingly the only TO labelled modification causes increase in stability of formed duplex. As showed in Chapter 2 no direct correlation between ΔT_m and F_{ds}/F_{ss} could be observed. This general decrease of T_m and unfavourable fluorescence properties for TO/reporter dye combinations (low increase of fluorescence response) for both modifications indicates the inadequacy of this design for combinational probes, although this thymidine modification could be used as a versatile monomer for selective incorporation of labels on a single nucleobase in oligonucleotide sequences (Table 6.12). A solution to this problem would be a new modification (Scheme 4.3) where one propargyl group is protected with TIPS which will allow for selective incorporation of fluorescent dyes according to the published procedure[199] into the exact probe system developed previously in our group.[118] This simple procedure would allow for easy and convenient probe synthesis and further studies.

4.9. Conclusions

In summary, based on previously published work[118] a new approach was developed involving synthesis of two new monomers AP-C_3 and AP-C_6 equipped with amino and propargyl groups for orthogonal labelling of oligonucleotides with various dyes. A successful and efficient protocol for single tube labelling of oligonucleotides resulted in a range of probes with various combinations of dyes. An intercalating fluorescent anchor (TO) attached by its benzothiazole moiety gave good fluorescence signals with DNA and RNA targets when no reporter dye was present, as well good thermal duplex stabilisation with DNA targets. Incorporation of the reporter dye resulted in highly efficient energy transfer via FRET in both ss and ds states which unfortunately led to either no fluorescence change or small F_{ds}/F_{ss} for various TO derivatives (TO_{B6}, TO_{B10}, TO_{B3}) and reporter dyes (Alexa555, Alexa594 and ATOT647N). A general decrease of thermal stability in TO/dye systems, was observed, whereas for TO-only probes, good fluorescent increases against DNA and small increases against RNA targets were observed. This suggest non-specific interactions between dyes and inefficient collisional quenching when AP-C_3 or AP-C_6 were used. Although these new monomers were not suitable for this study, synthetic versatility and an established protocol for single tube labelling with two molecules on a single nucleobase provides a base for further studies. Additionally, good F_{ds}/F_{ss} responses of TO-only labelled probes suggests an opportunity of incorporation of other functional molecules (e.g. metallodrugs).[215]

5. Conclusions and future work

In summary, new highly promising groove directing fluorescent duplex stabilising modifications (C6 – major groove and AE – minor groove) conjugated with thiazole orange (TO) were synthesised and evaluated. An Important aim of the work was to exploit the properties of the modifications (PA, C6 and AE) with respect to two different DNA attachment position of TO (TO_B or TO_Q). A strong correlation between attachment position and fluorescence response was most noticeable for C6-TO_B and AE-TO_Q, similar to previous studies on TO attached to oligonucleotides by a chiral phosphate linkage (R_p and R_s).[111] In my work, both F_{ds}/F_{ss} (up to 2.7-fold compared to up to 11.1-fold) and thermal melting (+1.5 °C and +6.5 °C compared to up to +14.3 °C) were superior to the published work, even in case of DNA-based (2'-deoxyribose) probes. Further development involved modification of the probe scaffold. Introduction of 2'-OMe sugar modifications greatly improved F_{ds}/F_{ss}, mostly by reducing F_{ss} and to some extent by improving F_{ds} especially in the case of the AE modification. Improvement was mostly visible for DNA targets resulting in 50 and 34-fold enhancements for AE-TO_{B6}. Detection of RNA targets for potential 'live cell imagining' is of great importance. Fluorescence enhancements for RNA targets were impressive, up to 21-fold for C6-TO_{B6}. Those values are comparable or higher than published ones, which gave from 7 to 30-fold enhancement for ECHO probes[122] and up to 13.4-fold for DNA FIT probes.[134,135] Fluorescence increases both in the published work and in this thesis are strongly sequence dependent. Generally, a pyrimidine environment shows favourable F_{ds}/F_{ss}, relative to purines, especially in the case of guanine. This unfavourable F_{ds}/F_{ss} for guanine is caused by strong fluorescence of the single stranded probe caused by self-dimerization[165] or G-stacking.[103] Replacement of guanine for inosine did solve the issue of strong single stranded fluorescence, and led to unspecific binding to other sequences. In conclusion it is wise to avoid guanine stacking environments around TO, as previously shown in case of ECHO probes.

The fluorescence properties of our developed system makes it an ideal candidate for live cell studies as already demonstrated for two other probe systems (ECHO and FIT).[122,134] Additionally high quantum

yields (up to 0.58) of our probe system were on a par with or higher than FIT probes (up to 0.32)[130] or ECHO probes (up to 0.44)[122]. An added benefit of our probe system is its ease of synthesis (the C6 thymidine modification is commercially available). In addition, the protocol for rapid (5 min) labelling with the NHS-ester of TO is simple and high yielding.

The intercalating properties of thiazole orange are of most importance, resulting in both increased fluorescence upon binding to the target oligonucleotide and increased melting temperature of the duplex. The probe systems produced in this work give impressive increases in duplex stability, up to 19.3 °C for AE-TO_{Q6} even with a single TO moiety, which is comparable to the ECHO probe system[122]. Hence, the probe length can be reduced whilst still maintaining good target affinity. This allows for an increase in mismatch discrimination. Interestingly the C6-TO_{B6} combination gave higher increases in T_m than TO_{Q6}. This was not observed in case of AE modification where both (TO_B and TO_Q) gave similar increases of T_m. In terms of mismatch discrimination by melting temperature, for C6-TO_{B6} and AE-TO_{Q6} highly favourable mismatch discrimination is obtained when the mispaired base is placed at positions -1 or +1 relative to the TO-nucleotide. Mismatch discrimination by T_m is not as good if the TO-thymidine nucleotide is the mismatched base pair. In conclusion, excellent duplex melting and fluorescence intensity changes give the probe systems described in Chapter 2 have great potential for SNP detection. In some cases they exceed the fluorescence and thermal stabilisation properties of existing probes.

The next step with this design will be to use the nucleobase sequence of the FDA-approved oligonucleotide drug Mipomersen, which targets ApoB-100 mRNA.[216] An *in vitro* assay will be used to determine the optimal TO incorporation pattern that retains cleavage of the target RNA by human RNase HC, using Mipomersen as a benchmark. Potency will be evaluated by measuring ApoB-100 mRNA levels in Hep3B cells using RT qPCR.

The AE-TO_{Q6} and C6-TO_{B6} modifications will also be evaluated in exon skipping assays using oligonucleotides with 2´-OMe sugars combined with a phosphorothioate backbone. A splice-switching Luciferase assays will be conducted to determine the exon-skipping activity. This model is commonly used in the field.[217] It uses HeLa cells that are stably transfected with a recombinant plasmid pLuc/705 which is a luciferase gene interrupted by the insertion of a single-point mutation from the human *β*-globin intron 2 (IVS2-705), which causes *β*-thalassemia. Gymnotic oligonucleotide delivery will be conducted in addition to the use of transfection agents. TO is slightly lipophilic and has a positive charge which might increase the interaction of the oligonucleotide with the membrane. Nuclease stability of the oligonucleotide might also be improved by the presence of TO, and this might negate the need for heavy modification of the oligonucleotide.

A different approach was explored in Chapter 3 where a new L-threoninol backbone was evaluated in a FIT probe design. Attempts were made to conjugate the amino-group of this new acyclic backbone with short linker carboxylic acid TO derivatives, but unfortunately, the desired products were not obtained. However, CuAAC-catalysed labelling of the probes with TO-alkyne after amine to azide conversion using the diazotransfer reagent ISAHC provided a straightforward synthesis protocol for the desired conjugate. Unfortunately the fluorescence properties of this system were not satisfactory and further investigations are warranted.

Finally, new promising thymidine monomers for orthogonal oligonucleotide labelling by the CuAAC reaction and by amide bond formation were synthesized (AP-C_3 and AP-C_6, Chapter 4). These new modifications were designed to simplify the previously developed FRET probe signalling system (combination probes) for multicolour readout where thiazole orange is the donor dye. The fluorescence responses were hindered by the high fluorescence background in the unbound single stranded probe, resulting in low F_{ds}/F_{ss} ratios. Nevertheless, highly efficient FRET transfer from TO to the reporter dye was obtained. The fluorescence properties were improved with the double incorporation of the new monomer containing both TO and the reporter dye, and in addition, good

fluorescence increases in the TO-only probes were obtained. These findings suggest the need for further detailed studies on this system, ideally involving fluorescence lifetime measurements. The amine/alkyne T-monomer could also be useful for dense orthogonal labelling of oligonucleotides with other reporter groups. Future work will involve multiple incorporation of monomer with a reporter dye in order to overcome low F_{ds}/F_{ss} values, followed by studies in human cells.

Experimental

6. Chapter 6 - Experimental

6.1. General synthetic procedures

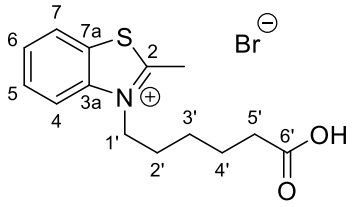
All reagents were purchased from Sigma-Aldrich, Acros Organics, Invitrogen or Fisher Scientific and used without further purification. 3 Å Molecular sieves (beads, 4 – 8 mesh, Sigma-Aldrich) were used to dry MeOH and EtOH. Anhydrous CH_2Cl_2, DMF and MeCN were collected from a Grubbs-type SPS. Thin layer chromatography (TLC) was performed using Merck TLC silica gel 60 F_{254} plates (0.22 mm thickness, aluminium backed) and the compounds were visualized by irradiation at 254/365 nm and stained with *p*-anisaldehyde (*p*-anisaldehyde (11.5 mL), glacial acetic acid (4.8 mL), conc. sulfuric acid (15.7 mL) and 95% EtOH (423 mL)) or potassium permanganate ($KMnO_4$ (1.5 g), K_2CO_3 (10 g), and NaOH (10%, 1.25 mL) in H_2O (200 mL)).

^{1}H NMR spectra were measured at 400 MHz on a Bruker DPX400 (AVIIIHD 400) spectrometer or at 500 MHz on a Bruker AVIIIHD 500 spectrometer. ^{13}C NMR spectra were measured at 101 MHz on a Bruker DPX400 spectrometer or at 126 MHz on a Bruker AVIIIHD 500 spectrometer. ^{31}P NMR and ^{19}F NMR spectra were recorded on a Bruker AVIIIHD 400 spectrometer at 162 MHz and 376 MHz respectively. ^{1}H were internally referenced to the appropriate residual undeuterated solvent signal; ^{13}C NMR spectra referenced to the deuterated solvent. Assignment of the signals was aided by COSY (^{1}H - ^{1}H), HSQC-DEPT, HSQC (^{1}H - ^{13}C) and HMBC (^{1}H - ^{13}C) experiments. Aromatic carbon without attached proton was abbreviated with Ar and aromatic carbon with the proton attached was abbreviated Ar-H.

Low-resolution mass spectra (LRMS) were recorded using electrospray ionisation (ESI^+ or ESI^-) on a Waters ZMD quadrupole mass spectrometer in HPLC grade methanol. High-resolution mass spectra (HRMS) were recorded in HPLC grade methanol using electrospray ionisation (EI) on a Bruker APEX III FT-ICR mass spectrometer.

6.2. Synthesised compounds

6.2.1. Synthesis of 3-(5-carboxypentyl)-2-methylbenzothiazol-3-ium bromide (**1**)

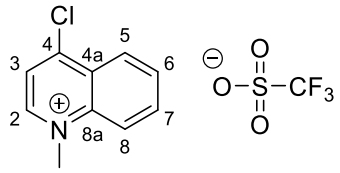


To a stirred solution of 2-methylbenzothiazole (9.11 mL, 71.7 mmol, 1.4 eq) in anhydrous MeCN (10 mL) under an argon atmosphere, 6-bromohexanoic acid (10.0 g, 51.2 mmol, 1.0 eq) was added. The solution was heated under reflux for 48 h and cooled to RT The precipitate was collected by filtration and washed with Et_2O (2 × 15 mL), to give the product as an off-white solid (7.2 g, 20.9 mmol, 41%).

^{1}H NMR (400 MHz, d_6-DMSO): δ 12.04 (br s, 1H, OH), 8.49 (dd, *J* = 8.3, 1.3 Hz, 1H, H^4 or H^7), 8.36 (d, *J* = 8.5 Hz, 1H, H^4 or H^7), 7.88 (ddd, *J* = 8.5, 7.2, 1.3 Hz, 1H, H^5 or H^6), 7.80 (ddd, *J* = 8.3, 7.2, 1.0 Hz, 1H, H^5 or H^6), 4.72 (t, *J* = 8.0 Hz, 2H, $H^{1'}$), 3.23 (s, 3H, CH_3), 2.22 (t, *J* = 7.2 Hz, 2H, $H^{5'}$), 1.85 (app. p, *J* = 8.0 Hz, 2H, $H^{2'}$), 1.56 (app. p, *J* = 7.2 Hz, 2H, $H^{4'}$), 1.50 – 1.40 (m, 2H, $H^{4'}$);

^{13}C NMR (101 MHz, d_6-DMSO): δ 177.6 (C2), 174.8 (C6'), 141.3 (C3a or C7a), 129.8 (C5 or C6), 129.6 (C3a or C7a), 128.5 (C5 or C6), 125.2 (C4 or C7), 117.4 (C4 or C7), 49.6 (C1'), 33.9 (C5'), 28.0 (C2'), 25.9 (C3'), 24.5 (C4'), 17.4 (CH_3); LRMS (ESI$^+$) *m/z* (%): 264.1 ([M-Br]$^+$, 100). Spectral data were in agreement with literature values.[218,114]

6.2.2. Synthesis of 4-chloro-1-methylquinolin-1-ium trifluoromethanesulfonate (**2**)



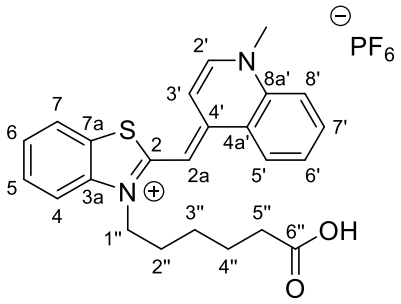
To a stirred solution of 4-chloroquinoline (0.49 g, 3.0 mmol, 1.0 eq) in anhydrous MeCN (6 mL), methyl trifluoromethanesulfonate was added (0.34 mL, 3.0 mmol, 1.0 eq). The mixture was stirred for 3 h under an argon atmosphere at RT. The reaction mixture was precipitated by addition of Et_2O (10 mL), filtration and washed with Et_2O (2 × 5 mL) to give the product as a white solid (0.89 g, 2.7 mmol, 90%).

^{1}H NMR (400 MHz, d_6-DMSO): δ 9.51 (d, *J* = 6.4, 1H, H^2), 8.64 – 8.56 (m, 2H, H^5 and H^8), 8.51 (d, *J* = 6.4 Hz, 1H, H^3), 8.38 (ddd, *J* = 8.8, 7.0, 1.4 Hz, 1H, H^6 or H^7), 8.18 (ddd, *J* = 8.1, 7.0, 0.9 Hz, 1H, H^6 or H^7), 4.62 (s, 3H, CH_3);

^{13}C NMR (101 MHz, d_6-DMSO): δ 151.8 (C4), 150.1 (C2), 139.1 (C4a or C8a), 136.3 (C6 or C7), 131.3 (C6 or C7), 126.9 (C4a or C8a), 126.1 (C5 or C8), 122.7 (C3), 120.2 (C5 or C8), 45.4 (CH_3);

LRMS (ESI^+) *m/z* (%): 178.0 ($[M\text{-}SO_3CF_3]^+$, 100); LRMS (ESI^-) *m/z* (%): 149.0 ($[SO_3CF_3]^-$, 100); HRMS (ESI^+) *m/z* $[M\text{-}SO_3CF_3]^+$ for $C_{10}H_9NCl^+$ calc. 178.0418 found: 178.0419; R_f = 0.49 (MeOH:CH_2Cl_2, *v*:*v* = 2:8), UV.

6.2.3. Synthesis of N-(5-carboxypentyl)-2-[(1,4-dihydro-1-methylquinolin-4-ylidene) methyl]benzothiazol-3-ium hexafluorophosphate (**3**, **TO$_{B6}$**)

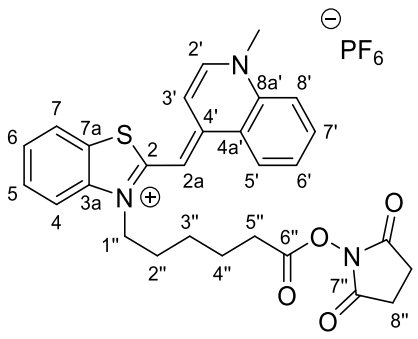


To a stirred solution of **1** (0.93 g, 2.7 mmol, 1.0 eq) and **2** (1.1 g, 3.2 mmol, 1.2 eq) in a mixture of anhydrous MeOH (34 mL) and anhydrous CH_2Cl_2 (34 mL) under an argon atmosphere at RT, was added anhydrous Et_3N (0.94 mL, 6.8 mmol, 2.5 eq). The solution turned red instantly and was stirred for 15 min. Et_2O (400 mL) was added, and the resulting solid was collected by filtration and washed with Et_2O (2 x 20 mL). The crude red solid was dissolved in THF (26 mL) and H_2O (24 mL), LiOH (0.21 g, 8.6 mmol, 3.2 eq) was added and the reaction mixture was stirred for 8 h. To the stirring suspension was added HCl (2.5%, 16 mL) to give a red solution, the aqueous layer was extracted with CH_2Cl_2:2-propanol (*v*:*v* = 3:1, 5 × 80 mL). The organic layer was dried with $MgSO_4$, filtered and evaporated to give the product as a red solid (0.97 g, 1.8 mmol). Salt metathesis was performed as follows: $NaPF_6$ (0.79 g, 4.7 mmol, 2.8 eq to the crude product) was added to a stirred solution of the crude product in H_2O:2-propanol (*v*:*v* = 3.4:1.0; 800 mL). A red solid precipitated and was collected by filtration and washed with CH_2Cl_2:2-propanol (*v*:*v* = 8:2, 2 × 10 mL) and H_2O (2 × 15 mL) to give the product as a red solid (0.59 g, 1.1 mmol, 41%).

^{1}H NMR (400 MHz, d_6-DMSO): δ 8.69 (d, *J* = 8.4 Hz, 1H, $H^{8'}$), 8.57 (d, *J* = 7.2 Hz, 1H, $H^{2'}$), 8.10 – 7.93 (m, 3H, H^4 or H^7, $H^{5'}$, $H^{6'}$), 7.78 (ddd, *J* = 8.4, 6.5, 1.5 Hz, 1H, $H^{7'}$), 7.72 (d, *J* = 8.3 Hz, 1H, H^4 or H^7), 7.62 – 7.54 (m, 1H, H^5 or H^6), 7.39 (app. t, *J* = 7.6 Hz, 1H, H^5 or H^6), 7.34 (d, *J* = 7.2 Hz, 1H, $H^{3'}$), 6.88 (s, 1H, H^{2a}), 4.56 (t, *J* = 7.5 Hz, 2H, $H^{1''}$), 4.15 (s, 3H, CH_3), 2.15 (t, *J* = 7.2 Hz, 2H, $H^{5''}$), 1.77 (app. p, *J* = 7.5 Hz, 2H, $H^{2''}$), 1.58 (app. p, *J* = 7.2 Hz, 2H, $H^{4''}$), 1.51 – 1.41 (m, 2H, $H^{3''}$);

^{13}C NMR (101 MHz, d_6-DMSO): δ 174.7 (C6''), 159.1 (C2), 148.6 (C4'), 145.0 (C2'), 139.9 (C3a or C7a), 138.0 (C4a' or C8a'), 133.2 (C4 or C7 or C5' or C6'), 128.2 (C5 or C6), 127.1 (C7'), 125.3 (C8'), 124.4 (C5 or C6), 124.0 (C4a' or C8a'), 123.8 (C3a or C7a), 122.9 (C4 or C7 or C5' or C6'), 118.2 (C4 or C7 or C5' or C6'), 112.9 (C4 or C7 or C5 or C6'), 107.9 (C3'), 87.4 (C2a), 45.6 (C1''), 42.3 (CH_3), 34.6 (C5''), 26.7 (C2''), 25.8 (C3''), 24.6 (C4''); LRMS (ESI^+): *m/z* (%): 405.2 ($[M\text{-}PF_6]^+$, (100); LRMS (ESI^-): *m/z* (%): 145.0 ($[PF_6]^-$, 100); HRMS (ESI^+) *m/z* $[M\text{-}PF_6]^+$ for $C_{24}H_{25}N_2O_2S^+$ calc. 405.1631 found: 405.1629.; R_f = 0.22 (MeOH:CH_2Cl_2, *v*:*v* = 1:9), UV. Spectral data were in agreement with literature values.[114]

6.2.4. Synthesis of N-hydroxysuccinimide ester of N-(5-carboxypentyl)-2-[(1,4-dihydro-1-methylquinolin-4-ylidene)methyl]benzothiazol-3-ium hexafluorophosphate (**4**, **TO$_{B6}$-NHS**)



To a stirred solution of **3** (0.20 g, 0.36 mmol, 1.0 eq) and DIPEA (0.31 mL, 1.8 mmol, 5.1 eq) in anhydrous DMF (3.5 mL) under an argon atmosphere at RT, was added *N*,*N*,*N*′,*N*′-tetramethyl-*O*-(*N*-succinimidyl)uronium tetrafluoroborate (TSTU) (0.23 g, 0.76 mmol, 2.1 eq). The solution was stirred for 0.5 h and evaporated, CH_2Cl_2 (15 mL) was added and the solution was washed with HCl (5%, 15 mL) and H_2O (25 mL). The organic layer was dried with Na_2SO_4 filtered and evaporated, followed by purification by column chromatography on silica gel (5-60% MeCN/CH_2Cl_2) to give the product as a red solid (0.11 g, 0.17 mmol, 47%).

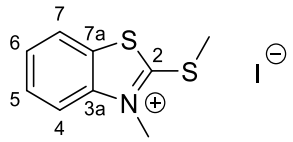
^{1}H NMR (400 MHz, d_6-DMSO): δ 8.68 (dd, *J* = 8.5, 1.2 Hz, 1H, $H^{8'}$), 8.57 (d, *J* = 7.2 Hz, 1H, $H^{2'}$), 8.08 – 7.95 (m, 3H, $H^{5'}$, $H^{6'}$, H^4 or H^7), 7.77 (ddd, *J* = 8.5, 6.4, 1.7 Hz, 1H, $H^{7'}$), 7.72 (d, *J* = 8.4 Hz, 1H, H^4 or H^7), 7.58 (ddd, *J* = 8.4, 7.4, 1.2 Hz, 1H, H^5 or H^6), 7.40 (t, *J* = 7.4 Hz, 1H, H^5 or H^6), 7.35 (d, *J* = 7.2 Hz, 1H, $H^{3'}$),

6.88 (s, 1H, H^{2a}), 4.58 (t, *J* = 7.5 Hz, 2H, $H^{1''}$), 4.15 (s, 3H, CH_3), 2.80 (s, 4H, $H^{8''}$), 2.69 (t, *J* = 7.3 Hz, 2H, $H^{5''}$), 1.83 (app. p, *J* = 7.5 Hz, 2H, $H^{2''}$), 1.73 (app. p, *J* = 7.3 Hz, 2H, $H^{4''}$), 1.57 (m, 2H, $H^{3''}$);

^{13}C NMR (101 MHz, d_6-DMSO): δ = 170.2 (C7''), 168.9 (C6''), 159.2 (C2), 148.7 (C4'), 145.0 (C2'), 139.9 (C3a or C7a), 138.0 (C4a' or C8a'), 133.2 (C4 or C7 or C5' or C6') 128.2 (C5 or C6), 127.0 (C7'), 125.4 (C8'), 124.5 (C5 or C6), 124.0 (C4a' or C8a'), 123.8 (C3a or C7a), 122.9 (C4 or C7 or C5' or 6'), 118.2 (C4 or C7 or C5' or 6'), 112.9 (C4 or C7 or C5' or 6'), 108.0 (C3'), 87.5 (C2a), 45.5 (C1''), 42.4 (CH_3), 30.0 (C5''), 26.4 (C2''), 25.4 (C8''), 25.2 (C3''), 24.0 (C4'');

LRMS (ESI^-): *m/z* (%): 145.0 ($[PF_6]^-$, 100); LRMS (ESI^+): *m/z* (%): 502.2 ($[M\text{-}PF_6]^+$, 100); HRMS (ESI^+) *m/z* $[M\text{-}PF_6]^+$ for $C_{28}H_{28}N_3O_4S^+$ calc. 502.1795 found: 502.1795; R_f = 0.67 (MeOH:CH_2Cl_2, *v*:*v* = 1:9), UV.

6.2.5. Synthesis of 3-methyl-2-(methylthio)benzothiazol-3-ium iodide (**5**)



2-(Methylthio)benzothiazole (1.0 g, 5.6 mmol, 1.0 eq) was dissolved in anhydrous MeCN (3 mL) in a pressure vial under an argon atmosphere. Iodomethane (0.70 mL, 11.2 mmol, 2.0 eq) was added to the stirring solution. The mixture was stirred at 50 °C for 24 h, cooled to RT, precipitated by addition of Et_2O (10 mL). Obtained solid was collected by filtration and washed with Et_2O (2 × 5 mL) to give the product as a yellow solid (0.84 g, 2.6 mmol, 46%).

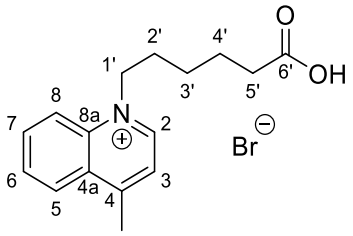
^{1}H NMR (400 MHz, d_6-DMSO): δ 8.40 (dd, *J* = 8.2, 1.0 Hz, 1H, H^4 or H^7), 8.20 (d, *J* = 8.5 Hz, 1H, H^4 or H^7), 7.84 (ddd, *J* = 8.5, 7.3, 1.0 Hz, 1H, H^5 or H^6), 7.73 (ddd, *J* = 8.2, 7.3, 1.0 Hz, 1H, H^5 or H^6), 4.11 (s, 3H, N-CH_3), 3.13 (s, 3H, S-CH_3);

^{13}C NMR (101 MHz, d_6-DMSO): δ 181.7 (C2), 143.0 (C3a or C7a), 129.7 (C5 or C6), 128.7 (C3a or C7a), 127.5 (C5 or C6), 124.5 (C4 or C7), 116.2 (C4 or C7), 37.1 (N-CH_3), 18.7 (S-CH_3);

LRMS (ESI$^+$) *m/z* (%): 196.0 ([M-I]$^+$, 100); LRMS (ESI$^-$) *m/z* (%): 127.0 ([I]$^-$, 100);

Spectral data were in agreement with literature values.[191]

6.2.6. Synthesis of 1-(5-carboxypentyl)-4-methylquinolin-1-ium bromide (**6**)

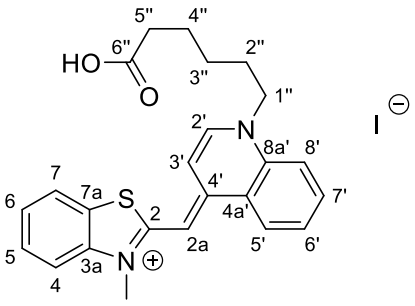


A mixture of lepidine (1.86 mL, 14.0 mmol, 1.0 eq) and 6-bromohexanoic acid (3.00 g, 15.4 mmol, 1.1 eq) was heated at 130 °C for 20 h under an argon atmosphere. The mixture was cooled to RT and stirred with acetone (30 mL) for 0.5 h. Obtained solid was collected by filtration and washed with Et_2O (15 mL) to give the product as a white solid (2.9 g, 8.6 mmol, 61%).

^{1}H NMR (400 MHz, d_6-DMSO): δ 9.47 (d, *J* = 6.0 Hz, 1H, H^2), 8.61 (d, *J* = 8.9 Hz, 1H, H^5 or H^8), 8.54 (dd, *J* = 8.5, 1.4 Hz, 1H, H^5 or H^8), 8.25 (ddd, *J* = 8.9, 6.9, 1.4 Hz, 1H, H^6 or H^7), 8.11 – 8.01 (m, 2H, H^3 and H^6 or H^7), 5.02 (t, *J* = 7.5 Hz, 2H, H$^{1'}$), 3.00 (s, 3H, CH_3), 2.21 (t, *J* = 7.3 Hz, 2H, H$^{5'}$), 2.01 – 1.88 (m, 2H, H$^{2'}$), 1.54 (app. p, *J* = 7.3 Hz, 2H, H$^{4'}$), 1.45 – 1.33 (m, 2H, H$^{3'}$);

^{13}C NMR (101 MHz, d_6-DMSO): δ 174.3 (C6'), 158.6 (C4), 148.4 (C2), 136.7 (C4a or C8a), 135.1 (C3 or C6 or C7), 129.6 (C3 or C6 or C7), 129.0 (C4a or C8a), 127.2 (C5 or C8), 122.7 (C3 or C6 or C7), 119.4 (C5 or C8), 56.7 (C1'), 33.4 (C5'), 29.2 (C2'), 25.3 (C3'), 23.9 (C4'), 19.7 (CH_3); LRMS (ESI$^+$): *m/z* (%): 258.2 ([M-Br]$^+$, 100). Spectral data were in agreement with literature values.[219]

6.2.7. Synthesis of N-(methyl)-2-[(1,4-dihydro-1-(5-carboxypentyl)quinolin-4-ylidene) methyl]benzothiazol-3-ium iodide (**7, TO_{Q6}**)



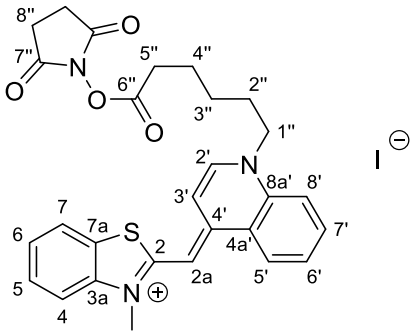
To a stirred solution of **5** (1.1 g, 3.4 mmol, 1.4 eq) and **6** (0.81 g, 2.4 mmol, 1.0 eq) in anhydrous DMF (8.0 mL), under an argon atmosphere at RT, was added anhydrous Et_3N (1.0 mL, 7.2 mmol, 3.0 eq). The solution turned red instantly and stirring was continued for 0.5 h. H_2O (80 mL) was added and the mixture was acidified with 37% HCl to pH 2. The obtained precipitate was collected by filtration and washed with H_2O (15 mL) to give the product as red solid (1.0 g, 1.9 mmol, 79%).

^{1}H NMR (400 MHz, d_6-DMSO): δ 12.0 (br s, 1H, COOH), 8.73 (d, *J* = 8.7 Hz, 1H, $H^{5'}$ or $H^{8'}$), 8.60 (d, *J* = 7.2 Hz, 1H, $H^{2'}$), 8.05 (d, *J* = 8.7 Hz, 1H, $H^{5'}$ or $H^{8'}$), 7.98 (dd, *J* = 8.1, 1.3 Hz, 1H, H^4), 7.94 (ddd, *J* = 8.7, 6.9, 1.2 Hz, 1H, $H^{6'}$ or $H^{7'}$), 7.74 – 7.66 (m, 2H, H^7 and $H^{6'}$ or $H^{7'}$), 7.54 (ddd, *J* = 8.4, 7.2, 1.3 Hz, 1H, H^6), 7.33 (ddd, *J* = 8.1, 7.2, 1.0 Hz, 1H, H^5), 7.24 (d, *J* = 7.2 Hz, 1H, $H^{3'}$), 6.82 (s, 1H, H^{2a}), 4.53 (t, *J* = 7.5 Hz, 2H, $H^{1''}$), 3.96 (s, 3H, CH_3), 2.22 (t, *J* = 7.3 Hz, 2H, $H^{5''}$), 1.83 (app. p, *J* = 7.5 Hz, 2H, $H^{2''}$), 1.55 (app. p, *J* = 7.3 Hz, 2H, $H^{4''}$), 1.42 – 1.32 (m, 1H, $H^{3''}$);

^{13}C NMR (101 MHz, d_6-DMSO): δ = 174.3 (C6''), 159.8 (C2), 148.3 (C4'), 144.2 (C2'), 140.3 (C3a or C7a), 136.8 (C4a' or C8a'), 133.1 (C7 or C6' or C7'), 128.0 (C6), 126.7 (C7 or C6' or C7'), 125.7 (C5' or C8'), 124.3 (C5), 124.1 (C4a'or C8a'), 123.8 (C3a or C7a), 122.8 (C4), 117.9 (C5' or C8'), 112.8 (C7 or C6' or C7'), 107.7 (C3'), 88.0 (C2a), 53.9 (C1''), 33.9 (CH_3), 33.5 (C5''), 28.5 (C2''), 25.4 (C3''), 24.0 (C4'');

LRMS (ESI$^+$): *m/z* (%): 405.2 ([M-I]$^+$, 100); HRMS (ESI$^+$) *m/z* for [M-I]$^+$ $C_{24}H_{25}N_2O_2S^+$ calc. 405.1631 found: 405.1630; R_f = 0.26 (MeOH:CH_2Cl_2, *v*:*v* = 1:9), UV. Spectral data were in agreement with literature values.[220]

6.2.8. Synthesis of N-hydroxysuccinimide ester of N-(methyl)-2-[(1,4-dihydro-1-(5-carboxypentyl)quinolin-4-ylidene)methyl]benzothiazol-3-ium iodide (**8**, **TO$_{Q6}$-NHS**)



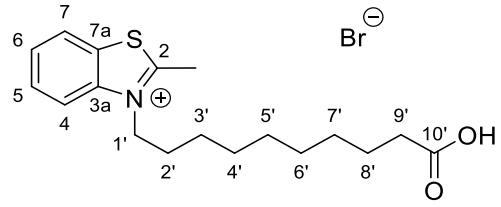
To a stirred solution of **7** (0.30 g, 0.56 mmol, 1.0 eq) and DIPEA (0.49 mL, 2.8 mmol, 5.0 eq) in anhydrous DMF (5.0 mL), under an argon atmosphere at RT, was added TSTU (0.34 g, 1.1 mmol, 2.0 eq). The solution was stirred for 0.5 h and HCl (5%, 20 mL) was added. The mixture was stirred for an additional 10 min. The obtained precipitate was collected by filtration and washed with H_2O (10 mL) to give the product as red solid (0.29 g, 0.45 mmol, 80%).

^{1}H NMR (400 MHz, *d$_6$*-DMSO): δ 8.80 (d, *J* = 8.7 Hz, 1H, H$^{5'}$ or H$^{8'}$), 8.63 (d, *J* = 7.3 Hz, 1H, H$^{2'}$), 8.14 (d, *J* = 8.7 Hz, 1H, H$^{5'}$ or H$^{8'}$), 8.05 (dd, *J* = 7.6, 1.2 Hz, 1H, H^4), 7.99 (ddd, *J* = 8.7, 6.9, 1.3 Hz, 1H, H$^{6'}$ or H$^{7'}$), 7.85 – 7.68 (m, 2H, H^7 and H$^{6'}$ or H$^{7'}$), 7.62 (ddd, *J* = 8.4, 7.6, 1.2 Hz, 1H, H^6), 7.42 (td, *J* = 7.6, 1.0 Hz, 1H, H^5), 7.37 (d, *J* = 7.3 Hz, 1H, H$^{3'}$), 6.93 (s, 1H, H^{2a}), 4.60 (t, *J* = 7.4 Hz, 2H, H$^{1''}$), 4.02 (s, 3H, CH_3), 2.80 (s, 4H, H$^{8''}$), 2.71 (t, *J* = 7.2 Hz, 2H, H$^{5''}$), 1.90 (app. p, *J* = 7.6 Hz, 2H, H$^{2''}$), 1.70 (app. p, *J* = 7.3 Hz, 2H, H$^{4''}$), 1.58 – 1.42 (m, 2H, H$^{3''}$);

^{13}C NMR (101 MHz, *d$_6$*-DMSO): δ 170.3 (C7''), 168.9 (C6''), 160.0 (C2), 148.5 (C4'), 144.3 (C2'), 140.4 (C3a or C7a), 137.0 (C4a' or C8a'), 133.3 (C7 or C6' or C7'), 128.2 (C6), 126.8 (C7 or C6' or C7'), 125.8

(C5' or C8'), 124.5 (C5), 124.2 (C4a' or C8a'), 123.9 (C3a or C7a), 122.9 (C4), 118.1 (C5' or C8'), 113.0 (C7 or C6' or C7'), 107.9 (C3'), 88.1 (C2a), 53.9 (C1''), 33.8 (CH_3), 30.0 (C5''), 28.3 (C2''), 25.4 (C8''), 25.0 (C3''), 23.7 (C4''); LRMS (ESI^+): *m/z* (%): 502.2 ($[M-I]^+$, 100); HRMS (ESI^+) *m/z* $[M-I]^+$ for $C_{28}H_{28}N_3O_4S^+$ calc. 502.1795 found: 502.1793; R_f = 0.50 (MeOH:CH_2Cl_2, *v*:*v* = 1:9), UV. Compound was described without spectroscopic data.[221]

6.2.9. Synthesis of 3-(9-carboxynonyl)-2-methylbenzothiazol-3-ium bromide (**9**)



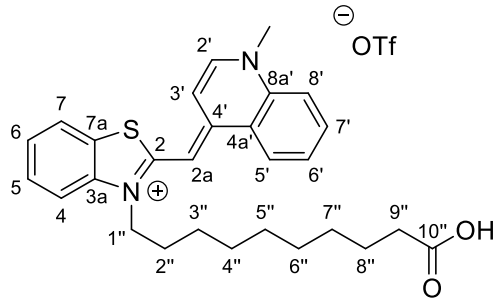
A mixture of 2-methylbenzothiazole (2.3 mL, 18 mmol, 1.0 eq) and 10-bromodecanoic acid (5.0 g, 20 mmol, 1.1 eq) was heated at 110 °C for 5 h under an argon atmosphere. The reaction mixture was dissolved in MeOH (5 mL) and precipitated by addition of Et_2O (60 mL), solid was collected by filtration and washed with Et_2O (30 mL). The crude product was purified by column chromatography on silica gel (1-15% MeOH/CH_2Cl_2) to give the product as a white solid (1.3 g, 3.3 mmol, 18%).

^{1}H NMR (400 MHz, d_6-DMSO): δ 11.94 (br s, 1H, COOH), 8.49 (dd, *J* = 8.2, 1.3 Hz, 1H, H^4 or H^7), 8.35 (d, *J* = 8.6 Hz, 1H, H^4 or H^7), 7.88 (ddd, *J* = 8.6, 7.3, 1.3 Hz, 1H, H^5 or H^6), 7.80 (ddd, *J* = 8.2, 7.3, 1.0 Hz, 1H, H^5 or H^6), 4.72 (t, *J* = 7.8 Hz, 2H, $H^{1'}$), 3.22 (s, 3H, CH_3), 2.17 (t, *J* = 7.4 Hz, 2H, $H^{9'}$), 1.84 (app. p, *J* = 7.8 Hz, 2H, $H^{2'}$), 1.51 – 1.38 (m, 4H, CH_2), 1.35 – 1.19 (m, 8H, CH_2);

^{13}C NMR (101 MHz, d_6-DMSO): δ 177.0 (C2), 174.4 (C10'), 140.8 (C3a or C7a), 129.3 (C5 or C6), 129.1 (C3a or C7a), 128.0 (C5 or C6), 124.7 (C4 or C7), 116.9 (C4 or C7), 49.2 (C1'), 33.6 (C9'), 28.7 (CH_2), 28.6 (CH_2), 28.49 (CH_2), 28.45 (CH_2), 27.8 (C2'), 25.8 (CH_2), 24.4 (CH_2), 16.9 (CH_3);

LRMS (ESI$^+$): *m/z* (%): 320.2 ([M-Br]$^+$, 100); HRMS (ESI$^+$) *m/z* [M-Br]$^+$ for $C_{18}H_{26}NO_2^+$ calc. 320.1679 found: 320.1677; R_f = 0.53 (MeOH:CH_2Cl_2, *v*:*v* = 1.5:8.5), UV.

6.2.10. Synthesis of N-(9-carboxynonyl))-2-[(1,4-dihydro-1-methylquinolin-4-ylidene)methyl] benzothiazol-3-ium trifluoromethanesulfonate (**10**, **TO$_{B10}$**)



To a stirred solution of **9** (0.096 g, 0.24 mmol, 1.0 eq) and **2** (0.079 g, 0.24 mmol, 1.0 eq) in a mixture of anhydrous MeCN (1.0 mL) and anhydrous CH_2Cl_2 (2.0 mL) under an argon atmosphere at RT, was added anhydrous Et_3N (0.10 mL, 0.72 mmol, 3.0 eq). The solution turned red instantly and was stirred for 0.5 h, HCl (5%, 10 mL) was added and the mixture was stirred for a further 10 min. The reaction mixture was extracted with CH_2Cl_2 (2 x 10 mL), dried with Na_2SO_4 filtered and evaporated, followed by purification by column chromatography on silica gel (1-10% MeOH/CH_2Cl_2) to give the product as a red solid (0.090 g, 0.15 mmol, 63%).

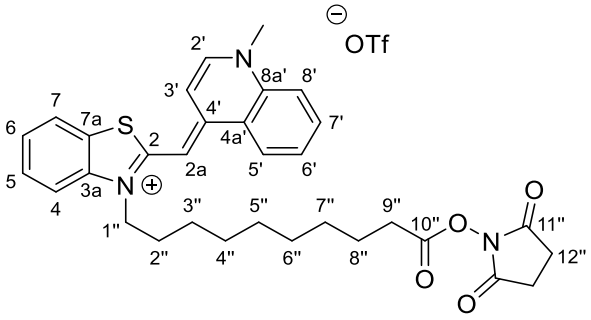
^{1}H NMR (400 MHz, *d*$_6$-DMSO): δ 8.67 (t, *J* = 6.5 Hz, 1H, H$^{8'}$), 8.58 – 8.53 (app. m, 1H, H$^{2'}$), 8.04 – 7.95 (m, 3H, H^4 or H^7, H$^{5'}$, H$^{6'}$ or H$^{7'}$), 7.80 – 7.73 (m, 1H, H$^{6'}$ or H$^{7'}$), 7.72 – 7.67 (m, 1H, H^4 or H^7), 7.57 (t, *J* = 7.8, 1H, H^5 or H^6), 7.38 (t, *J* = 7.8, 1H, H^5 or H^6), 7.34 – 7.30 (app. m, 1H, H$^{3'}$), 6.87 (s, 1H, H^{2a}), 4.65 – 4.50 (m, 2H, H$^{1''}$), 4.14 (s, 3H, CH_3), 2.12 (t, *J* = 7.4 Hz, 2H, H$^{9''}$), 1.79 – 1.72 (m, 2H, H$^{2''}$), 1.48 – 1.36 (m, 4H, CH_2), 1.36 – 1.27 (m, 2H, CH_2), 1.25 – 1.17 (m, 6H, CH_2);

^{13}C NMR (101 MHz, *d*$_6$-DMSO): δ 174.5 (C10''), 159.1 (C2), 148.5 (C4'), 144.9 (C2'), 139.8 (C3a or C7a), 137.9 (C4a' or C8a'), 133.1 (Ar-H), 128.1 (C5 or C6), 126.9 (Ar-H), 125.2 (C8'), 124.4 (C5 or C6), 123.9 (C4a' or C8a'), 123.8 (C3a or C7a), 122.8 (Ar-H), 118.2 (Ar-H), 112.8 (Ar-H), 107.8 (C3'), 87.5 (C2a), 45.6

(C1''), 42.3 (CH_3), 33.8 (C9''), 28.7 (CH_2), 28.58 (CH_2), 28.56 (CH_2), 28.5 (CH_2), 26.8 (C2''), 25.9 (CH_2), 24.5 (CH_2); Ar-H = C5' – C7' or C4 or C7;

LRMS (ESI^+): *m/z* (%): 461.2 ($[M\text{-}SO_3CF_3]^+$, 100); HRMS (ESI^+) *m/z* $[M\text{-}SO_3CF_3]^+$ for $C_{28}H_{33}N_2O_2S^+$ calc. 461.2257 found: 461.2258; R_f = 0.33 (MeOH:CH_2Cl_2, *v*:*v* = 1:9), UV.

6.2.11. Synthesis of N-hydroxysuccinimide ester of N-(9-carboxynonyl))-2-[(1,4-dihydro-1-methylquinolin-4-ylidene)methyl]benzothiazol-3-ium trifluoromethanesulfonate (**11**, **TO_{B10}-NHS**)

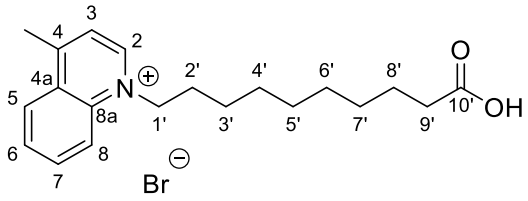


To a stirred solution of **10** (0.045 g, 0.074 mmol, 1.0 eq) and DIPEA (0.071 mL, 0.41 mmol, 5.5 eq) in anhydrous DMF (1.0 mL), under an argon atmosphere at RT, was added TSTU (0.054 g, 0.18 mmol, 2.4 eq). The solution was stirred for 0.5 h and evaporated, CH_2Cl_2 (5 mL) was added and extracted with 5% HCl (10 mL) and H_2O (10 mL). The organic layer was dried with Na_2SO_4, filtered and evaporated, followed by purification by column chromatography on silica gel (5-60% MeCN/CH_2Cl_2) to give the product as a red solid (0.040 g, 0.057 mmol, 77%).

^1H NMR (400 MHz, d_6-DMSO): δ 8.71 (d, *J* = 8.6 Hz, 1H, $H^{8'}$), 8.59 (d, *J* = 7.2 Hz, 1H, $H^{2'}$), 8.10 – 7.97 (m, 3H, $H^{5'}$, $H^{6'}$, H^4 or H^7), 7.78 (ddd, *J* = 8.6, 6.9, 1.7 Hz, 1H, $H^{7'}$), 7.75 (d, *J* = 8.4 Hz, 1H, H^4 or H^7), 7.60 (ddd, *J* = 8.4, 7.5, 1.3 Hz, 1H, H^5 or H^6), 7.41 (t, *J* = 7.5 Hz, 1H, H^5 or H^6), 7.38 (d, *J* = 7.2 Hz, 1H, $H^{3'}$), 6.92 (s, 1H, H^{2a}), 4.61 (t, *J* = 7.5 Hz, 2H, $H^{1''}$), 4.17 (s, 3H, CH_3), 2.81 (s, 4H, $H^{12''}$), 2.60 (t, *J* = 7.2 Hz, 2H, $H^{9''}$), 1.80 (app. p, *J* = 7.5 Hz, 2H, $H^{2''}$), 1.56 (app. p, *J* = 7.2 Hz, 2H, $H^{8''}$), 1.45 (app. p, *J* = 7.5, Hz, 2H, $H^{3''}$), 1.38 – 1.18 (m, 8H, C4'' – C7'');

^{13}C NMR (101 MHz, d_6-DMSO): δ 170.2 (C11'), 168.9 (C10''), 159.2 (C2), 148.6 (C4'), 145.0 (C2'), 140.0 (C3a or C7a), 138.0 (C4a' or C8a'), 133.2 (Ar-H), 128.2 (C5 or C6), 127.0 (Ar-H), 125.3 (C8'), 124.5 (C5 or C6), 124.0 (C3a or C7a), 123.9 (C4a' or C8a'), 122.9 (Ar-H), 118.3 (Ar-H), 112.9 (Ar-H), 107.9 (C3'), 87.5 (C2a), 45.6 (C1''), 42.4 (CH_3), 30.1 (C9''), 28.6 (CH_2), 28.5 (CH_2), 28.3 (CH_2), 27.9 (CH_2), 26.9 (C2''), 25.9 (C3''), 25.4 (C12''), 24.2 (C8''); Ar-H = C5' – C7' or C4 or C7; LRMS (ESI$^+$): *m/z* (%): 558.2 ([M-SO_3CF_3]$^+$, 100); HRMS (ESI$^+$) *m/z* [M-SO_3CF_3]$^+$ for $C_{32}H_{36}N_3O_4S^+$ calc. 558.2421 found: 558.2421; R_f = 0.38 (MeOH:CH_2Cl_2, *v*:*v* = 1:9), UV.

6.2.12. Synthesis of 1-(9-carboxynonyl)-4-methylquinolin-1-ium bromide (**12**)



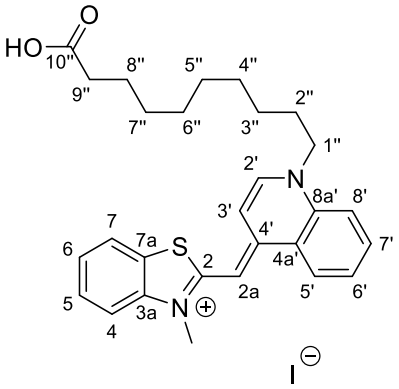
A mixture of lepidine (1.86 mL, 14.0 mmol, 1.0 eq) and 10-bromodecanoic acid (3.87 g, 15.4 mmol, 1.1 eq) was heated to 110 °C for 3 h under an argon atmosphere. The mixture was cooled to RT and stirred with acetone (30 mL) for 0.5 h. The obtained solid was collected by filtration and washed with Et_2O, followed by purification by column chromatography on silica gel (1-15% MeOH/CH_2Cl_2) to give the product as a white solid (1.0 g, 2.5 mmol, 18%).

^{1}H NMR (400 MHz, d_6-DMSO): δ 11.97 (br s, 1H, COOH), 9.49 (d, *J* = 6.4 Hz, 1H, H^2), 8.62 (d, *J* = 8.9 Hz, 1H, H^5 or H^8), 8.55 (dd, *J* = 8.4, 1.4 Hz, 1H, H^5 or H^8), 8.26 (ddd, *J* = 8.9, 7.0, 1.4 Hz, 1H, H^6 or H^7), 8.09 (d, *J* = 6.4 Hz, 1H, H^3), 8.06 (ddd, *J* = 8.4, 7.0, 0.8 Hz, 1H, H^6 or H^7), 5.03 (t, *J* = 7.5 Hz, 2H, $H^{1'}$), 3.01 (s, 3H, CH_3), 2.17 (t, *J* = 7.4 Hz, 2H, $H^{9'}$), 1.94 (app. p, *J* = 7.5 Hz, 2H, $H^{2'}$), 1.46 (app. p, *J* = 6.8 Hz, 2H, $H^{8'}$), 1.40 – 1.33 (m, 2H, $H^{3'}$), 1.33 – 1.20 (m, 8H, CH_2);

^{13}C NMR (101 MHz, d_6-DMSO): δ 174.5 (C10'), 158.5 (C4a or C8a), 148.4 (C2), 136.7 (C4a or C8a), 135.1 (C6 or C7), 129.6 (C6 or C7), 129.0 (C4), 127.2 (C5 or C8), 122.7 (C3), 119.4 (C5 or C8), 56.9 (C1'), 33.6 (C9'), 29.4 (C2'), 28.7 (CH_2), 28.6 (CH_2), 28.5 (CH_2), 28.4 (CH_2), 25.7 (C3'), 24.4 (C8'), 19.7 (CH_3);

LRMS (ESI^+): *m/z* (%): 314.2 ($[M\text{-}Br]^+$, 100); HRMS (ESI^+) *m/z* $[M\text{-}Br]^+$ for $C_{20}H_{28}NO_2^+$ calc. 314.2115 found: 314.2110; R_f = 0.12 (MeOH:CH_2Cl_2, *v*:*v* = 1:9), UV.

6.2.13. Synthesis of N-(methyl)-2-[(1,4-dihydro-1-(9-carboxynonyl) quinolin-4-ylidene)methyl] benzothiazol-3-ium iodide (**13**, **TO$_{Q10}$**)



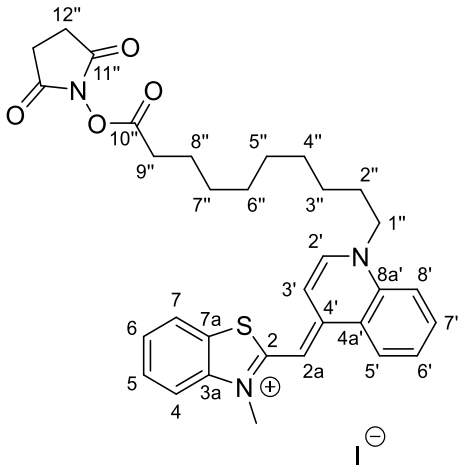
To a stirred solution of **12** (0.19 g, 0.47 mmol, 1.0 eq) and **5** (0.15 g, 0.47 mmol, 1.0 eq) in anhydrous DMF (3.0 mL), under an argon atmosphere at RT, was added anhydrous Et_3N (0.19 mL, 1.4 mmol, 3.0 eq). The solution turned red instantly and stirring was continued for 0.5 h, H_2O (16 mL) was added and the mixture was acidified with 37% HCl to pH 2. Obtained precipitate was collected by filtration and washed with H_2O to give the product as a red solid (0.14 g, 0.24 mmol, 51%).

^{1}H NMR (400 MHz, d_6-DMSO): δ 12.00 (br s, 1H, COOH), 8.77 (d, *J* = 8.6 Hz, 1H, $H^{8'}$), 8.65 (d, *J* = 7.2 Hz, 1H, $H^{2'}$), 8.09 (dd, *J* = 8.7, 1.1 Hz, 1H, $H^{5'}$ or $H^{6'}$), 8.01 (dd, *J* = 7.6, 1.2 Hz, 1H, H^4), 7.96 (ddd, *J* = 8.7, 6.9, 1.2 Hz, 1H, $H^{5'}$ or $H^{6'}$), 7.77 – 7.67 (m, 2H, H^7, $H^{7'}$), 7.57 (ddd, *J* = 8.3, 7.6, 1.2 Hz, 1H, H^6), 7.38 (td, *J* = 7.6, 1.0 Hz, 1H, H^5), 7.29 (d, *J* = 7.2 Hz, 1H, $H^{3'}$), 6.87 (s, 1H, H^{2a}), 4.56 (t, *J* = 7.4 Hz, 2H, $H^{1''}$), 3.99 (s, 3H, CH_3), 2.17 (t, *J* = 7.2 Hz, 2H, $H^{9''}$), 1.82 (app. p, *J* = 7.4 Hz, 2H, $H^{2''}$), 1.45 (app. p, *J* = 7.2 Hz, 2H, $H^{8''}$), 1.39 – 1.25 (m, 4H, CH_2), 1.26 – 1.18 (m, 6H, CH_2);

^{13}C NMR (101 MHz, d_6-DMSO): δ 174.4 (C10''), 159.9 (C2), 148.4 (C4'), 144.3 (C2'), 140.4 (C3a or C7a), 136.9 (C4a' or C8a'), 133.2 (C6'), 128.1 (C5 or C6), 126.7 (C7' or C7), 125.8 (C8'), 124.4 (C5 or C6), 124.2 (C4a' or C8a'), 123.8 (C3a or C7a), 122.8 (C4), 118.0 (C5'), 112.9 (C7' or C7), 107.8 (C3'), 88.1 (C2a), 54.1 (C1''), 33.8 (CH_3), 33.7 (C9''), 28.8 (C2''), 28.7 (CH_2), 28.6 (CH_2), 28.5 (CH_2), 28.4 (CH_2), 25.8 (CH_2), 24.5 (C8'');

LRMS (ESI$^+$): *m/z* (%): 461.2 ([M-I]$^+$, 100); HRMS (ESI$^+$) *m/z* [M-I]$^+$ for $C_{28}H_{33}N_2O_2S^+$ calc. 461.2257 found: 461.2255; R_f = 0.32 (MeOH:CH_2Cl_2, *v*:*v* = 1:9), UV.

6.2.14. Synthesis of N-hydroxysuccinimide ester of N-(methyl)-2-[(1,4-dihydro-1-(9-carboxynonyl)quinolin-4-ylidene)methyl] benzothiazol-3-ium iodide (**14**, **TO$_{Q10}$-NHS**)



To a stirred solution of **13** (0.14 g, 0.23 mmol, 1.0 eq) and DIPEA (0.21 mL, 1.2 mmol, 5.2 eq) in anhydrous DMF (2.0 mL), under an argon atmosphere at RT, was added TSTU (0.15 g, 0.48 mmol, 2.1 eq). The solution was stirred for 0.5 h and 5% HCl (20 mL) was added. The mixture was stirred for an additional 10 min. The obtained precipitate was collected by filtration and washed with H_2O (5 mL) to give the product as a red solid (0.14 g, 0.20 mmol, 87%).

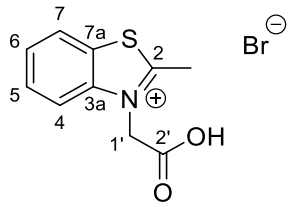
^{1}H NMR (400 MHz, d_6-DMSO): δ 8.76 (d, *J* = 8.5 Hz, 1H, H$^{8'}$), 8.61 (d, *J* = 7.2 Hz, 1H, H$^{2'}$), 8.08 (app. d, *J* = 8.7 Hz, 1H, H$^{5'}$), 8.00 (d, *J* = 7.8 Hz, 1H, H^4), 7.96 (t, *J* = 7.8 Hz, 1H, H$^{6'}$), 7.77 – 7.69 (m, 2H, H^7, H$^{7'}$), 7.57

(t, *J* = 7.8 Hz, 1H, H^5 or H^6), 7.38 (t, *J* = 7.8 Hz, 1H, H^5 or H^6), 7.28 (d, *J* = 7.2 Hz, 1H, $H^{3'}$), 6.86 (s, 1H, H^{2a}), 4.55 (t, *J* = 7.4 Hz, 2H. $H^{1''}$), 3.98 (s, 3H, CH_3), 2.81 (s, 4H, $H^{12''}$), 2.64 (t, *J* = 7.2 Hz, 2H, $H^{9''}$), 1.82 (app. p, *J* = 7.4 Hz, 2H, $H^{2''}$), 1.59 (app. p, *J* = 7.2 Hz, 2H, $H^{8''}$), 1.42 – 1.15 (m, 10H, $H^{3''}$– $H^{7''}$);

^{13}C NMR (101 MHz, d_6-DMSO): δ 170.3 (C11'), 169.0 (C10''), 159.9 (C2), 148.4 (C4'), 144.3 (C2'), 140.4 (C3a or C7a), 136.9 (C4a' or C8a'), 133.2 (C6'), 128.1 (C5 or C6), 126.8 (C7 or C7'), 125.8 (C8'), 124.4 (C5 or C6), 124.2 (C4a' or C8a'), 123.8 (C3a or C7a), 122.8 (C4), 118.0 (C5'), 112.9 (C7 or C7'), 107.8 (C3'), 88.0 (C2a), 54.1 (C1''), 33.8 (CH_3), 30.2 (C9''), 28.8 (C2''), 28.6 (CH_2), 28.4 (CH_2), 28.3 (CH_2), 27.9 (CH_2), 25.8 (CH_2), 25.5 (C12''), 24.3 (C8'');

LRMS (ESI^+): *m/z* (%): 558.2 ($[M-I]^+$, 100); HRMS (ESI^+) *m/z* $[M-I]^+$ for $C_{32}H_{36}N_3O_4S^+$ calc. 558.2421 found: 558.2421; R_f = 0.50 (MeOH:CH_2Cl_2, *v*:*v* = 1:9), UV.

6.2.15. Synthesis of 3-(carboxymethyl)-2-methylbenzothiazol-3-ium bromide (**15**)



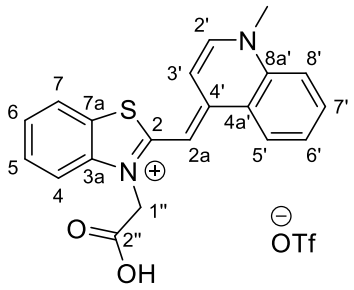
A mixture of 2-methylbenzothiazole (0.22 mL, 1.7 mmol, 1.0 eq), bromoacetic acid (0.26 g, 1.9 mmol, 1.1 eq) and anhydrous MeCN (2.3 mL) was heated under reflux for 24 h under an argon atmosphere. The reaction mixture was cooled to RT, precipitated by addition of Et_2O (10 mL), obtained solid was collected by filtration and washed with Et_2O (10 mL). Recrystallisation from MeCN (28 mL) followed by washing with MeCN (5 mL) and Et_2O (5 mL) gave the product as a white solid (0.28 g, 0.97 mmol, 57%).

^{1}H NMR (400 MHz, d_6-DMSO): δ 14.22 (br s, 1H, COOH), 8.49 (dd, *J* = 8.2, 1.1 Hz, 1H, H^4 or H^7), 8.30 (dd, *J* = 8.2, 1.1 Hz, 1H, H^4 or H^7), 7.90 (ddd, *J* = 8.2, 7.3, 1.1 Hz, 1H, H^5 or H^6), 7.82 (ddd, *J* = 8.2, 7.3, 1.1 Hz, 1H, H^5 or H^6), 5.78 (s, 2H, $H^{1'}$), 3.21 (s, 3H, CH_3);

^{13}C NMR (101 MHz, d_6-DMSO): δ 179.6 (C2'), 167.1 (C2), 141.6 (C3a or C7a), 130.1 (C5 or C6), 129.1 (C3a or C7a), 128.7 (C5 or C6), 125.4 (C4 or C7), 117.1 (C4 or C7), 50.5 (C1'), 17.6 (CH_3);

LRMS (ESI$^+$) *m/z* (%): 208 ([M-Br]$^+$, 100). Spectral data were in agreement with literature values.[192]

6.2.16. Synthesis of N-(carboxymethyl)-2-[(1,4-dihydro-1-methylquinolin-4-ylidene)methyl] benzothiazol-3-ium trifluoromethanesulfonate (**16, TO$_{B2}$**)



To a stirred solution of **15** (0.20 g, 0.70 mmol, 1.0 eq) and **2** (0.25 g, 0.77 mmol, 1.1 eq) in a mixture of anhydrous MeOH (2 mL) and CH_2Cl_2 (2 mL) under argon atmosphere at RT, was added anhydrous Et_3N (0.24 mL, 1.7 mmol, 2.4 eq). The solution turned red instantly and was stirred for 3 h. Mixture was evaporated and purified by column chromatography on silica gel (20% MeOH/CH_2Cl_2) to give the product as a dark red solid (0.14 g, 0.27 mmol, 39%).

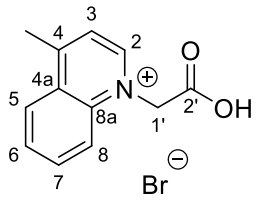
^{1}H NMR (400 MHz, d_6-DMSO): δ 8.53 (dd, *J* = 8.3, 1.0 Hz, 1H, H$^{8'}$), 8.49 (d, *J* = 7.2 Hz, 1H, H$^{2'}$), 8.03 (dd, *J* = 8.1, 1.1 Hz, 1H, H^4 or H^7), 8.01 – 7.92 (m, 2H, H$^{6'}$ or H$^{7'}$ and H$^{5'}$), 7.72 (ddd, *J* = 8.3, 6.6, 1.6 Hz, 1H, H$^{6'}$ or H$^{7'}$), 7.63 (dd, *J* = 8.1, 1.1 Hz, 1H, H^4 or H^7), 7.57 (ddd, *J* = 8.1, 7.3, 1.1 Hz, 1H, 1H, H^5 or H^6), 7.40 (ddd, *J* = 8.1, 7.3, 1.1 Hz, 1H, H^5 or H^6), 7.21 (d, *J* = 7.2 Hz, 1H, H$^{3'}$), 6.81 (s, 1H, H^{2a}), 4.82 (s, 2H, H$^{1''}$), 4.08 (s, 3H, CH_3);

^{13}C NMR (126 MHz, d_6-DMSO): δ 165.5 (C2''), 159.9 (C2), 147.9 (C4'), 144.5 (C2'), 140.9 (C3a or C7a), 138.1 (C4a' or C8a'), 133.0 (C5' or C6' or C7'), 128.0 (C5 or C6), 126.7 (C5' or C6' or C7'), 125.0 (C8'),

124.3 (C5 or C6), 124.0 (C4a' or C8a'), 123.8 (C3a or C7a), 122.6 (C4 or C7), 118.1 (C5' or C6' or C7'), 113.5 (C4 or C7), 107.1 (C3'), 88.4 (C2a), 51.5 (C1''), 42.5 (CH_3);

LRMS (ESI^+): *m/z* (%): 349.0 ($[M\text{-}SO_3CF_3]^+$, 100), 290.0 ($[M\text{-}(SO_3CF_3)\text{-}(CH_2COOH)$, 100); LRMS ($ESI^-$): *m/z* (%): 149.0 ($[SO_3CF_3]^-$, 100), 113 (90); HRMS ($ESI^+$) *m/z* $[M\text{-}SO_3CF_3]^+$ for $C_{20}H_{17}N_2O_2S^+$ calc. 349.1005 found: 349.1006; R_f = 0.2 ($MeOH:CH_2Cl_2$, *v*:*v* = 2:8), UV.

6.2.17. Synthesis of 1-(carboxymethyl)-4-methylquinolin-1-ium bromide (**17**)



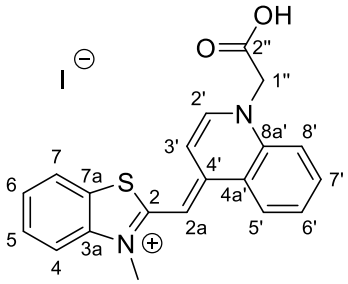
To a stirred solution of bromoacetic acid (0.97 g, 6.8 mmol, 1.0 eq) in anhydrous MeCN (3.0 mL), methyl 4-methylquinoline (1.0 g, 7.5 mmol, 1.1 eq) was added. The mixture was stirred overnight, under an argon atmosphere at reflux. The reaction mixture evaporated and recrystalized from MeCN, solid was collected by filtration and washed with Et_2O to obtain the product as a pale yellow solid (0.23 g, 0.82 mmol, 12%).

^1H NMR (400 MHz, d_6-DMSO): δ 9.45 (d, *J* = 6.1 Hz, 1H, H^2), 8.57 (d, *J* = 8.5 Hz, 1H, H^5 or H^8), 8.40 (d, *J* = 8.9 Hz, 1H, H^5 or H^8), 8.26 (ddd, *J* = 8.5, 7.0, 1.2 Hz, 1H, H^6 or H^7), 8.17 (d, *J* = 6.1 Hz, 1H, H^3), 8.06 (app. t, *J* = 7.7 Hz, 1H, H^6 or H^7), 6.02 (s, 2H, $H^{1'}$), 3.05 (s, 3H, CH_3);

^{13}C NMR (101 MHz, d_6-DMSO): δ 167.6 (C2'), 160.3 (C4), 149.6 (C2), 137.6 (C4a or C8a), 135.5 (C6 or C7), 129.7 (C3), 128.6 (C4a or C8a), 127.2 (C5 or C8), 122.7 (C6 or C7), 119.2 (C5 or C8), 57.4 (C1'), 20.0 (CH_3);

LRMS (ESI^+) *m/z* (%): 202.2 ($[M\text{-}Br]^+$, 100); Spectral data were in agreement with literature values.[193]

6.2.18. Synthesis of N-(methyl)-2-[(1,4-dihydro-1-(Carboxymethyl) quinolin-4-ylidene) methyl]benzothiazol-3-ium iodide (**18**, **TO_{Q2}**)



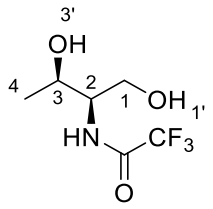
To a stirred solution of **5** (0.22 g, 0.69 mmol, 1.0 eq) and **17** (0.25 g, 0.90 mmol, 1.3 eq) in anhydrous EtOH (10 mL) under an argon atmosphere at RT, was added anhydrous Et_3N (0.32 mL, 2.3 mmol, 3.3 eq). The solution turned red instantly and stirring was continued for 2 h. The mixture was evaporated and purified by column chromatography (20% MeOH/CH_2Cl_2) to give the product as a dark red solid (0.17 g, 0.36 mmol, 52%).

^{1}H NMR (500 MHz, d_6-DMSO): δ 8.76 (dd, *J* = 8.6, 1.2 Hz, 1H, $H^{8'}$), 8.56 (d, *J* = 7.2 Hz, 1H, $H^{2'}$), 8.01 (dd, *J* = 8.3, 1.2 Hz, 1H, H^4), 7.93 (ddd, *J* = 8.6, 6.8, 1.2 Hz, 1H, $H^{6'}$), 7.86 (dd, *J* = 8.6, 1.2 Hz, 1H, $H^{5'}$), 7.74 (d, *J* = 8.3 Hz, 1H, H^7), 7.73 (ddd, *J* = 8.6, 6.8, 1.2 Hz, 1H, $H^{7'}$), 7.59 (ddd, *J* = 8.3, 7.4, 1.2 Hz, 1H, H^5), 7.40 (d, *J* = 7.2 Hz, 1H, $H^{3'}$), 7.38 (ddd, *J* = 8.3, 7.4, 1.2 Hz, 1H, H^6), 6.91 (s, 1H, H^{2a}), 4.87 (s, 2H, $H^{1''}$), 3.99 (s, 3H, CH_3);

^{13}C NMR (126 MHz, d_6-DMSO): δ 165.9 (C2''), 159.0 (C2), 148.5 (C4'), 145.3 (C2'), 140.6 (C3a or C7a), 138.2 (C4a' or C8a'), 132.7 (C6'), 128.0 (C5), 126.6 (C7'), 125.3 (C8'), 124.2 (C6), 124.1 (C4a' or C8a'), 123.6 (C3a or C7a), 122.8 (C4), 118.8 (C5'), 112.6 (C7), 108.1 (C3'), 87.4 (C2a), 59.4 (C1''), 33.6 (CH_3);

LRMS (ESI^+) *m/z* (%): 349.0 ($[M-I]^+$, 100); R_f = 0.36 (MeOH:CH_2Cl_2, *v*:*v* = 2:8), UV. Spectral data were in agreement with literature values.[193]

6.2.19. Synthesis of N-trifluoroacetamide-L-threoninol (**19**)



To a stirring solution of *L*-threoninol (0.977 g, 9.30 mmol, 1.0 eq) in an anhydrous MeOH (15 mL) under an argon atmosphere at 0 °C, ethyl trifluoroacetate (1.22 mL, 10.2 mmol, 1.1 eq) was added. The mixture was stirred for 2.5 h after which it was evaporated and dried under high vacuum to give the product as a white crystalline solid (1.74 g, 8.65 mmol, 93%).

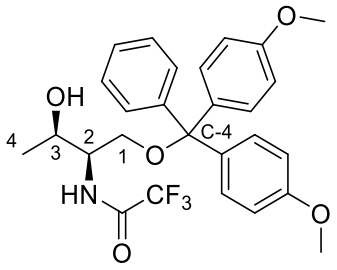
^{1}H NMR (400 MHz, d_6-DMSO): δ 8.85 (d, *J* = 8.8 Hz, 1H, NH), 4.71 (d, *J* = 5.5 Hz, 1H, $OH^{3'}$), 4.70 (d, *J* = 5.6 Hz, 1H, $OH^{1'}$), 3.87 – 3.76 (m, 1H, H^3), 3.76 – 3.67 (m, 1H, H^2), 3.56 (dt, *J* = 10.9, 5.6 Hz, 1H, H^{1a}), 3.44 (ddd, *J* = 10.9, 7.3, 5.6 Hz, 1H, H^{1b}), 1.02 (d, *J* = 6.4 Hz, 3H, H^4);

^{13}C NMR (126 MHz, d_6-DMSO): δ 156.6 (q, *J* = 35.9 Hz, CO-CF_3), 116.09 (q, *J* = 288.3 Hz, CF_3), 64.9 (C3), 60.6 (C1), 58.3 (C2), 20.5 (C4);

^{19}F NMR (376 MHz, d_6-DMSO): δ -73.89;

LRMS (ESI^-) *m/z* (%): 200.1 ($[M-H]^-$, 100); HRMS (ESI^-) *m/z* $[M-H]^-$ for $C_6H_9F_3NO_3^-$ calc 200.0540 found: 200.0541; R_f = 0.33 (MeOH:CH_2Cl_2, *v*:*v* = 1:9), $KMnO_4$. Spectral data were in agreement with literature values.[222]

6.2.20. Synthesis of N-trifluoroacetamide-1-*O*-(4,4'-dimethoxytritryl)-L-threoninol (**20**)



To a stirred solution of **19** (1.74 g, 8.63 mmol, 1.0 eq) in freshly distilled pyridine (20 mL) and DIPEA (1.8 mL, 10.4 mmol, 1.2 eq) under an argon atmosphere at 0 °C, a solution of 4,4'-dimethoxytrityl chloride (3.52 g, 10.4 mmol, 1.2 eq) and 4-dimethylaminopyridine (0.16 g, 1.3 mmol, 0.15 eq) in CH_2Cl_2 (15 mL) was added. The mixture was allowed to warm to RT and stirred for 3 h. The solvent was evaporated followed by column chromatography on silica gel (*v*:*v*:*v* = 80:20:3 → 60:40:3, Hexane:EtOAc:Et_3N) to give the product as a pale yellow foam (2.87 g, 5.70 mmol, 66%).

^{1}H NMR (400 MHz, d_6-DMSO): δ 9.24 (d, *J* = 8.3 Hz, 1H, NH), 7.37 (d, *J* = 7.5 Hz, 2H, Ar-H), 7.29 (t, *J* = 7.5 Hz, 2H, Ar-H), 7.26 – 7.21 (m, 5H, Ar-H), 6.87 (d, *J* = 8.9 Hz, 4H, Ar-H), 4.69 (d, *J* = 5.5 Hz, 1H, OH), 3.89 (m, 2H, H^2 and H^3), 3.73 (s, 6H, OCH_3), 3.15 (dd, *J* = 9.2, 3.8 Hz, 1H, H^{1a}), 2.96 (dd, *J* = 9.2, 6.6 Hz, 1H, H^{1b}), 0.93 (d, *J* = 6.0 Hz, 3H, H^4);

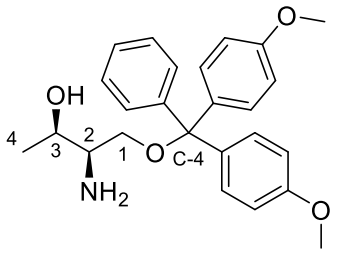
^{13}C NMR (101 MHz, d_6-DMSO): δ 158.5 (Ar), 145.4 (Ar), 136.1 (Ar), 130.1 (Ar-H), 128.2 (Ar-H), 128.1 (Ar-H), 127.1 (Ar-H), 113.6 (Ar-H), 85.7 (C-4), 65.2 (C2 or C3), 63.0 (C1), 56.6 (C2 or C3), 55.5 (OCH_3), 20.6 (C4); (weak ^{13}C no CO and CF_3)

^{19}F NMR (376 MHz, d_6-DMSO): δ -73.85;

LRMS (ESI^-) *m/z* (%): 502.2 ($[M-H]^-$, 100), 248.9 (80), 538.1 (25); HRMS (ESI^+) *m/z* $[M+Na]^+$ for $C_{27}H_{28}F_3NO_5Na$ calc. 526.1812 found 526.1811; R_f = 0.15 (EtOAc:Hexane:Et_3N, *v*:*v*:*v* = 20:80:3); R_f =

0.875 (EtOAc:MeOH:NH_3, *v*:*v*:*v* = 5:1:1), *p*-anisaldehyde. Compound was reported without proper analysis.[223]

6.2.21. Synthesis of 1-*O*-(4,4'-dimethoxytritryl)-L-threoninol (**21**)



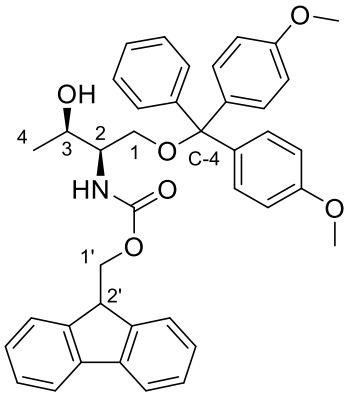
To a stirred solution of **20** (2.9 g, 5.7 mmol) in ethanol (80 mL) under an argon atmosphere at RT was added aqueous ammonia (160 mL) and stirred for 4 days. The mixture was evaporated to give the product as a yellow solid which was used without further purification (2.32 g, 5.7 mmol, quantitative).

^{1}H NMR (400 MHz, d_6-DMSO): δ 7.40 (br s, 2H, NH_2), 7.44 – 7.20 (m, 9H, Ar-H), 6.90 (d, *J* = 7.9 Hz, 4H, Ar-H), 5.38 (d, *J* = 4.8 Hz, 1H, OH), 3.80 – 3.74 (m, 1H, H^3), 3.74 (s, 6H, OCH_3), 3.20 (dd, *J* = 9.8, 4.5 Hz, 1H, H^{1a}), 2.95 (dd, *J* = 9.8, 5.5 Hz, 1H, H^{1b}), 2.85 (app. quartet, *J* = 5.5 Hz, 1H, H^2), 0.91 (d, *J* = 6.3 Hz, 3H, H^4);

^{13}C NMR (101 MHz, d_6-DMSO): δ 158.6 (Ar), 145.2 (Ar), 135.9 (Ar), 130.3 (Ar-H), 130.3 (Ar-H), 128.3 (Ar-H), 127.2 (Ar-H), 113.6 (Ar-H), 86.2 (C-4), 65.2 (C3), 62.6 (C1), 56.9 (C2), 55.5 (OCH_3), 20.4 (C4);

HRMS (ESI^+) *m/z* $[M+Na]^+$ for $C_{25}H_{29}NO_4Na$ calc. 430.1989 found 430.1984; R_f = 0.13 (CH_2Cl_2:MeOH:Et_3N, *v*:*v*:*v* = 95:5:0.1), *p*-anisaldehyde. Spectral data were in agreement with literature values.[224]

6.2.22. Synthesis of N-fluorenylmethyloxycarbonyl-1-*O*-(4,4'-dimethoxytritryl)-L-threoninol (**22**)



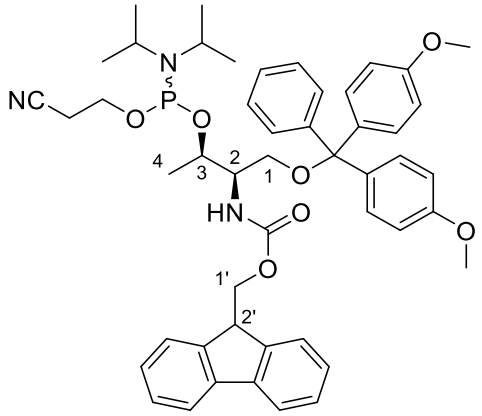
To a stirred solution of **21** (0.15 g, 0.37 mmol, 1.00 eq) in anhydrous CH_2Cl_2 (5 mL), under an argon atmosphere at RT, was added Fmoc-OSu (0.13 g, 0.39 mmol, 1.05 eq) and DIPEA (0.13 mL, 0.74 mmol, 2.0 eq). The mixture was stirred for 2 h, extracted and the aqueous layer washed with a saturated solution of $NaHCO_3$ and saturated KCl solution. The organic layer was dried with Na_2SO_4, filtered and purified by gel chromatography on silica gel (10-40% EtOAc/petroleum ether 40-60 with NEt_3 0.1%) to give the product as a white foam (0.19 g, 0.30 mmol, 81%).

^{1}H NMR (400 MHz, d_6-DMSO): δ 7.89 (d, *J* = 7.6 Hz, 2H, Ar-H), 7.78 – 7.73 (m, 2H, Ar-H), 7.43 – 7.36 (m, 4H, Ar-H), 7.31 – 7.15 (m, 9H, Ar-H), 7.03 (d, *J* = 9.2 Hz, 1H, NH), 6.86 – 6.80 (m, 4H, Ar-H), 4.47 (d, *J* = 5.8 Hz, 1H, OH), 4.36 (dd, *J* = 9.9, 6.6 Hz, 1H, $H^{1'a}$), 4.30 – 4.19 (m, 2H, $H^{1'b}$ and $H^{2'}$), 3.91 – 3.82 (m, 1H, H^3), 3.70 (d, *J* = 2.6 Hz, 6H, OCH_3), 3.68 – 3.61 (m, 1H, H^2), 3.11 (dd, *J* = 9.0, 5.4 Hz, 1H, H^{1a}), 2.92 (dd, *J* = 9.0, 6.7 Hz, 1H, H^{1b}), 0.98 (d, *J* = 6.4 Hz, 3H, H^4);

^{13}C NMR (101 MHz, d_6-DMSO): δ 158.4 (Ar), 156.8 (CO-CF_3), 145.6 (Ar), 144.3 (Ar), 141.2 (Ar), 136.4 (Ar), 130.2 (Ar-H), 128.2 (Ar-H), 128.1 (Ar-H), 127.54 (Ar-H), 127.49 (Ar-H), 127.0 (Ar-H), 125.8, (Ar-H), 120.6 (Ar-Fmoc-H), 113.5 (Ar-H), 85.6 (C-4), 66.0 (C1'), 65.7 (C3), 63.5 (C1), 57.0 (C2), 55.4 (OCH_3), 47.3 (C2'), 20.6 (C4);

LRMS (ESI$^+$) *m/z* (%): 652.2 ([M+Na]$^+$, 30), 303.2 ([DMTr]$^+$, 100); HRMS (ESI$^+$) *m/z* [M+Na]$^+$ for $C_{40}H_{39}NO_6Na$ calc. 652.2670 found 652.2670; R_f = 0.36 (EtOAc:Hexane:Et_3N, *v*:*v*:*v* = 50:50:0.5), *p*-anisaldehyde. Compound was reported in $CDCl_3$.[225]

6.2.23. Synthesis of N-fluorenylmethyloxycarbonyl-1-*O*-(4,4′-dimethoxytritryl)-L-threoninol phosphoramidite (**23**)



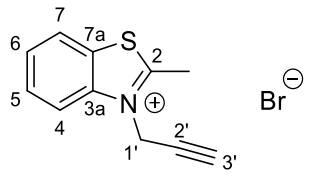
To a solution of **22** (0.19 g, 0.30 mmol, 1.0 eq) and anhydrous degassed DIPEA (0.12 mL, 0.69 mmol, 2.3 eq) in anhydrous degassed CH_2Cl_2 (7.0 mL) under an argon atmosphere, was added 2-cyanoethyl *N*,*N*-diisopropylchlorophosphoramidite (0.080 mL, 0.36 mmol, 1.2 eq). The reaction was stirred for 1 h, quenched with argon saturated KCl solution (30 mL) and the organic phase was passed through a layer of anhydrous Na_2SO_4 followed by evaporation to give a yellow foam. The crude product was purified by gel chromatography on silica gel (degassed 70% EtOAc/hexane) pre-equilibrated with pyridine, under an argon pressure to give the product as white foam (0.15 g, 0.19 mmol, 63%).

^{1}H NMR (400 MHz, CD_3CN): δ 7.86 – 7.77 (m, 2H, Ar-H), 7.68 (dd, *J* = 11.6, 7.4 Hz, 2H, Ar-H), 7.46 – 7.35 (m, 4H, Ar-H), 7.33 – 7.16 (m, 9H, Ar-H), 6.82 (dd, *J* = 8.8, 6.1 Hz, 4H, Ar-H), 5.43 (m, 1H, $H^{2'}$), 4.51 – 4.29 (m, 2H, $H^{1'}$), 4.25 (app. t, *J* = 6.7 Hz, 1H, CH), 4.21 – 4.02 (m, 1H, CH), 3.87 – 3.79 (m, 1H, OC$\underline{H}_2^a$CH$_2$-CN), 3.73 (s, 6H, OCH_3), 3.67 – 3.60 (m, 1H, OC$\underline{H}_2^b$CH$_2$-CN), 3.58 – 3.42 (m, 2H, iPr-CH), 3.20 – 2.99 (m, 2H, H^1), 2.59 (t, *J* = 6.0 Hz, 1H, CH_2^a-CN), 2.44 (t, *J* = 6.0 Hz, 1H, CH_2^b-CN), 1.16 – 1.05 (m, 12H, iPr-CH_3), 0.97 (d, *J* = 6.8 Hz, 3H, H^4);

^{31}P NMR (162 MHz, CD_3CN): δ 147.58 (s), 146.95 (s);

HRMS (ESI$^+$) *m/z* $[M+H]^+$ for $C_{49}H_{57}N_3O_7P$ calc. 830.3929 found 830.3929; R_f = 0.57 and 0.43 for two isomers (EtOAc:Hexane:Et_3N, *v*:*v*:*v* = 50:50:0.5), *p*-anisaldehyde. Compound was reported in $CDCl_3$.[225]

6.2.24. Synthesis of 3-(propargyl)-2-methylbenzothiazol-3-ium bromide **(24)**



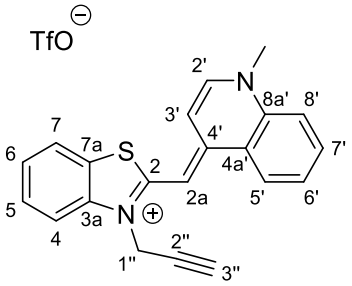
A mixture of 2-methylbenzothiazole (0.33 mL, 2.6 mmol, 1.0 eq) and propargyl bromide (80 wt. % in toluene, 0.32 mL, 2.9 mmol, 1.1 eq) in anhydrous MeCN (5 ml) was heated overnight at 100 °C in a pressure vial under an argon atmosphere. The reaction mixture was cooled to RT, the obtained solid was collected by filtration and washed with Et_2O (10 mL), to give the product as a grey solid (0.21 g, 0.78 mmol, 30%).

^{1}H NMR (400 MHz, d_6-DMSO): δ 8.54 (app. d, *J* = 7.4 Hz, 1H, H^4 or H^7), 8.39 (app. d, *J* = 8.5 Hz, 1H, 1H, H^4 or H^7), 7.93 (ddd, *J* = 8.5, 7.2, 1.2 Hz, 1H, H^5 or H^6), 7.82 (ddd, *J* = 8.2, 7.4, 1.0 Hz, 1H, H^5 or H^6), 5.81 (d, *J* = 2.6 Hz, 2H, $H^{1'}$), 3.85 (t, *J* = 2.6 Hz, 1H, $H^{3'}$), 3.30 (s, 3H, CH_3);

^{13}C NMR (101 MHz, d_6-DMSO): δ 179.0 (C2), 140.7 (C3a or C7a), 130.1 (C5 or C6), 129.5 (C3a or C7a), 128.8 (C5 or C6), 125.5 (C4 or C7), 117.2 (C4 or C7), 79.5 (C3'), 75.1 (C2'), 39.4 (C1'), 17.8 (CH_3);

LRMS (ESI$^+$) *m/z* (%): 188.0 ($[M-Br]^+$, 100); Spectral data were in agreement with literature values.[195]

6.2.25. Synthesis of N-(propargyl))-2-[(1,4-dihydro-1-methylquinolin-4-ylidene)methyl]benzothiazol-3-ium trifluoromethanesulfonate (**25, TO$_{BPr}$**)



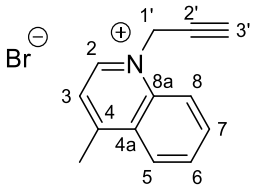
To a stirred solution of **2** (0.49 g, 1.5 mmol, 2.0 eq) and **24** (0.20 g, 0.75 mmol, 1.0 eq) in anhydrous EtOH (2.0 mL), under an argon atmosphere at RT, was added anhydrous Et_3N (0.21 mL, 1.5 mmol, 2.0 eq). The solution turned red instantly and stirring was continued for 20 min. The mixture was evaporated, followed by purification by column chromatography on silica gel (2-20% MeOH/CH_2Cl_2) to give the product as a red solid (0.088 g, 0.19 mmol, 25%).

^{1}H NMR (400 MHz, *d*$_6$-DMSO): δ 8.78 (dd, *J* = 8.8, 1.3 Hz, 1H, H$^{8'}$), 8.71 (d, *J* = 7.1 Hz, 1H, H$^{2'}$), 8.13 – 7.99 (m, 3H, H$^{5'}$ and H$^{6'}$ or H$^{7'}$ and H^4 or H^7), 7.84 (ddd, *J* = 8.3, 7.0, 1.3 Hz, 1H, H$^{6'}$ or H$^{7'}$), 7.77 (d, *J* = 8.3 Hz, 1H, H^4 or H^7), 7.61 (ddd, *J* = 8.5, 7.3, 1.2 Hz, 1H, H^5 or H^6), 7.43 (d, *J* = 7.1 Hz, 1H, H$^{3'}$), 7.42 – 7.37 (m, 1H, H^5 or H^6), 7.03 (s, 1H, H^{2a}), 5.56 (d, *J* = 2.4 Hz, 2H, H$^{1''}$), 4.22 (s, 3H, CH_3), 3.53 (t, *J* = 2.4 Hz, 1H, H$^{3''}$);

^{13}C NMR (101 MHz, *d*$_6$-DMSO): δ 158.3 (C2), 149.1 (C4'), 145.6 (C2'), 139.2 (C3a or C7a), 138.1 (C4a' or C8a'), 133.5 (Ar-H), 128.2 (C5 or C6), 127.3 (Ar-H), 125.4 (C8'), 124.6 (C5 or C6), 124.3 (C4a' or 8a'), 123.5 (Ar-H), 123.1 (C3a or C7a), 118.5 (Ar-H), 112.5 (Ar-H), 108.8 (C3'), 88.1 (C2a), 77.0 (C3''), 76.5 (C2''), 42.7 (CH_3), 35.4 (C1'');

LRMS (ESI$^+$) *m/z* (%): 329.0 ([M-SO_3CF_3]$^+$, 100), 290.0 ([M-(SO_3CF_3)-(propargyl)]$^+$, 40); HRMS (ESI$^+$) *m/z* [M--SO_3CF_3]$^+$ for $C_{21}H_{17}N_2S^+$ calc. 329.1107 found 329.1106; R_f = 0.51 (MeOH:CH_2Cl_2, *v*:*v* = 12:78), UV.

6.2.26. Synthesis of 1-(propargyl)-4-methylquinolin-1-ium bromide (**26**)



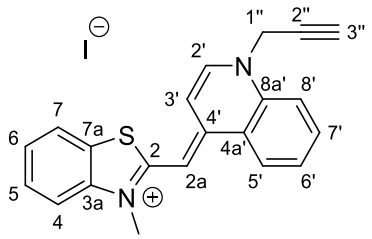
A mixture of 4-methylquinoline (0.80 mL, 6.0 mmol, 1.0 eq) and propargyl bromide (80 wt. % in toluene, 0.87 mL, 7.8 mmol, 1.3 eq) in MeCN (10 ml) was stirred at RT for 72 h under an argon atmosphere. The reaction mixture was cooled to RT, the obtained solid was collected by filtration and washed with Et_2O (10 mL), to give the product as a grey solid (0.67 g, 2.6 mmol, 43%).

^{1}H NMR (400 MHz, d_6-DMSO): δ 9.62 (d, *J* = 6.2 Hz, 1H, H^2), 8.62 – 8.55 (m, 2H, H^5 and H^8), 8.34 (ddd, *J* = 8.8, 7.0, 1.4 Hz, 1H, H^6 or H^7), 8.15 (d, *J* = 6.2 Hz, 1H, H^3), 8.10 (ddd, *J* = 8.2, 7.0, 1.0 Hz, 1H, H^6 or H^7), 6.07 (d, *J* = 2.5 Hz, 2H, $H^{1'}$), 4.01 (t, *J* = 2.5 Hz, 1H, $H^{3'}$), 3.04 (s, 3H, CH_3);

^{13}C NMR (101 MHz, d_6-DMSO): δ 160.6 (C4), 148.7 (C2), 136.9 (C4a or C8a), 135.8 (C6 or C7), 130.4 (C6 or C7), 129.4 (C4a or C8a), 127.8 (C5 or C8), 123.4 (C3), 119.9 (C5 or C8), 81.7 (C3'), 76.3 (C2'), 47.3 (C1'), 20.4 (CH_3);

LRMS (ESI^+) *m/z* (%): 182.0 ($[M-Br]^+$, 100). Spectral data were in agreement with literature values.[196]

6.2.27. Synthesis of N-(methyl)-2-[(1,4-dihydro-1-(propargyl)quinolin-4-ylidene) methyl]benzothiazol-3-ium iodine (**27, TO$_{QPr}$**)



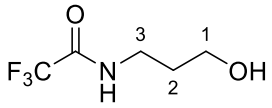
To a stirred solution of **26** (0.32 g, 1.2 mmol, 1.0 eq) and **5** (0.78 g, 2.4 mmol, 2.0 eq) in anhydrous EtOH (3.0 mL), under an argon atmosphere at RT was added anhydrous Et_3N (0.34 mL, 2.4 mmol, 2.0 eq). The solution turned red instantly and stirring was continued for 10 min. The mixture was evaporated, followed by purification by column chromatography on silica gel (2-30% MeOH/CH_2Cl_2) to give the product as a red solid (0.11 g, 0.24 mmol, 20%).

^{1}H NMR (400 MHz, d_6-DMSO): δ 8.75 (d, *J* = 8.4 Hz, 1H, H$^{8'}$), 8.56 (d, *J* = 7.4 Hz, 1H, H$^{2'}$), 8.08 – 7.95 (m, 3H, H^4 or H^7 and H^5 or H^6 and H$^{6'}$ or H$^{7'}$), 7.80 – 7.69 (m, 2H, H^4 or H^7 and H$^{6'}$ or H$^{7'}$), 7.59 (ddd, *J* = 8.4, 7.3, 1.2 Hz, 1H, H^5 or H^6), 7.41 (app. t, *J* = 7.6 Hz, 1H, H$^{5'}$), 7.30 (d, *J* = 7.4 Hz, 1H, H$^{3'}$), 6.91 (s, 1H, H^{2a}), 5.46 (d, *J* = 2.5 Hz, 2H, H$^{1''}$), 4.02 (s, 3H, CH_3), 3.76 (t, *J* = 2.5 Hz, 1H, H$^{3''}$);

^{13}C NMR (101 MHz, d_6-DMSO): δ 161.4 (C2), 149.0 (C4'), 143.9 (C2'), 140.8 (C3a or C7a), 137.1 (C4a' or C8a'), 133.7 (Ar-H), 128.7 (Ar-H), 127.3 (Ar-H), 126.2 (C8'), 125.3 (C5'), 124.6 (C3a or C7a), 124.4 (C4a' or C8a'), 123.4 (Ar-H), 118.5 (Ar-H), 113.8 (Ar-H), 108.1 (C3'), 89.4 (C2a), 79.5 (C3''), 77.6 (C2''), 44.1 (C1''), 34.5 (CH_3);

LRMS (ESI$^+$) *m/z* (%): 329.0 ([M-I]$^+$, 100), 290.0 ([M-(I)-(propargyl)]$^+$, 10); R_f = 0.50 (MeOH:CH_2Cl_2, *v*:*v* = 1:9), UV. Spectral data were in agreement with literature values.[197]

6.2.28. Synthesis of N-(1-hydroxypropyl)trifluoroacetamide (**28**)



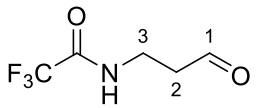
To a stirred 3-aminopropanol (6.11 mL, 6.00 g, 79.9 mmol, 1.0 eq) ethyl trifluoroacetate (17.3 mL, 144 mmol, 1.8 eq) was added dropwise under an argon atmosphere at 0 °C. The solution was stirred for 3 h, evaporated, followed by purification by column chromatography on silica gel (10% MeOH/CH_2Cl_2) to give the product as pale yellow liquid (13.3 g, 77.7 mmol, 97%).

^{1}H NMR (400 MHz, $CDCl_3$): δ 7.80 (br s, 1H, NH), 3.72 (t, *J* = 5.6 Hz, 2H, H^1), 3.47 (app. q, *J* = 6.0 Hz, 2H, H^3), 3.19 (s, 1H, OH), 1.83 – 1.74 (m, 2H, H^2);

^{13}C NMR (101 MHz, $CDCl_3$): δ 158.0 (q, *J* = 36.7 Hz, CO-CF_3), 116.1 (q, *J* = 287.3 Hz, CF_3), 60.7 (C1), 38.2 (C3), 30.6 (C2);

LRMS (ESI^-) *m/z* (%): 170.1 ($[M-H]^-$, 100); R_f = 0.60 (MeOH:CH_2Cl_2, *v*:*v* = 1:9), $KMnO_4$. Spectral data were in agreement with literature values.[226]

6.2.29. Synthesis of N-(1-oxopropyl)trifluoroacetamide (**29**)



To a stirred solution of **28** (3.20 g, 18.7 mmol, 1.0 eq) in CH_2Cl_2 (60 mL) was added Dess-Martin periodinane (11.9 g, 28.1 mmol, 1.5 eq) under an argon atmosphere at 0 °C. The suspension was stirred for 2 h at RT, quenched with sat. $NaHCO_3$ (120 mL) and the Et_2O (120 mL) was added and the biphasic mixture was stirred for 20 min. Precipitate formed which was removed by filtration and phases were separated, the aqueous phase was extracted with Et_2O (60 mL). The combined organic layers were washed with sat. NaCl (50 mL), dried with $MgSO_4$ filtered and evaporated. The crude product was

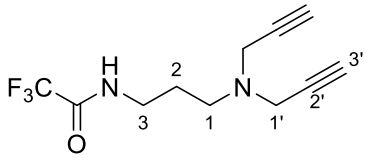
purified by column chromatography on silica gel (60% petroleum ether 40-60/EtOAc) to give the product as colourless liquid (1.61 g, 9.52 mmol, 51%). The product was used on the same day due to low stability.

^{1}H NMR (400 MHz, d_6-DMSO): δ 9.63 (t, *J* = 1.4 Hz, 1H, H^1), 9.46 (s, 1H, NH), 3.49 – 3.42 (m, 2H, H^3), 2.70 (td, *J* = 6.6, 1.4 Hz, 2H, H^2);

^{13}C NMR (101 MHz, d_6-DMSO): δ 201.9 (C1), 156.7 (q, *J* = 36.2 Hz, CO-CF_3), 116.3 (q, *J* = 288.0 Hz, CF_3), 42.3 (C2), 33.7 (C3);

^{19}F NMR (376 MHz, d_6-DMSO): δ -74.5 (CF_3); LRMS (ESI^-) *m/z* (%): 168.0 ($[M-H]^-$, 40), 321^- (100); R_f = 0.43 (EtOAc:*n*-Hexane, *v*:*v* = 2:3), $KMnO_4$. Spectral data of the compound were reported in $CDCl_3$.[227]

6.2.30. Synthesis of N-(1-(N,N-dipropargyl)propyl)trifluoroacetamide (**30**)



To a stirred solution of **29** (1.78 g, 10.5 mmol, 1.5 eq) and dipropargylamine (0.72 mL, 7.0 mmol, 1.0 eq) in a anhydrous CH_2Cl_2 (23 mL) under an argon atmosphere at RT, was added $NaHB(OAc)_3$ (2.97 g, 14.0 mmol, 2.0 eq). The solution was stirred for 2 h, quenched with sat. $NaHCO_3$ (10 mL) and stirred for 20 min. The mixture was extracted with CH_2Cl_2 (2 x 15 mL), organic phase was washed with water, NaCl, dried with Na_2SO_4, filtered and evaporated. The crude product was purified by column chromatography on silica gel (10-70% EtOAc/petroleum ether 40-60) to give the product as a white solid (1.63 g, 6.62 mmol, 95%).

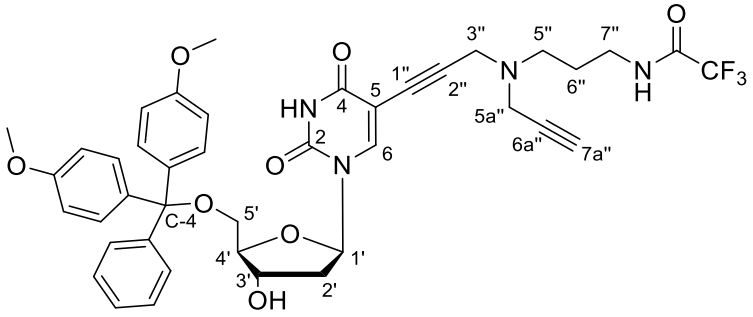
^{1}H NMR (400 MHz, $CDCl_3$): δ 8.18 (br s, 1H, NH), 3.42 (app. q, *J* = 5.8 Hz, 2H, H^{3}), 3.37 (d, *J* = 2.4 Hz, 4H, $H^{1'}$), 2.72 – 2.67 (m, 2H, H^{1}), 2.19 (t, *J* = 2.4 Hz, 2H, $H^{3'}$), 1.71 – 1.63 (m, 2H, H^{2});

^{13}C NMR (101 MHz, $CDCl_3$): δ 157.1 (q, *J* = 36.7 Hz, CO-CF_3), 117.4 (q, *J* = 287.9, CF_3), 77.9 (C2'), 73.6 (C3'), 51.5 (C1), 42.2 (C1'), 39.9 (C3), 24.4 (C2);

^{19}F NMR (376 MHz, $CDCl_3$): δ -76.10 (CF_3);

LRMS (ESI^+) *m/z* (%): 126.0 ($[M-(C_2H_4–N(propargyl)_2)]^+$, 100), 154.0 ($[M-(N(propargyl)_2)]^+$, 90); HRMS ($ESI^+$) *m/z* $[M+H]^+$ for $C_{11}H_{14}F_3N_2O$ calc. 247.1053 found 247.1052; R_f = 0.60 (MeOH:CH_2Cl_2, *v*:*v* = 1:9), $KMnO_4$.

6.2.31. Synthesis of 5-pargylamino(N-propargyl-N-propyltrifluoroacetamide)-5′-*O*-(4,4'-dimethoxytritryl)-2′-deoxythymidine (**31**)



To a stirred solution of 5-iodo-5'-DMTr-deoxythymidine (4.20 g, 6.40 mmol, 1.0 eq), **30** (3.2 g, 12.8 mmol, 2.0 eq), $PdCl_2(PPh_3)_2$ (0.494 g, 0.704 mmol, 0.11 eq) and CuI (0.0720 g, 0.378 mmol, 0.059 eq) in degassed DMF (60.6 mL) under an argon atmosphere at RT, degassed NEt_3 (5.35 ml) was added. The mixture was stirred for 12 h, evaporated to dryness and the resulting residue was dissolved in EtOAc (100 mL). The organic layer was washed with an EDTA solution (4%, 50 mL), H_2O (50 mL) and sat. NaCl (50 mL). The organic phase was dried with Na_2SO_4 and evaporated, followed by purification by gel chromatography on silica gel (17-100% EtOAc/CH_2Cl_2) to give the product as a pale yellow foam (2.92 g, 3.76 mmol, 59%).

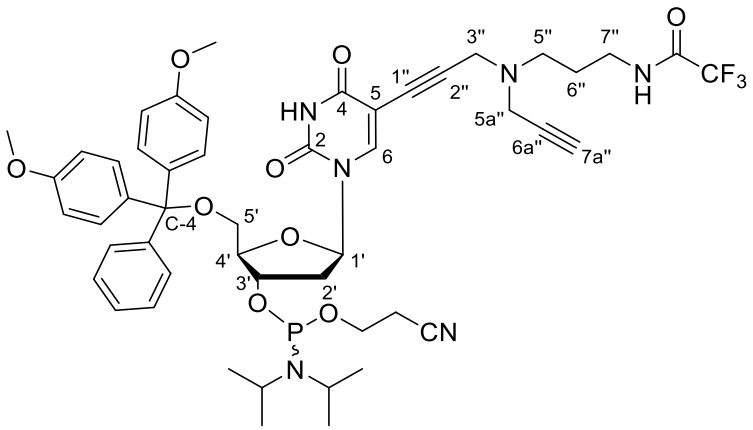
^{1}H NMR (500 MHz, $CDCl_3$): δ 9.66 (s, 1H, NH-thymidine), 8.26 (t, *J* = 5.3 Hz, 1H, NH-chain), 8.12 (s, 1H, H^{6}), 7.46 – 7.42 (m, 2H, Ar-H), 7.37 – 7.33 (m, 4H, Ar-H), 7.33 – 7.29 (m, 2H, Ar-H), 7.26 – 7.21 (m, 1H, Ar-H), 6.88 – 6.84 (m, 4H, Ar-H), 6.34 (t, *J* = 7.5 Hz, 1H, $H^{1'}$), 4.56 – 4.52 (m, 1H, $H^{3'}$), 4.11 (app. q, *J* = 3.1 Hz, 1H, $H^{4'}$), 3.80 (s, 6H, OCH_3), 3.46 (dd, *J* = 10.8, 3.1 Hz, 1H, $H^{5'a}$), 3.38 – 3.29 (m, 5H, $H^{5'b}$, $H^{3''}$and $H^{7''}$), 3.19 (d, *J* = 2.5 Hz, 2H, $H^{5a''}$), 2.56 – 2.51 (m, 3H, $H^{2'a}$ and $H^{5''}$), 2.30 (ddd, *J* = 13.6, 7.6, 6.0 Hz, 1H, $H^{2'b}$), 2.21 (t, *J* = 2.5 Hz, 1H, $H^{7a''}$), 1.54 (app. p, *J* = 6.1 Hz, 2H, $H^{6''}$).

^{13}C NMR (126 MHz, $CDCl_3$): δ 162.1 (C4), 158.6 (Ar), 157.2 (q, *J* = 36.5 Hz, CO-CF_3), 149.4 (C2), 144.5 (Ar), 142.3 (C6), 135.6 (Ar), 130.0 (Ar-H), 128.1 (Ar-H), 127.9 (Ar-H), 127.0 (Ar-H), 116.2 (q, *J* = 287.8 Hz, CF_3), 113.3 (Ar-H), 99.9 (C5), 88.8 (C2''), 87.0 (C-4), 86.6 (C4'), 85.7 (C1'), 78.6 (C6a''), 76.0 (C1''), 73.3 (C7a''), 72.2 (C3'), 63.4 (C5'), 55.3 (OCH_3), 50.8 (C5''), 43.1 (C3''), 42.7 (C5a''), 41.6 (C2'), 39.4 (C7''), 24.6 (C6'').

^{19}F NMR (376 MHz, $CDCl_3$): δ -75.91 (CF_3);

HRMS (ESI^+) *m/z* $[M+H]^+$ for $C_{41}H_{42}N_4O_8F_3$ calc. 775.2949 found: 775.2940; R_f = 0.20 (EtOAc:CH_2Cl_2, *v*:*v* = 7:3), *p*-anisaldehyde, UV.

6.2.32. Synthesis of 5-pargylamino(N-propargyl-N-propyltrifluoroacetamide)-5′-*O*-(4,4’-dimethoxytritryl)-2′-deoxythymidine phosphoramidite (**32**)



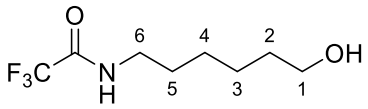
To a solution of **31** (2.01 g, 2.60 mmol, 1.0 eq) and anhydrous degassed DIPEA (1.27 mL, 7.28 mmol, 2.8 eq) in anhydrous degassed CH_2Cl_2 (60 mL) under an argon atmosphere, was added 2-cyanoethyl *N*,*N*-diisopropylchlorophosphoramidite (0.755 mL, 3.38 mmol, 1.3 eq). The reaction was stirred for 1.5 h, quenched with argon saturated KCl solution (30 mL) and the organic phase was passed through a layer of anhydrous Na_2SO_4 followed by evaporation to give a yellow foam. The crude product was purified by gel chromatography on silica gel (degassed 60-85% EtOAc/hexane) pre-equilibrated with pyridine, under an argon pressure to give the product as white foam (1.82 g, 1.87 mmol, 72%).

^{1}H NMR (400 MHz, $CDCl_3$) δ 8.31 (s, 1H, NH-chain), 8.08 (s, 0.5H, H^6 isomer a), 8.04 (s, 0.5H, H^6 isomer b), 7.39 – 7.33 (m, 2H, Ar-H), 7.30 – 7.20 (m, 6H, Ar-H), 7.19 – 7.10 (m, 1H, Ar-H), 6.80 – 6.73 (m, 4H, Ar-H), 6.28 – 6.18 (m, 1H, $H^{1'}$), 4.57 – 4.48 (m, 1H, $H^{3'}$), 4.15 – 4.05 (m, 1H, $H^{4'}$), 3.72 (s, 6H, OCH_3), 3.79 – 3.33 (m, 5H, $H^{5'a}$ and iPr-CH and $OC\underline{H}_2CH_2$-CN), 3.30 – 3.15 (m, 5H, $H^{3''}$and $H^{5'b}$ and $H^{7''}$), 3.06 (app. dd, *J* = 6.1, 2.4 Hz, 2H, $H^{5a''}$), 2.55 (t, *J* = 6.3 Hz, 1H, CH_2^b-CN), 2.48 (ddd, *J* = 13.7, 5.7, 2.8 Hz, 1H, $H^{2'a}$), 2.44 – 6.73 (m, 2H, $H^{5''}$), 2.35 (t, *J* = 6.3 Hz, 1H, CH_2^a-CN), 2.25 (dt, *J* = 13.7, 7.0 Hz, 1H, $H^{2'b}$), 2.11 (app. q, *J* = 2.4 Hz, 1H, $H^{7a''}$), 1.45 – 1.34 (m, 2H, $H^{6''}$), 1.12 – 1.07(m, 9H, iPr-CH_3), 0.98 (d, *J* = 6.8 Hz, 3H, iPr-CH_3).

^{31}P NMR (162 MHz, $CDCl_3$): δ 149.08 (s), 148.68 (s);

HRMS (ESI$^+$) *m/z* $[M+H]^+$ for $C_{50}H_{59}F_3N_6O_9P$ calc. 975.4028 found 975.4018; HRMS (ESI$^-$) *m/z* $[M-H]^-$ for $C_{50}H_{57}F_3N_6O_9P$ calc. 973.3882 found 973.3872; R_f = 0.31 and 0.48 for two isomers (EtOAc:Hexane, *v*:*v* = 7:3), *p*-anisaldehyde, UV.

6.2.33. Synthesis of N-(1-hydroxyhexyl)trifluoroacetamide (**33**)



To a stirred 6-aminohexanol (4.00 g, 34.1 mmol, 1.0 eq) ethyl trifluoroacetate (5.70 mL, 47.7 mmol, 1.4 eq) was added dropwise under an argon atmosphere at RT. The solution was stirred for 2.5 h, evaporated, followed by purification by column chromatography on silica gel (20-100% EtOAc/CH_2Cl_2) to give the product as white solid (4.94 g, 23.2 mmol, 68%).

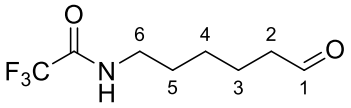
^{1}H NMR (400 MHz, $CDCl_3$): δ 6.84 (br s, 1H, NH), 3.62 (td, *J* = 6.5, 3.3 Hz, 2H, H^1), 3.34 (app. q, *J* = 6.8 Hz, 2H, H^6), 1.90 (br s, 1H, OH), 1.63 – 1.50 (m, 4H, CH_2), 1.43 – 1.30 (m, 4H, CH_2);

^{13}C NMR (101 MHz, $CDCl_3$): δ 157.4 (q, *J* = 36.6 Hz, $\underline{C}O$-CF_3), 115.9 (q, *J* = 287.8 Hz, CF_3), 62.6 (C1), 39.8 (C6), 32.3 (CH_2), 28.8 (CH_2), 26.3 (CH_2), 25.2 (CH_2);

^{19}F NMR (376 MHz, $CDCl_3$): δ -75.97 (CF_3);

LRMS (ESI$^-$) *m/z* (%): 212.1 ($[M-H]^-$, 100); R_f = 0.57 (EtOAc:CH_2Cl_2, *v*:*v* = 8:2), $KMnO_4$. Spectral data were in agreement with literature values.[228]

6.2.34. Synthesis of N-(1-oxohexyl)trifluoroacetamide (**34**)



To a stirred solution of **33** (3.65 g, 17.1 mmol, 1.0 eq) in CH_2Cl_2 (100 mL) was added Dess-Martin periodinane (10.1 g, 23.9 mmol, 1.4 eq) under an argon atmosphere at 0 °C. The suspension was stirred for 2 h at RT, quenched with sat. $NaHCO_3$ (120 mL) and the Et_2O (120 mL) was added and the biphasic mixture was stirred for 20 min. Precipitate formed which was removed by filtration and phases were separated, the aqueous phase was extracted with Et_2O (60 mL). The combined organic layers were washed with sat. NaCl (50 mL), dried with $MgSO_4$ filtered and evaporated. The crude product was purified by column chromatography on silica gel (40% petroleum ether 40-60/EtOAc) to give the product as colourless liquid (3.21 g, 15.2 mmol, 89%).

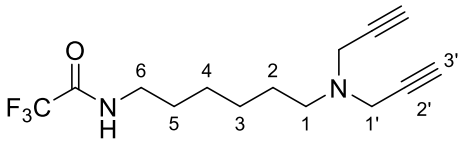
^{1}H NMR (400 MHz, d_6-DMSO): δ 9.67 (t, *J* = 1.6 Hz, 1H, H^1), 9.39 (t, *J* = 6.5 Hz, 1H, NH), 3.17 (app. q, *J* = 6.5 Hz, 2H, H^6), 2.43 (td, *J* = 7.2, 1.6 Hz, 2H, H^2), 1.59 – 1.43 (m, 4H, CH_2), 1.32 – 1.20 (m, 2H, CH_2);

^{13}C NMR (101 MHz, d_6-DMSO): δ 203.8 (C1), 156.6 (q, *J* = 35.9 Hz, C̲O-CF_3), 116.4 (q, *J* = 288.4 Hz, CF_3), 43.3 (C2), 39.4 (C6), 28.5 (CH_2), 26.1 (CH_2), 21.5 (CH_2);

^{19}F NMR (376 MHz, d_6-DMSO): δ -74.45 (CF_3);

LRMS (ESI^-) *m/z* (%): 210.1 ($[M-H]^-$, 100); R_f = 0.49 (EtOAc:*n*-Hexane, *v*:*v* = 3:2), $KMnO_4$. Spectral data of the compound were reported in $CDCl_3$.[229]

6.2.35. Synthesis of N-(1-(N,N-dipropargyl)hexyl)trifluoroacetamide (**35**)



To a stirred solution of **34** (3.02 g, 14.3 mmol, 1.9 eq) and dipropargylamine (0.780 mL, 7.54 mmol, 1.0 eq) in a anhydrous CH_2Cl_2 (25 mL) under an argon atmosphere at RT, was added $NaHB(OAc)_3$ (3.20 g, 15.1 mmol, 2.0 eq). The solution was stirred for 2 h, quenched with sat. $NaHCO_3$ (20 mL) and stirred for 20 min. The mixture was extracted with CH_2Cl_2 (2 x 15 mL), organic phase was washed with water, NaCl, dried with Na_2SO_4 filtered and evaporated. The crude product was purified by column chromatography on silica gel (5-50% EtOAc/petroleum ether 40-60) to give the product as a colourless liquid (2.13 g, 7.39 mmol, 98%).

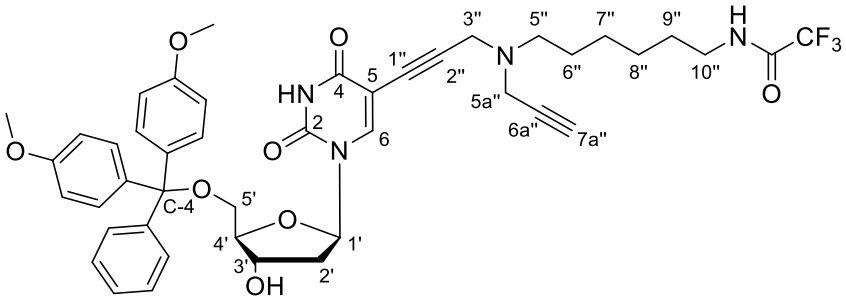
^{1}H NMR (400 MHz, $CDCl_3$): δ 6.60 (br s, 1H, NH), 3.40 (d, *J* = 2.4 Hz, 4H, $H^{1'}$), 3.33 (app. q, *J* = 6.8 Hz, 2H, H^6), 2.35 – 2.47 (m, 2H, H^1), 2.20 (t, *J* = 2.4 Hz, 2H, $H^{3'}$), 1.61 – 1.52 (m, 2H, H^5), 1.50 – 1.41 (m, 2H, H^2), 1.37 – 1.30 (m, 4H, CH_2);

^{13}C NMR (101 MHz, $CDCl_3$): δ 157.2 (q, *J* = 36.7 Hz, CO-CF_3), 115.9 (q, *J* = 287.9 Hz, CF_3), 78.7 (C2'), 72.9 (C3'), 52.6 (C1), 42.1 (C1'), 39.9 (C6), 28.8 (C5), 27.1 (C2), 26.7 (CH_2), 26.4 (CH_2);

^{19}F NMR (377 MHz, $CDCl_3$): δ -75.94 (CF_3);

HRMS (ESI$^+$) *m/z* $[M+H]^+$ for $C_{14}H_{20}F_3N_2O$ calc. 289.1522 found 289.1521; R_f = 0.43 (MeCN:CH_2Cl_2, *v*:*v* = 1:9), $KMnO_4$.

6.2.36. Synthesis of 5-pargylamino(N-propargyl-N-hexyltrifluoroacetamide) -5′-*O*-(4,4’-dimethoxytritryl)-2′-deoxythymidine (**36**)



To a stirred solution of 5-iodo-5'-DMTr-deoxythymidine (0.50 g, 0.76 mmol, 1.0 eq), **35** (0.55 g, 1.9 mmol, 2.5 eq), $PdCl_2(PPh_3)_2$ (64 mg, 0.091 mmol, 0.12 eq) and CuI (9.0 mg, 0.047 mmol, 0.062 eq) in anhydrous degassed DMF (12 mL) under an argon atmosphere at RT, anhydrous degassed NEt_3 (3.6 mL) was added. The mixture was stirred for 24 h, evaporated and redissolved in EtOAc (100 mL). The organic layer was washed with an EDTA solution (4%, 50 mL), H_2O (50 mL) and sat. NaCl (50 mL). The organic phase was dried with Na_2SO_4, filtered and evaporated, followed by purification by gel chromatography on silica gel (20-100% EtOAc/CH_2Cl_2) to give the product as a pale yellow foam (0.33 g, 0.41 mmol, 54%).

^{1}H NMR (500 MHz, $CDCl_3$): δ 9.59 (s, 1H, NH-thymidine), 8.01 (s, 1H, H^6), 7.44 – 7.39 (m, 2H, Ar-H), 7.35 – 7.30 (m, 4H, Ar-H), 7.30 – 7.26 (m, 2H, Ar-H), 7.24 – 7.18 (m, 1H, Ar-H), 6.86 – 6.80 (m, 4H, Ar-H), 6.27 (t, *J* = 6.7 Hz, 1H, $H^{1'}$), 4.50 (app. dt, *J* = 5.8, 3.1 Hz, 1H, $H^{3'}$), 4.08 (app. q, *J* = 3.1 Hz, 1H, $H^{4'}$), 3.77 (s, 6H, OCH_3), 3.41 – 3.27 (m, 6H, $H^{3''}$ and $H^{5'}$ and $H^{10''}$), 3.20 (d, *J* = 2.5 Hz, 2H, $H^{5a''}$), 2.51 – 2.40 (m, 3H, $H^{2'a}$ and $H^{5''}$), 2.29 – 2.20 (m, 1H, $H^{2'b}$), 2.15 (t, *J* = 2.5 Hz, 1H, $H^{7a''}$), 1.54 (app. p, *J* = 7.0 Hz, 2H, $H^{9''}$), 1.42 – 1.27 (m, 6H, $H^{6''}$and $H^{7''}$and $H^{8''}$);

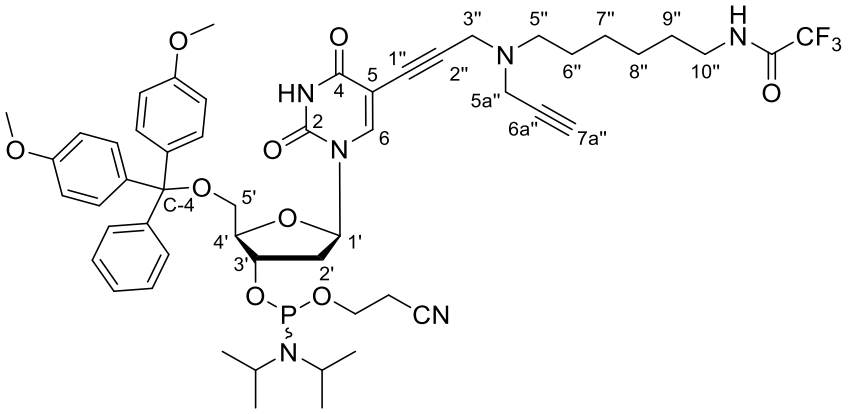
^{13}C NMR (126 MHz, $CDCl_3$): δ 162.0 (C4), 158.6 (Ar) 157.3 (q, *J* = 36.7 Hz, CO-CF_3), 149.5 (C2), 144.5 (Ar), 142.2 (C6), 135.6 (Ar), 130.0 (Ar-H), 128.1 (Ar-H), 127.9 (Ar-H), 127.0 (Ar-H), 116.0 (q, *J* = 287.8 Hz, CF_3), 113.3 (Ar-H), 100.2 (C5), 89.4 (C2''), 87.0 (C-4), 86.5 (C4'), 85.7 (C1'), 79.0 (C6a''), 75.6 (C1''), 73.0

(C7a''), 72.2 (C3'), 63.5 (C5'), 55.3 (OCH_3), 52.1 (C5''), 43.0 (C3''), 42.4 (C5a''), 41.4 (C2'), 39.9 (C10''), 28.5 (C9''), 26.64, 26.47, 26.12 (C6'' – C8'');

^{19}F NMR (376 MHz, $CDCl_3$): δ -75.74 (CF_3);

HRMS (ESI^+) *m/z* $[M+H]^+$ for $C_{44}H_{48}F_3N_4O_8$ calc. 817.3419 found 817.3411; R_f = 0.60 (MeCN:Toluene, *v*:*v* = 1:1), *p*-anisaldehyde, UV.

6.2.37. Synthesis of 5-pargylamino(N-propargyl-N-hexyltrifluoroacetamide) -5′-O-(4,4'-dimethoxytritryl)-2′-deoxythymidine phosphoramidite (**37**)



To a solution of **36** (0.27 g, 0.33 mmol, 1.0 eq) and anhydrous degassed DIPEA (0.16 mL, 0.93 mmol, 2.8 eq) under an argon atmosphere in anhydrous degassed CH_2Cl_2 (9.0 mL), was added 2-cyanoethyl *N*,*N*-diisopropylchlorophosphoramidite (0.10 mL, 0.46 mmol, 1.4 eq). The reaction was stirred for 1.5 h, quenched with argon saturated KCl solution (5 mL) and the organic phase was passed through a layer of anhydrous Na_2SO_4 followed by evaporation to give a yellow foam. The crude product was purified by gel chromatography on silica gel (degassed 60-75% EtOAc/hexane) pre-equilibrated with pyridine, under an argon pressure to give the product as white foam (0.20 g, 0.20 mmol, 61%).

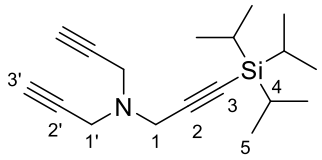
^1H NMR (400 MHz, $CDCl_3$): δ 8.77 (s, 1H, NH-thymidine), 8.06 (s, 0.5H, H^6 isomer a), 8.02 (s, 0.5H, H^6 isomer b), 7.47 – 7.39 (m, 2H, Ar-H), 7.38 – 7.24 (m, 6H, Ar-H), 7.24 – 7.15 (m, 1H, Ar-H), 6.90 – 6.79

(m, 4H, Ar-H), 6.33 – 6.22 (m, 1H, $H^{1'}$), 4.61 – 4.54 (m, 1H, $H^{3'}$), 4.22 – 4.13 (m, 1H, $H^{4'}$), 3.79 (s, 6H, OCH_3), 3.88 – 3.36 (m, 6H, $OC\underline{H}_2CH_2$-CN and iPr-CH and $H^{10''}$), 3.36 – 3.25 (m, 4H, $H^{3''}$ and $H^{5'}$), 3.18 – 3.10 (m, 2H, $H^{5a''}$), 2.62 (t, *J* = 6.3 Hz, 1H, CH_2^a-CN), 2.58 – 2.49 (m, 1H, $H^{2'a}$), 2.47 – 2.37 (m, 3H, CH_2^b-CN and $H^{5''}$), 2.33 – 2.24 (m, 1H, $H^{2'b}$), 2.14 (app. q, *J* = 2.3 Hz, 1H, $H^{7a''}$), 1.55 (app. p, *J* = 7.0 Hz, 2H, $H^{9''}$), 1.41 – 1.23 (m, 6H, $H^{6''}$ – $H^{8''}$), 1.20 – 1.15 (m, 9H, iPr-CH_3), 1.07 (d, *J* = 6.8 Hz, 3H, iPr-CH_3);

^{31}P NMR (162 MHz, $CDCl_3$): δ 148.99 (s), 148.61 (s);

HRMS (ESI^+) *m/z* $[M+H]^+$ for $C_{53}H_{65}F_3N_6O_9P$ calc. 1017.4497 found 1017.4462; R_f = 0.71 and 0.61 for two isomers (EtOAc:*n*-Hexane, *v*:*v* = 7:3), *p*-anisaldehyde, UV.

6.2.38. Synthesis of N,N-dipropargyl-N-3-(triisopropylsilyl)propargylamine (**38**)



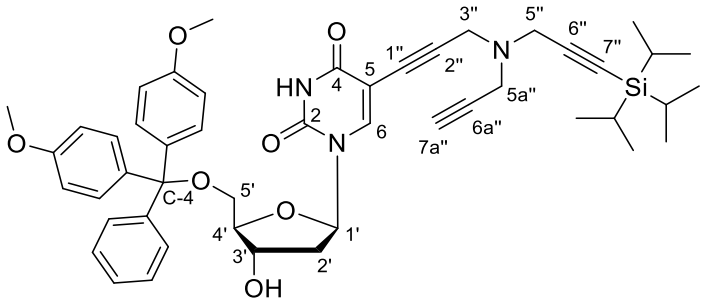
To a stirred solution of tripropargylamine (5.39 mL, 38.1 mmol, 1.0 eq) in THF (100 mL) lithium bis(trimethylsilyl)amide (1.0 M in THF, 38.1 mL, 38.1 mmol, 1.0 eq) was added dropwise under an argon atmosphere at -78 °C and stirred for 45 min. Triisopropyl chloride (8.97 mL, 41.9 mmol, 1.1 eq) was added dropwise and stirred for 2 h at -78 °C. The reaction mixture was warmed to RT, quenched with H_2O (200 mL) and extracted with Et_2O (2 x 150 mL). The organic phase was washed with HCl (3.5%, 50 mL), dried with Na_2SO_4, filtered and evaporated. The crude mixture was distilled under vacuum (160 °C, pressure 8×10^{-1} mbar) to give the product as colourless liquid (5.69 g, 19.8 mmol, 52%).

^{1}H NMR (400 MHz, $CDCl_3$): δ 3.54 (s, 2H, H^1), 3.48 (d, *J* = 2.5 Hz, 4H, $H^{1'}$), 2.24 (t, *J* = 2.5 Hz, 2H, $H^{3'}$), 1.09 – 1.03 (m, 21H, H^4 and H^5);

^{13}C NMR (101 MHz, $CDCl_3$): δ 101.9 (C2), 86.7 (C3), 78.8 (C2'), 73.3 (C3'), 43.2 (C1), 41.9 (C1'), 18.7 (C5), 11.3 (C4);

LRMS (ESI$^+$) *m/z* (%): 288.2 ([M+H]$^+$, 100); HRMS (ESI$^+$) *m/z* [M+H]$^+$for $C_{18}H_{30}NSi$ calc. 288.2142 found 288.2140; bp. at 8×10^{-1} mbar = 120 °C.

6.2.39. Synthesis of 5-pargylamino(N-propargyl-N-7''-(triisopropylsilyl) propargyl)-5′-*O*-(4,4’-dimethoxytritryl)-2′-deoxythymidine (**39**)



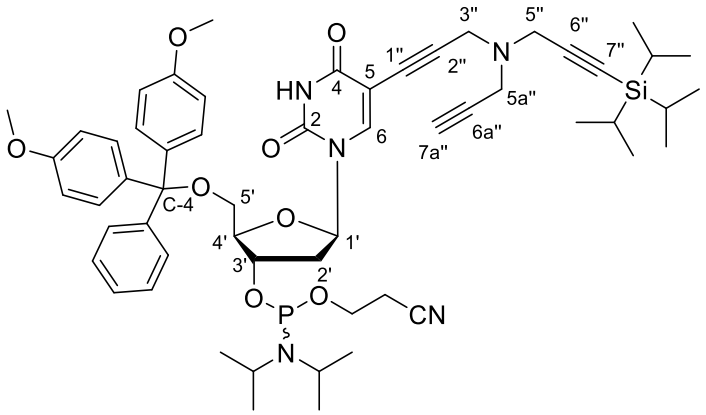
To a stirred solution of 5-iodo-5'-DMTr-deoxythymidine (0.50 g, 0.76 mmol, 1.00 eq), **38** (0.83 g, 2.9 mmol, 2.9 eq), Pd $(PPh_3)_4$ (88 mg, 0.076 mmol, 0.10 eq) and CuI (27 mg, 0.14 mmol, 0.18 eq) in anhydrous degassed DMF (2.5 mL) under an argon atmosphere at RT, anhydrous degassed NEt_3 (2.5 mL) was added. The mixture was stirred for 12 h, evaporated and redissolved in EtOAc (20 mL). The organic phase was washed with an EDTA solution (4%, 10 mL), H_2O (10 mL) and sat. NaCl (10 mL). The organic layer was dried with Na_2SO_4 filtered and evaporated, followed by purification by gel chromatography on silica gel (degassed 10-100% EtOAc/hexane) to give the product as a pale yellow foam (0.31 g, 0.38 mmol, 50%).

^{1}H NMR (500 MHz, $CDCl_3$): δ 9.61 (s, 1H, NH), 7.96 (s, 1H, H^6), 7.46 – 7.41 (m, 2H, Ar-H), 7.36 – 7.33 (m, 4H, Ar-H), 7.32 – 7.28 (m, 2H, Ar-H), 7.25 – 7.20 (m, 1H, Ar-H), 6.88 – 6.82 (m, 4H, Ar-H), 6.29 (t, *J* = 6.3 Hz, 1H, H$^{1'}$), 4.51 (app. dt, *J* = 5.9, 2.8 Hz, 1H, H$^{3'}$), 4.13 – 4.1 (m, 1H, H$^{4'}$), 3.79 (s, 6H, OCH_3), 3.44 – 3.32 (m, 8H, H$^{3''}$and H$^{5'}$ and H$^{5''}$and H$^{5a''}$), 2.53 (ddd, *J* = 13.6, 6.3, 2.8 Hz, 1H, H$^{2'a}$), 2.22 – 2.21 (m, 1H, H$^{2'b}$), 2.20 (t, *J* = 2.4 Hz, 1H, H$^{7a''}$), 1.11 – 1.02 (m, 21H, $SiCH(CH_3)_2$);

13C NMR (126 MHz, $CDCl_3$): δ 161.7 (C4), 158.6 (Ar), 149.53 (C2), 144.6 (Ar), 142.3 (C6), 135.5 (Ar), 130.0 (Ar-H), 128.0 (Ar-H), 127.9 (Ar-H), 127.0 (Ar-H), 113.3 (Ar-H), 102.0 (C6''), 100.1 (C5) 89.3 (C2''), 86.9 (C-4), 86.5 (C4'), 86.4 (C7''), 85.8 (C1'), 78.8 (C6a''), 75.8 (C1''), 73.2 (C7a''), 72.3 (C3'), 63.7 (C5'), 55.2 (OCH_3), 43.1 (C3''), 43.0 (C5a''), 41.5 (C5''), 41.3 (C2'), 18.6 (Si-CH($\underline{C}H_3)_2$), 11.2 (SiCH);

HRMS (ESI^+) *m/z* $[M+H]^+$ for $C_{45}H_{58}O_7N_3Si$ calc. 816.4039 found 816.4038; R_f = 0.40 (MeCN:Toluene, *v*:*v* =1:1), *p*-anisaldehyde, UV.

6.2.40. Synthesis of 5-pargylamino(N-propargyl-N-7''-(triisopropylsilyl) propargyl)-5′-*O*-(4,4’-dimethoxytritryl)-2′-deoxythymidine phosporamidite (**40**)



To a solution of **39** (0.30 g, 0.37 mmol, 1.0 eq) in anhydrous degassed CH_2Cl_2 (9.0mL) and anhydrous degassed DIPEA (0.19 mL, 1.1 mmol, 3.0 eq) under an argon atmosphere, was added 2-cyanoethyl *N*,*N*-diisopropylchlorophosphoramidite (0.12 mL, 0.52 mmol, 1.4 eq). The reaction was stirred for 1.5 h, quenched with argon saturated KCl solution (5 mL) and the organic phase was passed through a layer of anhydrous Na_2SO_4 followed by evaporation to give a yellow foam. The crude product was purified by gel chromatography on silica gel (degassed 40-50% EtOAc/hexane) pre-equilibrated with pyridine, under an argon pressure to give the product as white foam (0.19 g, 0.19 mmol, 51%).

^{1}H NMR (400 MHz, $CDCl_3$): δ 8.04 (s, 1H, NH-thymidine), 7.93 (s, 0.5H, H^6 isomer a), 7.88 (s, 0.5H, H^6 isomer b), 7.38 – 7.32 (m, 2H, Ar-H), 7.30 – 7.20 (m, 6H, Ar-H), 7.18 – 7.10 (m, 1H, Ar-H), 6.81 – 6.73 (m, 4H, Ar-H), 6.24 – 6.15 (m, 1H, $H^{1'}$), 4.54 – 4.46 (m, 1H, $H^{3'}$), 4.16 – 4.07 (m, 1H, $H^{4'}$), 3.72 (s, 6H, OCH_3), 3.72 – 3.43 (m, 4H, N-C<u>H</u> and O<u>CH_2</u>CH_2-CN), 3.33 – 3.25 (m, 8H, $H^{3''}$ and $H^{5'}$ and $H^{5''}$ and $H^{5a''}$), 2.56 (t, *J* = 6.4 Hz, 1H, CH_2^a-CN), 2.48 (ddd, *J* = 13.7, 5.8, 2.7 Hz, 1H, $H^{2'a}$), 2.38 (t, *J* = 6.4 Hz, 1H, CH_2^b-CN), 2.25 – 2.15 (m, 1H, $H^{2'b}$), 2.11 (app. dt, *J* = 2.3 Hz, 1H, $H^{7a''}$), 1.11 (dd, *J* = 6.7, 3.1 Hz, 9H, N-CH(C<u>H</u>$_3$)$_2$), 1.04 – 0.93 (m, 24H, SiCH(CH_3)$_2$ and N-CH(C<u>H</u>$_3$)$_2$);

^{31}P NMR (162 MHz, $CDCl_3$): δ 149.00 (s), 148.59 (s);

HRMS (ESI^+) *m/z* $[M+H]^+$ for $C_{57}H_{75}N_5O_8PSi$ calc. 1016.5117 found 1016.5112; R_f = 0.36 and 0.31 for two isomers (EtOAc:*n*-Hexane, *v*:*v* = 1:1), *p*-anisaldehyde, UV.

6.3. Synthesis and purification of oligonucleotides

6.3.1. Synthesis of DNA oligonucleotides

Standard DNA phosphoramidites, solid supports and additional reagents including amino-C6 dT phosphoramidite (C6, Figure 2.1) were purchased from Link Technologies and Applied Biosystems Ltd. Oligonucleotides were synthesized using an Applied Biosystems 394 automated DNA/RNA synthesizer using a standard 1.0 μmol phosphoramidite cycle of acid-catalyzed detritylation, coupling, capping and iodine oxidation. Stepwise coupling efficiencies and overall yields were determined by an automated trityl cation conductivity monitoring facility and in all cases were >98.0%. β-Cyanoethyl phosphoramidite monomers were dissolved in anhydrous acetonitrile to a concentration of 0.1 M immediately prior to use. The coupling time for normal A, G, C and T monomers was 35 s and the coupling time for the modified monomers (PA[53], AE[54,55], C6, TH, AP-C_3 and AP-C_6 Figure 2.1, Scheme 3.2 and Figure 4.1B) was 360 s. Cleavage of the oligonucleotides from the solid support and deprotection was achieved by exposure to concentrated aqueous ammonia solution (1 h, RT) followed by heating in a sealed tube (5 h, 55 °C). After evaporation of the ammonia *in vacuo*, the fully deprotected oligonucleotides were purified by reverse-phase HPLC (RP-HPLC) on a Gilson system using a Luna 10 μm C8 100 Å pore Phenomenex 10x250 mm column with a gradient of acetonitrile (HPLC grade) in water (Sterile, Millipore system) with TEAA buffer (buffer A: 0.1 M triethylammonium acetate, pH 7.0; buffer B: 0.1 M triethylammonium acetate with 50% acetonitrile, pH 7.0; gradient: 0% to 100% buffer B over 20 min, flow rate: 4 mL/min) or TEAB buffer (buffer A: 0.1 M triethylammonium bicarbonate, pH 7.5; buffer B: 0.1 M triethylammonium bicarbonate, pH 7.5, with 50% acetonitrile) were used (0% to 100% buffer B over 20 min). Elution was monitored by UV absorption at 260-299 nm. Oligonucleotides purified with TEAA buffers were desalted with GE Healthcare Life Sciences illustra NAP 25 then NAP 10 gel filtration columns. After RP-HPLC purification, all oligonucleotides were characterised by electrospray mass spectrometry using a Bruker micrOTOF II focus ESI-TOF MS or UPLC-MS Waters XEVO G2-QTOF instrument in ESI^- mode. Data were processed using MaxEnt or MassLynx v4.1.

6.3.2. Synthesis of RNA oligonucleotides

2′-TBDMS (Tert-butyldimethylsilyl) protected RNA phosphoramidite monomers with *t*-butylphenoxyacetyl protection of the A, G and C nucleobases were used purchased from Sigma-Aldrich and used to assemble RNA oligonucleotides. Benzylthiotetrazole (BTT) was used as the coupling agent, *t*-butylphenoxyacetic anhydride as the capping agent and 0.1 M iodine as the oxidizing agent (Sigma-Aldrich). Coupling time of 10 min was used and coupling efficiencies of >97% were obtained. Cleavage of oligonucleotides from the solid support and protecting groups from the nucleobase and backbone were removed by exposure to concentrated aqueous ammonia : ethanol (*v*:*v* = 3:1) for 2 h at room temperature followed by heating in a sealed tube for 2 h at 55 °C.

6.3.3. Removal of 2′-TBDMS of RNA oligonucleotides

After cleavage from the solid support and removal of the protecting groups from the nucleobases and phosphodiesters in ammonia/ethanol as described above, oligonucleotides were concentrated to a small volume in vacuo, transferred to 15 mL plastic tubes and freeze dried (lyophilised). The residue was dissolved in DMSO (300 µL) and triethylamine trihydrofluoride (300 µL) was added after which the reaction mixtures were kept at 65 °C for 2.5 h. Sodium acetate (3 M, 50 µL) and butanol (3 mL) were added with vortexing and the samples were kept at -80 °C for 30 min then centrifuged at 13000 rpm at 4 °C for 10 min. The supernatant was decanted and the precipitate was washed twice with ethanol (0.75 mL) then dried under vacuum. The fully deprotected oligonucleotides were purified in similar matter as DNA equivalents.

6.3.4. Synthesis of 2′-OMe–RNA oligonucleotides

Phosphoramidites, solid supports and additional reagents were purchased from Link Technologies, the procedure was identical to the DNA oligonucleotides apart from extended coupling time, 10 min, for each step including modifications.

6.4. Labelling of oligonucleotides

6.4.1. NHS ester labelling

6.4.1.1. TO-NHS ester labelling (Method 1)

To a solution of thiazole orange $TO_{Q/B6}$ (20 eq) in DMF (120 µL), DSC[165,230] or PyBop[164] (20 eq) and NMM (60 eq) were added and the mixture was shaken for 30 min at 30 °C (DSC) or 10 min at 37 °C (PyBOP) at 400 rpm. The mixture was added to an equal volume of the oligonucleotide (200 nmol, 1.0 eq) dissolved in carbonate buffer ($NaHCO_3$/Na_2CO_3, 0.5 M, pH = 8.75) in an Eppendorf tube and shaken for 4 h at 37 °C. The mixture was desalted by NAP gel filtration column, lyophilised and purified by RP-HPLC to obtain desired pure labelled oligonucleotide, isolated yields with DSC were 40-50%, and with PyBop were 50-70%.

PyBOP was found to give higher coupling efficiencies (conversion calculated by crude HPLC chromatograms at 260 nm after gel filtration, Figure 2.3) and higher isolated yields (amount of nmol obtained after HPLC purification) than DSC.

6.4.1.2. TO-NHS ester labelling (Method 2)

A solution of thiazole orange $TO_{Q/B6}$ NHS ester (5 eq) in DMF (80 µL) was added to an oligonucleotide (200 nmol) dissolved in carbonate buffer ($NaHCO_3$/Na_2CO_3, 0.5 M, pH = 8.75, 120 µL) and shaken for 5 min at 20 °C. The mixture was desalted by NAP gel filtration column, lyophilised and purified by RP-HPLC to obtain the desired labelled oligonucleotide. Complete conversion to the product was observed by HPLC, and isolated yields were 60-75% (Figure 2.4). A summary of sequences is in Table 6.1 and Table 6.2.

Table 6.1 Masses of oligonucleotide probes (ODNs) labelled with $TO_{B/Q6}$ and DNA targets.

ODN	X =	Sequence	Mass calculated	Mass found
ODN1 5′-GCATXTTACG	PA	5′-GCATPATTACG	3057	3057
	AE	5′-GCATAETTACG	3077	3077
	C6	5′-GCATC6TTACG	3172	3172
	PA-TO_{B6}	5′-GCATPA-TO_{B6}TTACG	3444	3444
	AE-TO_{B6}	5′-GCATAE-TO_{B6}TTACG	3464	3464
	C6-TO_{B6}	5′-GCATC6-TO_{B6}TTACG	3559	3559
	PA-TO_{Q6}	5′-GCATPA-TO_{Q6}TTACG	3444	3444
	AE-TO_{Q6}	5′-GCATAE-TO_{Q6}TTACG	3464	3464
	C6-TO_{Q6}	5′-GCATC6-TO_{Q6}TTACG	3559	3560
Unmodified ODN1	T	5′-GCATTTTACG	3018	3018
ODN1 – T target	A	5′-CGTAA**T**ATGC	3027	3027
ODN1 – A target	T	5′-CGTAA**A**ATGC	3036	3036
ODN2 5′-GCAAXATACG	PA	5′-GCAAPAATACG	3075	3075
	AE	5′-GCAAAEATACG	3095	3096
	C6	5′-GCAAC6ATACG	3190	3190
	PA-TO_{B6}	5′-GCAAPA-TO_{B6}ATACG	3462	3462
	AE-TO_{B6}	5′-GCAAAE-TO_{B6}ATACG	3482	3482
	C6-TO_{B6}	5′-GCAAC6-TO_{B6}ATACG	3577	3577
	PA-TO_{Q6}	5′-GCAAPA-TO_{Q6}ATACG	3462	3462
	AE-TO_{Q6}	5′-GCAAAE-TO_{Q6}ATACG	3482	3482
	C6-TO_{Q6}	5′-GCAAC6-TO_{Q6}ATACG	3577	3577
Unmodified ODN2	T	5′-GCAATATACG	3036	3036
ODN2 – T target	A	5′-CGTAT**T**TTGC	3009	3009
ODN2 – A target	T	5′-CGTAT**A**TTGC	3018	3018
ODN 3 5′-GCACXCTACG	PA	5′-GCACPACTACG	3027	3027
	AE	5′-GCACAECTACG	3047	3048
	AE	5′-GCAGC6GTACG	3142	3142
	PA-TO_{B6}	5′-GCACPA-TO_{B6}CTACG	3414	3413
	AE-TO_{B6}	5′-GCACAE-TO_{B6}CTACG	3434	3433
	C6-TO_{B6}	5′-GCACC6-TO_{B6}CTACG	3529	3529
	PA-TO_{Q6}	5′-GCACPA-TO_{Q6}CTACG	3414	3414
	AE-TO_{Q6}	5′-GCACAE-TO_{Q6}CTACG	3434	3434
	C6-TO_{B6}	5′-GCACC6-TO_{Q6}CTACG	3529	3529
Unmodified ODN3	T	5′-GCACTCTACG	2988	2988
ODN3 – T target (0)	A	5′-CGTAG**T**GTGC	3059	3059
ODN3 – A target	T	5′-CGTAG**A**GTGC	3068	3068
ODN3 – target (-2)		5′-CGTAGAG**A**GC	3077	3077
ODN3 – target (-1)		5′-CGTAGA**T**TGC	3043	3043
ODN3 – target (+1)		5′-CGTA**T**AGTGC	3043	3043
ODN3 – target (+2)		5′-CGT**T**GAGTGC	3059	3059
ODN4 5′-GCAGXGTACG	PA	5′-GCAGPAGTACG	3107	3108
	AE	5′-GCAGAEGTACG	3127	3128
	C6	5′-GCAGC6GTACG	3222	3221
	PA-TO_{B6}	5′-GCAGPA-TO_{B6}GTACG	3494	3494
	AE-TO_{B6}	5′-GCAGAE-TO_{B6}GTACG	3514	3514
	C6-TO_{B6}	5′-GCAGC6-TO_{B6}GTACG	3609	3609
	PA-TO_{Q6}	5′-GCAGPA-TO_{Q6}GTACG	3494	3494
	AE-TO_{Q6}	5′-GCAGAE-TO_{Q6}GTACG	3514	3514
	C6-TO_{Q6}	5′-GCAGC6-TO_{Q6}GTACG	3609	3609
ODN4′ 5′-GCAIXITACG I = Inosine	C6	5′-GCAIC6ITACG	3192	3192
	C6-TO_{B6}	5′-GCAIC6-TO_{B6}ITACG	3579	3579
	C6-TO_{Q6}	5′-GCAIC6-TO_{Q6}ITACG	3579	3579
Unmodified ODN4	T	5′-GCAGTGTACG	3068	3068
ODN4 – T target	A	5′-CGTAC**T**CTGC	2979	2979
ODN4 – A target	T	5′-CGTAC**A**CTGC	2988	2988

Table 6.2 Masses of oligonucleotide probes (2′-OMe–(ORNs)) labelled with $TO_{B/Q\,6/10}$ and RNA targets.

2′-OMe–(ORN)	X =	Sequence	Mass calculated	Mass found
2′-OMe–(ORN1) 5′-GCAUXUUACG	AE	5′-GCAUAEUUACG	3304	3305
	C6	5′-GCAUC6UUACG	3400	3400
	AE-TO_{B6}	5′-GCAUAE-TO_{B6}UUACG	3691	3692
	C6-TO_{B6}	5′-GCAUC6-TO_{B6}UUACG	3787	3787
	AE-TO_{Q6}	5′-GCAUAE-TO_{Q6}UUACG	3691	3692
	C6-TO_{Q6}	5′-GCAUC6-TO_{Q6}UUACG	3787	3786
	AE-TO_{B10}	5′-GCAUAE-TO_{B10}UUACG	3747	3748
	C6-TO_{B10}	5′-GCAUC6-TO_{B10}UUACG	3843	3843
	AE-TO_{Q10}	5′-GCAUAE-TO_{Q10}UUACG	3747	3748
	C6-TO_{Q10}	5′-GCAUC6-TO_{Q10}UUACG	3843	3843
2′-OMe– 5′-GCAXUUXACG	2 x AE	5′-GCAAEUUAEACG	3348	3348
	2 x AE-TO_{Q6}	5′-GCAAE-TO_{Q6}UUAE-TO_{Q6}ACG	4122	4122
2′-OMe– 5′-GCAUXXUACG-3′-propanol	2 x AE	5′-GCAUAEAEUACG-3′-propanol	3409	3409
	2 x AE-TO_{Q6}	5′-GCAUAE-TO_{Q6}AE-TO_{Q6} UACG-3′-propanol	4183	4183
2′-OH–(ORN1)	U	5′-GCAU**U**UUACG	3121	3122
(ORN1) – RNA target A	A	5′-CGUAA**A**AUGC	3167	3167
(ORN1) – RNA target U	U	5′-CGUAA**U**AUGC	3144	3146
2′-OMe–(ORN2) 5′-GCAAXAUACG	AE	5′-GCAAAEAUACG	3351	3352
	C6	5′-GCAAC6AUACG	3446	3446
	AE-TO_{B6}	5′-GCAAAE-TO_{B6}AUACG	3738	3738
	C6-TO_{B6}	5′-GCAAC6-TO_{B6}AUACG	3833	3833
	AE-TO_{Q6}	5′-GCAAAE-TO_{Q6}AUACG	3738	3739
	C6-TO_{Q6}	5′-GCAAC6-TO_{Q6}AUACG	3833	3833
2′-OH–(ORN2)	U	5′-GCAA**U**AUACG	3168	3167
(ORN2) – RNA target A	A	5′-CGUAU**A**UUGC	3121	3122
(ORN2) – RNA target U	U	5′-CGUAU**U**UUGC	3098	3099
2′-OMe–(ORN3) 5′-GCACXCUACG	AE	5′-GCACAECUACG	3302	3303
	C6	5′-GCACC6CUACG	3398	3399
	AE-TO_{B6}	5′-GCACAE-TO_{B6}CUACG	3689	3690
	C6-TO_{B6}	5′-GCACC6-TO_{B6}CUACG	3785	3785
	AE-TO_{Q6}	5′-GCACAE-TO_{Q6}CUACG	3689	3690
	C6-TO_{Q6}	5′-GCACC6-TO_{Q6}CUACG	3785	3786
2′-OH–(ORN3)	U	5′-GCAC**U**CUACG	3120	3119
(ORN3) – RNA target A	A	5′-CGUAG**A**GUGC	3200	3200
(ORN3) – RNA target U	U	5′-CGUAG**U**GUGC	3177	3178
2′-OMe–(ORN4) 5′-GCAGXGUACG	AE	5′-GCAGAEGUACG	3383	3384
	C6	5′-GCAGC6GUACG	3478	3478
	AE-TO_{B6}	5′-GCAGAE-TO_{B6}GUACG	3770	3771
	C6-TO_{B6}	5′-GCAGC6-TO_{B6}GUACG	3865	3864
	AE-TO_{Q6}	5′-GCAGAE-TO_{Q6}GUACG	3770	3771
	C6-TO_{Q6}	5′-GCAGC6-TO_{Q6}GUACG	3865	3864
2′-OH–(ORN4)	U	5′-GCAG**U**GUACG	3200	3200
(ORN4) – RNA target A	A	5′-CGUAC**A**CUGC	3120	3119
(ORN4) – RNA target U	U	5′-CGUAC**U**CUGC	3097	3096

6.4.2. General procedure for labelling of $TO_{B/Q2}$ on solid support

To thiazole orange (TO_{XY} where X = B or Q, Y = 2 or 6, **z** eq, Table 6.3) was added solution of PPTS (**z** eq) in solvent (**f/2** µL). The mixture was vortexed (mixture not soluble), followed by the addition of solution (**f/2** µL) of coupling reagent in solvent (**k**) eq). To a reaction mixture NMM was added (**g** eq) stirred for

5 min and added to a NH_2–TH–ODN3 oligonucleotide on CPG in (a vial or a column) (**h** µm, 1.0 eq) previously deprotected with piperdine : DMF (v : v 1 : 9 mL) for 20 minutes. The suspension was shaken for 12 h at (j) °C. The mixture was washed with PPTS solution of DMF (5 mL; 10 mg for 1 mL), DMF (5 mL), DCM (5 mL) and MeCN (5 mL). The CPG was treated for 1 hour with NH_3(aq), transferred to a vial and deprotected for 5 h at 55°C, evaporated, freeze dried and analysed by ESI-TOF MS.

Table 6.3 Conditions for solid phase labelling of $TO_{B2/Q2}$ into 5'-GCAC**TH**CTACG (ODN3-TH) sequence.

Reaction	A-1	A-2	A-3	A-4	A-5	A-6	A-7	A-8	A-9	A-10
Dye	TO_{Q2}	TO_{B2}	TO_{Q2}	TO_{B2}	TO_{Q2}	TO_{B2}	TO_{Q2}	TO_{Q2}	TO_{B2}	TO_{Q2}
Solvent	DMF	DMF	DMF	DMF	DMF	DMSO	DMF	DMSO	DMSO	DMSO
Vol. / uL(f)	300	300	200	200	300	200	300	200	300	300
PPTS eq	80	80	-	-	100	100	100	100	100	100
Coupling reagent	PyBOP	PyBOP	HBTU	HBTU	PyBOP	PyBOP	PyBOP	PyBOP	PyBOP	PyBOP
Base	NMM	NMM	DIPEA	DIPEA	DIPEA	DIPEA	DIPEA	DIPEA	DIPEA	DIPEA
eq of base to dye (g)	1	1	9	9	5	5	5	5	5	5
Scale uM (h)	0.25	0.25	0.25	0.25	0.1	0.1	0.1	0.1	0.1	0.1
eq of dye (z)	80	80	10	10	100	100	100	100	100	100
eq of C-reag (k)	80	80	20	20	250	250	250	250	250	250
Temperature (j)	30	30	RT	RT	RT	55	55	55	55	55
Reaction vessel (v = vial; c =column)	v	v	c	c	c	c	c	c	c	c

A-25	A-24	A-23	A-22	A-21	A-20	A-19	A-18	A-17	A-16	A-15	A-14	A-13	A-12	A-11
TO_{B6}	$TO_{Q2}/3x^{a}$	$TO_{B2}/3x^{a}$	$TO_{Q2}/3x^{a}$	$TO_{B2}/3x^{a}$	TO_{Q2}	TO_{B2}	TO_{B2}	TO_{B2}	TO_{B2}	TO_{Q2}	TO_{Q2}	TO_{Q2}	TO_{B2}	TO_{B2}
DMSO	DMSO	DMSO	DMSO	DMSO	DMSO	DMSO	DMF	DMF	DMSO	DMSO	DMSO	DMSO	DMSO	DMSO
100	50	50	100	100	200	200	300	300	300	300	400	400	400	400
100	50	50	50	50	100	100	100	100	100	100	100	100	100	100
PyBOP	PyBOP	PyBOP	PyBOP	PyBOP	PyBOP	PyBOP	PyBOP	PyBOP	PyBOP	PyBOP	DSC	HATU	DSC	HATU
DIPEA	DIPEA	DIPEA	DIPEA	DIPEA	DIPEA	DIPEA	DIPEA	DIPEA	DIPEA	DIPEA	DIPEA	DIPEA	DIPEA	DIPEA
5	2	2	5	5	5	5	5	5	5	5	2	5	2	5
0.05	0.05	0.05	0.1	0.1	0.1	0.1	0.1	0.1	0.1	0.1	0.1	0.1	0.1	0.1
100	50	50	50	50	100	100	100	100	100	100	100	100	100	100
250	50	50	125	125	250	250	250	250	250	250	99	99	99	99
55	55	55	55	55	55	55	55	RT	RT	RT	55	55	55	55
v	v	v	v	v	v	v	c	c	c	c	c	c	c	c

[a]Amount of labelling procedures repeated on the same sample

6.4.3. General procedure for amine to azide conversion on the oligonucleotides

To a solution of NH_2-olignuclotide (1.0 eq, 70 nmol) in buffer ($NaHCO_3$, 50 mM, pH = 8.5, 1:3 MeOH/H_2O; 200 µL) was added a stock of $CuSO_4$ (100 mM in H_2O; 2.00 µL) and stock of ISHAC (Synthesized according to literature procedure,[77] 25 mg / 1 mL of MeOH:H_2O 1:1; 11.7 µL) and shaken for 2 h at 55 °C. The mixture was desalted by NAP gel filtration column, lyophilised and purified by RP-HPLC to obtain the desired labelled oligonucleotide. Complete conversion to the product was observed by HPLC, examples are given in Figure 3.5.

6.4.4. General procedure Copper-Click 1,3-dipolar cycloaddition (CuAAC)

To a solution of alkyne/azide containing oligonucleotide (40 nmol, 1.0 eq) in H_2O (600 µL), TEAA buffer (2M, pH = 7.0; 200 µL), DMSO (590 µL) and stock of terminal azide/alkyne containing dye (10 nmol/µL in DMSO, 12 µL, 3.0 eq) and freshly prepared sodium ascorbate (0.9 mg/ 1.0 mL of H_2O; 200 µL) were vortexed together. Mixture was degassed by bubbling Argon gas for 5 min followed by addition of Cu^{II}:THPTA (Tris(3-hydroxypropyltriazolylmethyl)amine) complex (10 mM in 55%/45% DMSO/H_2O; 100 µL, Cu source: $CuSO_4$). Reaction was shaken for 2 h at 25 °C, desalted with GE Healthcare Life Sciences illustra NAP 25 and was purified by reverse-phase HPLC (RP-HPLC) to obtain pure product with full conversion. Example of copper 'Click' labelling are given in Figure 6.1.

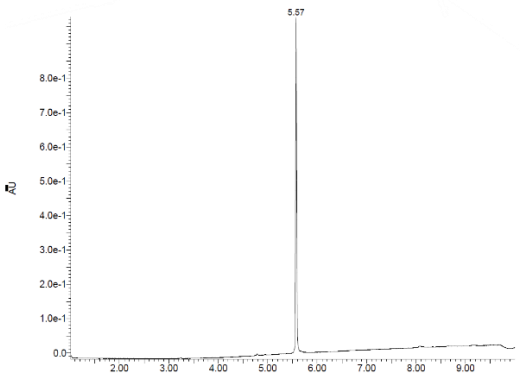


Figure 6.1 Example of HPLC chromatograms at 260 nm of purified oligonucleotide ODN1-TO_{QPr}– DNA (5'-GCATTh-TO_{QPr}TTACG) mass calculated: 3236 mass found: 3235

Table 6.4 Masses of Threoninol modified oligonucleotide probes (ODN1) labelled with $TO_{B/QPr}$.

ODN	X =	Sequence	Mass calculated	Mass found
ODN1 5′-GCATXTTACG	TH-NH_2	5′-GCATTH-NH_2TTACG	2881	2881
	TH-N_3	5′-GCATTH-N_3TTACG	2907	2908
	TH-triazole-TO_{BPr}	5′-GCATTH-TO_{BPr}TTACG	3236	3235
	TH-triazole-TO_{QPr}	5′-GCATTH-TO_{QPr}TTACG	3236	3235
ODN1 – T target	T	5′-CGTAA**T**ATGC	3027	3027
ODN1 – A target	A	5′-CGTAA**A**ATGC	3036	3036
ODN3 5′-GCACXCTACG	TH-NH_2	5′-GCACTH-NH_2CTACG	2851	2851

Table 6.5 Masses of oligonucleotide probes ODN7 with amino-C_3-propargyl dT modification labelled with various dyes and appropriate target.

Sequence	X =	Sequence	Mass calculated	Mass found
ODN7	Amino-propargyl-C_3	5′-CGCTTC**APC3(NH$_2$/propargyl)**GTATCTATATTCATC	6760	6761
		5′-CGCTTC**APC$_3$(TO$_{B6}$/propargyl)**GTATCTATATTCATC	7147	7149
		5′-CGCTTC**APC$_3$(NH$_2$/ATTO647N)**GTATCTATATTCATC	7606	7607
		5′-CGCTTC**APC$_3$(TO$_{B6}$/ATTO647N)**GTATCTATATTCATC	7992	8057 (+Cu)
		5′-CGCTTC **APC$_3$(TO$_{B10}$/propargyl)**GTATCTATATTCATC	7203	7204
		5′-CGCTTC**APC$_3$(TO$_{B10}$/ATTO647N)**GTATCTATATTCATC	8049	8112 (+Cu)
		5′-CGCTTC**APC$_3$(ATTO647N/propargyl)**GTATCTATATTCATC	7388	7705 (+5 Cu)
		5′-CGCTTC**APC$_3$(ATTO647N/TO$_{B3}$)**GTATCTATATTCATC	7762	7762
		5′-CGCTTC**APC$_3$(NH$_2$/propargyl)**GTATCTA**APC$_3$ (NH$_2$/propargyl)**ATTCATC	6894	6895
		5′-CGCTTC**APC$_3$(ATTO647N/TO$_{B3}$)**GTATCTA**APC$_3$ (ATTO647N/TO$_{B3}$)**ATTCATC	8899	8898
	Target	5′-CTATGATGAATATAGATACAGAAGCGTCAT	9262	9263

Table 6.6 Masses of oligonucleotide 2′-OMe–ORN3 probes with amino-$C_{3/6}$-propargyl dT modification labelled with various dyes.

Sequence	X =	Sequence	Mass calculated	Mass found
2′-OMe–ORN3 5′-GCACXCUACG	Amino-propargyl-C_3	5′-GCAC**APC$_3$(NH$_2$/propargyl)**CUACG	3378	3379
		5′-GCAC**APC$_3$(TO$_{B6}$/propargyl)**CUACG	3765	3765
		5′-GCAC**APC$_3$(TO$_{B6}$/Alexa555)**CUACG	4506	4506
		5′-GCAC**APC$_3$(NH$_2$/Alexa555)**CUACG	4119	4120
		5′-GCAC**APC$_3$(TO$_{B6}$/Alexa594)**CUACG	4612	4612
	Amino-propargyl-C_6	5′-GCAC**APC$_6$(NH$_2$/propargyl)**CUACG	3420	3421
		5′-GCAC**APC$_6$(TO$_{B6}$/propargyl)**CUACG	3807	3807
		5′-GCAC**APC$_6$(TO$_{B6}$/Alexa555)**CUACG	4548	4548
		5′-GCAC**APC$_6$(NH$_2$/Alexa555)**CUACG	4161	4162
		5′-GCAC**APC$_6$(TO$_{B6}$/Alexa594)**CUACG	4654	4654
		5′-GCAC**APC$_6$(TO$_{B6}$/ATTO647N)**CUACG	4654	4653

6.5. Steady state fluorescence measurements

Fluorescence studies were performed on a Perkin Elmer LS50B luminescence spectrometer fitted with Perkin Elmer PTP-1 Peltier temperature controller. FLWinlabTempScan software was used with settings of 400 nm s^{-1} scan speed. For TO the emission wavelength was recorded from 510 nm to 700 nm, excitation wavelength 484 nm, gain: high (900V), excitation slit width 7.0 nm, emission slit width 7.0 nm. For Alexa555 the range of emission was 560 nm to 800 nm at excitation wavelength of 553 nm; for Alexa594 the range of emission was recorded from 600 nm to 800 nm at excitation 590 nm; ATTO647N the range of emission was recorded from 655 nm to 800 nm at excitation 645 nm; the gain and slits width were identical as for TO for all dyes.

Experiment: Samples were prepared in 250 µL cuvettes with 0.25 µM probe containing TO, 200 mM NaCl, 10 mM Na-phosphate buffer pH = 7.0 at 20 °C. Spectra were recorded for the single stranded oligonucleotide probe, and then titrated with 1.1 eq of the desired target oligonucleotide and recorded again. F_{ds}/F_{ss} was calculated by comparison of the surface area under both curves (from 510 to 650 nm unless stated otherwise), each probe – target pair was recorded at least in duplicate and values are given in the charts as an averaged values (From Table 6.13 to Table 6.26). Examples of fluorescence emission spectra are given in Figure 6.9.

It is important to clarify that in this study the ratio of double to single stranded fluorescence (F_{ds}/F_{ss}) was calculated in selected range (see above). More favourable F_{ds}/F_{ss} ratios can be obtained if a narrower band is selected, e.g. For ODN3 C6-TO_{B6} against its complementary DNA target between 510 nm and 555 nm F_{ds}/F_{ss} = 7.7 compared to 6.9 in the region 510 nm to 650 nm, and in case of 2'-OMe–(ORN3) AE-TO_{Q6} against its complementary DNA target the relevant values are 43.9 compared to 33.9, this differences are showed in paragraph 0.

6.6. UV melting studies

UV melting measurements were made on a Varian Cary 4000 UV-Vis spectrophotometer with a Cary temperature controller. Cary Win UV Thermal software was used with an absorbance wavelength of 260 nm. Samples were analysed in 1 mL quartz cuvettes (1 cm path length) and were made to 3.0 µM oligonucleotide probe concentration (X = $TO_{Q/B6}$ strand) and 3.3 µM oligonucleotide target concentration (target strand: A-match, T/U-mismatch) in phosphate buffer (NaH_2PO_4, 10 mM, NaCl 200 mM at pH 7.0, unless stated otherwise). The samples were initially denatured by heating to 85 °C at 10 °C min^{-1} then cooled to 15 °C at -1 °C min^{-1} and then maintained at 15 °C for 2 min before heating to 85 °C at 1 °C min^{-1}. UV absorption was recorded every 0.1 °C. The melting temperature (T_m) values were derived from the derivatives of the melting curves and calculated at 260 nm using Cary Win UV Thermal application software. Four successive melting curves were measured and averaged (Table 6.7, Table 6.8, Table 6.9, Table 6.10 and Table 6.11). Examples of melting curves and derivatives are given in Figure 6.10, Figure 6.11, Figure 6.12 and Figure 6.13.

6.7. Quantum yield measurements

Method 1

Quantum yield measurements were made using UV-Vis and fluorescence spectrometers as described above. Samples were prepared in 250 µL 10 mm pathlength cuvettes with increasing concentration of oligonucleotide in 200 mM NaCl, 10 mM Na-phosphate buffer pH = 7.0 at 20 °C. Fluorescence emission and UV absorption spectra were recorded for five concentrations (from 0.1 to 1.25 µM range). The oligonucleotide probe was treated with 1.1 eq of the desired target and recorded again for five dilution steps. Values of Φ yields were calculated by comparison of linear plot of surface area under fluorescence curve to absorption (R^2 ≥0.98) at 484 nm at given concentration, with comparison to fluorescein in 0.1 M NaOH as a standard.

Method 2

The absolute fluorescence quantum yields were measured using a SC-30 integrating sphere module (Edinburgh Instruments) and the re-absorption effect was corrected when possible. For all ODNs/2'-OMe–(ORNs) and double stranded duplexes with DNA or RNA targets, the excitation wavelength was 488 nm, the wavelength step size 0.1 nm and integration dwell time 0.25 s. All fluorescence samples were prepared with optical densities under 0.1 under ambient conditions (1 µM of ODN/2'-OMe–ORN in 1000 µL of buffer, 200 mM NaCl, 10 mM Na-phosphate pH = 7.0). Sample spectra were recorded for the single stranded ODNs/2'-OMe–(ORNs) and then titrated with 1.1 eq of the target (DNA or RNA), allowed to anneal for 2 min and recorded again at 20 °C. Three scans were repeated for both the ss and ds sample solutions and the buffer. The scattering region between 483 nm and 593 nm, and emission region between 500 and 700 nm were chosen for the calculation of the observed quantum yields. Both method 1 and method 2 were found to give comparable values, with results within 0.4% of each other.

6.8. CD spectroscopy

CD spectra (200−550 nm) were recorded on a Jasco J-815 spectropolarimeter using a Quartz optical cell with a path length of 5.0 mm. Scans were performed at 20 °C using a step size of 0.2 nm, a time per point of 1.0 s and a bandwidth of 1 nm, with 100 nm min^{-1} scanning speed; the average of eight scans is shown (Figure 2.28 - Figure 2.32). Samples from UV melting studies (3.0 µM of each oligonucleotide probe and 3.3 µM of DNA/RNA target in a 10 mM Na-phosphate buffer containing 200 mM NaCl at pH 7.0) were used directly. The average trace was smoothed (20 points) using in-built software. A CD spectrum of only buffer was also recorded and was subtracted from the collected data.

6.9. Oligonucleotide duplex melting temperatures

Table 6.7 Melting temperatures for TO-modified ODN1-4 duplexes with DNA targets (T_m), with comparison to unmodified duplexes (ΔT_m). Mismatch target refers to a T mismatch opposite the TO-modified base.

ODN	X =	T_m DNA match target			ΔT_m match target[a]			T_m DNA mismatch target			ΔT_m mismatch target		
ODN1 5′-GCATXTTACG	PA-TO$_{Q6}$	42.9	±	0.3	1.3	±	0.8	27.2	±	0.5	2.7	±	0.6
	PA-TO$_{B6}$	48.2	±	0.2	6.6	±	0.7	33.5	±	0.4	9.0	±	0.5
	AE-TO$_{Q6}$	49.3	±	0.4	7.7	±	0.8	37.4	±	0.5	12.9	±	0.6
	AE-TO$_{B6}$	47.9	±	0.4	6.3	±	0.8	36.7	±	0.5	12.2	±	0.6
	C6-TO$_{Q6}$	43.9	±	0.4	2.3	±	0.8	36.3	±	0.5	11.8	±	0.6
	C6-TO$_{B6}$	50.0	±	0.2	8.4	±	0.7	36.7	±	0.3	12.2	±	0.4
ODN2 5′-GCAAXATACG	PA-TO$_{Q6}$	45.6	±	0.5	6.0	±	0.8	35.1	±	0.6	9.8	±	0.8
	PA-TO$_{B6}$	52.4	±	0.4	12.8	±	0.7	39.9	±	0.4	14.6	±	0.6
	AE-TO$_{Q6}$	50.4	±	0.5	10.8	±	0.8	37.6	±	0.4	12.3	±	0.6
	AE-TO$_{B6}$	50.9	±	0.3	11.3	±	0.7	38.0	±	0.2	12.7	±	0.5
	C6-TO$_{Q6}$	44.4	±	0.5	4.8	±	0.8	38.8	±	0.4	13.5	±	0.6
	C6-TO$_{B6}$	49.5	±	0.7	9.9	±	0.9	39.1	±	0.1	13.8	±	0.5
ODN3 5′-GCACXCTACG	PA-TO$_{Q6}$	54.7	±	0.4	7.1	±	0.7	43.2	±	0.6	9.4	±	0.9
	PA-TO$_{B6}$	62.2	±	0.6	14.6	±	0.8	48.9	±	0.1	15.1	±	0.7
	AE-TO$_{Q6}$	56.9	±	0.4	9.3	±	0.7	48.3	±	0.4	14.5	±	0.8
	AE-TO$_{B6}$	55.5	±	0.7	7.9	±	0.9	45.2	±	0.3	11.4	±	0.8
	C6-TO$_{Q6}$	52.3	±	0.4	4.7	±	0.7	51.8	±	0.4	18.0	±	0.8
	C6-TO$_{B6}$	59.1	±	0.1	11.5	±	0.6	49.4	±	0.4	15.6	±	0.8
ODN4 5′-GCAGXGTACG	PA-TO$_{Q6}$	55.4	±	0.5	6.3	±	0.5	42.9	±	0.8	10.5	±	0.9
	PA-TO$_{B6}$	61.4	±	0.6	12.3	±	0.6	47.0	±	0.7	14.6	±	0.8
	AE-TO$_{Q6}$	58.6	±	0.5	9.5	±	0.5	45.9	±	0.7	13.5	±	0.8
	AE-TO$_{B6}$	58.0	±	0.2	8.9	±	0.3	46.0	±	0.1	13.6	±	0.4
	C6-TO$_{Q6}$	53.1	±	0.4	4.0	±	0.4	47.7	±	0.3	15.3	±	0.5
	C6-TO$_{B6}$	59.4	±	0.2	10.3	±	0.3	47.4	±	0.5	15.0	±	0.6
ODN4′ 5′-GCAIXITACG I = Inosine	C6-TO$_{Q6}$	39.7	±	0.4	-9.4	±	0.4	35.7	±	0.4	3.3	±	0.6
	C6-TO$_{B6}$	44.8	±	0.4	-4.3	±	0.4	33.8	±	0.5	1.4	±	0.6
Unmodified 5′-GCAYTYTACG	Y = T	41.6	±	0.7	-			24.5	±	0.3	-		
	Y = A	39.6	±	0.6	-			25.3	±	0.5	-		
	Y = C	47.6	±	0.6	-			33.8	±	0.7	-		
	Y = G	49.1	±	0.2	-			32.4	±	0.4	-		

Table 6.8 Melting temperatures for TO-modified 2′-OMe–(ORN1-4) duplexes with DNA targets (T_m), with comparison to unmodified duplexes (ΔT_m). Mismatch target refers to a T mismatch opposite the TO-modified base.

2′-OMe–(ORN)	X =	T_m DNA match target			ΔT_m DNA match target			T_m DNA mismatch target			ΔT_m DNA mismatch target		
2′-OMe–(ORN1) 5′-GCAUXUUACG	AE-TO_{Q6}	43.2	±	0.4	18.0	±	0.6	31.6	±	0.3	-[b]		
	AE-TO_{B6}	44.5	±	0.4	19.3	±	0.6	32.1	±	0.4	-[b]		
	C6	24.9	±	0.1	-0.3	±	0.5		-[c]				
	C6-TO_{Q6}	34.9	±	0.2	9.7	±	0.5	27.1	±	0.1	-[b]		
	C6-TO_{B6}	39.5	±	0.5	14.3	±	0.7	28.7	±	0.4	-[b]		
	AE-TO_{Q10}	43.0	±	0.4	17.8	±	0.6		-[c]				
	AE-TO_{B10}		-[c]			-[c]	0.5		-[c]				
	C6-TO_{Q10}	30.5	±	0.6	5.3	±	0.8		-[c]				
	C6-TO_{B10}	35.7	±	0.6	10.5	±	0.8		-[c]				
2′-OMe– 5′-GCAXUUXACG	2 × AE	30.9	±	0.7	5.7	±	0.9		-[c]		-[b]		
	2 × AE-TO_{Q6}	54.3	±	0.4	29.1	±	0.6	46.0	±	0.6	-[b]		
2′-OMe– 5′-GCAUXXUACG-3′-propanol	2 × AE-TO_{Q6}	46.2	±	0.1	21.1	±	0.5	40.1	±	0.1	-[b]		
2′-OMe–(ORN2) 5′-GCAAXAUACG	AE-TO_{Q6}	46.1	±	0.9	10.3	±	1.0	31.9	±	0.6	-[b]		
	AE-TO_{B6}	44.6	±	0.3	8.8	±	0.6	29.5	±	0.2	-[b]		
	C6-TO_{Q6}	40.1	±	0.1	4.3	±	0.5	30.9	±	0.4	-[b]		
	C6-TO_{B6}	42.6	±	0.3	6.8	±	0.6	31.2	±	0.2	-[b]		
2′-OMe–(ORN3) 5′-GCACXCUACG	AE-TO_{Q6}	54.3	±	0.9	11.1	±	1.1	44.4	±	0.5	15.9	±	0.7
	AE-TO_{B6}	58.2	±	0.5	15.0	±	0.8	45.2	±	0.7	16.7	±	0.9
	C6-TO_{Q6}	51.2	±	0.2	8.0	±	0.6	42.1	±	0.7	13.6	±	0.9
	C6-TO_{B6}	55.9	±	0.5	12.7	±	0.8	45.1	±	0.2	16.6	±	0.5
2′-OMe–(ORN4) 5′-GCAGXGUACG	AE-TO_{Q6}	57.5	±	0.5	8.4	±	0.6	44.8	±	0.4	12	±	0.5
	AE-TO_{B6}	57.6	±	0.6	8.5	±	0.7	43.3	±	0.5	10.5	±	0.6
	C6-TO_{Q6}	52.8	±	0.6	3.7	±	0.7	41.2	±	0.2	8.4	±	0.4
	C6-TO_{B6}	58.8	±	0.4	9.7	±	0.5	43.4	±	0.1	10.6	±	0.3
Unmodified 2′-OH–RNA 5′-GCAYUYUACG	Y = U	25.2	±	0.5	-				-[a]		-		
	Y = A	35.8	±	0.5	-				-[a]		-		
	Y = C	43.2	±	0.6	-			28.5	±	0.5	-		
	Y = G	49.1	±	0.3	-			32.8	±	0.3	-		

[a]-no melting observed, [b]-no reference melting curve, [c]-No data obtained/measurment wasn't performed

Table 6.9 Melting temperatures for TO-modified ODN1-4 duplexes with RNA targets (T_m), with comparison to unmodified duplexes (ΔT_m). Mismatch target refers to a U mismatch opposite the TO-modified base.

ODN	X =	T_m RNA match target			ΔT_m RNA match target			T_m RNA mismatch target			ΔT_m RNA mismatch target		
ODN1 5′-GCATXTTACG	AE-TO_{Q6}	41.6	±	0.2	5.6	±	0.4	27.8	±	0.4	-[b]	±	0.4
	AE-TO_{B6}		-[c]						-[c]		-		
	C6-TO_{Q6}	39.2	±	0.3	3.3	±	0.4	25.0	±	0.4	-[b]	±	0.4
	C6-TO_{B6}	44.1	±	0.1	8.1	±	0.3	27.7	±	0.5	-[b]	±	0.5
ODN2 5′-GCAAXATACG	AE-TO_{Q6}		-[c]						-[c]				
	AE-TO_{B6}		-[c]						-[c]				
	C6-TO_{Q6}	33.3	±	0.4	1.3	±	0.4	22.9	±	0.5	-[b]	±	0.5
	C6-TO_{B6}	37.2	±	0.7	5.2	±	0.7	23.2	±	0.5	-[b]	±	0.5
ODN3 5′-GCACXCTACG	AE-TO_{Q6}		-[c]						-[c]				
	AE-TO_{B6}		-[c]					38.0	±	0.9	4.8	±	0.9
	C6-TO_{Q6}	49.5	±	0.5	0.6	±	0.6	34.4	±	0.4	1.2	±	0.5
	C6-TO_{B6}	54.8	±	0.7	5.9	±	0.8	38.6	±	0.4	5.4	±	0.5
ODN4 5′-GCAGXGTACG	AE-TO_{Q6}		-[c]						-[c]				
	AE-TO_{B6}		-[c]						-[c]				
	C6-TO_{Q6}	45.4	±	0.6	0.8	±	0.8	32.6	±	0.7	5.6	±	1.0
	C6-TO_{B6}	50.9	±	0.4	6.3	±	0.6	34.8	±	0.9	7.8	±	1.1
ODN4′ 5′-GCAIXITACG I = Inosine	C6-TO_{Q6}	33.2	±	0.5	-11.4	±	0.7	24.2	±	0.9	-2.8	±	1.1
	C6-TO_{B6}	37.2	±	0.6	-7.4	±	0.8	24.1	±	0.1	-2.9	±	0.7
Unmodified 5′-GCAYTYTACG	Y = T	35.9	±	0.3	-				-[a]		-		
	Y = A	32.0	±	0.2	-				-[a]		-		
	Y = C	48.9	±	0.3	-			33.2	±	0.3	-		
	Y = G	44.6	±	0.5	-			27.0	±	0.7	-		

[a]-no melting observed, [b]-no reference melting curve, [c]-no data obtained/measurement wasn't performed

Table 6.10 Melting temperatures for TO-modified 2′-OMe–(ORN1-4) duplexes with RNA targets (T_m), with comparison to unmodified duplexes (ΔT_m). Mismatch target refers to a U mismatch opposite the TO-modified base.

2′-OMe–(ORN)	X =	T_m RNA match target			ΔT_m RNA match target			T_m RNA mismatch target			ΔT_m RNA mismatch target		
2′-OMe–(ORN1) 5′-GCAUXUUACG	AE-TO$_{Q6}$	50.4	±	0.3	7.8	±	0.6	39.9	±	0.4	9.5	±	0.7
	AE-TO$_{B6}$	50.3	±	0.4	7.7	±	0.6	40.4	±	0.4	10	±	0.7
	C6	47.4	±	0.6	4.8	±	0.8		-[a]				
	C6-TO$_{Q6}$	47.3	±	0.5	4.7	±	0.7	36.7	±	0.5	6.3	±	0.8
	C6-TO$_{B6}$	50.0	±	0.2	7.4	±	0.5	39.2	±	0.3	8.8	±	0.7
	AE-TO$_{Q10}$	44.8	±	1.1	2.2	±	1.2		-[a]				
	AE-TO$_{B10}$		-[a]				0.5		-[a]				
	C6-TO$_{Q10}$	43.2	±	0.6	0.6	±	0.8		-[a]				
	C6-TO$_{B10}$	47.1	±	0.03	4.5	±	0.5		-[a]				
2′-OMe– 5′-GCAXUUXACG	2 × AE	48.7	±	0.7	6.1	±	0.9		-[a]				
	2 × AE-TO$_{Q6}$	57.2	±	0.4	14.6	±	0.6	48.5	±	0.3	18.1	±	0.7
2′-OMe– 5′-GCAUXXUACG-3′-propanol	2 × AE-TO$_{Q6}$	53.1	±	0.1	10.5	±	0.6	45.0	±	0.2	14.6	±	0.2
2′-OMe–(ORN2) 5′-GCAAXAUACG	AE-TO$_{Q6}$	50.8	±	0.5	6.2	±	0.8	37.4	±	0.6	6.4	±	0.6
	AE-TO$_{B6}$	49.5	±	0.6	4.9	±	0.8	36.5	±	0.5	5.5	±	0.5
	C6-TO$_{Q6}$	44.8	±	0.4	0.2	±	0.7	32.2	±	0.7	1.2	±	0.7
	C6-TO$_{B6}$	45.3	±	0.5	0.7	±	0.8	32.7	±	0.6	1.7	±	0.6
2′-OMe–(ORN3) 5′-GCACXCUACG	AE-TO$_{Q6}$	64.1	±	0.6	4.0	±	0.6	53.4	±	0.7	7.3	±	0.7
	AE-TO$_{B6}$	64.9	±	0.4	4.8	±	0.4	52.7	±	0.7	6.6	±	0.7
	C6-TO$_{Q6}$	60.6	±	0.5	0.5	±	0.5	49.0	±	0.8	2.9	±	0.8
	C6-TO$_{B6}$	64.7	±	0.6	4.6	±	0.6	53.0	±	0.6	6.9	±	0.6
2′-OMe–(ORN4) 5′-GCAGXGUACG	AE-TO$_{Q6}$	65.4	±	0.8	6.5	±	0.9	52.6	±	0.6	6.8	±	0.7
	AE-TO$_{B6}$	64.2	±	0.7	5.3	±	0.8	52.2	±	0.7	6.4	±	0.8
	C6-TO$_{Q6}$	59.3	±	0.6	0.4	±	0.7	46.9	±	0.1	1.1	±	0.3
	C6-TO$_{B6}$	62.8	±	0.5	3.9	±	0.6	48.9	±	0.4	3.1	±	0.5
Unmodified 2′-OH–RNA 5′-GCAYUYUACG	Y = U	42.6	±	0.5	-			30.4	±	0.6	-		
	Y = A	44.6	±	0.6	-			31.0	±	0.1	-		
	Y = C	60.1	±	0.2	-			46.1	±	0.1	-		
	Y = G	58.9	±	0.3	-			45.8	±	0.3	-		

[a] -no data obtained/measurement wasn't performed

Table 6.11 Effect of the mismatch position on melting temperatures of TO-modified 2′-OMe–(ORN3) (5′-GCACXCUACG) duplexes at 1.0 µM with DNA targets at 1.1 µM (T_m), with comparison to fully match target (ΔT_m). Position of mismatch refers to a mismatch (Table S1) in the target strand counting from the TO-modified base, e.g. position "0" is directly opposite the TO modification and "-2" is two nucleobases towards the 5′ end of the probe sequence. ΔT_m wasn't referenced as previously to completely unmodified duplexes due to lack of detectable T_m of some of mismatched duplexes, data not shown.

	X =	Position of mismatch	T_m of appropriate DNA target	ΔT_m of appropriate DNA target to match target
2′-OMe–(ORN3) 5′-GCACXCUACG	AE-TO_{Q6}	-2	37.5 ± 0.9	14.1 ± 1.0
		-1	32.1 ± 0.9	19.6 ± 1.0
		0	42.4 ± 0.2	9.2 ± 0.4
		+1	30.0 ± 0.7	21.7 ± 0.8
		+2	41.2 ± 0.3	10.5 ± 0.5
		match	51.7 ± 0.4	-
	C6-TO_{B6}	-2	30.8 ± 0.5	21.7 ± 0.8
		-1	24.3 ± 0.8	28.2 ± 1.0
		0	40.4 ± 0.8	12.1 ± 1.0
		+1	30.4 ± 0.3	22.1 ± 0.7
		+2	41.1 ± 0.7	11.4 ± 0.9
		match	52.5 ± 0.6	-

Table 6.12 Detailed values for melting temperatures for ORN3 sequence modified with AP-C_3 and AP-C_6 modification labelled with TO_{B6}, Alexa555, Alexa594 and ATTO647N duplexes with DNA and RNA targets (T_m), with comparison to the unlabelled probe sequences (ΔT_m). Conditions: data obtained in a buffer containing 10 mM phosphate 200 mM NaCl at pH 7.0, oligonucleotide concentrations were 1.0 µM of probe and 1.1 µM of target strand.

ORN	X =	Target	T_m			ΔT_m[b]		
2′-OMe–(ORN3) 5′-GCACXCUACG	AP-C_3(TO_{B6}/propargyl)	DNA			no data			
		RNA	60.6	±	0.3	0.1[b]	±	0.4
	AP-C_3(NH_2/Alexa555)	DNA	38.5	±	0.6	-4.2[b]	±	0.6
		RNA	56.1	±	0.2	-4.4[b]	±	0.4
	AP-C_3(TO_{B6}/Alexa555)	DNA	45.0	±	0.2	2.3[b]	±	0.3
		RNA	56.2	±	0.4	-4.3[b]	±	0.5
	AP-C_3(TO_{B6}/Alexa594)	DNA	39.5	±	0.3	-3.2[b]	±	0.4
		RNA	55.1	±	0.4	-5.4[b]	±	0.5
	AP-C_3(NH_2/propargyl)	DNA	42.7	±	1.1	3.2[a]	±	1.1
		RNA	60.5	±	0.5	5.0[a]	±	0.6
	AP-C_6(TO_{B6}/propargyl)	DNA	51.3	±	0.3	9.9[b]	±	0.4
		RNA	62.4	±	0.2	1.5[b]	±	0.4
	AP-C_6(NH_2/Alexa555)	DNA	35.3	±	0.5	-6.1[b]	±	0.5
		RNA	56.2	±	0.3	-4.7[b]	±	0.4
	AP-C_6(TO_{B6}/Alexa555)	DNA	45.3	±	0.4	3.9[b]	±	0.4
		RNA	58.5	±	0.2	-2.4[b]	±	0.4
	AP-C_6(TO_{B6}/Alexa594)	DNA	39.4	±	0.4	-2.0[b]	±	0.4
		RNA	54.8	±	0.4	-6.1[b]	±	0.5
	AP-C_6(TO_{B6}/ATTO647N)	DNA	42.9	±	0.3	1.5[b]	±	0.4
		RNA	54.9	±	0.2	-6.0[b]	±	0.4
	AP-C_6(NH_2/propargyl)	DNA	41.4	±	0.4	1.9[a]	±	0.4
		RNA	60.9	±	0.1	5.4[a]	±	0.3
	2′-OH–GCACUCUACG	DNA	39.5	±	0.2			
		RNA	55.5	±	0.3			

[a]-in comparison to unmodified 2′-OH–GCACUCUACG – target duplex, [b]-in comparison to the unlabelled probe sequences.

6.10. Fluorescence data

Table 6.13 Fluorescence emssion data for TO-modified ODN1-4 probes against DNA targets. F_{ds}/F_{ss} – ratio of integrated fluorescence emission of oligonucleotide duplexes to single stranded, I_0 – fluorescence emission intensity at $\lambda_{em,\,max}$ of single stranded TO-modified oligonucleotides probes, I_{max} – fluorescence emission intensity at $\lambda_{em,\,max}$ of TO-modified oligonucleotide probe-target duplexes. Mismatch target refers to a T mismatch opposite the TO-modified base.

ODN	X =	DNA target	Average F_{ds}/F_{ss}	Average I_0	Average I_{max}
ODN1 5′-GCATXTTACG	PA-TO_{Q6}	match	1.0	130.4 ± 6.0	126.0 ± 8.2
		mismatch	0.9	139.2 ± 12.3	118.7 ± 8.6
	PA-TO_{B6}	match	3.7	48.4 ± 1.7	199.4 ± 6.6
		mismatch	1.1	51.2 ± 6.4	59.4 ± 7.8
	AE-TO_{Q6}	match	2.8	49.8 ± 0.3	159.6 ± 1.9
		mismatch	1.5	48.4 ± 0.7	78.2 ± 1.8
	AE-TO_{B6}	match	0.8	30.8 ± 1.1	22.4 ± 1.2
		mismatch	0.9	31.7 ± 0.1	26.2 ± 0.9
	C6-TO_{Q6}	match	1.0	99.0 ± 8.6	83.3 ± 1.4
		mismatch	0.5	111.4 ± 7.5	56.8 ± 9.6
	C6-TO_{B6}	match	6.6	48.3 ± 2.8	393.8 ± 21.1
		mismatch	2.3	47.5 ± 3.9	120.3 ± 7.2
ODN2 5′-GCAAXATACG	PA-TO_{Q6}	match	1.4	14.6 ± 0.5	20.3 ± 0.9
		mismatch	1.3	14.7 ± 0.4	17.4 ± 0.8
	PA-TO_{B6}	match	5.5	28.4 ± 0.8	179.2 ± 4.3
		mismatch	3.8	26.0 ± 1.0	101.8 ± 0.7
	AE-TO_{Q6}	match	7.4	12.4 ± 0.1	102.0 ± 0.5
		mismatch	3.2	12.3 ± 0.1	38.1 ± 1.6
	AE-TO_{B6}	match	1.0	6.5 ± 1.7	7.1 ± 1.8
		mismatch	1.2	6.3 ± 1.5	9.1 ± 3.8
	C6-TO_{Q6}	match	3.7	19.4 ± 2.7	75.6 ± 7.1
		mismatch	2.5	20.2 ± 0.5	58.0 ± 0.4
	C6-TO_{B6}	match	8.6	21.4 ± 1.3	228.4 ± 4.2
		mismatch	5.5	19.3 ± 1.3	122.4 ± 2.7
ODN3 5′-GCACXCTACG	PA-TO_{Q6}	match	1.5	32.1 ± 0.5	45.9 ± 1.4
		mismatch	2.6	30.8 ± 0.1	61.7 ± 1.2
	PA-TO_{B6}	match	5.3	11.7 ± 1.1	64.2 ± 1.4
		mismatch	3.3	12.4 ± 1.7	49.5 ± 3.2
	AE-TO_{Q6}	match	4.1	33.7 ± 0.2	199.9 ± 2.7
		mismatch	1.5	34.1 ± 0.6	56.8 ± 1.1
	AE-TO_{B6}	match	1.9	13.9 ± 1.3	24.6 ± 1.3
		mismatch	1.3	14.8 ± 0.8	17.4 ± 0.6
	C6-TO_{Q6}	match	3.1	37.5 ± 2.1	116.4 ± 4.8
		mismatch	0.9	36.2 ± 2.4	33.8 ± 4.2
	C6-TO_{B6}	match	6.9	25.7 ± 1.6	200.1 ± 11.0
		mismatch	2.6	26.8 ± 0.3	70.7 ± 3.8

ODN4 5′-GCAGXGTACG	PA-TO_{Q6}	match	0.9	62.1	±	0.1	54.8	±	0.6
		mismatch	1.3	56.6	±	0.4	60.7	±	0.6
	PA-TO_{B6}	match	2.7	61.9	±	1.3	194.9	±	2.3
		mismatch	1.3	65.9	±	1.8	94.1	±	2.3
	AE-TO_{Q6}	match	1.3	66.2	±	2.0	88.2	±	1.0
		mismatch	0.6	65.0	±	2.5	41.1	±	1.8
	AE-TO_{B6}	match	0.8	120.1	±	3.7	108.0	±	0.6
		mismatch	0.6	121.4	±	3.4	70.7	±	0.8
	C6-TO_{Q6}	match	1.4	49.0	±	7.0	77.3	±	8.4
		mismatch	0.6	48.4	±	7.1	36.0	±	5.2
	C6-TO_{B6}	match	3.0	87.5	±	5.5	332.7	±	1.8
		mismatch	1.1	71.3	±	4.4	86.6	±	14.2
ODN4′ 5′-GCAIXITACG I = Inosine	C6-TO_{Q6}	match	1.1	47.5	±	0.9	62.7	±	0.4
		mismatch	1.0	46.2	±	1.2	39.6	±	2.0
	C6-TO_{B6}	match	6.2	35.7	±	0.7	273.2	±	8.3
		mismatch	1.1	34.8	±	0.8	62.3	±	2.2

Table 6.14 Fluorescence emssion data for TO-modified ODN1-4 probes against DNA targets. F_{ds}/F_{ss} – ratio of integrated fluorescence emission of oligonucleotide duplexes to single stranded at $\lambda_{em,\ max}$ of double stranded probe, I_0 – fluorescence emission intensity at $\lambda_{em,\ max}$ of double stranded TO-modified oligonucleotides probes, I_{max} – fluorescence emission intensity at $\lambda_{em,\ max}$ of TO-modified oligonucleotide probe-target duplexes. Mismatch target refers to a T mismatch opposite the TO-modified base.

ODN	X =	Average I_0			Average I_{max} DNA target A			Average I_{max} DNA target T			F_{ss}/F_{ds} target A	F_{ss}/F_{ds} target T	$\lambda_{em,\ max}$ target A	$\lambda_{em,\ max}$ target T
ODN1 5′-GCATXTTACG	PA-TO_{Q6}	130.7	±	9.2	125.2	±	5.4	105.6	±	1.4	1.0	0.9	533	534
	PA-TO_{B6}	45.0	±	2.4	197.6	±	7.5	59.4	±	7.8	4.4	1.2	528	533
	AE-TO_{Q6}	47.5	±	0.2	159.6	±	1.9	78.2	±	1.8	3.4	1.6	527	528
	AE-TO_{B6}	45.6	±	0.2	37.8	±	1.6	42.4	±	1.7	0.8	0.8	542	538
	C6-TO_{Q6}	101.1	±	7.2	83.4	±	1.2	56.9	±	10.0	0.8	0.6	531	530
	C6-TO_{B6}	41.9	±	2.7	390.9	±	21.0	119.9	±	7.2	9.4	2.7	525	528
ODN2 5′-GCAAXATACG	PA-TO_{Q6}	14.2	±	0.3	20.2	±	0.9	17.6	±	0.8	1.4	1.2	532	531
	PA-TO_{B6}	28.6	±	0.6	179.2	±	0.4	101.8	±	0.7	6.3	4.0	530	530
	AE-TO_{Q6}	12.2	±	0.1	102.0	±	0.5	38.1	±	1.6	8.3	3.1	529	530
	AE-TO_{B6}	6.4	±	1.8	25.1	±	0.4	7.1	±	1.8	1.4	1.1	533	533
	C6-TO_{Q6}	18.9	±	2.7	75.6	±	7.1	58.0	±	0.3	4.0	3.1	530	528
	C6-TO_{B6}	20.6	±	0.5	228.4	±	4.2	122.4	±	1.9	11.1	6.6	528	528
ODN3 5′-GCACXCTACG	PA-TO_{Q6}	31.4	±	0.4	45.9	±	1.4	61.7	±	1.2	1.5	2.1	532	540
	PA-TO_{B6}	11.0	±	1.4	65.1	±	0.3	51.6	±	1.3	6.0	4.1	531	530
	AE-TO_{Q6}	43.6	±	0.9	199.1	±	6.8	56.8	±	1.5	4.6	1.2	530	534
	AE-TO_{B6}	5.3	±	0.5	16.3	±	0.5	12.3	±	0.6	3.1	2.1	536	534
	C6-TO_{Q6}	37.4	±	2.1	116.4	±	4.8	33.8	±	4.2	3.1	0.9	533	532
	C6-TO_{B6}	24.7	±	1.6	200.1	±	11.0	70.7	±	3.8	8.1	2.6	527	529
ODN4 5′-GCAGXGTACG	PA-TO_{Q6}	61.1	±	0.2	54.8	±	0.6	60.7	±	0.6	0.9	1.1	531	535
	PA-TO_{B6}	57.7	±	1.1	194.9	±	2.3	94.1	±	2.3	3.4	1.5	529	531
	AE-TO_{Q6}	60.4	±	3.2	108.0	±	1.8	70.7	±	1.6	1.3	0.6	530	531
	AE-TO_{B6}	111.2	±	3.2	108.0	±	0.6	70.7	±	0.8	1.0	0.6	532	536
	C6-TO_{Q6}	38.5	±	8.0	77.3	±	8.0	36.2	±	6.0	2.0	0.9	531	532
	C6-TO_{B6}	56.0	±	5.5	332.7	±	2.4	86.6	±	13.0	5.9	1.5	528	529
ODN4′ 5′-GCAIXITACG I = Inosine	C6-TO_{Q6}	62.5	±	0.4	62.7	±	0.4	39.6	±	2.0	1.0	1.0	531	530
	C6-TO_{B6}	34.3	±	0.2	273.2	±	8.3	62.3	±	2.2	8.0	1.7	527	530

Table 6.15 Fluorescence emssion data for TO-modified ODN4 and ODN4′ probes against RNA targets. F_{ds}/F_{ss} – ratio of integrated fluorescence emission of oligonucleotide duplexes to single stranded at $\lambda_{em,\,max}$ of double stranded probe, I_0 – fluorescence emission intensity at $\lambda_{em,\,max}$ of double stranded TO-modified oligonucleotides probes, I_{max} – fluorescence emission intensity at $\lambda_{em,\,max}$ of TO-modified oligonucleotide probe-target duplexes. Mismatch target refers to a U mismatch opposite the TO-modified base.

ODN	X =	Average I_0	Average I_{max} RNA target A	Average I_{max} RNA target U	F_{ss}/F_{ds} target A	F_{ss}/F_{ds} target U	$\lambda_{em,\,max}$ target A	$\lambda_{em,\,max}$ target U
ODN4 5′-GCAGXIGACG	C6-TO_{Q6}	38.5 ± 0.2	71.7 ± 0.1	40.9 ± 0.7	1.9	1.1	532	534
	C6-TO_{B6}	56.0 ± 0.3	189.1 ± 0.8	84.1 ± 7.7	3.1	1.5	530	532
ODN4′ 5′-GCAIXITACG I = Inosine	C6-TO_{Q6}	62.5 ± 0.8	63.1 ± 0.3	47.2 ± 3.0	1.3	0.9	532	531
	C6-TO_{B6}	34.3 ± 0.3	119.1 ± 7.6	44.8 ± 1.5	3.3	1.2	530	532

Table 6.16 Fluorescence emssion data for TO-modified 2′-OMe–(ORN1-4) probes against DNA targets. F_{ds}/F_{ss} – ratio of integrated fluorescence emission of oligonucleotide duplexes to single stranded, I_0 – fluorescence emission intensity at $\lambda_{em,\,max}$ of single stranded TO-modified oligonucleotides probes, I_{max} – fluorescence emission intensity at $\lambda_{em,\,max}$ of TO-modified oligonucleotide probe-target duplexes. Mismatch target refers to a T mismatch opposite the TO-modified base.

2′-OMe–(ORN)	X =	DNA target	Average F_{ds}/F_{ss}	Average I_0	Average I_{max}
2′-OMe–(ORN1) 5′-GCAUXUUACG	AE-TO_{Q6}	match	21.5	16.2 ± 1.5	472.8 ± 57.8
		mismatch	8.9	15.2 ± 0.9	169.4 ± 3.8
	AE-TO_{B6}	match	1.3	24.9 ± 0.5	31.7 ± 2.1
		mismatch	1.6	26.7 ± 0.4	41.0 ± 1.8
	C6-TO_{Q6}	match	4.2	20.4 ± 2.0	81.6 ± 2.2
		mismatch	1.7	22.5 ± 2.3	36.1 ± 3.8
	C6-TO_{B6}	match	14.6	14.5 ± 1.3	270.7 ± 17.0
		mismatch	2.7	15.1 ± 0.9	45.3 ± 7.2
	AE-TO_{Q10}	match	21.8	9.6 ± 4.0	273.5 ± 3.5
		mismatch	17.0	9.6 ± 4.0	193.2 ± 9.0
	AE-TO_{B10}	match	1.9	4.8 ± 0.01	8.6 ± 0.1
		mismatch	no data obtained/measurement wasn't performed		
	C6-TO_{Q10}	match	2.6	15.2 ± 0.1	41.4 ± 1.7
		mismatch	1.3	15.2 ± 0.1	19.4 ± 1.9
	C6-TO_{B10}	match	7.6	27.6 ± 0.5	241.4 ± 34.5
		mismatch	1.7	27.6 ± 0.5	50.1 ± 0.6

2′-OMe– 5′-GCAXUUXACG	2× AE-TO_{Q6}	match	14.1	9.5	±	0.5	239.3	±	22.1
		mismatch	9.0	9.5	±	0.6	128.7	±	4.2
2′-OMe– 5′-GCAUXXUACG- 3′-propanol	2× AE-TO_{Q6}	match	5.4	20.1	±	1.0	184.1	±	5.2
		mismatch	4.5	20.1	±	0.5	143.5	±	3.2
2′-OMe–(ORN2) 5′-GCAAXAUACG	AE-TO_{Q6}	match	7.6	44.9	±	1.7	450.8	±	15.0
		mismatch	3.0	46.0	±	1.0	172.1	±	1.4
	AE-TO_{B6}	match	0.9	43.2	±	1.4	34.5	±	1.2
		mismatch	1.6	44.1	±	1.7	78.1	±	4.9
	C6-TO_{Q6}	match	9.1	11.0	±	0.2	114.6	±	2.9
		mismatch	2.8	11.3	±	0.2	34.2	±	0.5
	C6-TO_{B6}	match	17.5	11.2	±	0.4	226.9	±	7.2
		mismatch	8.6	10.9	±	0.4	119.1	±	0.8
2′-OMe–(ORN3) 5′-GCACXCUACG	AE-TO_{Q6}	match	33.9	9.3	±	0.1	425.4	±	8.6
		mismatch	17.0	9.7	±	0.2	192.2	±	1.9
	AE-TO_{B6}	match	3.5	12.1	±	0.2	41.0	±	1.2
		mismatch	2.6	11.8	±	0.4	30.4	±	0.5
	C6-TO_{Q6}	match	6.4	9.3	±	1.1	58.4	±	5.1
		mismatch	2.0	10.6	±	0.4	20.1	±	0.6
	C6-TO_{B6}	match	17.2	12.5	±	1.4	251.7	±	30.9
		mismatch	3.9	15.8	±	3.2	65.4	±	10.6
2′-OMe–(ORN4) 5′-GCAGXGUACG	AE-TO_{Q6}	match	3.1	90.2	±	1.0	355.6	±	1.7
		mismatch	1.4	96.4	±	2.0	167.0	±	0.8
	AE-TO_{B6}	match	0.2	226.8	±	3.2	56.1	±	16.5
		mismatch	0.3	239.6	±	4.8	79.5	±	0.8
	C6-TO_{Q6}	match	1.0	52.3	±	6.0	55.2	±	6.3
		mismatch	0.7	64.4	±	0.8	42.9	±	1.7
	C6-TO_{B6}	match	3.7	94.3	±	3.1	420.5	±	5.4
		mismatch	1.2	87.1	±	1.1	107.3	±	3.5

Table 6.17 Fluorescence emssion data for TO-modified ODN1-4 probes against RNA targets. F_{ds}/F_{ss} – ratio of integrated fluorescence emission of oligonucleotide duplexes to single stranded, I_0 – fluorescence emission intensity at $\lambda_{em,\,max}$ of single stranded TO-modified oligonucleotides probes, I_{max} – fluorescence emission intensity at $\lambda_{em,\,max}$ of TO-modified oligonucleotide probe-target duplexes. Mismatch target refers to a U mismatch opposite the TO-modified base.

ODN	X =	RNA target	Average F_{ds}/F_{ss}	Average I_0	Average I_{max}
ODN1 5′-GCATXTTACG	AE-TO_{Q6}	match	2.5	49.5 ± 0.2	127.0 ± 2.1
		mismatch	1.0	48.2 ± 0.3	47.1 ± 0.9
	AE-TO_{B6}	match	2.5	30.5 ± 0.4	76.1 ± 0.2
		mismatch	1.3	30.5 ± 0.2	41.0 ± 1.6
	C6-TO_{Q6}	match	1.6	115.0 ± 7.6	171.6 ± 16.6
		mismatch	1.0	102.2 ± 0.7	100.2 ± 3.4
	C6-TO_{B6}	match	6.4	53.1 ± 4.1	404.0 ± 24.8
		mismatch	2.0	48.4 ± 0.6	99.7 ± 2.8
ODN2 5′-GCAAXATACG	AE-TO_{Q6}	match	5.2	14.0 ± 0.1	76.2 ± 7.4
		mismatch	1.8	14.0 ± 0.1	26.7 ± 2.4
	AE-TO_{B6}	match	3.3	6.2 ± 1.6	17.0 ± 3.8
		mismatch	1.2	7.8 ± 1.5	10.0 ± 3.5
	C6-TO_{Q6}	match	2.8	13.6 ± 0.3	37.1 ± 5.4
		mismatch	1.3	16.6 ± 1.7	17.2 ± 1.4
	C6-TO_{B6}	match	7.2	13.9 ± 0.1	111.5 ± 8.9
		mismatch	2.6	14.8 ± 0.4	40.7 ± 1.3
ODN3 5′-GCACXCTACG	AE-TO_{Q6}	match	3.8	34.5 ± 1.2	139.1 ± 0.3
		mismatch	1.8	34.5 ± 1.0	61.3 ± 1.0
	AE-TO_{B6}	match	3.8	18.8 ± 1.4	77.3 ± 2.6
		mismatch	3.7	18.9 ± 1.5	76.3 ± 5.3
	C6-TO_{Q6}	match	2.3	23.9 ± 6.8	56.7 ± 0.1
		mismatch	2.6	24.0 ± 7.2	68.7 ± 3.4
	C6-TO_{B6}	match	5.2	28.0 ± 0.6	158.5 ± 6.8
		mismatch	3.1	28.1 ± 0.2	90.2 ± 2.9
ODN4 5′-GCAGXGTACG	AE-TO_{Q6}	match	2.2	65.0 ± 3.1	150.2 ± 4.0
		mismatch	1.1	66.2 ± 2.2	71.1 ± 3.0
	AE-TO_{B6}	match	1.0	112.3 ± 4.2	118.3 ± 7.9
		mismatch	0.8	112.3 ± 4.4	93.7 ± 2.8
	C6-TO_{Q6}	match	1.8	37.9 ± 8.9	69.8 ± 3.7
		mismatch	1.0	38.4 ± 8.0	41.4 ± 8.8
	C6-TO_{B6}	match	2.8	73.7 ± 14.6	196.0 ± 9.9
		mismatch	1.4	73.5 ± 17.4	85.9 ± 6.8
ODN4′ 5′-GCAIXITACG I = Inosine	C6-TO_{Q6}	match	1.1	47.6 ± 0.9	63.1 ± 0.3
		mismatch	0.9	46.3 ± 1.2	47.2 ± 3.0
	C6-TO_{B6}	match	3.1	35.8 ± 0.7	119.1 ± 7.6
		mismatch	1.0	34.7 ± 0.8	44.8 ± 1.5

Table 6.18 Fluorescence emssion data for TO-modified 2′-OMe–(ORN1-4) probes against RNA targets. F_{ds}/F_{ss} – ratio of integrated fluorescence emission of oligonucleotide duplexes to single stranded, I_0 – fluorescence emission intensity at $\lambda_{em,\,max}$ of single stranded TO-modified oligonucleotides probes, I_{max} – fluorescence emission intensity at $\lambda_{em,\,max}$ of TO-modified oligonucleotide probe-target duplexes. Mismatch target refers to a U mismatch opposite the TO-modified base.

2′-OMe–(ORN)	X =	RNA target	Average F_{ds}/F_{ss}	Average I_0	Average I_{max}
2′-OMe–(ORN1) 5′-GCAUXUUACG	AE-TO_{Q6}	match	9.8	14.1 ± 1.6	158.4 ± 9.2
		mismatch	4.8	15.4 ± 3.0	79.5 ± 10.7
	AE-TO_{B6}	match	2.7	24.3 ± 1.7	66.2 ± 12.0
		mismatch	1.6	23.1 ± 1.9	35.6 ± 2.4
	C6-TO_{Q6}	match	5.0	20.3 ± 0.3	94.7 ± 4.1
		mismatch	3.1	20.9 ± 2.1	65.5 ± 3.8
	C6-TO_{B6}	match	15.8	13.4 ± 0.4	254.7 ± 17.6
		mismatch	5.1	15.2 ± 1.1	80.4 ± 2.0
	AE-TO_{Q10}	match	16.0	9.6 ± 4.0	282.7 ± 26.1
		mismatch	11.1	9.6 ± 4.0	108.4 ± 5.1
	AE-TO_{B10}	match	4.2	8.7 ± 0.2	31.4 ± 1.0
		mismatch	no data obtained/measurement wasn't performed		
	C6-TO_{Q10}	match	4.2	17.8 ± 4.2	68.2 ± 6.2
		mismatch	3.1	15.2 ± 0.1	51.0 ± 1.7
	C6-TO_{B10}	match	8.5	27.6 ± 0.6	246.0 ± 4.8
		mismatch	2.9	27.7 ± 0.5	76.8 ± 0.1
2′-OMe– 5′-GCAXUUXACG	2× AE-TO_{Q6}	match	8.2	9.7 ± 0.7	126.2 ± 3.6
		mismatch	7.0	9.5 ± 0.5	133.4 ± 2.5
2′-OMe– 5′-GCAUXXUACG -3′-propanol	2× AE-TO_{Q6}	match	7.0	20.1 ± 0.3	260.5 ± 14.5
		mismatch	4.8	20.1 ± 0.6	161.6 ± 5.1
2′-OMe–(ORN2) 5′-GCAAXAUACG	AE-TO_{Q6}	match	3.0	46.0 ± 1.0	196.3 ± 21.9
		mismatch	0.8	44.9 ± 1.7	63.2 ± 1.7
	AE-TO_{B6}	match	1.2	44.9 ± 0.8	53.4 ± 2.4
		mismatch	1.1	44.1 ± 0.8	45.1 ± 3.2
	C6-TO_{Q6}	match	8.9	11.6 ± 1.3	117.9 ± 30.1
		mismatch	3.5	12.0 ± 0.4	49.6 ± 1.4
	C6-TO_{B6}	match	11.3	11.2 ± 0.5	136.8 ± 16.3
		mismatch	5.1	12.1 ± 1.7	58.5 ± 3.5
2′-OMe–(ORN3) 5′-GCACXCUACG	AE-TO_{Q6}	match	12.7	9.5 ± 0.4	138.9 ± 1.3
		mismatch	8.4	9.5 ± 0.2	84.9 ± 17.4
	AE-TO_{B6}	match	2.5	11.8 ± 0.2	30.3 ± 1.4
		mismatch	4.7	11.6 ± 0.1	58.8 ± 2.5
	C6-TO_{Q6}	match	3.2	12.0 ± 0.2	38.0 ± 0.3
		mismatch	2.4	12.2 ± 0.2	27.5 ± 0.1
	C6-TO_{B6}	match	6.3	14.9 ± 0.5	101.1 ± 2.6
		mismatch	4.3	14.1 ± 0.2	65.2 ± 2.7
2′-OMe–(ORN4) 5′-GCAGXGUACG	AE-TO_{Q6}	match	3.4	98.4 ± 6.7	408.1 ± 7.0
		mismatch	1.0	119.4 ± 11.2	129.9 ± 2.8
	AE-TO_{B6}	match	0.5	232.4 ± 8.8	108.3 ± 3.3
		mismatch	0.3	227.9 ± 11.7	64.4 ± 5.0
	C6-TO_{Q6}	match	1.0	60.1 ± 1.3	57.3 ± 5.3
		mismatch	0.8	62.7 ± 1.3	48.8 ± 2.2
	C6-TO_{B6}	match	2.4	90.4 ± 1.7	246.3 ± 7.3
		mismatch	1.1	88.7 ± 0.2	93.6 ± 2.2

Table 6.19 Fluorescence emssion data for TO-modified ORN1-4 probes against DNA targets. F_{ds}/F_{ss} – ratio of integrated fluorescence emission of oligonucleotide duplexes to single stranded at $\lambda_{em,\ max}$ of double stranded probe, I_0 – fluorescence emission intensity at $\lambda_{em,\ max}$ of double stranded TO-modified oligonucleotides probes, I_{max} – fluorescence emission intensity at $\lambda_{em,\ max}$ of TO-modified oligonucleotide probe-target duplexes. Mismatch target refers to a T mismatch opposite the TO-modified base.

ODN	X =	Average I_0	Average I_{max} DNA target A	Average I_{max} DNA target T	F_{ss}/F_{ds} target A	F_{ss}/F_{ds} target T	$\lambda_{em,\ max}$ target A	$\lambda_{em,\ max}$ target T
5′-GCAUXUUACG	AE-TO_{Q6}	14.4 ± 3.0	485.3 ± 57.8	169.4 ± 2.7	34.5	11.6	527	527
	AE-TO_{B6}	24.3 ± 0.3	31.8 ± 2.1	39.8 ± 0.1	1.3	1.5	534	533
	C6-TO_{Q6}	19.9 ± 1.9	78.3 ± 1.8	32.8 ± 0.6	4.0	1.5	531	531
	C6-TO_{B6}	12.0 ± 1.7	234.6 ± 18.2	49.5 ± 0.6	19.8	3.2	527	530
	AE-TO_{Q10}	11.7 ± 3.0	274.5 ± 3.5	193.2 ± 2.7	23.4	18.5	529	529
	AE-TO_{B10}	4.7 ± 0.3	8.6 ± 0.1	No data	1.8	No data	533	No data
	C6-TO_{Q10}	15.2 ± 0.1	41.4 ± 1.7	19.4 ± 1.9	2.7	1.3	532	533
	C6-TO_{B10}	27.7 ± 0.3	250.6 ± 39.1	50.1 ± 0.6	9.0	1.8	528	531
2′-OMe–5′-GCAXUUXACG	2× AE-TO_{Q6}	7.5 ± 0.9	239.3 ± 22.1	128.7 ± 4.2	31.9	17.0	530	537
2′-OMe–5′-GCAUXXUACG-3′-propanol	2× AE-TO_{Q6}	19.9 ± 0.9	184.1 ± 5.2	143.5 ± 3.2	9.3	7.4	531	531
5′-GCAAXAUACG	AE-TO_{Q6}	40.7 ± 1.7	450.8 ± 15.0	172.1 ± 1.4	11.1	3.9	527	529
	AE-TO_{B6}	42.2 ± 1.6	34.5 ± 1.2	78.1 ± 4.9	0.8	1.7	535	532
	C6-TO_{Q6}	10.9 ± 0.2	114.6 ± 2.9	34.2 ± 0.4	10.5	3.0	530	532
	C6-TO_{B6}	11.1 ± 0.4	232.4 ± 7.2	119.1 ± 0.6	21.0	11.4	531	527
5′-GCACXCUACG	AE-TO_{Q6}	8.6 ± 0.1	425.4 ± 8.6	192.2 ± 1.9	49.4	20.5	527	528
	AE-TO_{B6}	11.5 ± 0.1	41.0 ± 1.2	30.4 ± 0.5	3.6	2.7	535	534
	C6-TO_{Q6}	9.2 ± 1.1	58.4 ± 5.1	20.1 ± 0.6	6.4	1.9	532	532
	C6-TO_{B6}	12.1 ± 1.5	251.7 ± 30.9	65.4 ± 10.6	20.9	4.2	528	532
5′-GCAGXGUACG	AE-TO_{Q6}	73.2 ± 0.1	355.6 ± 1.7	167.0 ± 0.8	4.6	1.9	526	529
	AE-TO_{B6}	225.0 ± 3.9	56.1 ± 16.5	79.5 ± 0.8	0.3	0.2	534	534
	C6-TO_{Q6}	57.2 ± 5.0	55.2 ± 6.3	42.9 ± 1.7	1.0	0.8	535	532
	C6-TO_{B6}	76.6 ± 3.2	420.5 ± 5.4	107.3 ± 3.5	5.4	1.3	529	531

Table 6.20 Fluorescence emssion data for TO-modified ORN1-4 probes against RNA targets. F_{ds}/F_{ss} – ratio of integrated fluorescence emission of oligonucleotide duplexes to single stranded at $\lambda_{em,\ max}$ of double stranded probe, I_0 – fluorescence emission intensity at $\lambda_{em,\ max}$ of double stranded TO-modified oligonucleotides probes, I_{max} – fluorescence emission intensity at $\lambda_{em,\ max}$ of TO-modified oligonucleotide probe-target duplexes. Mismatch target refers to a T mismatch opposite the TO-modified base.

ODN	X =	ss probe	RNA target A	RNA target U	F_{ss}/F_{ds} target A	F_{ss}/F_{ds} target U	$\lambda_{em,\ max}$ target A	$\lambda_{em,\ max}$ target T
ORN1 5′-GCAUXUUACG	AE-TO$_{Q6}$	14.4 ± 2.0	152.2 ± 9.2	68.2 ± 0.5	11.4	4.8	527	530
	AE-TO$_{B6}$	24.3 ± 1.7	63.6 ± 12.0	32.5 ± 0.6	2.6	1.4	530	532
	C6-TO$_{Q6}$	19.9 ± 0.3	94.7 ± 4.1	64.2 ± 3.7	4.7	3.0	531	530
	C6-TO$_{B6}$	12.0 ± 0.4	225.1 ± 17.6	68.2 ± 1.1	19.2	5.6	528	534
	AE-TO$_{Q10}$	11.7 ± 3.0	274.5 ± 17.9	108.4 ± 5.1	25.6	10	530	533
	AE-TO$_{B10}$	4.7 ± 0.3	8.6 ± 1.0	No data ± No data	3.7	No data	530	No data
	C6-TO$_{Q10}$	15.2 ± 0.1	41.4 ± 6.2	51.0 ± 1.7	4.0	3.8	532	530
	C6-TO$_{B10}$	27.7 ± 0.3	250.6 ± 4.8	76.8 ± 0.1	8.9	2.9	530	535
ORN2 5′-GCAAXAUACG	AE-TO$_{Q6}$	40.7 ± 4.7	196.3 ± 21.9	63.2 ± 1.7	4.7	1.4	528	533
	AE-TO$_{B6}$	42.2 ± 3.2	53.4 ± 2.4	46.0 ± 2.4	1.2	1.0	531	533
	C6-TO$_{Q6}$	10.9 ± 0.9	103.6 ± 30.1	49.6 ± 1.4	9.2	4.6	531	529
	C6-TO$_{B6}$	11.1 ± 3.5	114.7 ± 16.3	58.5 ± 2.1	10.1	4.9	533	531
ORN3 5′-GCACXCUACG	AE-TO$_{Q6}$	8.6 ± 0.1	138.9 ± 1.3	85.6 ± 1.3	15.7	9.2	533	528
	AE-TO$_{B6}$	11.5 ± 0.2	58.8 ± 1.4	30.3 ± 1.4	5.2	2.6	535	533
	C6-TO$_{Q6}$	9.2 ± 0.3	38.0 ± 0.1	27.5 ± 0.3	3.2	2.3	530	531
	C6-TO$_{B6}$	12.1 ± 0.6	101.1 ± 2.6	65.2 ± 2.7	6.9	4.6	532	535
ORN4 5′-GCAGXGUACG	AE-TO$_{Q6}$	73.2 ± 1.4	408.1 ± 7.0	129.9 ± 2.8	4.6	1.4	529	532
	AE-TO$_{B6}$	225.0 ± 2.0	108.3 ± 3.3	64.4 ± 5.0	0.5	0.3	534	534
	C6-TO$_{Q6}$	57.2 ± 0.9	57.3 ± 5.3	48.8 ± 2.2	1.0	0.8	534	532
	C6-TO$_{B6}$	76.6 ± 1.8	246.3 ± 7.3	93.6 ± 2.2	3.0	1.1	531	534

Table 6.21 Fluorescence emssion data for TO-modified 2′-OMe–(ORN3) (5′-GCAC**X**CUACG) probe against DNA targets with a range of positional mismatches. F_{ds}/F_{ss} – ratio of integrated fluorescence emission of oligonucleotide probe-target duplexes to single stranded probe, I_0 –fluorescence emission intensity at $\lambda_{em,\ max}$ of single stranded TO-modified oligonucleotides probes, I_{max} – fluorescence emission intensity at $\lambda_{em,\ max}$ of TO-modified oligonucleotide probe-target duplexes. Position of mismatch refers to a mismatch (Table 6.1) in the target strand counting from the TO-modified base, e.g.: position "0" is directly opposite modification and "-2" is two nucleobases towards 5′ end of the probe sequence. For mismatch values at position "0" or fully matched target: see Table S9.

	X =	Position of mismatch	Average F_{ds}/F_{ss}	Average I_0	Average I_{max}
2′-OMe–(ORN3) 5′-GCACXCUACG	AE-TO_{Q6}	-2	9.2	8.1 ± 0.2	86.2 ± 1.2
		-1	22.0	7.6 ± 0.2	217.1 ± 1.6
		+1	16.5	8.1 ± 0.1	178.4 ± 1.5
		+2	28.3	8.0 ± 0.3	295.3 ± 3.1
	C6-TO_{B6}	-2	12.8	12.8 ± 0.01	206.6 ± 1.1
		-1	4.6	12.7 ± 0.1	69.7 ± 1.1
		+1	5.8	11.8 ± 1.1	73.2 ± 1.2
		+2	13.8	9.3 ± 0.5	156.2 ± 5.9

Table 6.22 Fluorescence emssion data for TO-modified 2′-OMe–(ORN3) (5′-GCAC**X**CUACG) probe against DNA targets with a range of positional mismatches. F_{ds}/F_{ss} – ratio of $\lambda_{em,\ max}$ of oligonucleotide probe-target duplexes to single stranded probe at $\lambda_{em,\ max}$ of probe-target duplex, I_0 –fluorescence emission intensity at $\lambda_{em,\ max}$ of double stranded TO-modified oligonucleotides probes, I_{max} – fluorescence emission intensity at $\lambda_{em,\ max}$ of TO-modified oligonucleotide probe-target duplexes, Fds/Fss - ratio of integrated fluorescence emission of oligonucleotide duplexes to single stranded at $\lambda_{em,\ max}$ of double stranded probe. Position of mismatch refers to a mismatch (Table 6.1) in the target strand counting from the TO-modified base, e.g.: position "0" is directly opposite modification and "-2" is two nucleobases towards 5′ end of the probe sequence.

	X =	Position of mismatch	F_{ds}/F_{ss}	I_{max}	$\lambda_{em,\ max}$
2′-OMe–(ORN3) 5′-GCACXCUACG	AE-TO_{Q6}	-2	17.0	206.6 ± 1.1	527
		-1	5.6	69.7 ± 0.2	528
		0	4.2	65.4 ± 10.6	532
		+1	6.4	73.2 ± 0.2	530
		+2	16.5	201.3 ± 5.1	529
		Match	20.9	251.7 ± 30.9	532
	C6-TO_{B6}	-2	11.1	86.2 ± 0.1	530
		-1	29.4	217.1 ± 1.6	528
		0	20.5	192.2 ± 1.9	528
		+1	23.4	178.4 ± 0.7	527
		+2	41.1	250.6 ± 5.1	527
		Match	49.4	425.4 ± 8.6	528

Table 6.23 Fluorescence emssion data for TO-modified ODN1 probes against DNA targets. F_{ds}/F_{ss} – ratio of integrated fluorescence emission of oligonucleotide duplexes to single stranded, I_0 – fluorescence emission intensity at $\lambda_{em,\ max}$ of single stranded TO-modified oligonucleotides probes, I_{max} – fluorescence emission intensity at $\lambda_{em,\ max}$ of TO-modified oligonucleotide probe-target duplexes.

ODN	X =	DNA target	Average F_{ds}/F_{ss}	Average I_0	Average I_{max}
ODN1 5′-GCATXTTACG	TH-TO_{BPr}	match	1.5	18.9 ± 0.8	34.0 ± 1.3
	TH-TO_{QPr}	match	1.0	13.7 ± 1.1	13.4 ± 1.2

Table 6.24 Fluorescence emssion data for AP-C3 (NH_2/propargyl) ODN7 probe labelled with TO_{B6}-NHS and ATTO647N-N_3 against DNA target. Data obtained in 10 mM phosphate 200 mM NaCl at pH 7.0 buffer, DNA concentrations for F_{ds}/F_{ss} 0.25 µM of ODN7and 0.28 µM of target were used. Fluorescence data were measured at least as a duplicate. TO_{B6}: λ_{ex} = 484 nm, ATTO647N: λ_{ex} = 647 nm.

	X =	Y =	Average F_{ds}/F_{ss}	Average I_0	Average I_{max}
			Ex 488 nm		
ODN7 5′-CGCTTC**AP-C_3(X/Y)**GTATCTATATTCATC	TO_{B6}	-	1.7	94.3 ± 0.4	172.2 ± 8.5
	TO_{B6}	ATTO647N	1.0	169.0 ± 5.0	178.7 ± 3.8
	-	ATTO647N	-	- ± -	- ± -
			Ex 647 nm		
	TO_{B6}	-	-	- ± -	- ± -
	TO_{B6}	ATTO647N	1.1	306.0 ± 2.2	355.4 ± 4.8
	-	ATTO647N	1.0	328.9 ± 9.2	345.5 ± 11.1

Table 6.25 Fluorescence emssion data for AP-$C_{3/6}$ (NH_2/propargyl) 2′-OMe–(ORN3) probes labelled with various dyes against matched DNA and RNA target, λ_{ex} = 484 nm. Conditions see: Experimental 6.5.

ORN	X =	Target	Average F_{ds}/F_{ss}	Average I_0	Average I_{max}
2′-OMe–(ORN3) 5′-GCACXCUACG	APC_3(TO_{B6}/propargyl)	DNA	5.9	22.9 ± 1.8	134.8 ± 5.9
		RNA	7.1	21.3 ± 1.3	150.9 ± 3.7
	APC_3(NH_2/Alexa555)	DNA	1.0	55.4 ± 1.5	54.2 ± 0.7
		RNA	1.0	54.7 ± 1.7	54.5 ± 2.8
	APC_3(TO_{B6}/Alexa555)	DNA	1.8	79.6 ± 3.8	146.2 ± 6.5
		RNA	1.4	80.7 ± 0.9	116.1 ± 2.4
	APC_3(TO_{B6}/Alexa594)	DNA	3.2	46.1 ± 2.8	148.3 ± 6.1
		RNA	1.3	50.1 ± 1.7	65.3 ± 0.7
	APC_6(TO_{B6}/propargyl)	DNA	12.7	17.0 ± 0.5	216.2 ± 3.0
		RNA	8.3	20.5 ± 0.5	168.9 ± 4.9
	APC_6(NH_2/Alexa555)	DNA	1.0	82.2 ± 1.8	80.1 ± 0.1
		RNA	1.0	84.8 ± 0.5	84.9 ± 2.8
	APC_6(TO_{B6}/Alexa555)	DNA	1.9	84.5 ± 2.1	163.4 ± 3.8
		RNA	1.3	94.0 ± 2.9	120.3 ± 0.9
	APC_6(TO_{B6}/Alexa594)	DNA	3.2	59.2 ± 0.4	190.2 ± 5.0
		RNA	1.6	58.8 ± 0.4	95.6 ± 0.2
	APC_6(TO_{B6}/ATTO647N)	DNA	1.1	132.7 ± 3.3	141.0 ± 4.2
		RNA	1.0	118.4 ± 2.4	112.2 ± 9.2

Table 6.26 Fluorescence emssion data for AP-$C_{3/6}$ (NH_2/propargyl) 2'-OMe–(ORN3) probes labelled with various dyes against matched DNA and RNA target, λ_{ex} of Alexa555 (553 nm), Alexa594 (590 nm) and ATT647N (645 nm). Conditions see Experimental 6.5.

ORN	X =	Target	λ_{ex} / nm	Average F_{ds}/F_{ss}	Average I_0			Average I_{max}		
2'-OMe–(ORN3) 5'-GCACXCUACG	$APC_3(TO_{B6}$/propargyl)	DNA	-	-	-		-	-		-
		RNA	-	-	-		-	-		-
	$APC_3(NH_2$/Alexa555)	DNA	553	1.0	233.8	±	3.7	230.6	±	12.5
		RNA		1.0	239.2	±	10.0	239.9	±	16.7
	$APC_3(TO_{B6}$/Alexa555)	DNA		2.0	140.3	±	6.0	276.9	±	16.5
		RNA		1.3	146.7	±	4.3	186.8	±	0.5
	$APC_3(TO_{B6}$/Alexa594)	DNA	590	2.3	120.7	±	3.9	277.8	±	2.8
		RNA		1.2	119.2	±	3.6	145.7	±	3.2
	$APC_6(TO_{B6}$/propargyl)	DNA	-	-	-		-	-		-
		RNA	-	-	-		-	-		-
	$APC_6(NH_2$/Alexa555)	DNA	553	0.9	353.9	±	3.2	329.4	±	7.3
		RNA		1.0	356.7	±	5.6	355.2	±	9.0
	$APC_6(TO_{B6}$/Alexa555)	DNA		1.8	159.5	±	0.4	290.4	±	2.8
		RNA		1.2	171.5	±	7.2	197.8	±	7.0
	$APC_6(TO_{B6}$/Alexa594)	DNA	590	2.4	109.5	±	1.0	264.7	±	5.0
		RNA		1.4	125.9	±	8.6	177.1	±	4.7
	$APC_6(TO_{B6}$/ATTO647N)	DNA	645	1.4	121.4	±	2.6	170.0	±	2.4
		RNA		0.9	156.2	±	7.9	135.0	±	7.9

6.11. Graphical representation of fluorescence and thermal melting data

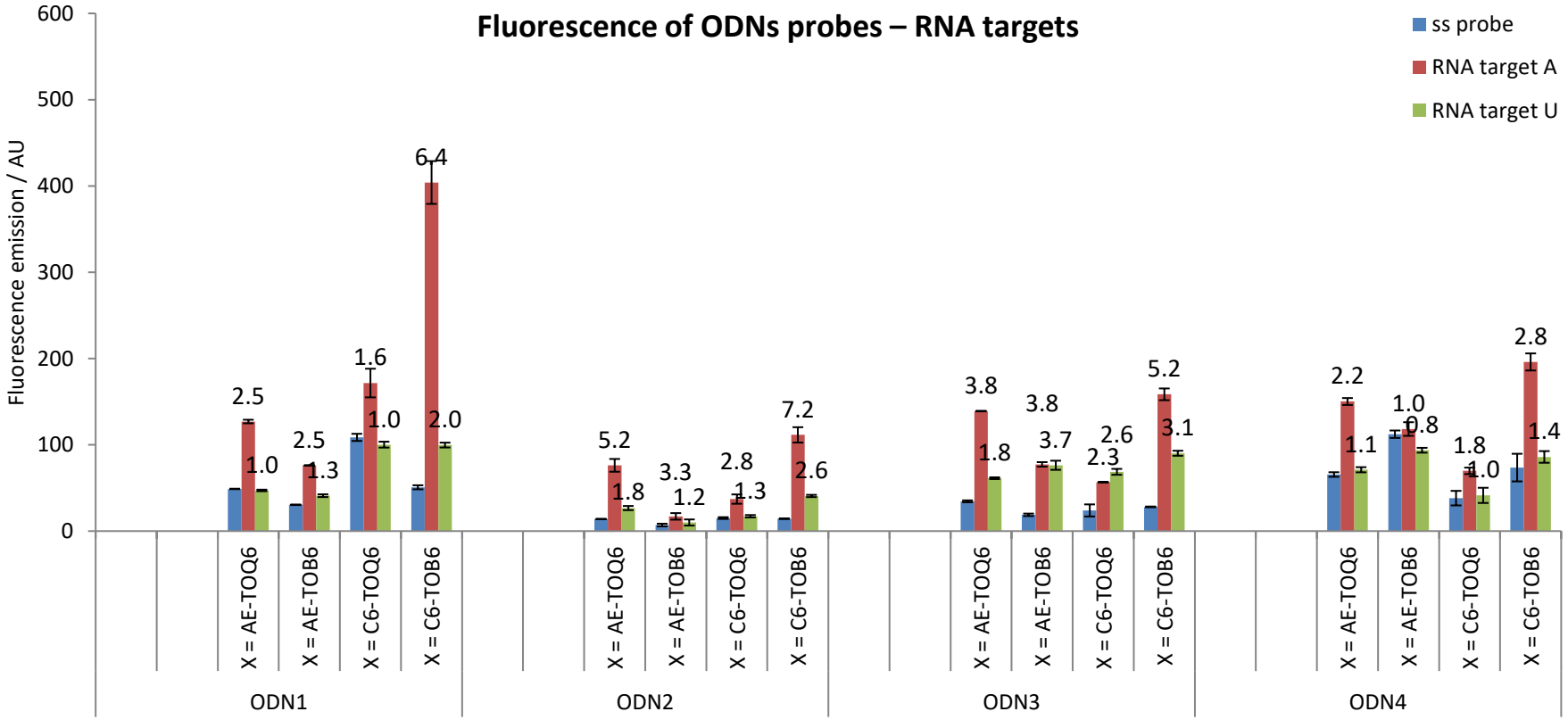


Figure 6.2 Fluorescence emssion intensity at $\lambda_{em,\,max}$ for TO-modified ODNs (ODN1 (5'-GCATXTTACG), ODN2 (5'-GCAAXATACG), ODN3 (5'-GCACXCTACG), ODN4 (5'-GCAGXGTACG)) probes against 2'-OH–RNA targets. The base opposite the TO is either A – match or U – mismatch, ss probe – fluorescence emission intensity of single stranded probe, RNA target A/U - fluorescence emission intensity of probe-target duplex, AU - arbitrary units, number above bar = F_{ds}/F_{ss}. Detailed values: see Table 6.17.

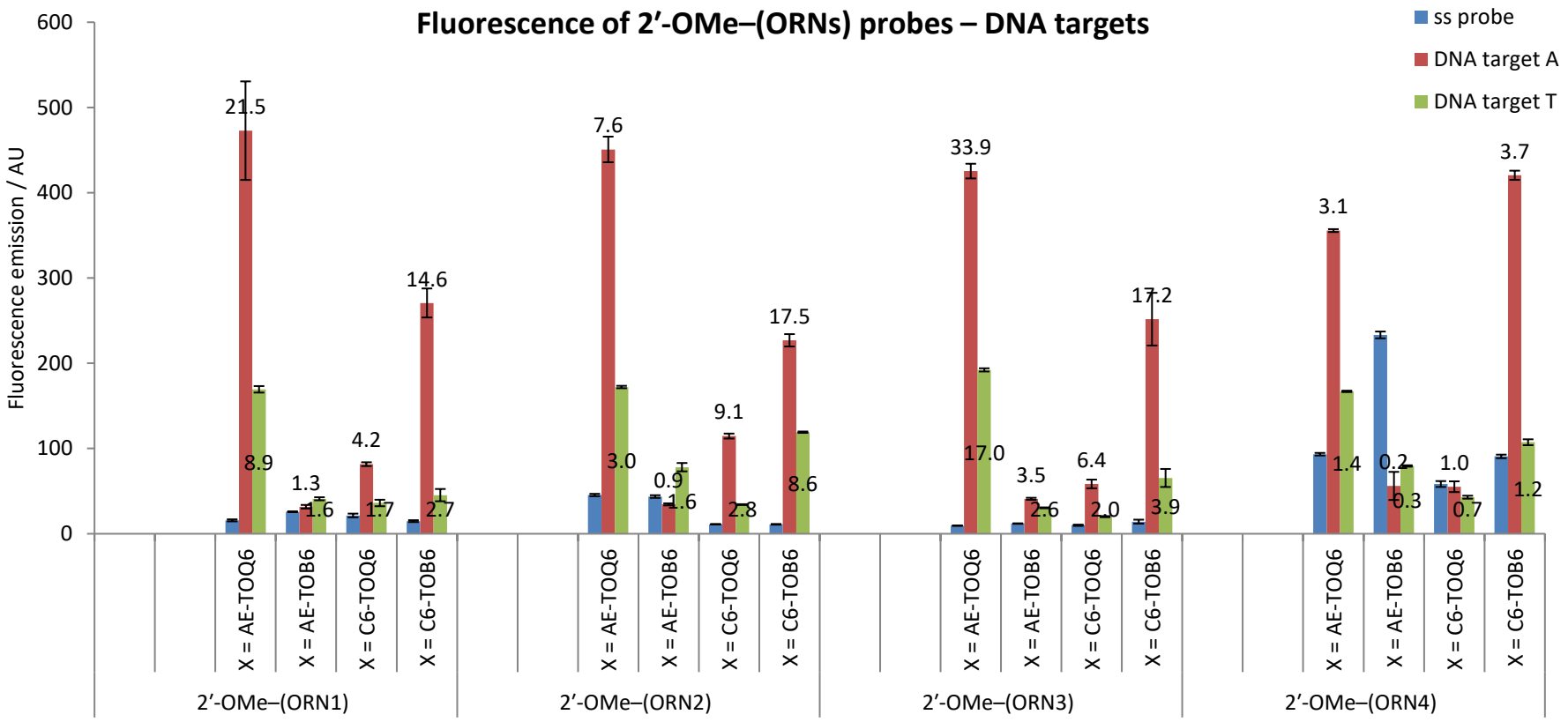


Figure 6.3 Fluorescence emssion intensity at $\lambda_{em,\ max}$ for TO-modified 2'-OMe–(ORNs) (2'-OMe–(ORN1) (5'-GCAUXUUACG), 2'-OMe–(ORN2) (5'-GCAAXAUACG), 2'-OMe–(ORN3) (5'-GCACXCUACG), 2'-OMe–(ORN4) (5'-GCAGXGUACG)) probes against DNA targets. The base opposite the TO is either A – match or T – mismatch, ss probe – fluorescence emission intensity of single stranded probe, DNA target A/T - fluorescence emission intensity of probe-target duplex, AU - arbitrary units, number above bar = F_{ds}/F_{ss}. Detailed values: see Table 6.16.

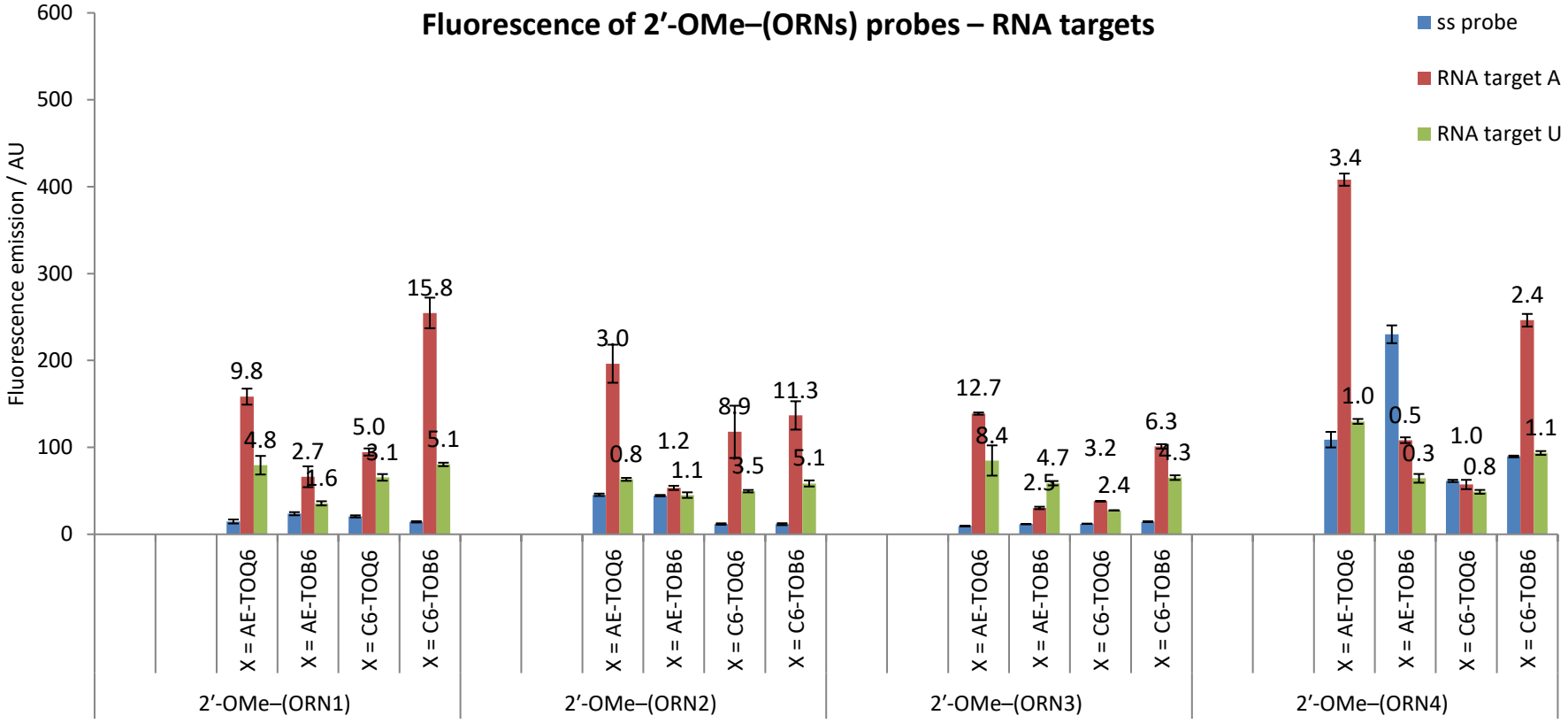


Figure 6.4 Fluorescence emssion intensity at $\lambda_{em,\ max}$ for TO-modified 2'-OMe–(ORNs) (2'-OMe–(ORN1) (5'-GCAUXUUACG), 2'-OMe–(ORN2) (5'-GCAAXAUACG), 2'-OMe–(ORN3) (5'-GCACXCUACG), 2'-OMe–(ORN4) (5'-GCAGXGUACG)) probes against RNA targets. The base opposite the TO is either A – match or U – mismatch, ss probe – fluorescence emission intensity of single stranded probe, RNA target A/U - fluorescence emission intensity of probe-target duplex, AU - arbitrary units, number above bar = F_{ds}/F_{ss}. Detailed values: see Table Table 6.18.

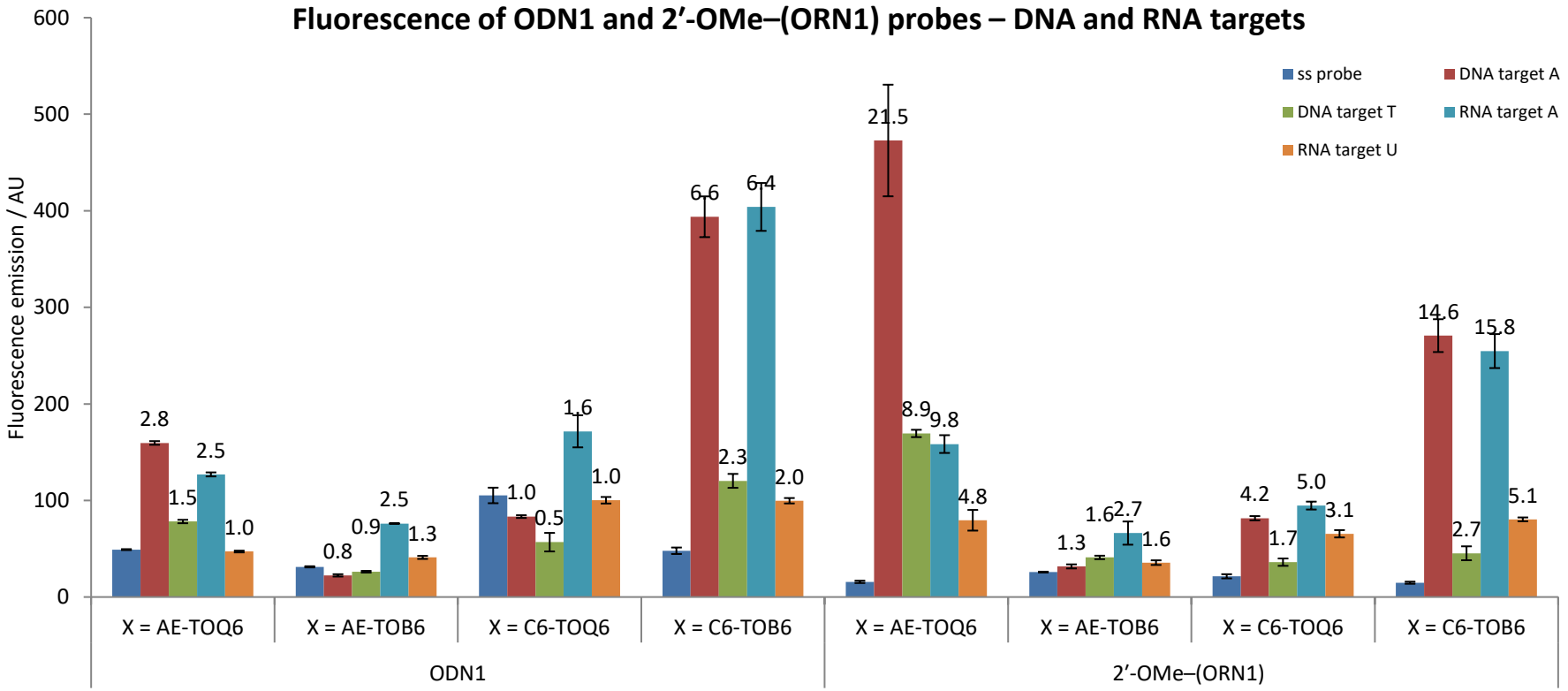


Figure 6.5 Fluorescence emssion intensity at $\lambda_{em,\ max}$ for TO-modified ODN1 (5'-GCATXTTACG) and 2'-OMe–(ORN1) (5'-GCAUXUUACG) probes against DNA and RNA targets. The base opposite the TO is either A – match or T/U – mismatch, ss probe – fluorescence emission intensity of single stranded probe, DNA target A/T and RNA target A/U - fluorescence emission intensity of probe-target duplex, AU - arbitrary units, number above bar = F_{ds}/F_{ss}. Detailed values: see Table 6.13, Table 6.16, Table 6.17 and Table 6.18.

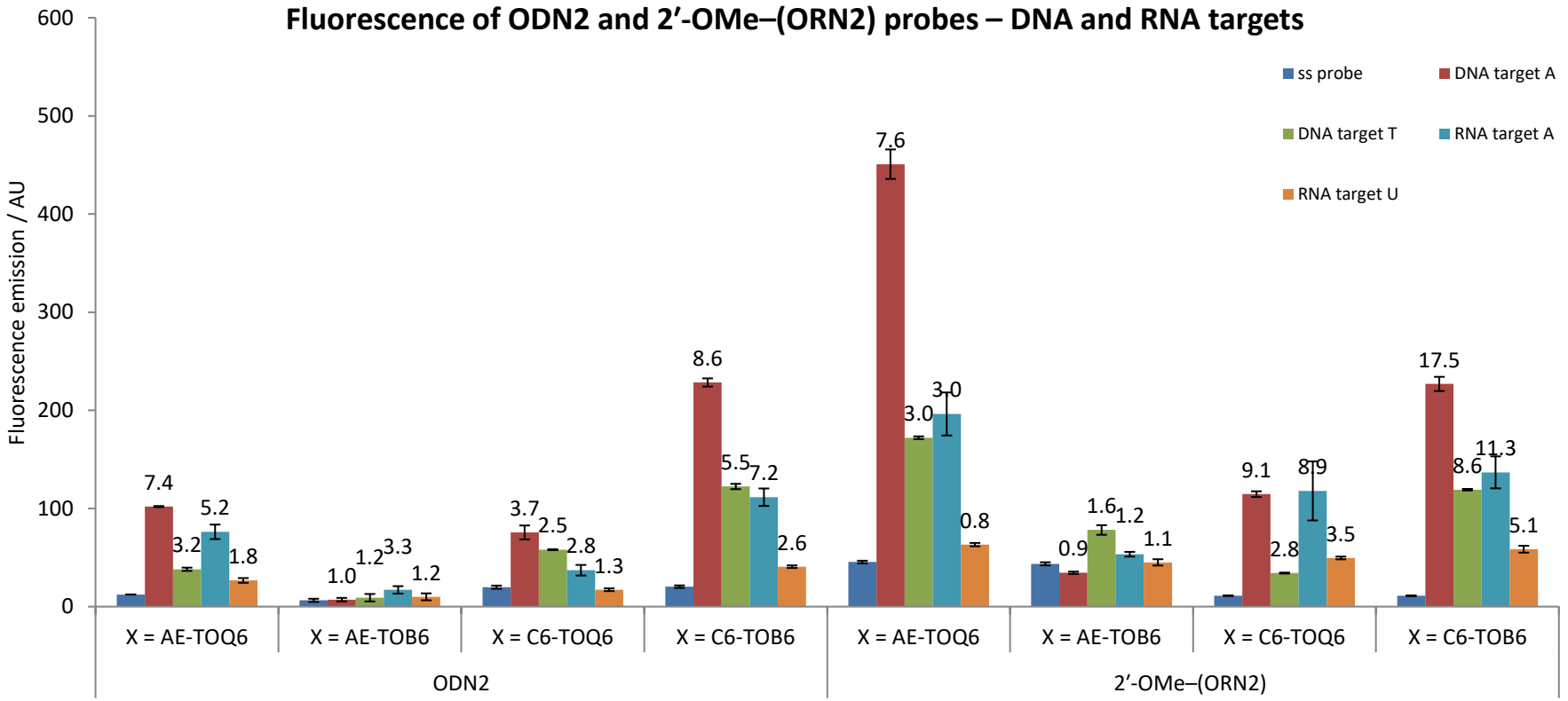


Figure 6.6 Fluorescence emssion intensity at $\lambda_{em,\,max}$ for TO-modified ODN2 (5'-GCAAXATACG) and 2'-OMe–(ORN2) (5'-GCAAXAUACG) probes against DNA and RNA targets. The base opposite the TO is either A – match or T/U – mismatch, ss probe – fluorescence emission intensity of single stranded probe, DNA target A/T and RNA target A/U - fluorescence emission intensity of probe-target duplex, AU - arbitrary units, number above bar = F_{ds}/F_{ss}. Detailed values: see Table 6.13, Table 6.16, Table 6.17 and Table 6.18.

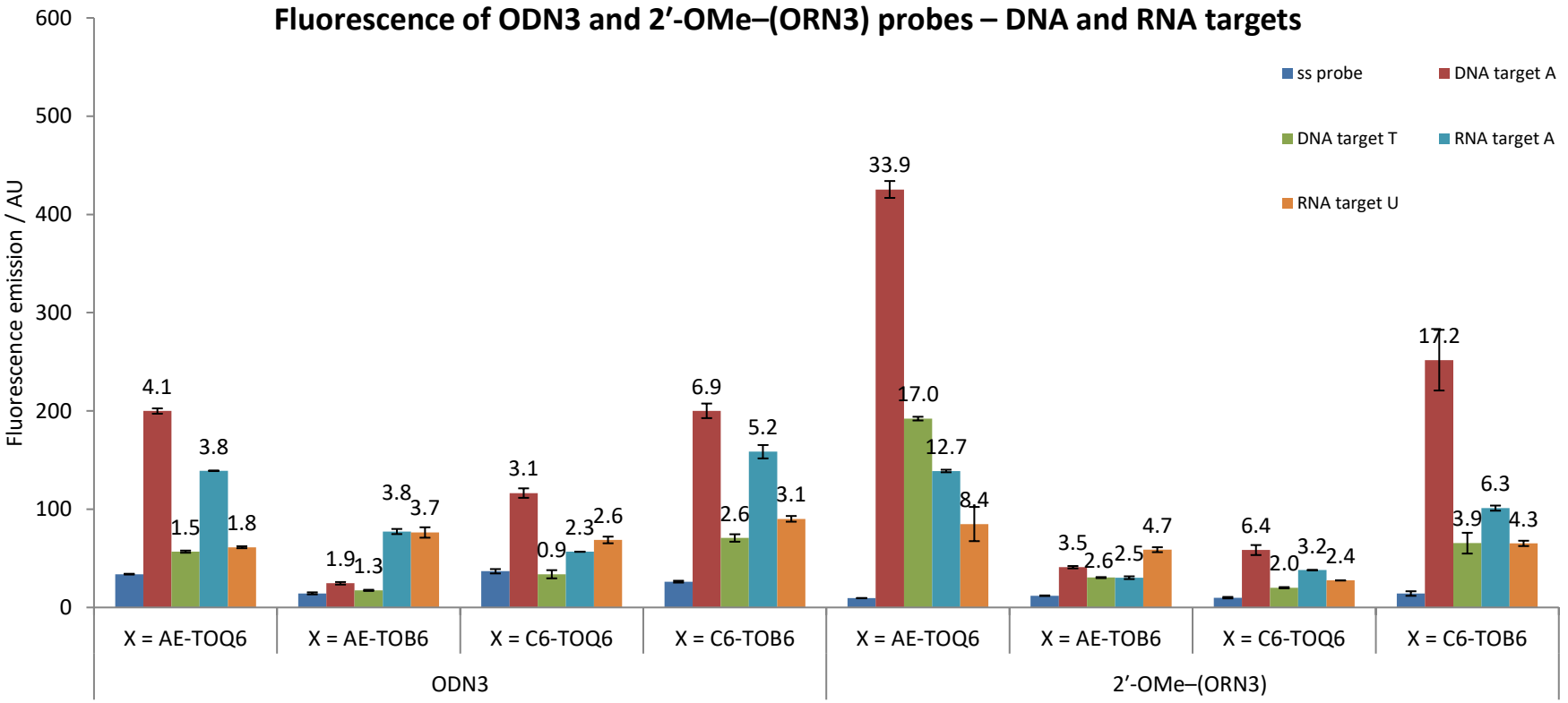


Figure 6.7 Fluorescence emssion intensity at $\lambda_{em,\ max}$ for TO-modified ODN3 (5'-GCACXCTACG) and 2'-OMe–(ORN3) (5'-GCACXCUACG) probes against DNA and RNA targets. The base opposite the TO is either A – match or T/U – mismatch, ss probe – fluorescence emission intensity of single stranded probe, DNA target A/T and RNA target A/U - fluorescence emission intensity of probe-target duplex, AU - arbitrary units, number above bar = F_{ds}/F_{ss}. Detailed values: see Table 6.13, Table 6.16, Table 6.17 and Table 6.18.

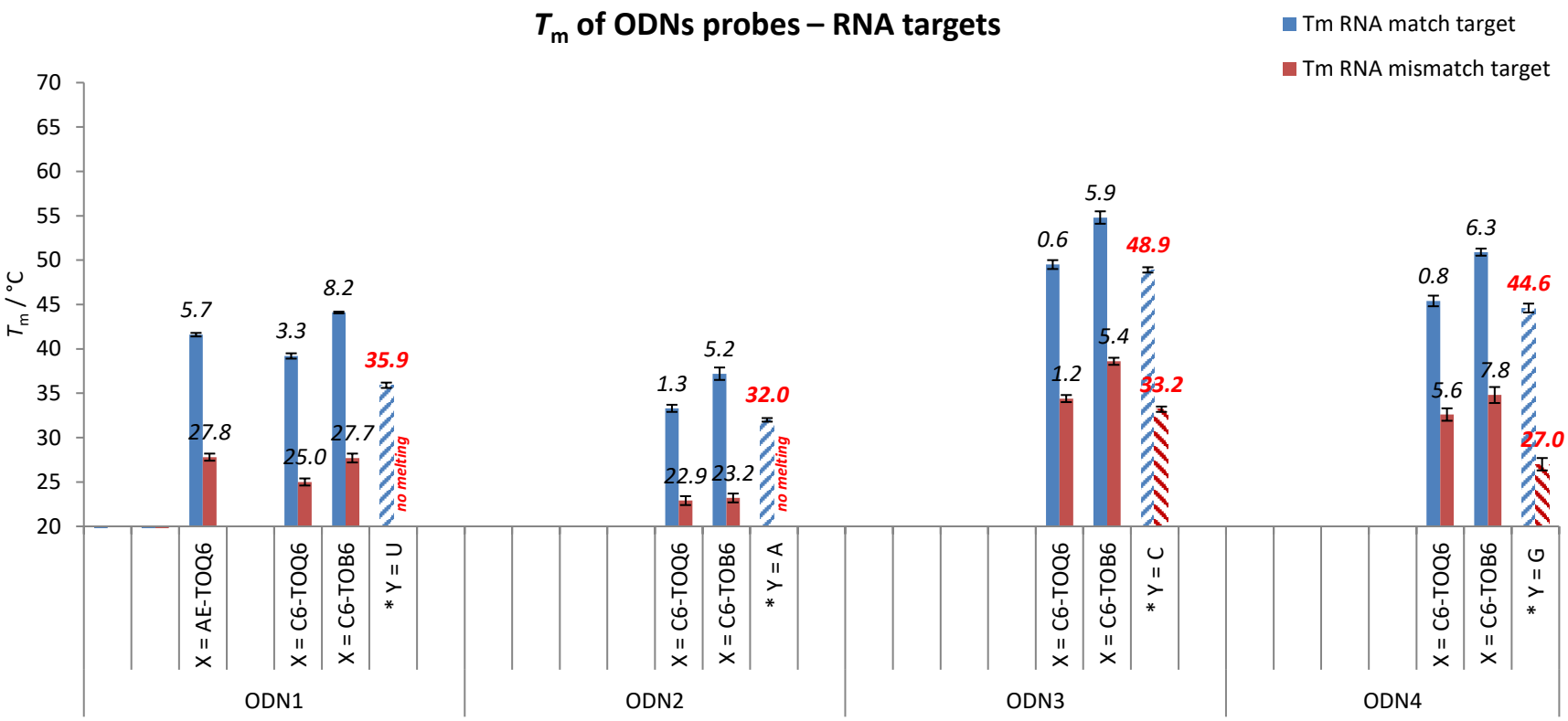


Figure 6.8 UV melting data for ODNs (ODN1 (5'-GCATXTTACG), ODN2 (5'-GCAAXATACG), ODN3 (5'-GCACXCTACG), ODN4 (5'-GCAGXGTACG)) probes against RNA targets. The base opposite the TO is either A – match or U – mismatch, number above bar = ΔT_m to unmodified target, * = T_m value of unmodified matched and mismatched duplexes. Detailed values: see Table 6.9.

6.12. Examples of fluorescence and UV melting curves

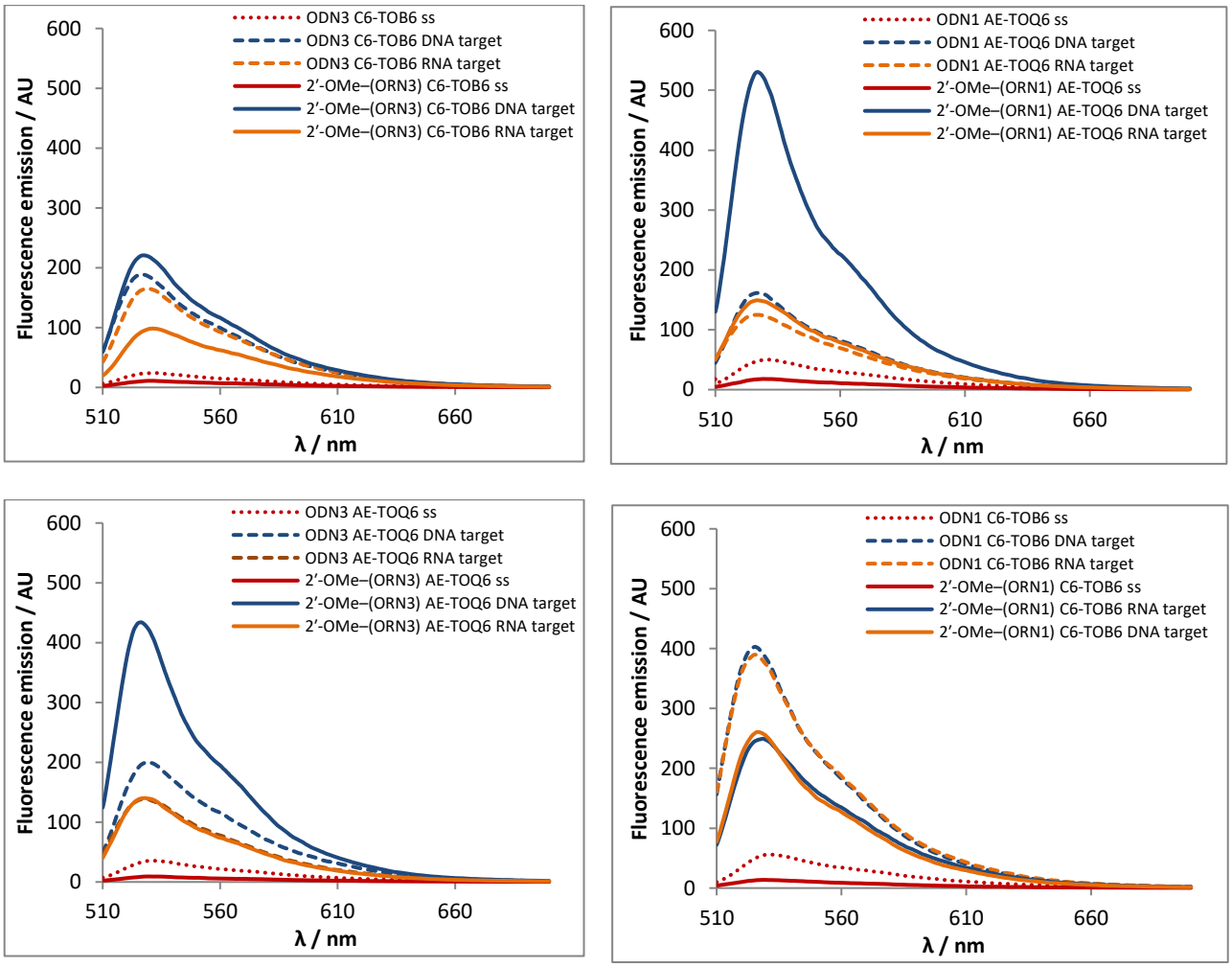


Figure 6.9 Examples of fluorescence emission spectra of ODN1 (5'GCAT**X**TTACG), 2'-OMe–(ORN1) (5'-GCAU**X**UUACG), ODN3 (5'-GCAC**X**CTACG) and 2'-OMe–(ORN3) (5'-GCAC**X**CUACG)) with C6-TO_{B6} and AE-TO_{Q6} probes with DNA or RNA targets. λ_{ex} = 484 nm, 200mM NaCl, 10 mM phosphate, pH = 7.0 at 20 °C.

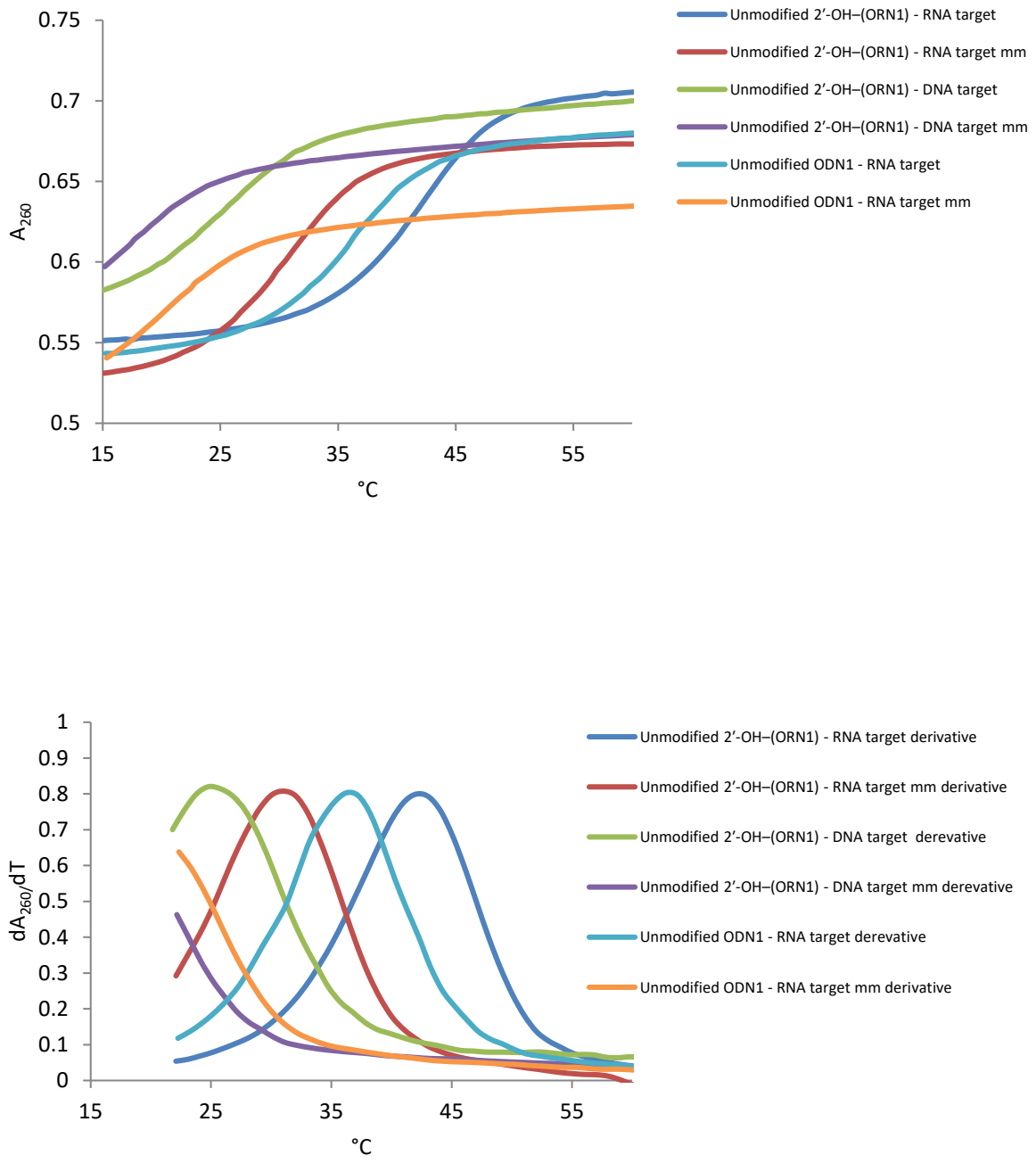


Figure 6.10 Examples of UV melting curves (top panel) and normalized derivatives (bottom panel) for unmodified 2'-OH–(ORN1) (5'-GCAU**U**UUACG) and ODN1 (5'-GCAT**T**TTACG) unmodified controls against match and mismatch (mm) DNA and RNA targets.

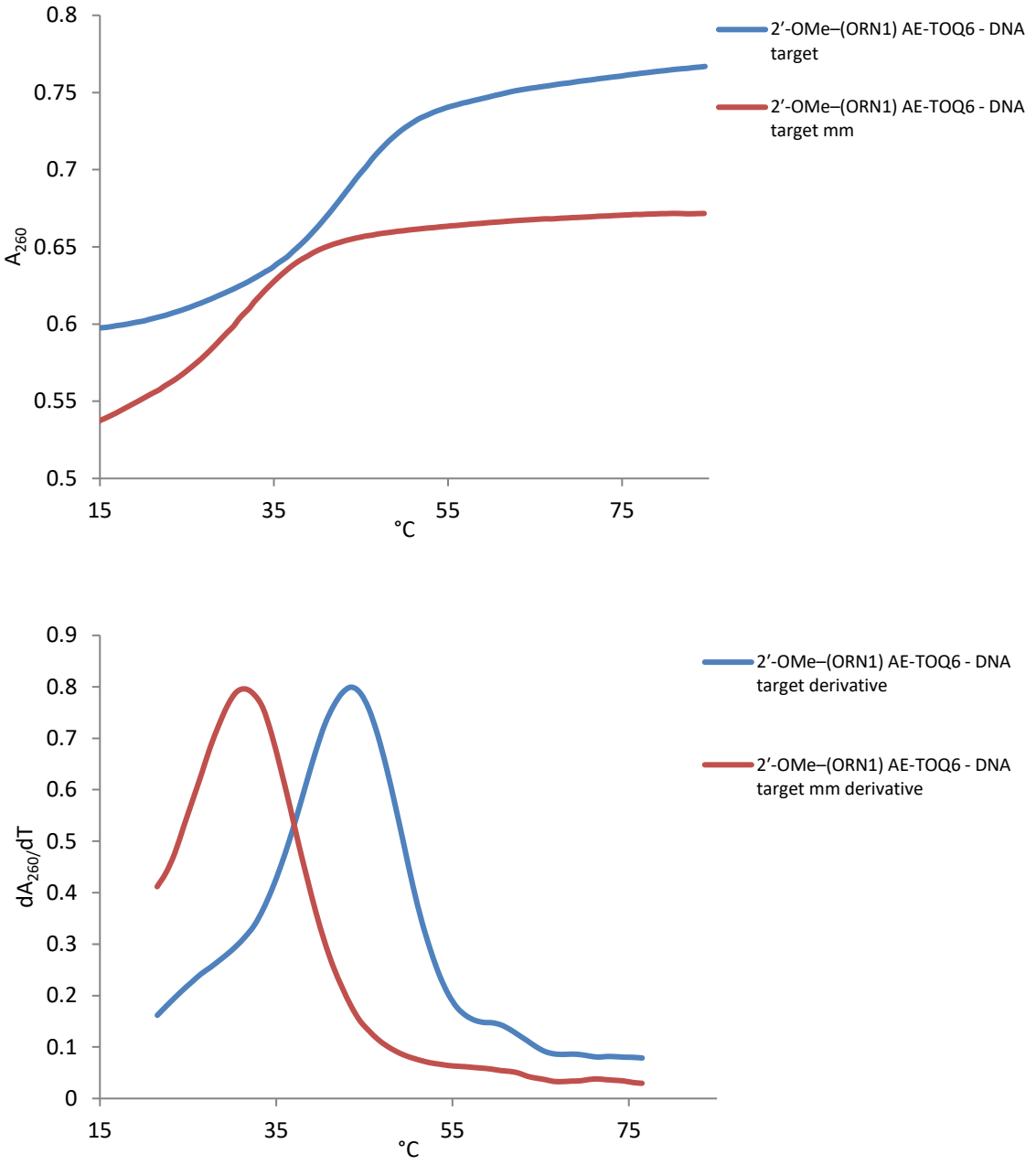


Figure 6.11 Examples of UV melting curves (top panel) and normalized derivatives (bottom panel) for 2′-OMe–(ORN1) (5′-GCAA**X**AUACG) probes with AE-TO_{Q6} against match and mismatch (mm) DNA targets.

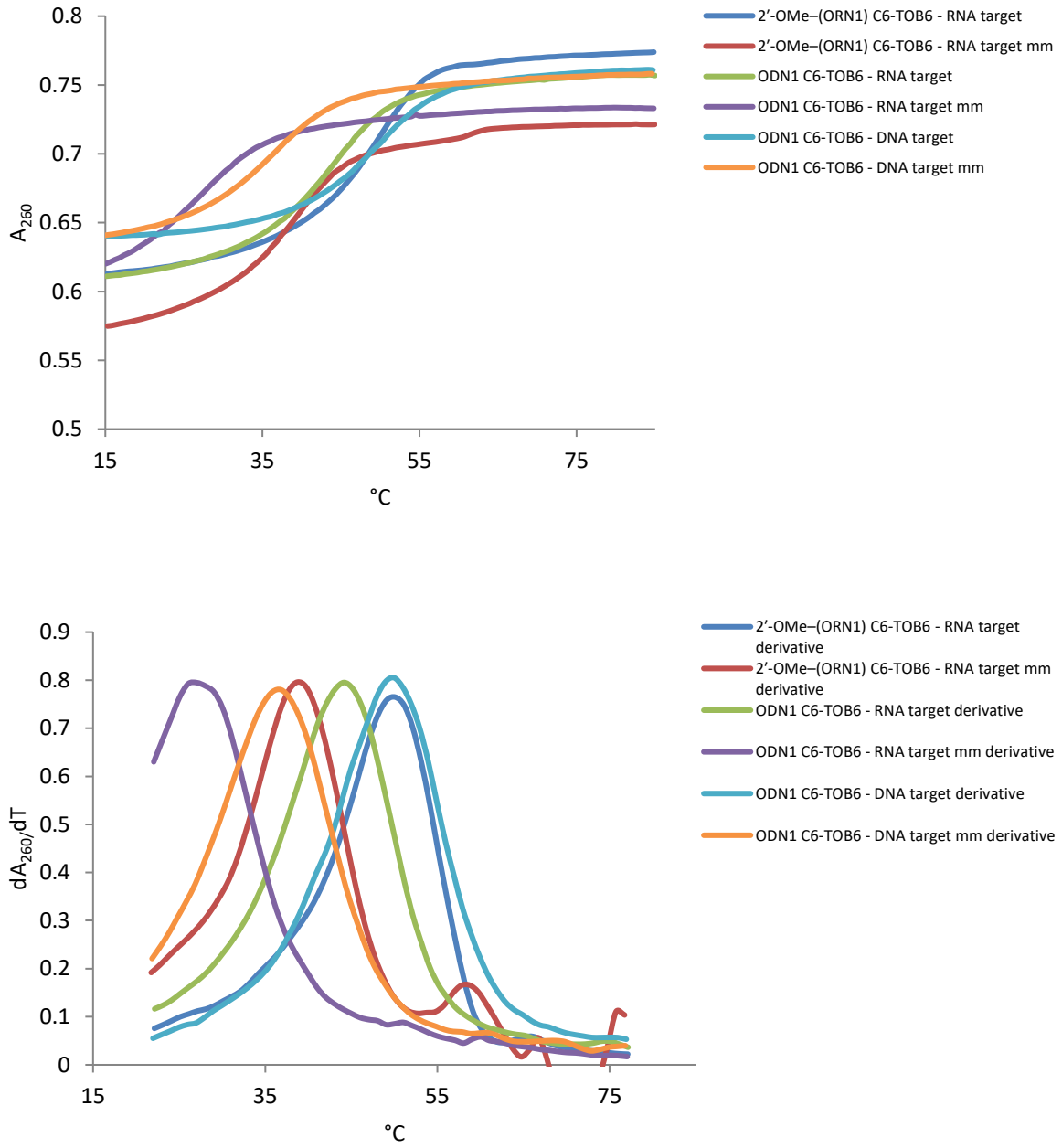


Figure 6.12 Examples of UV melting curves (top panel) and normalized derivatives (bottom panel) for 2'-OMe–(ORN1) (5'-GCAU**X**UUACG) and ODN1 (5'-GCAT**X**TTACG) probes with C6-TO_{B6} against match and mismatch (mm) DNA and RNA targets.

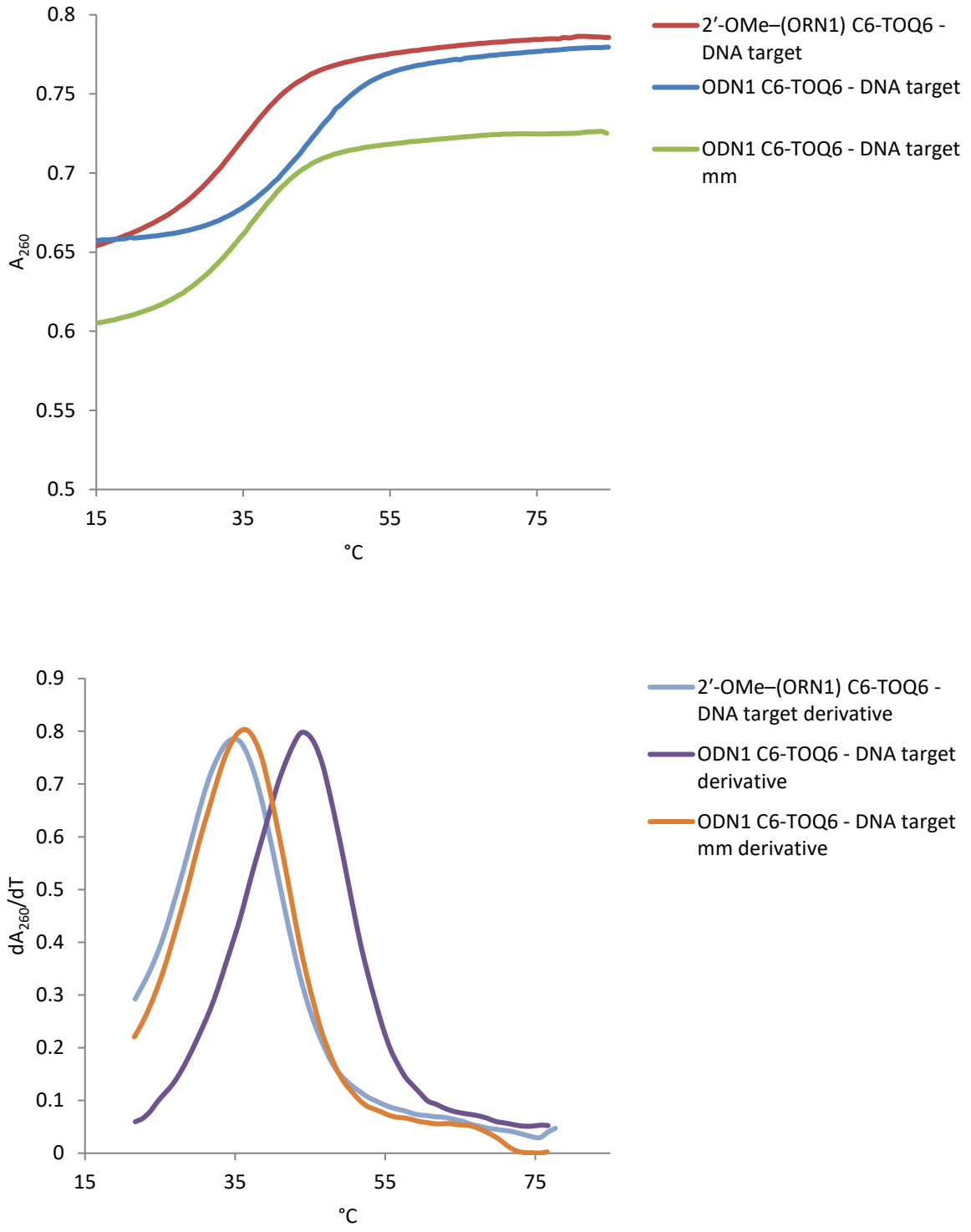


Figure 6.13 Examples of UV melting curves (top panel) and normalized derivatives (bottom panel) for 2'-OMe–(ORN1) 5'-GCAU**X**UUACG and ODN1 (5'-GCAT**X**TTACG) probes with C6-TO_{Q6} against match and mismatch (mm) DNA targets.

7. NMR spectra

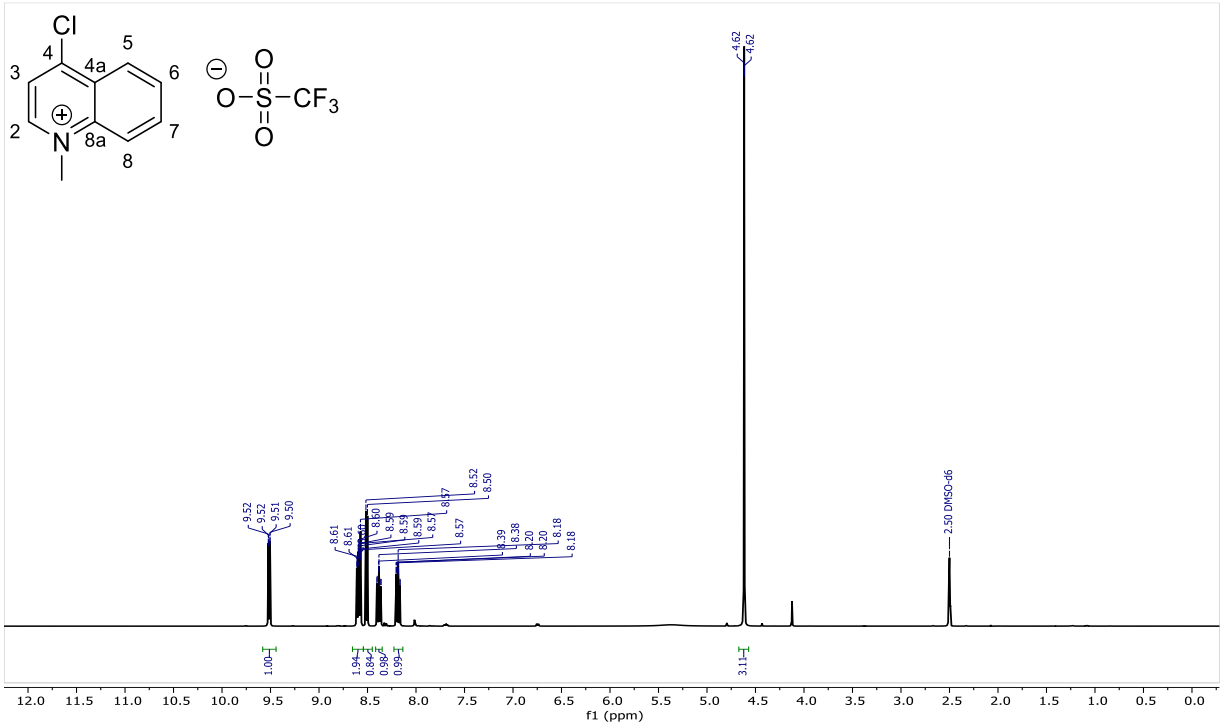


Figure 7.1 ^{1}H NMR d_6-DMSO spectrum of **2** at 400 MHz

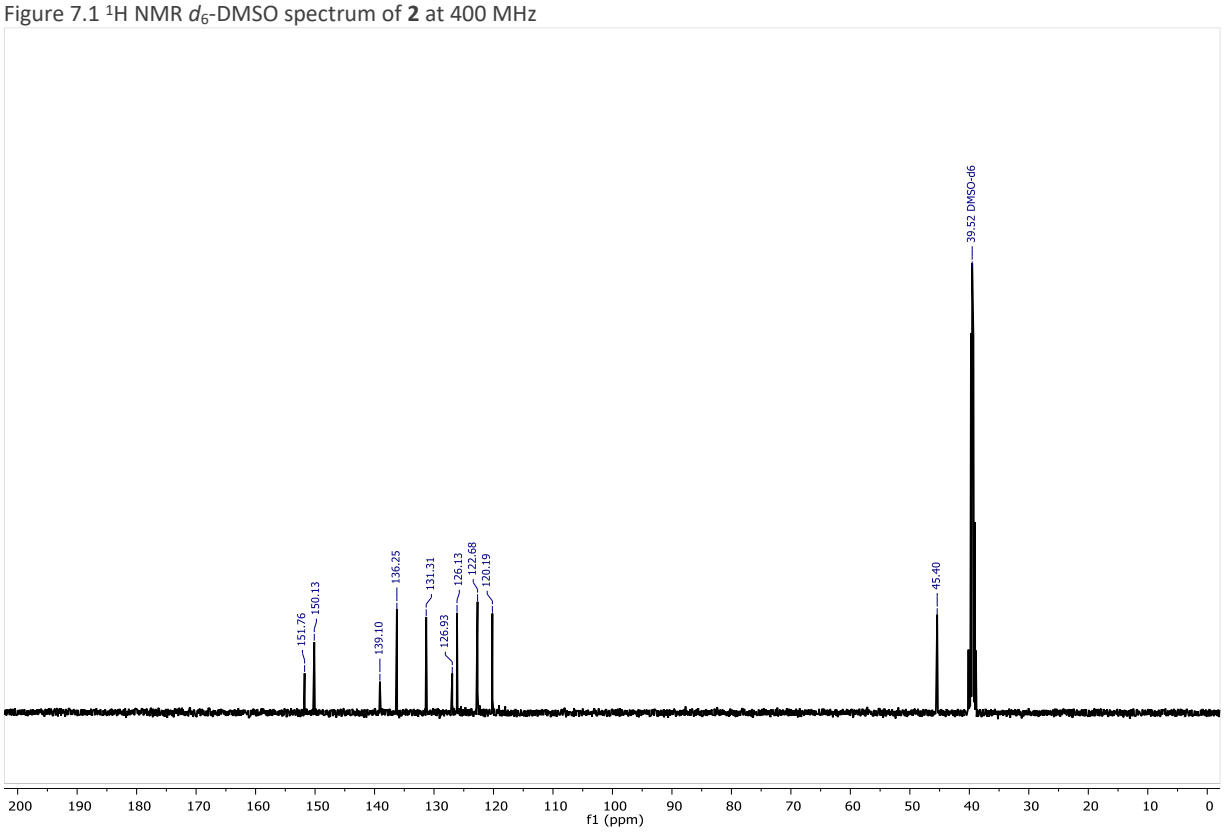


Figure 7.2 ^{13}C NMR d_6-DMSO spectrum of **2** at 101 MHz

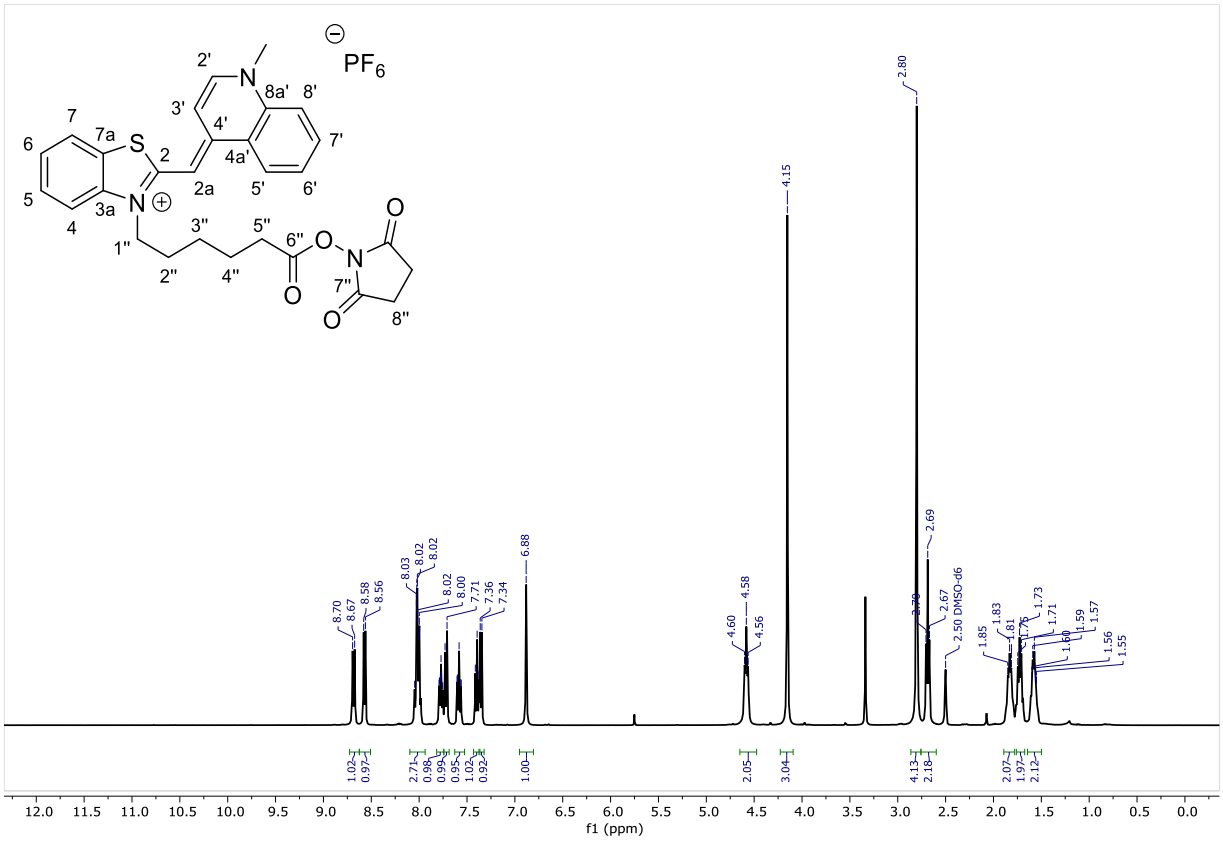


Figure 7.3 ^{1}H NMR d_6-DMSO spectrum of **4** at 400 MHz

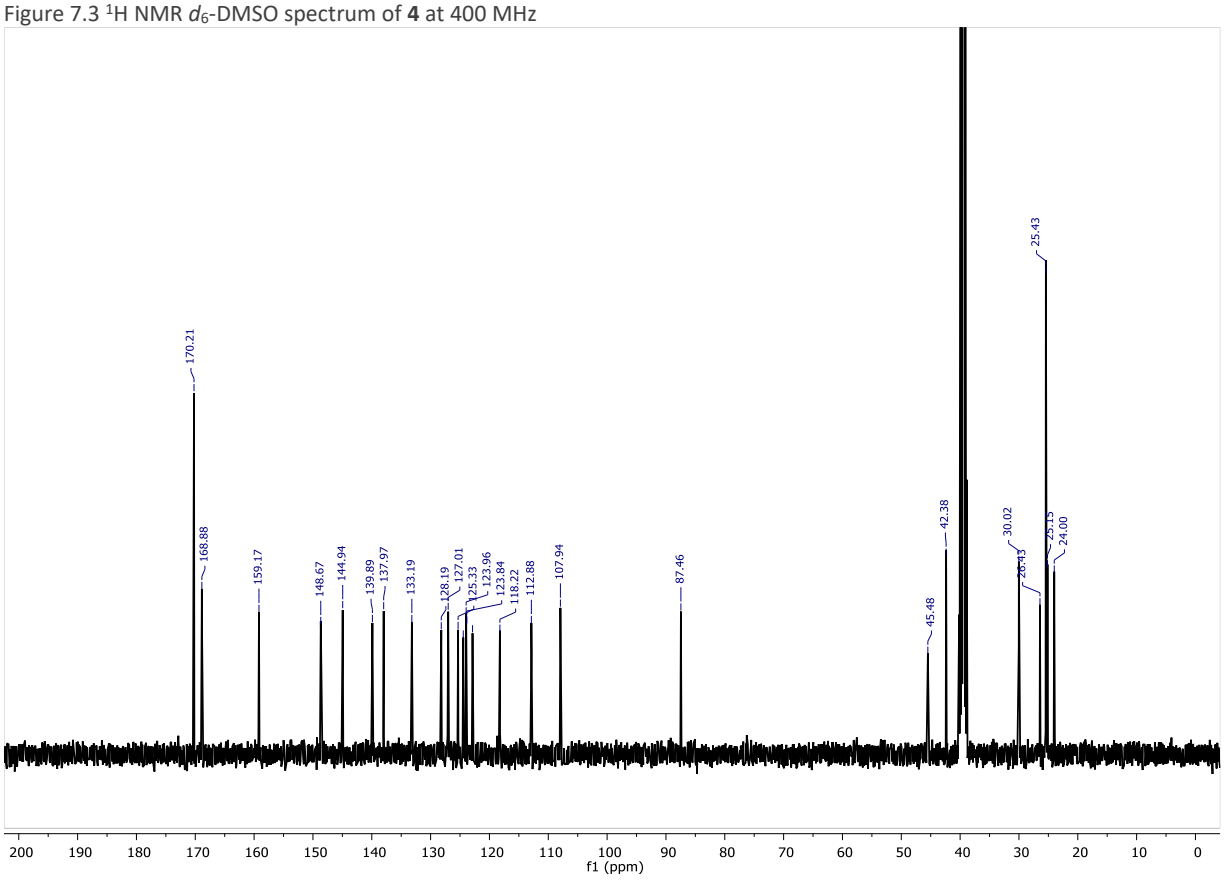


Figure 7.4 ^{13}C NMR d_6-DMSO spectrum of **4** at 101 MHz

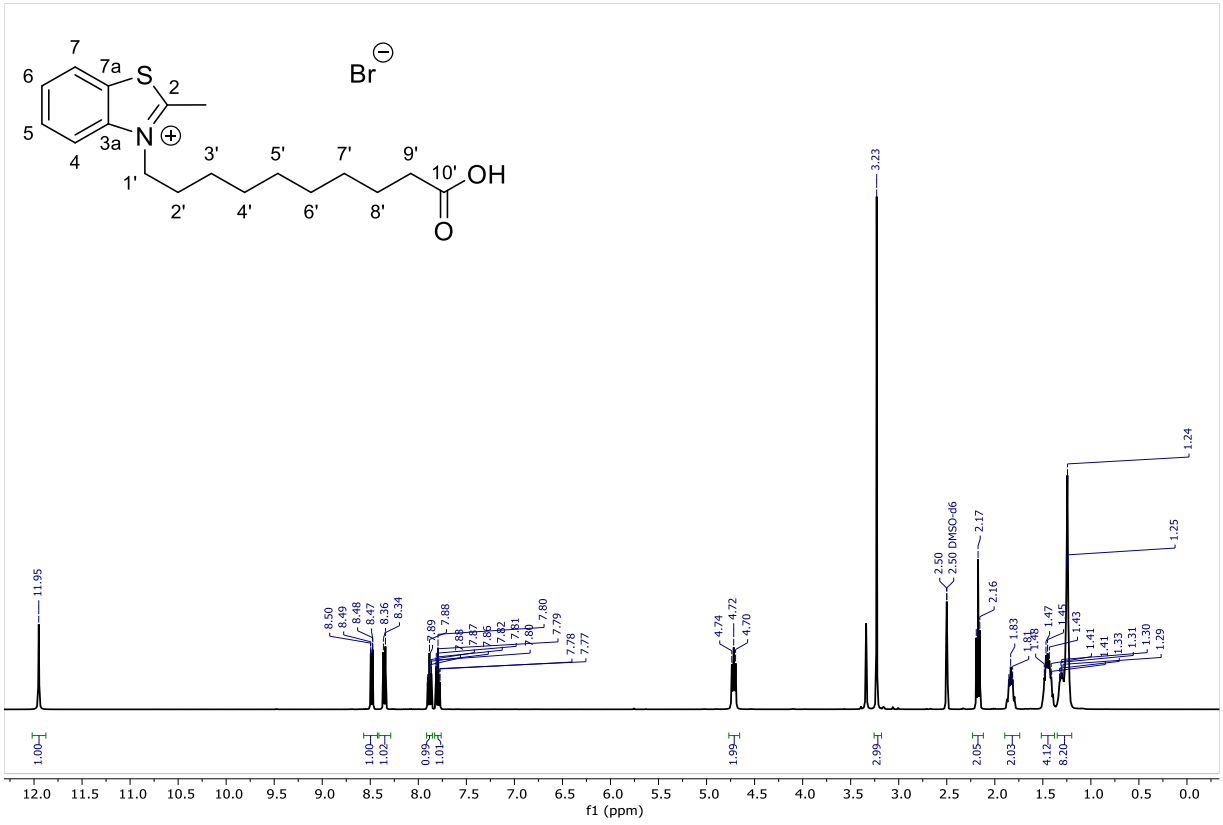


Figure 7.5 ^{1}H NMR d_6-DMSO spectrum of **9** at 400 MHz

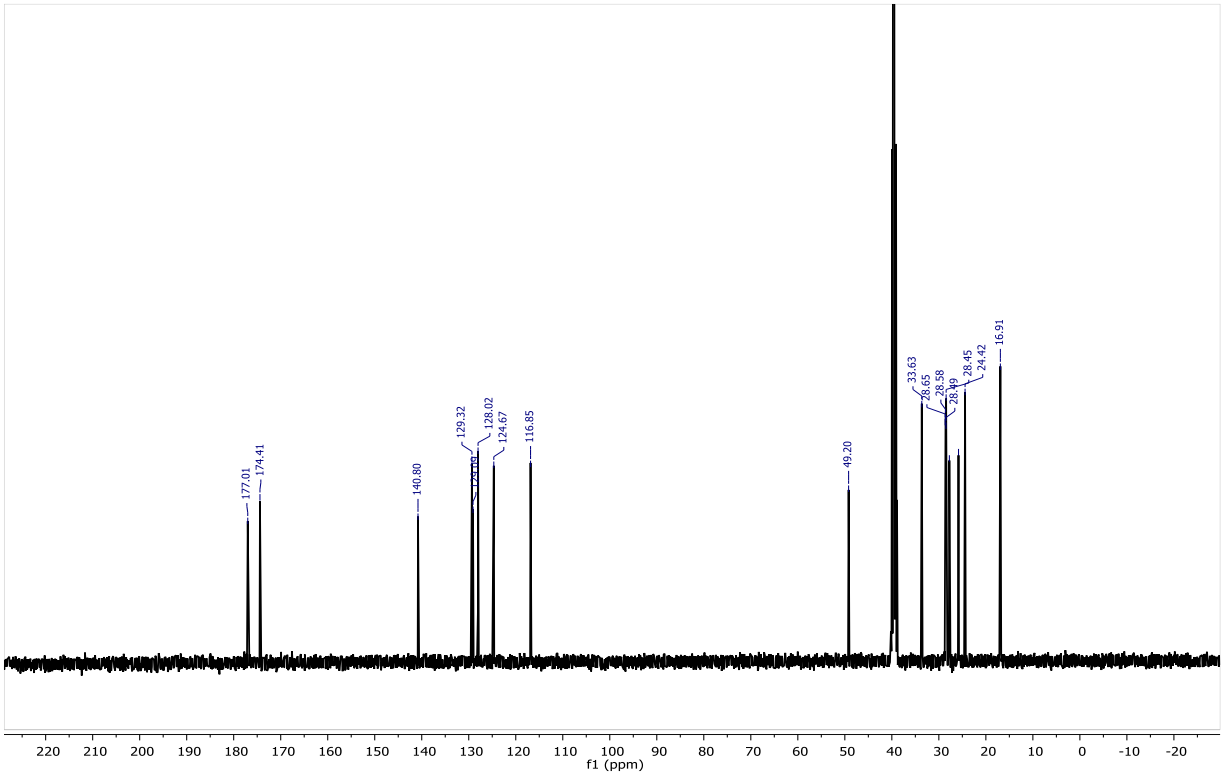


Figure 7.6 ^{13}C NMR d_6-DMSO spectrum of **9** at 101 MHz

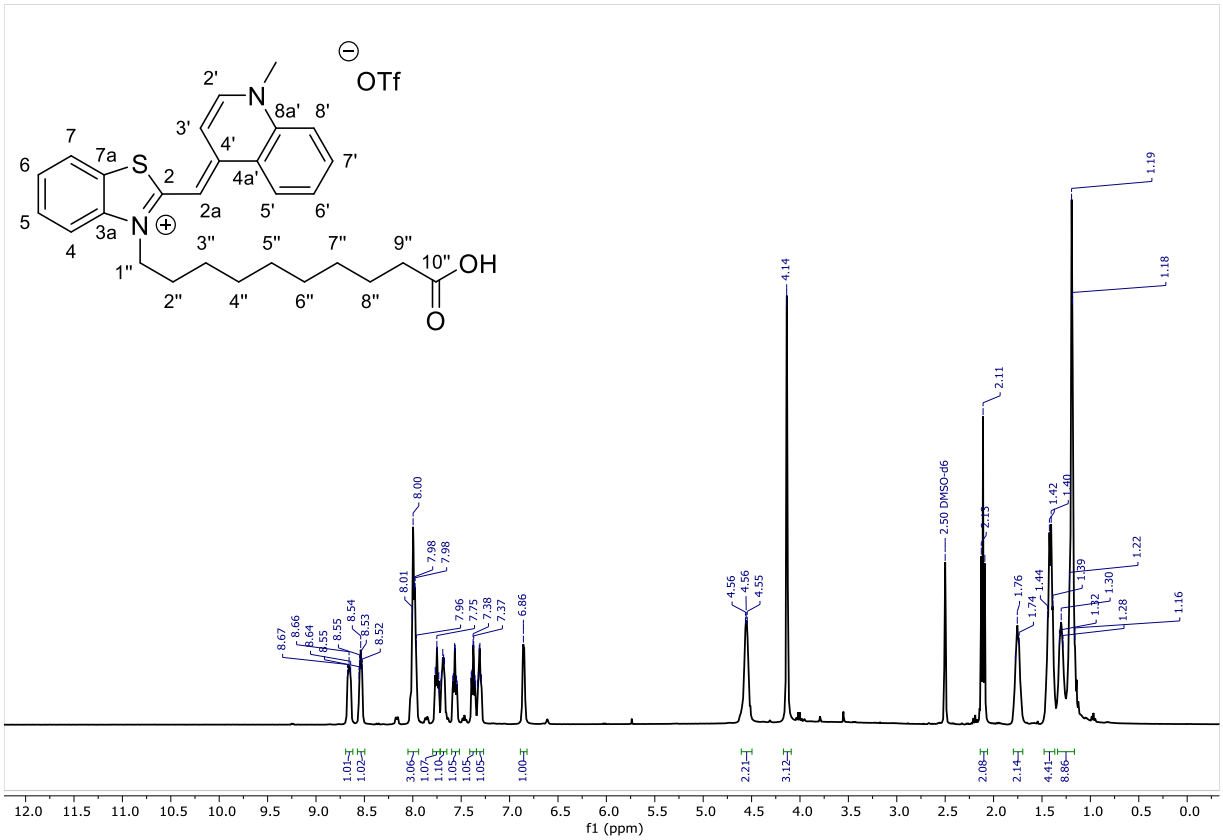


Figure 7.7 ^{1}H NMR d_6-DMSO spectrum of **10** at 400 MHz

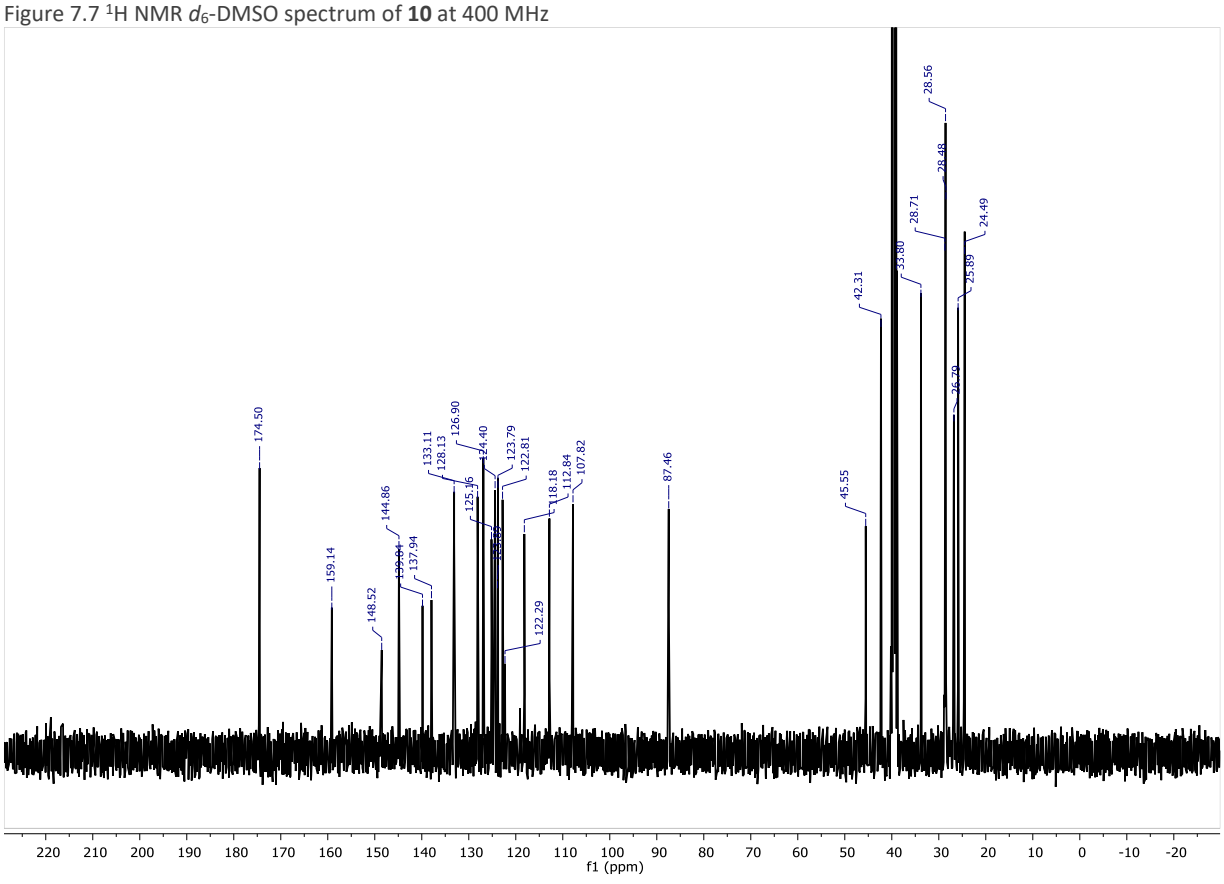


Figure 7.8 ^{13}C NMR d_6-DMSO spectrum of **10** at 101 MHz

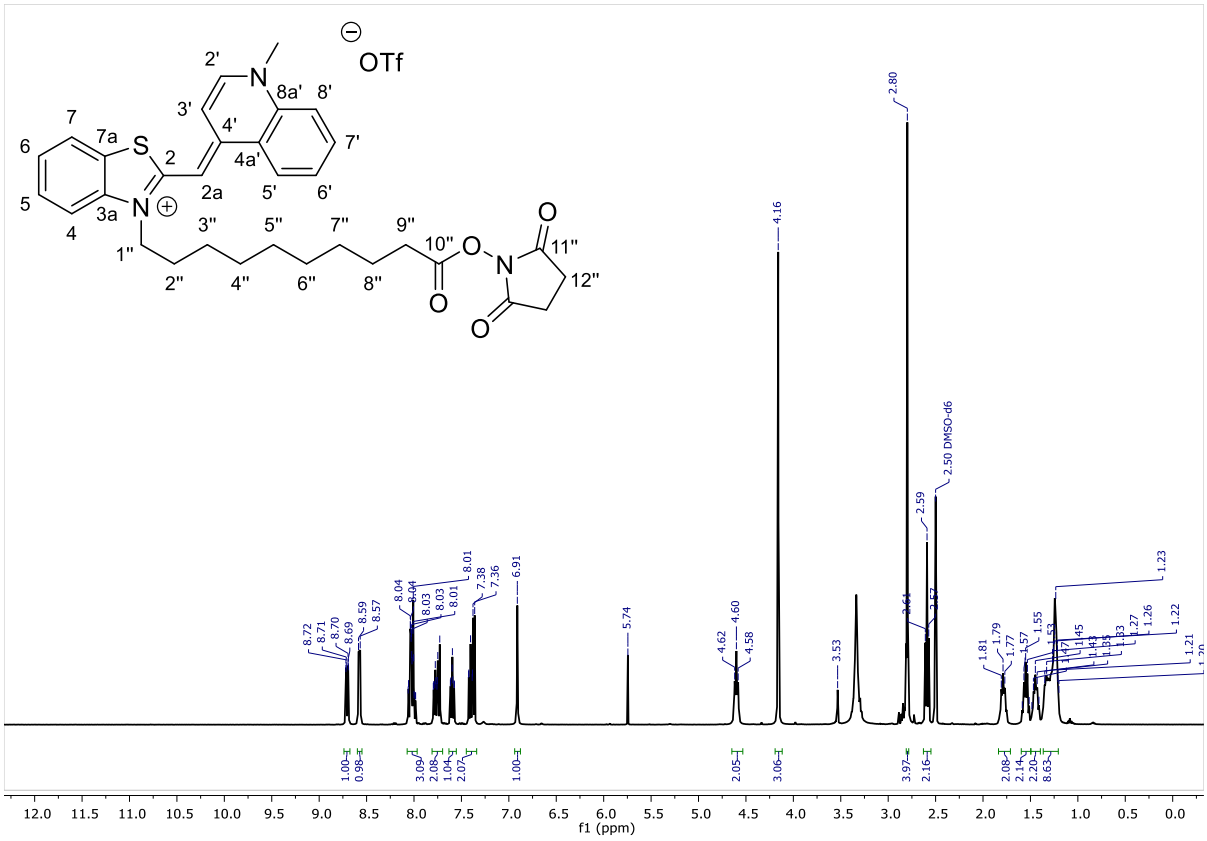


Figure 7.9 ^{1}H NMR d_6-DMSO spectrum of **11** at 400 MHz

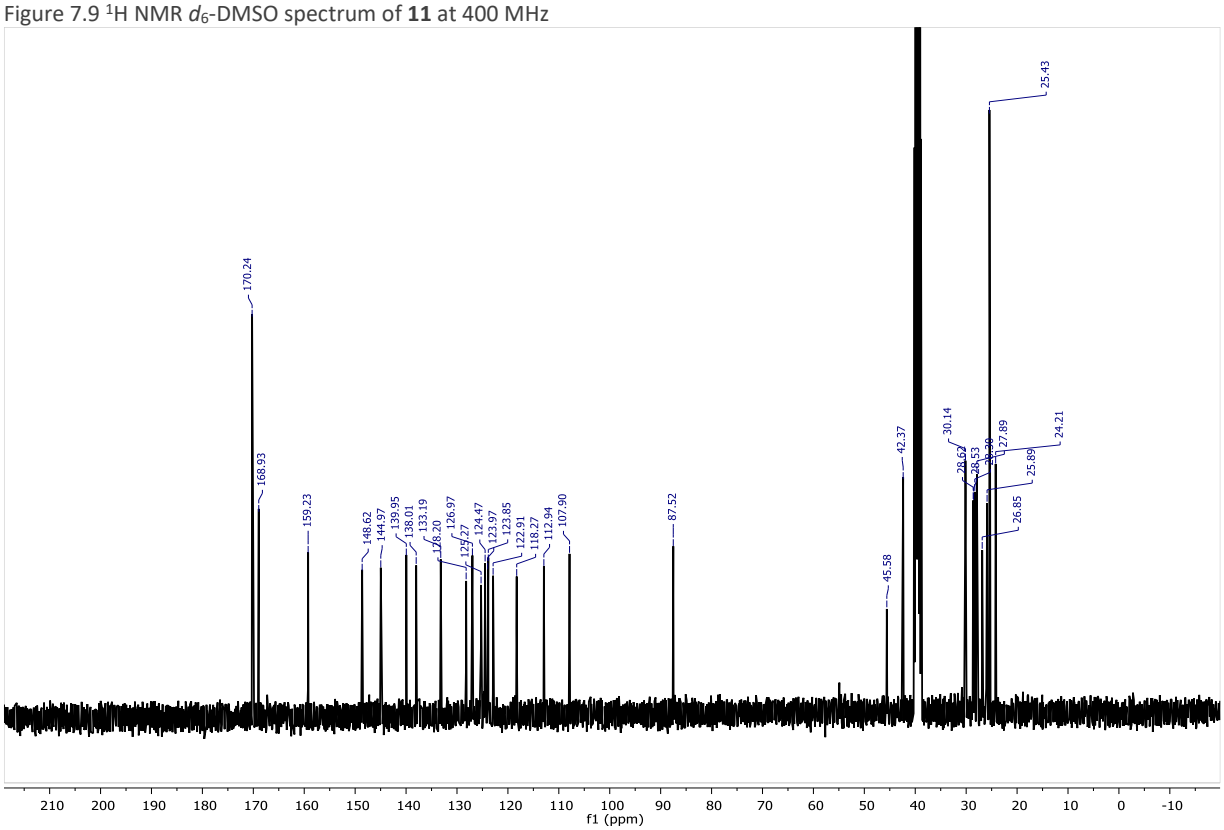


Figure 7.10 ^{13}C NMR d_6-DMSO spectrum of **11** at 101 MHz

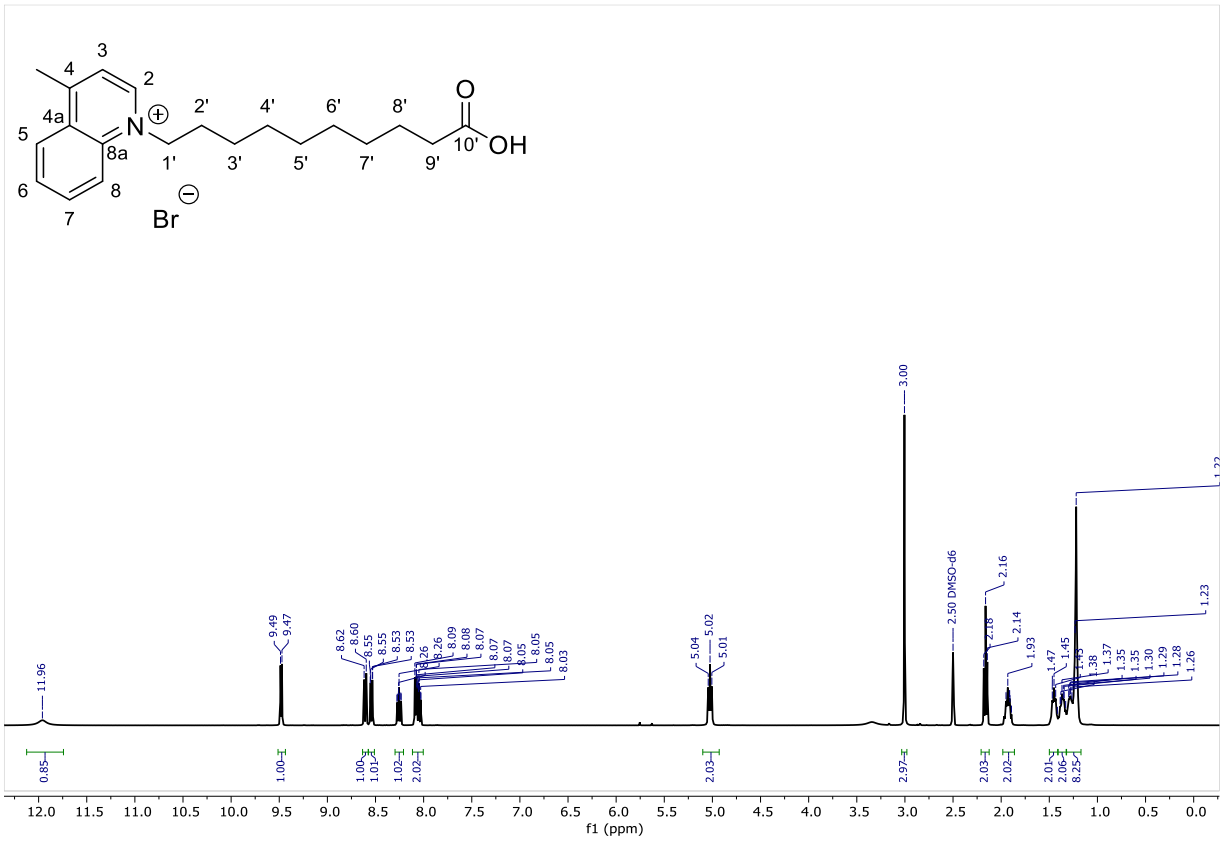


Figure 7.11 ^{1}H NMR d_6-DMSO spectrum of **12** at 400 MHz

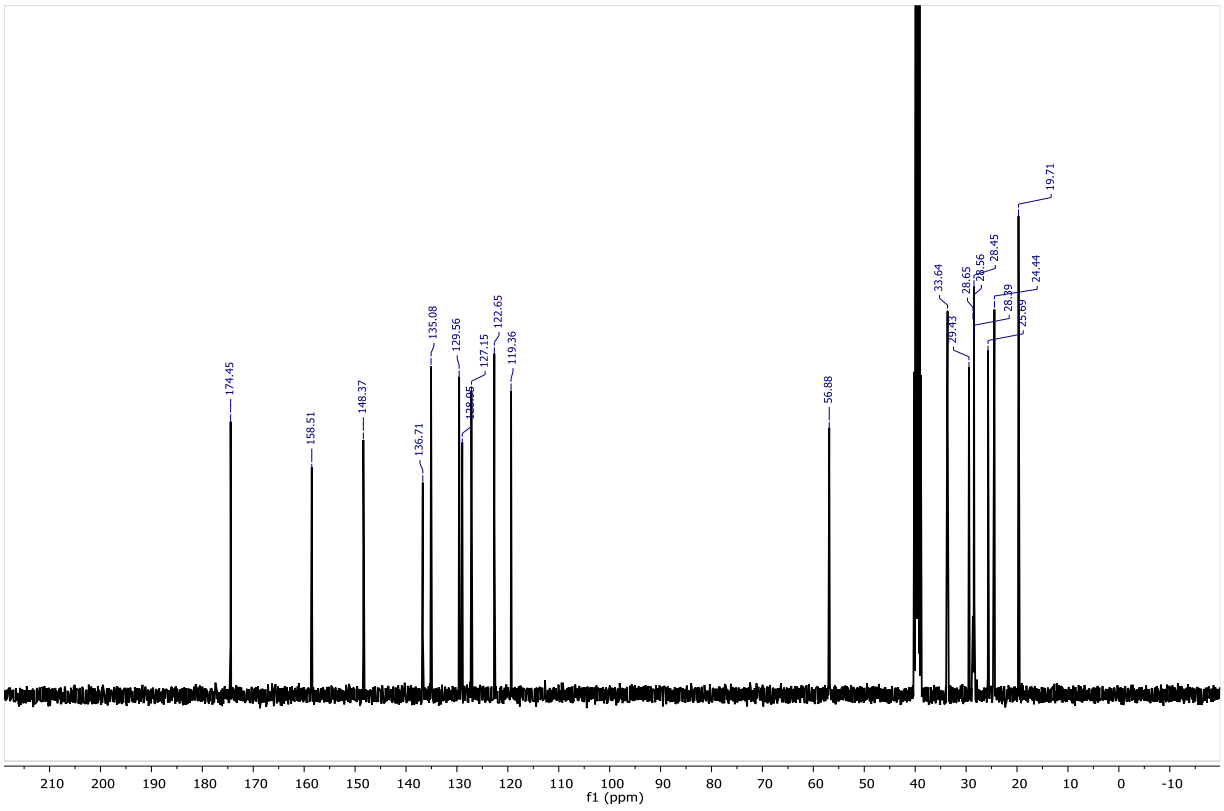


Figure 7.12 ^{13}CNMR d_6-DMSO spectrum of **12** at 101 MHz

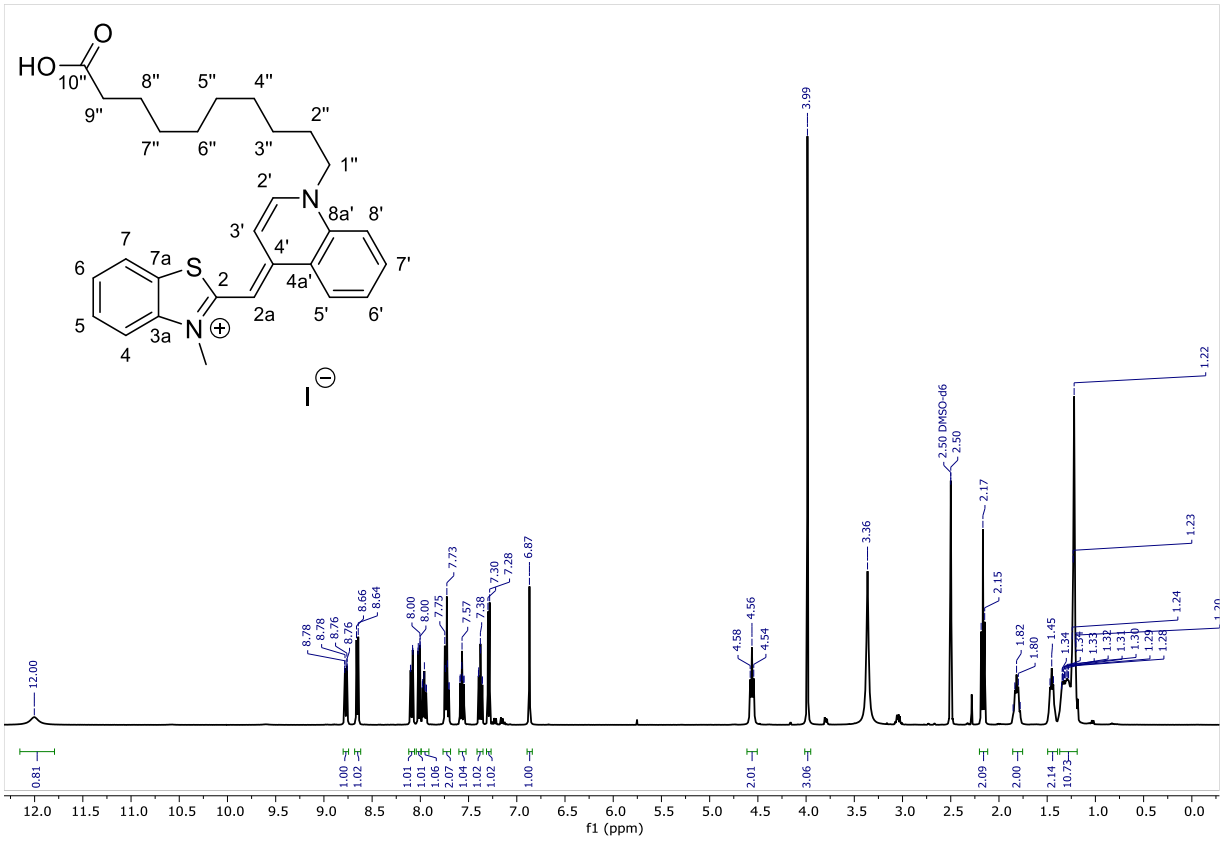


Figure 7.13 ^{1}H NMR d_6-DMSO spectrum of **13** at 400 MHz

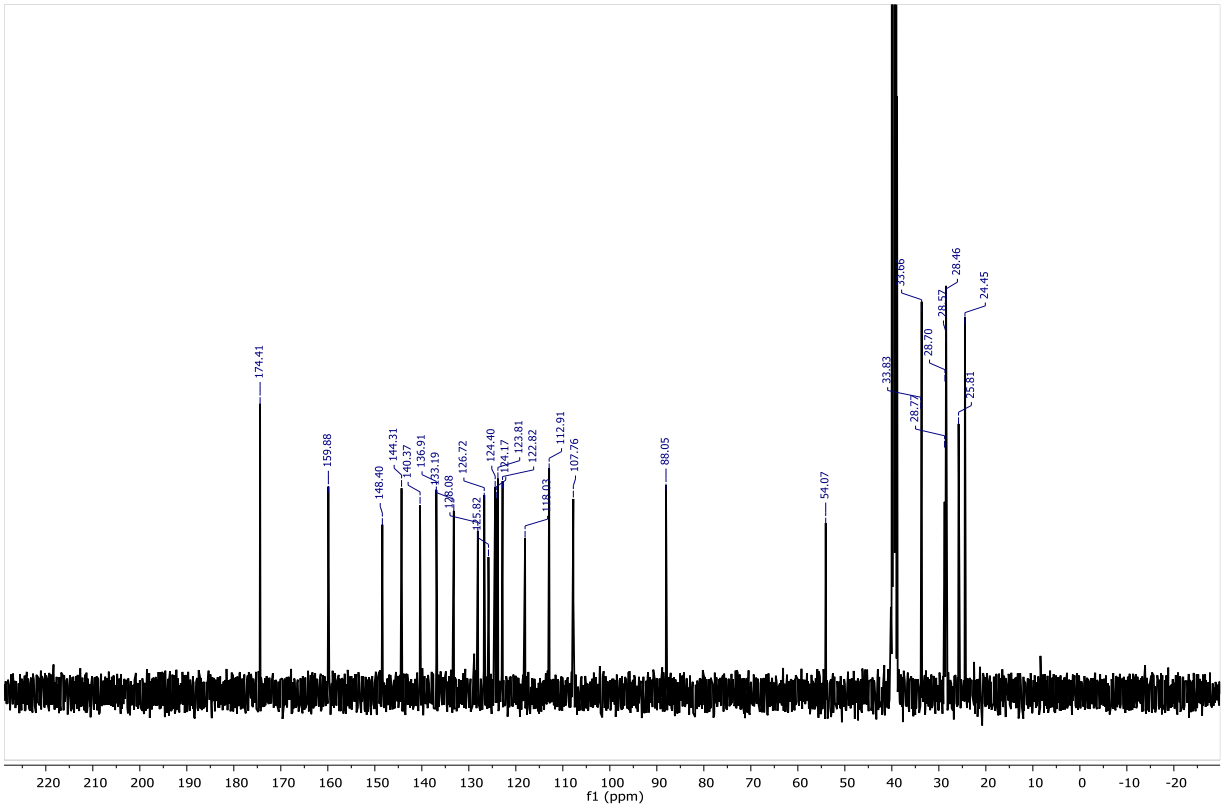


Figure 7.14 ^{13}C NMR d_6-DMSO spectrum of **13** at 101 MHz

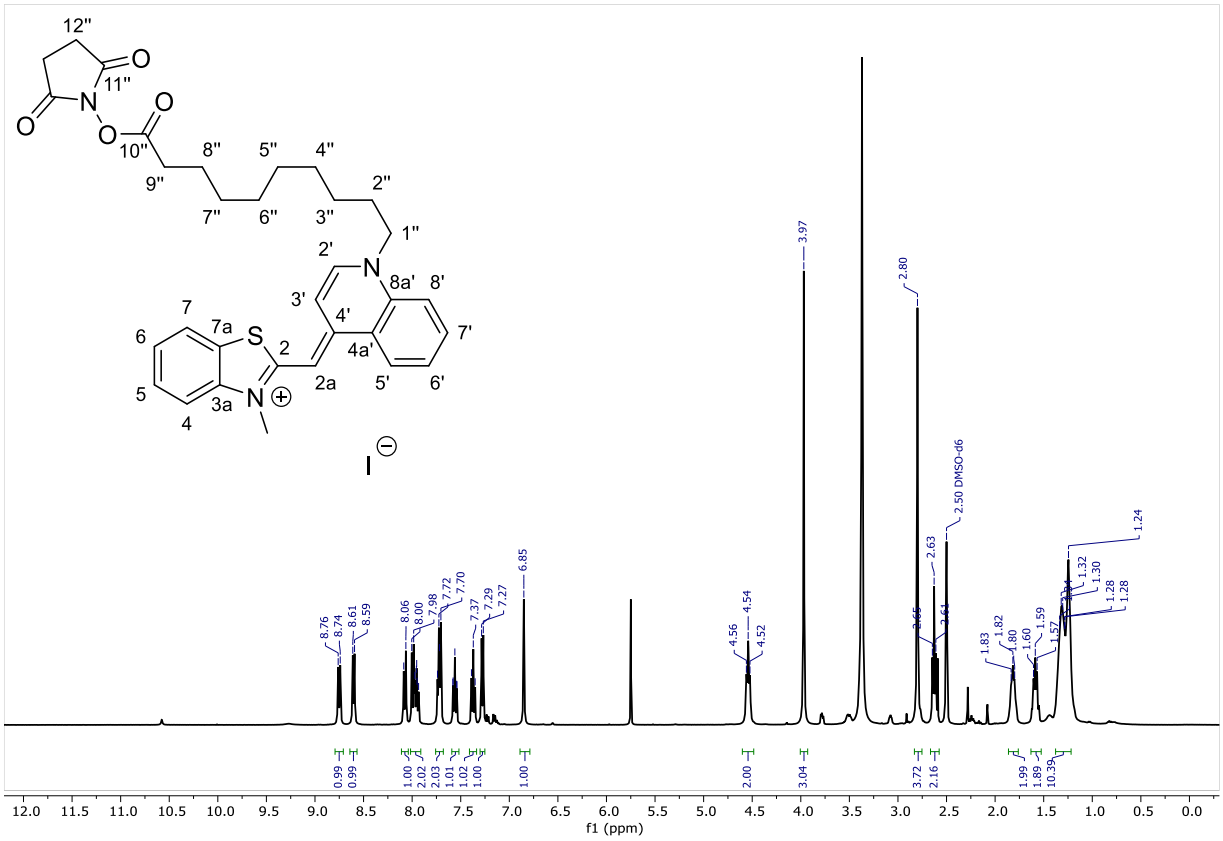


Figure 7.15 ^{1}H NMR d_6-DMSO spectrum of **14** at 400 MHz

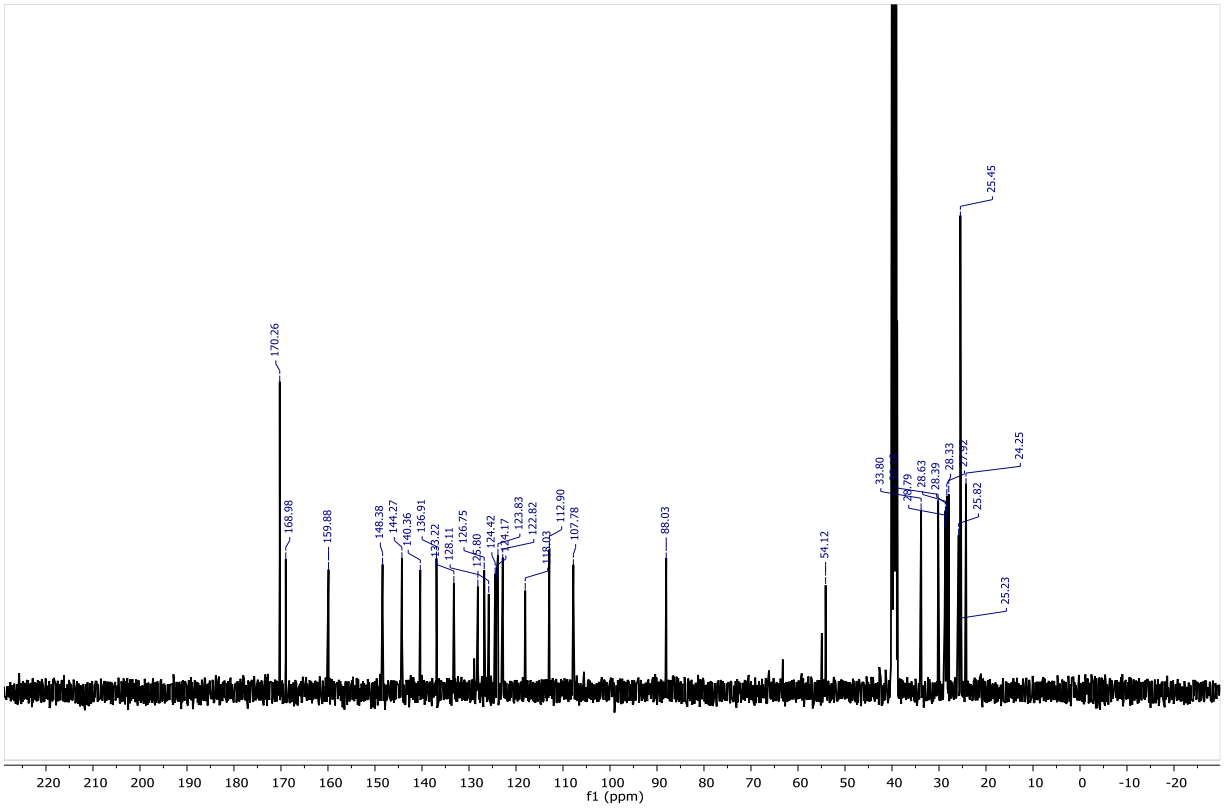


Figure 7.16 ^{13}C NMR d_6-DMSO spectrum of **14** at 101 MHz

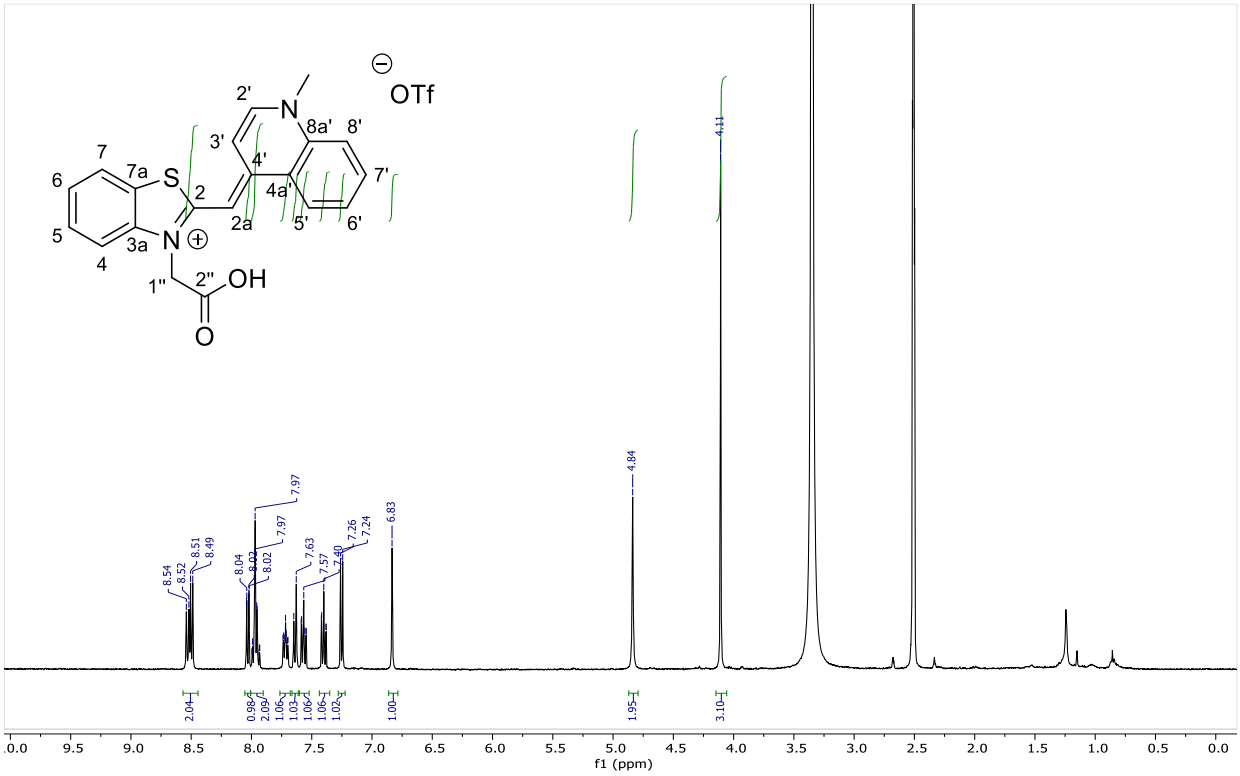


Figure 7.17 ^{1}H NMR d_6-DMSO spectrum of **16** at 400 MHz

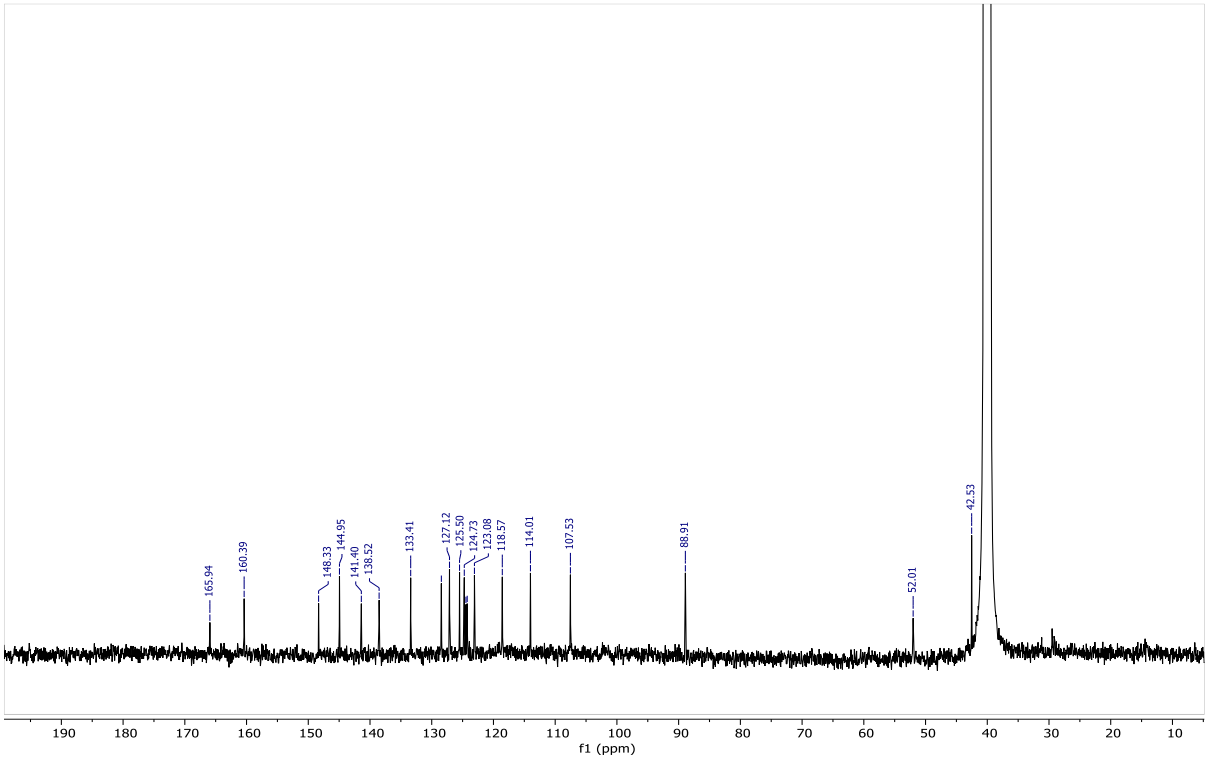


Figure 7.18 ^{13}C NMR d_6-DMSO spectrum of **16** at 101 MHz

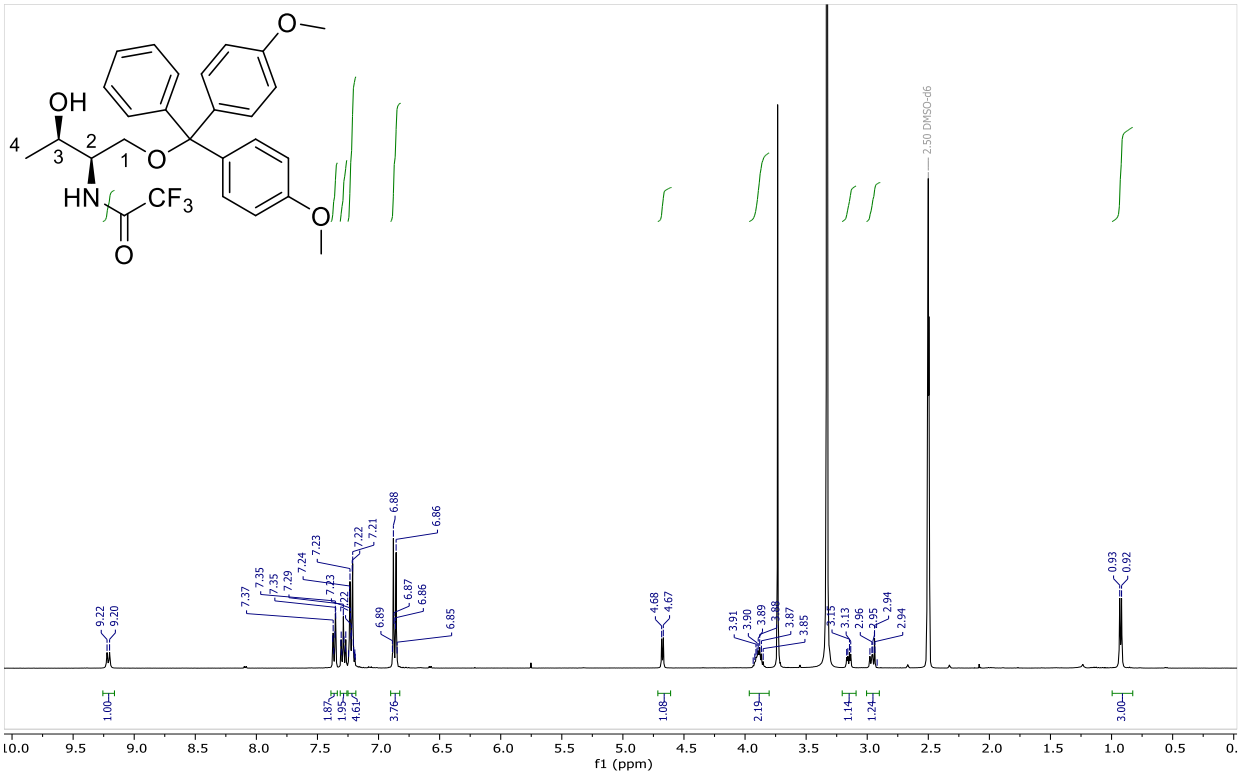


Figure 7.19 ^{1}H NMR d_6-DMSO spectrum of **20** at 400 MHz

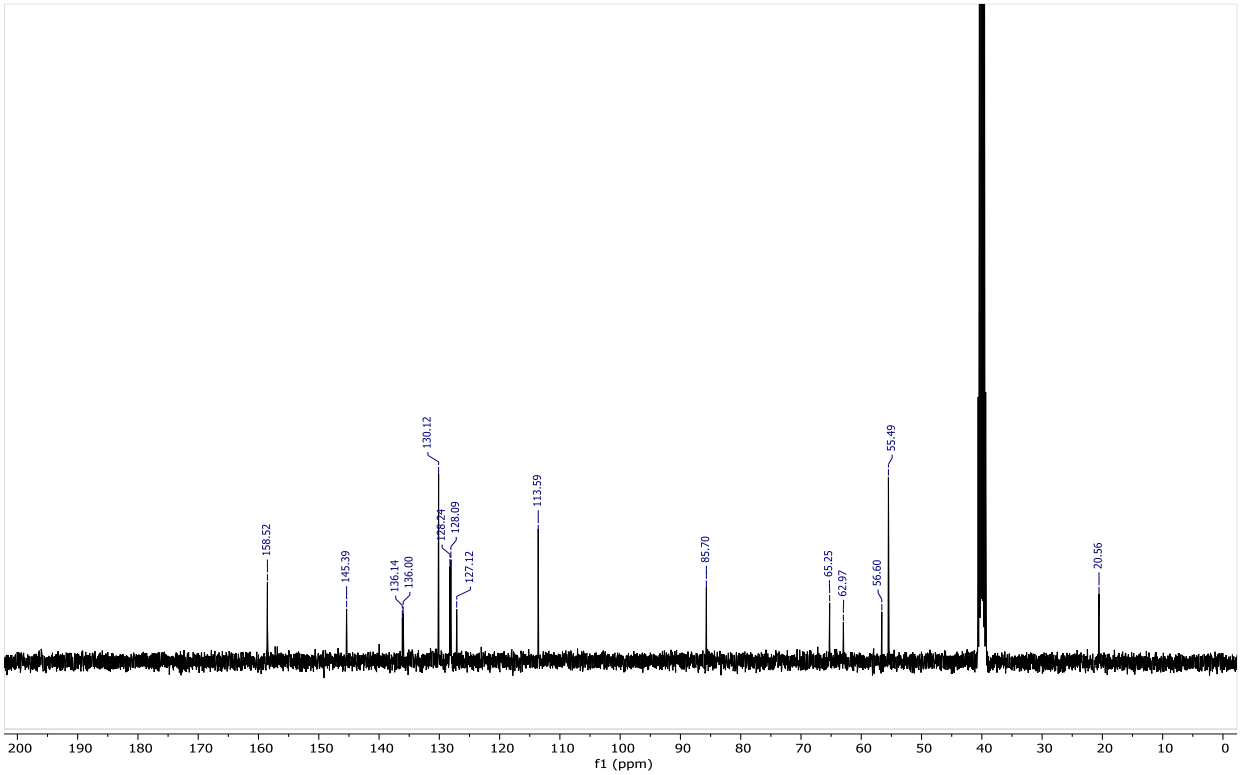


Figure 7.20 13C NMR d6-DMSO spectrum of **20** at 101 MHz

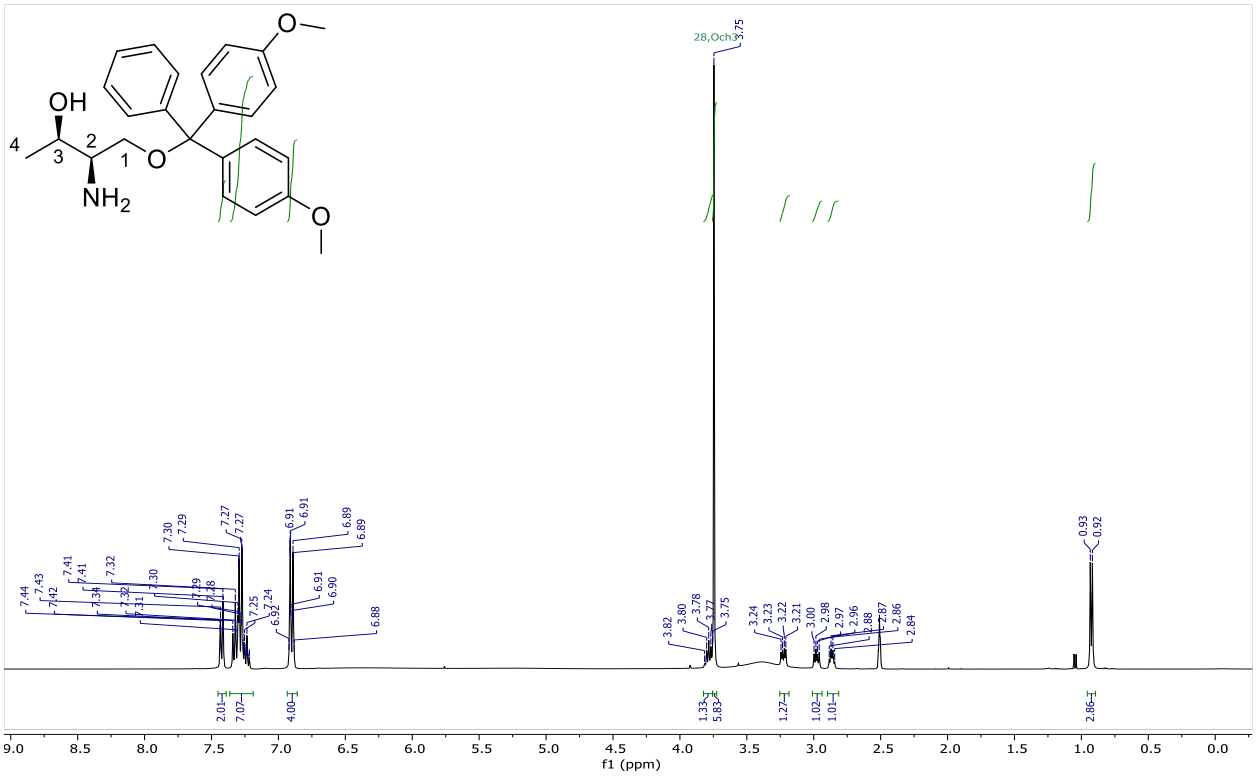


Figure 7.21 ^{1}H NMR d_6-DMSO spectrum of **21** at 400 MHz

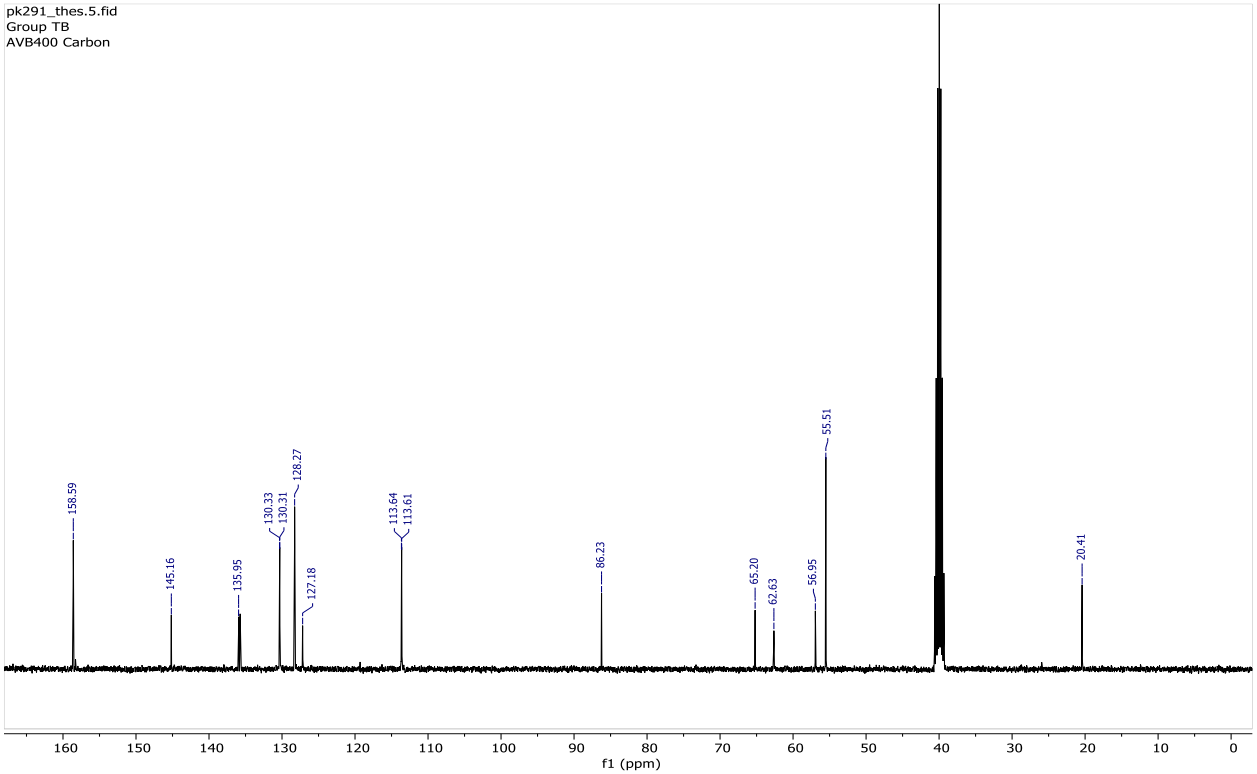


Figure 7.22 ^{13}C NMR d_6-DMSO spectrum of **21** at 101 MHz

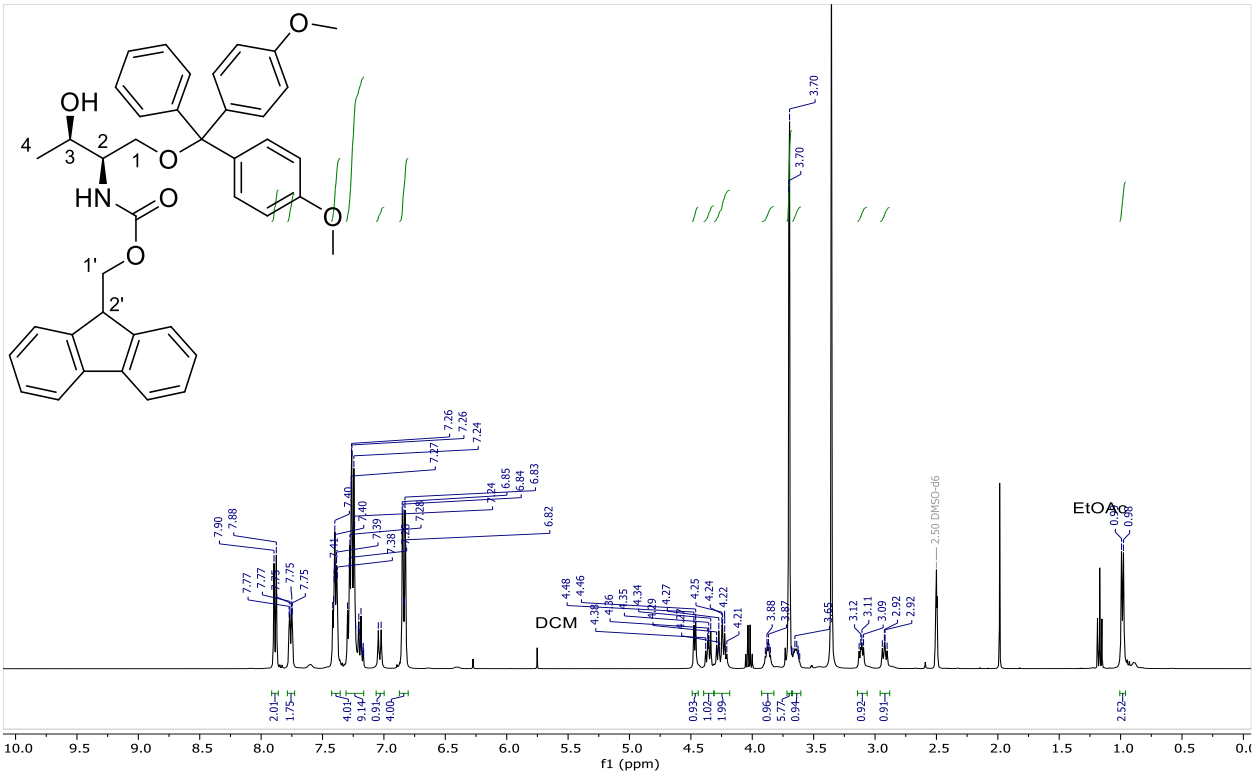


Figure 7.23 ^{1}H NMR d_6-DMSO spectrum of **22** at 400 MHz

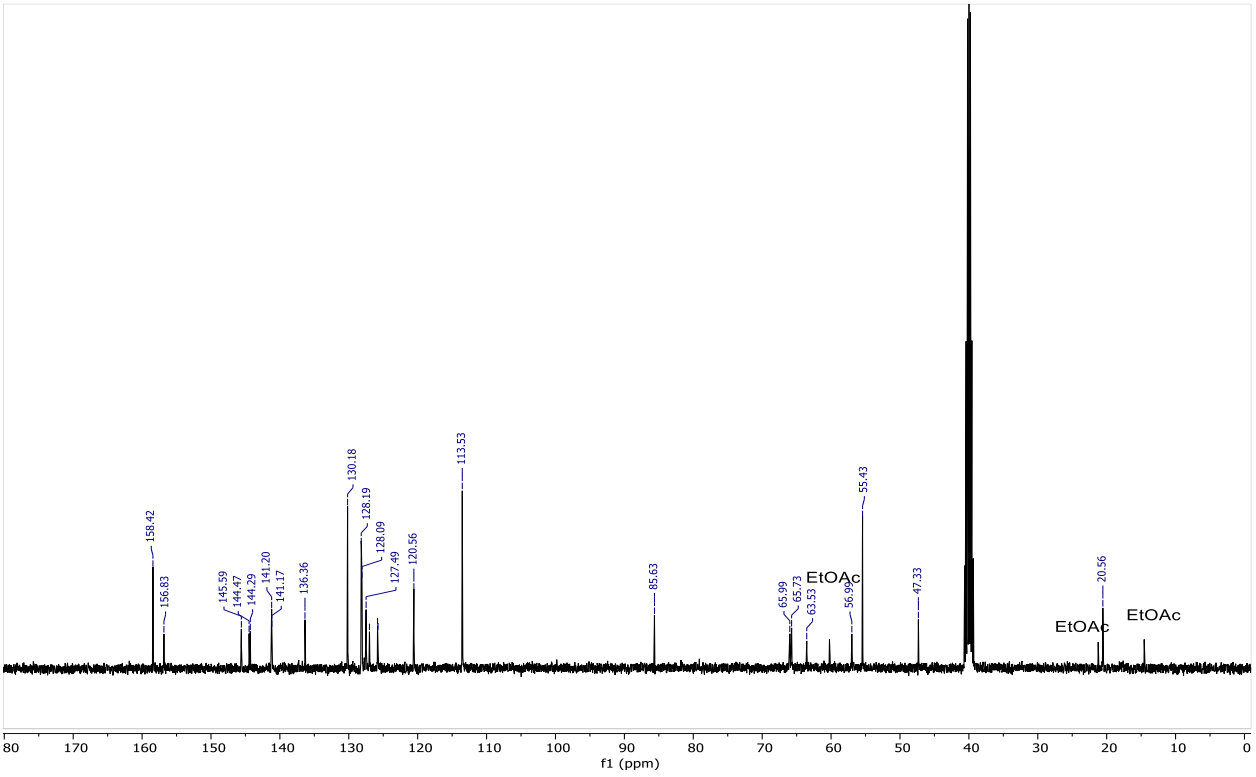


Figure 7.24 ^{13}C NMR d_6-DMSO spectrum of **22** at 101 MHz

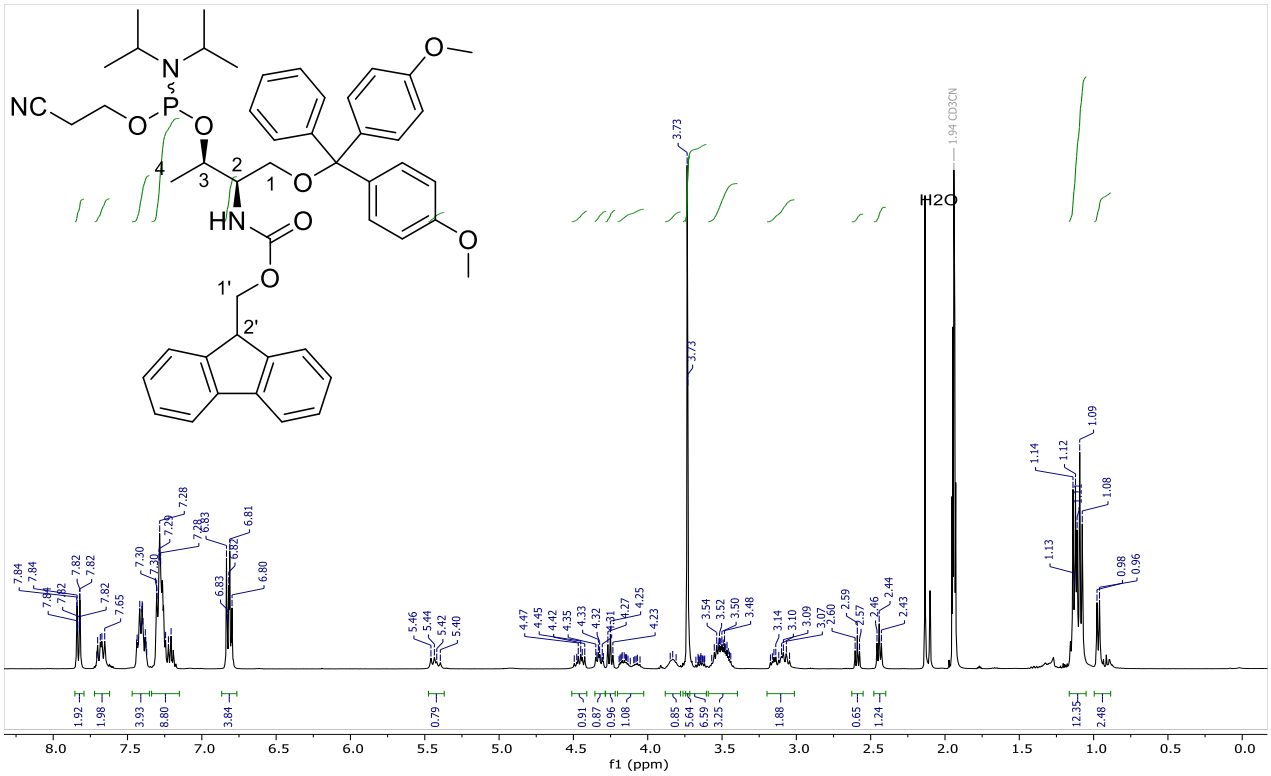


Figure 7.25 ^{1}H NMR CD_3CN spectrum of **23** at 400 MHz

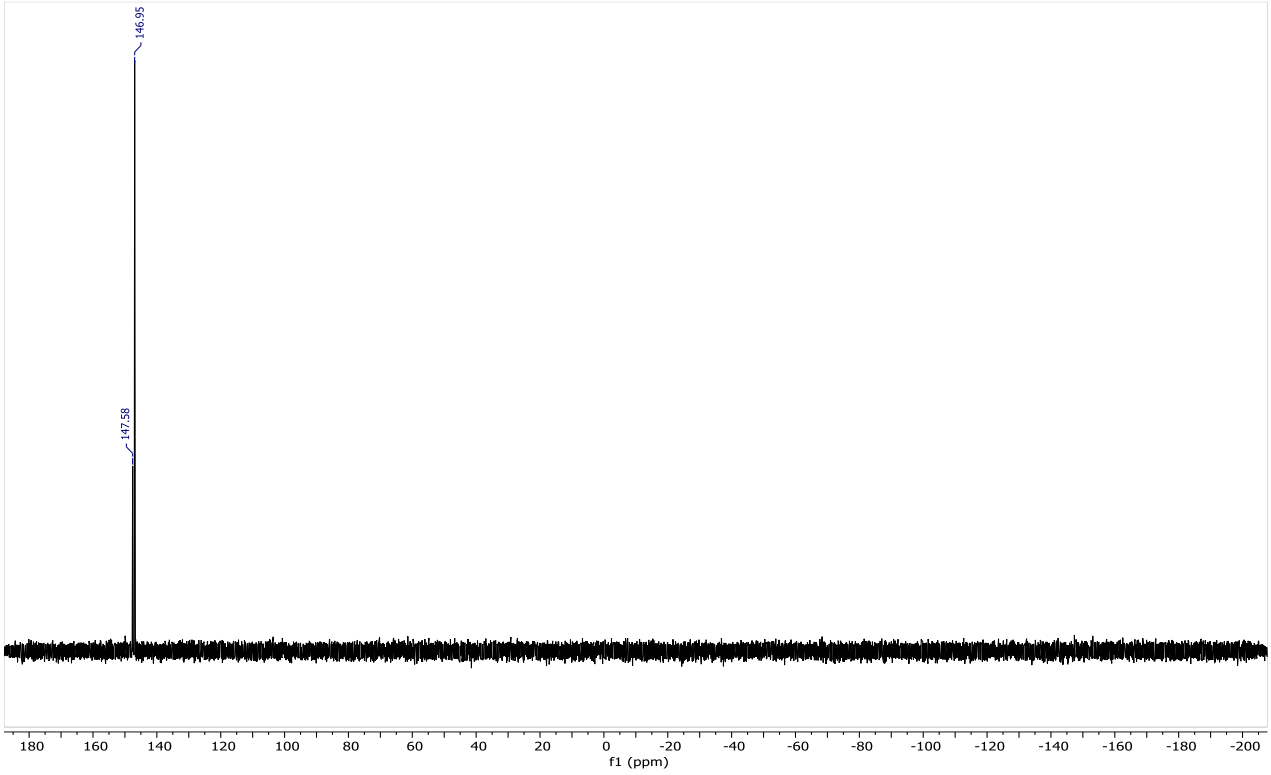


Figure 7.26 ^{31}P NMR CD_3CN spectrum of **23** at 126 MHz

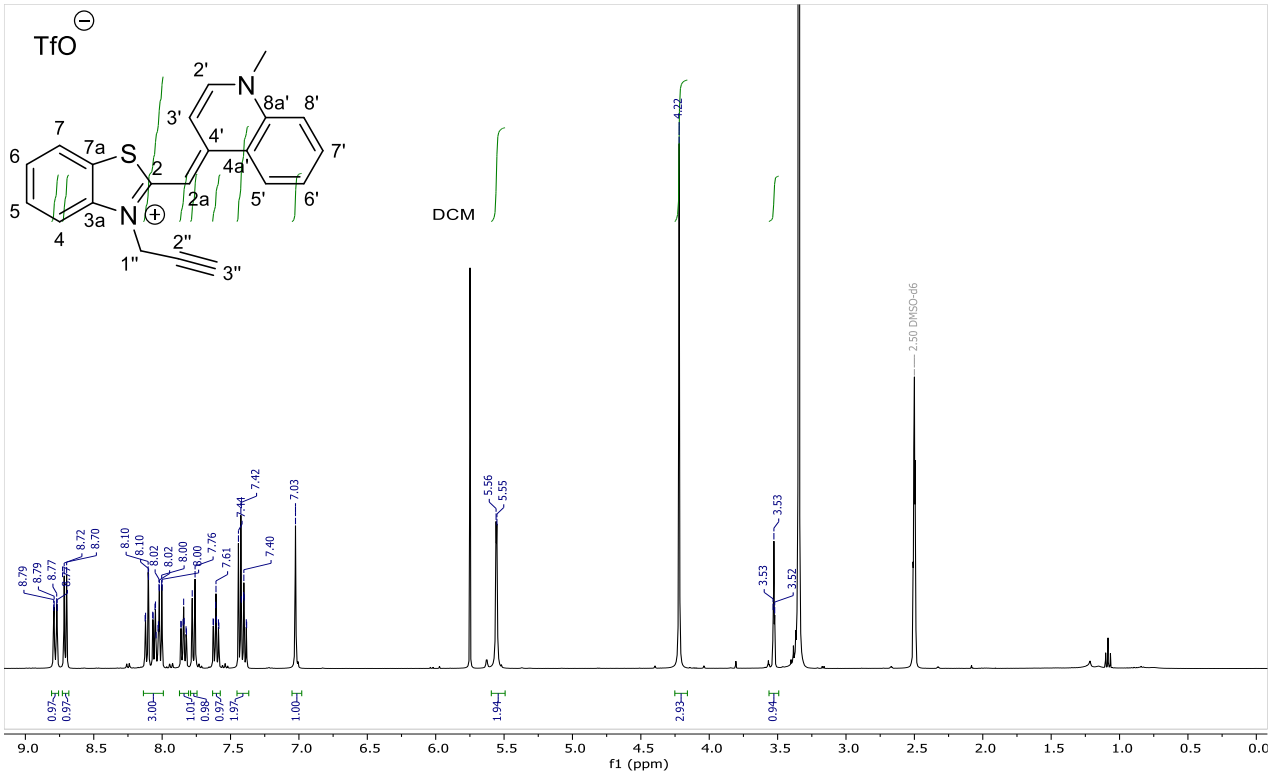


Figure 7.27 ^{1}H NMR d_6-DMSO spectrum of **25** at 400 MHz

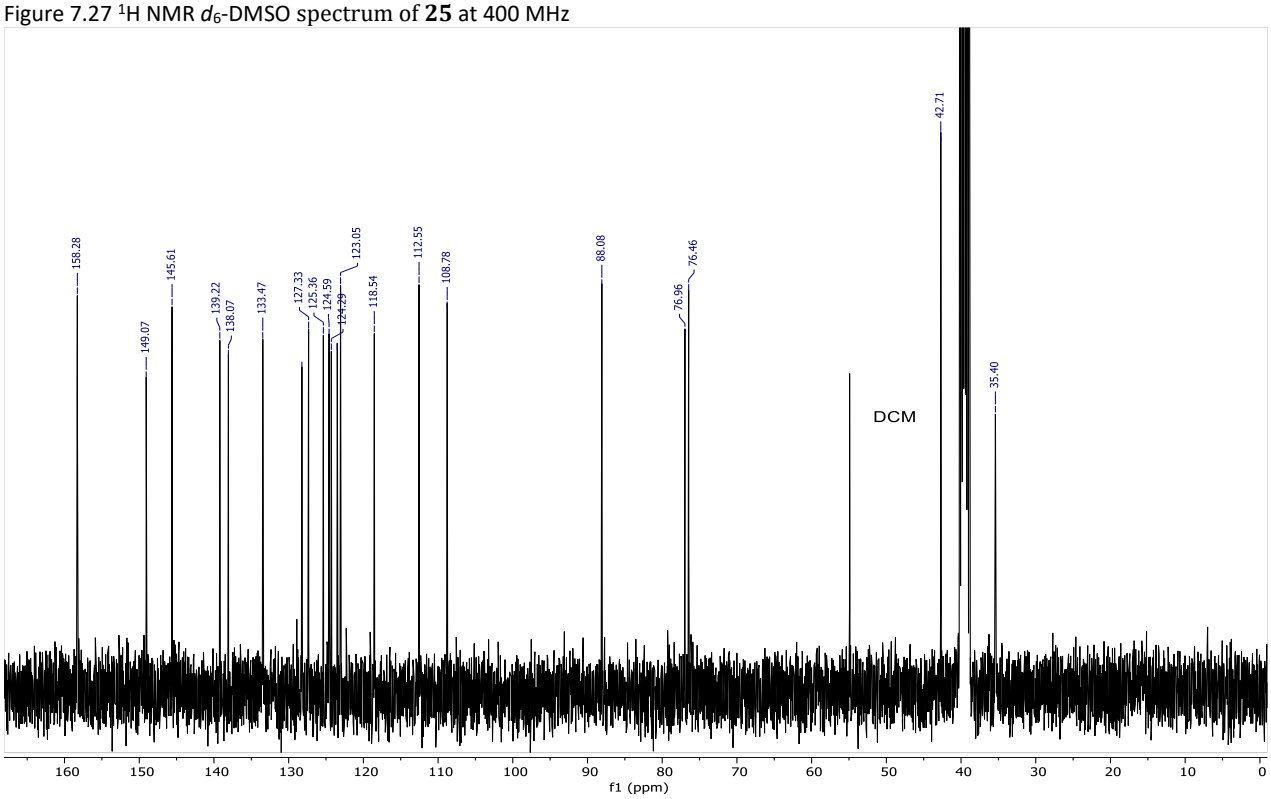


Figure 7.28 ^{13}C NMR d_6-DMSO spectrum of **25** at 101 MHz

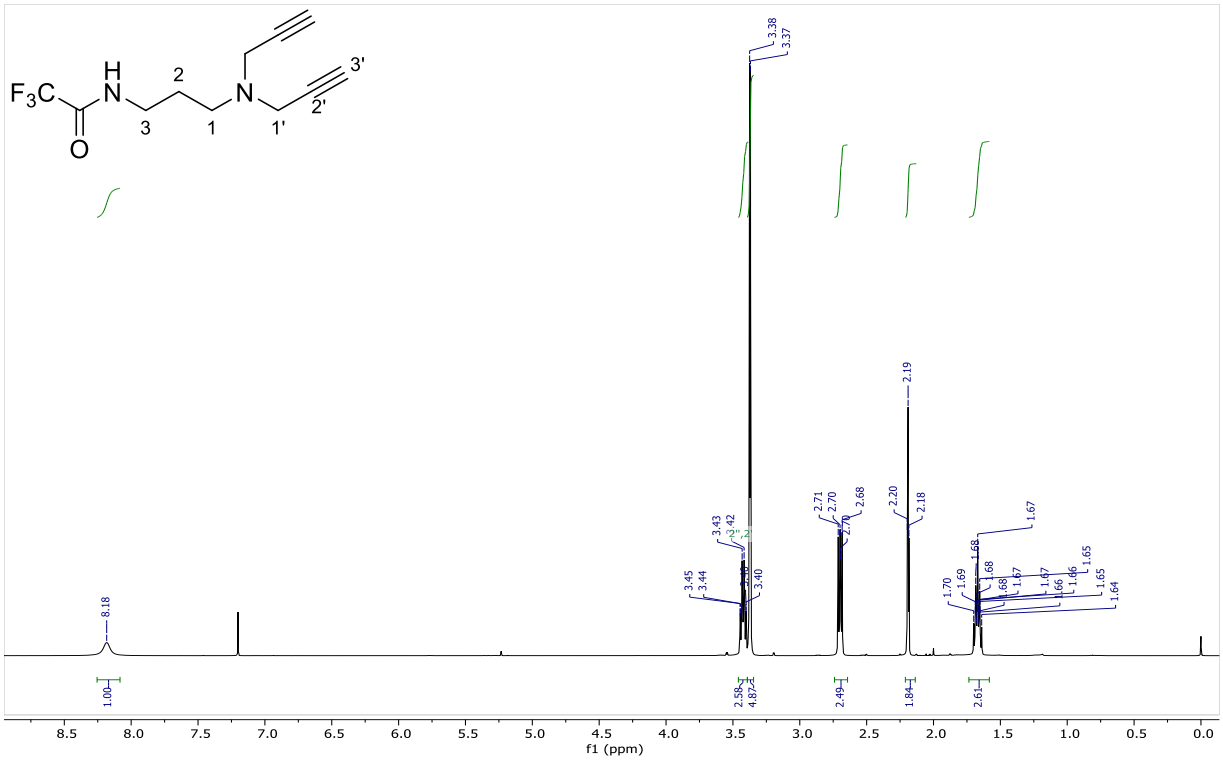


Figure 7.29 ^{1}H NMR $CDCl_3$ spectrum of **30** at 400 MHz

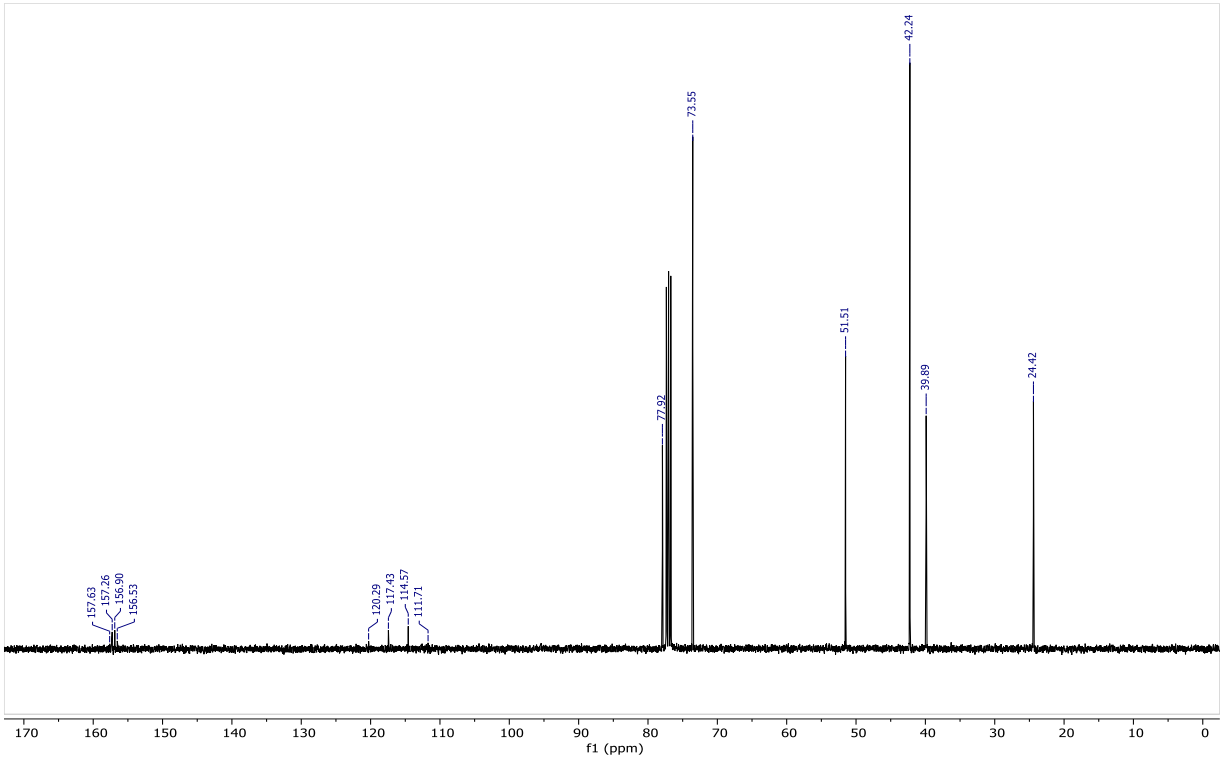


Figure 7.30 ^{13}C NMR $CDCl_3$spectrum of **30** at 101 MHz

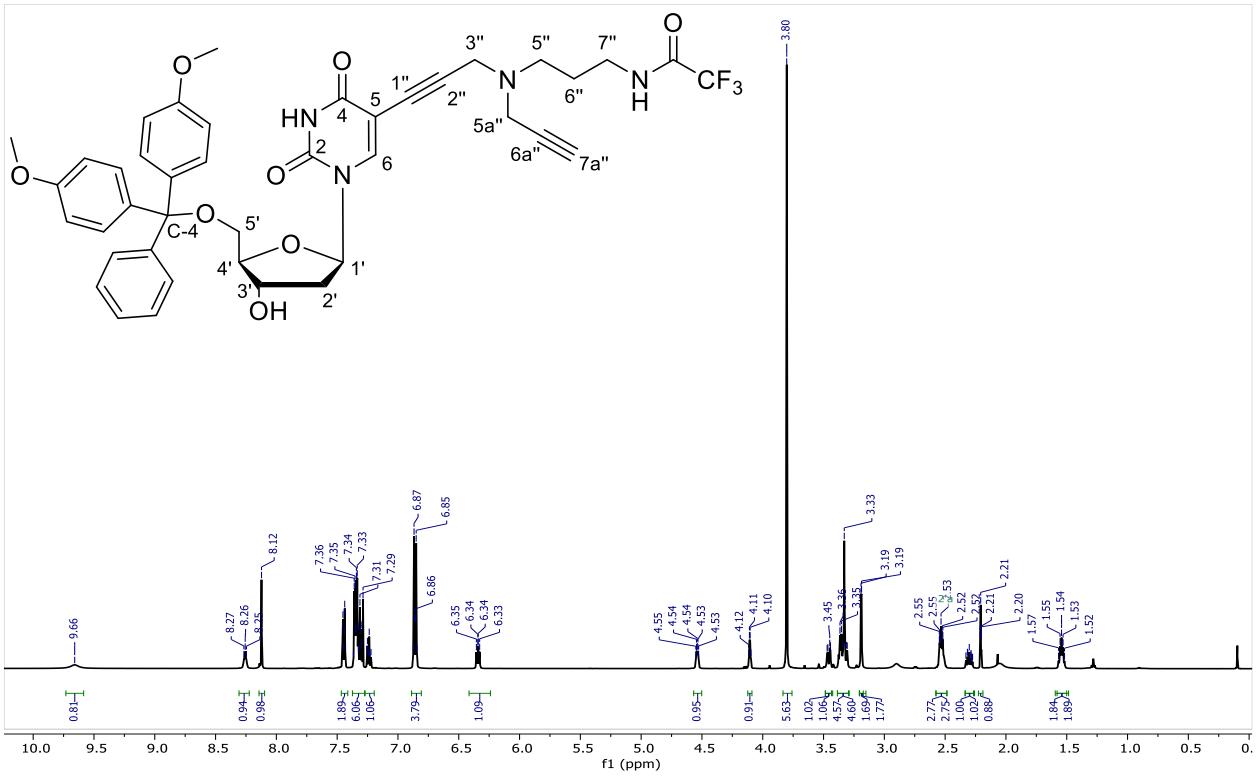


Figure 7.31 ^{1}H NMR $CDCl_3$ spectrum of **31** at 500 MHz

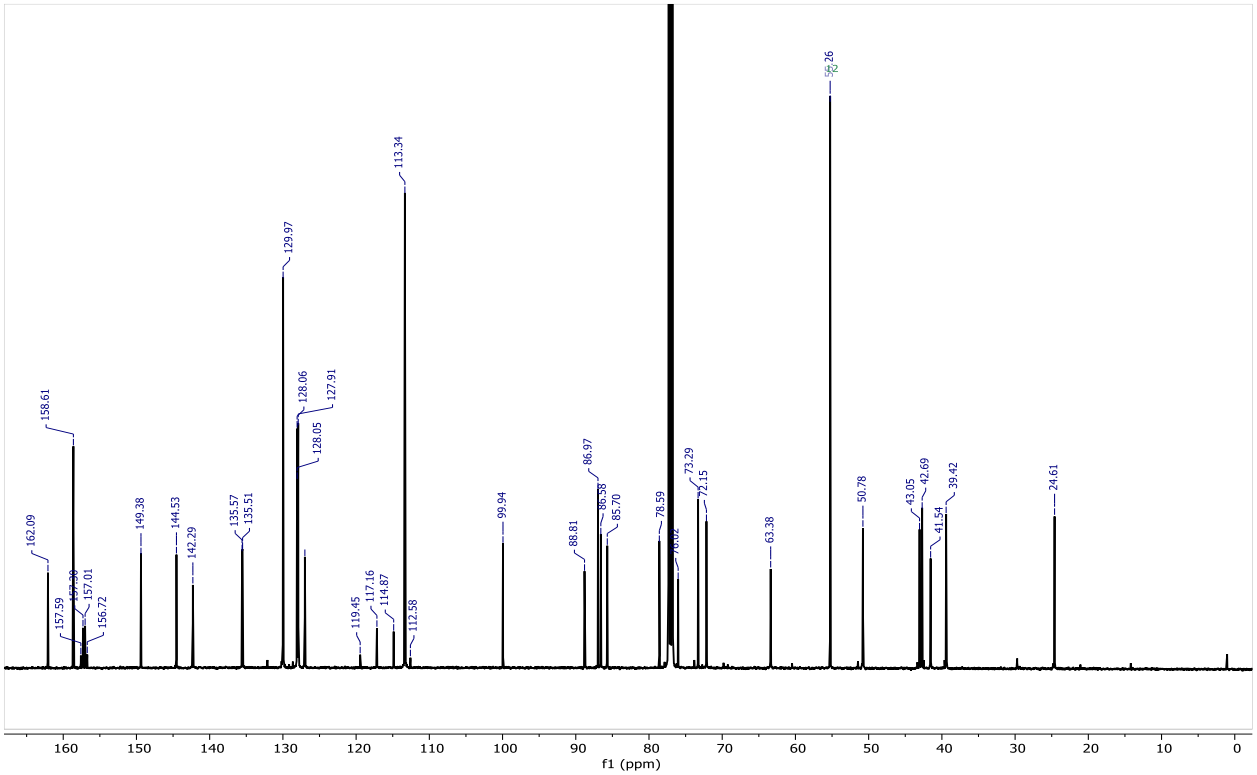


Figure 7.32 ^{13}C NMR $CDCl_3$ spectrum of **31** at 126 MHz

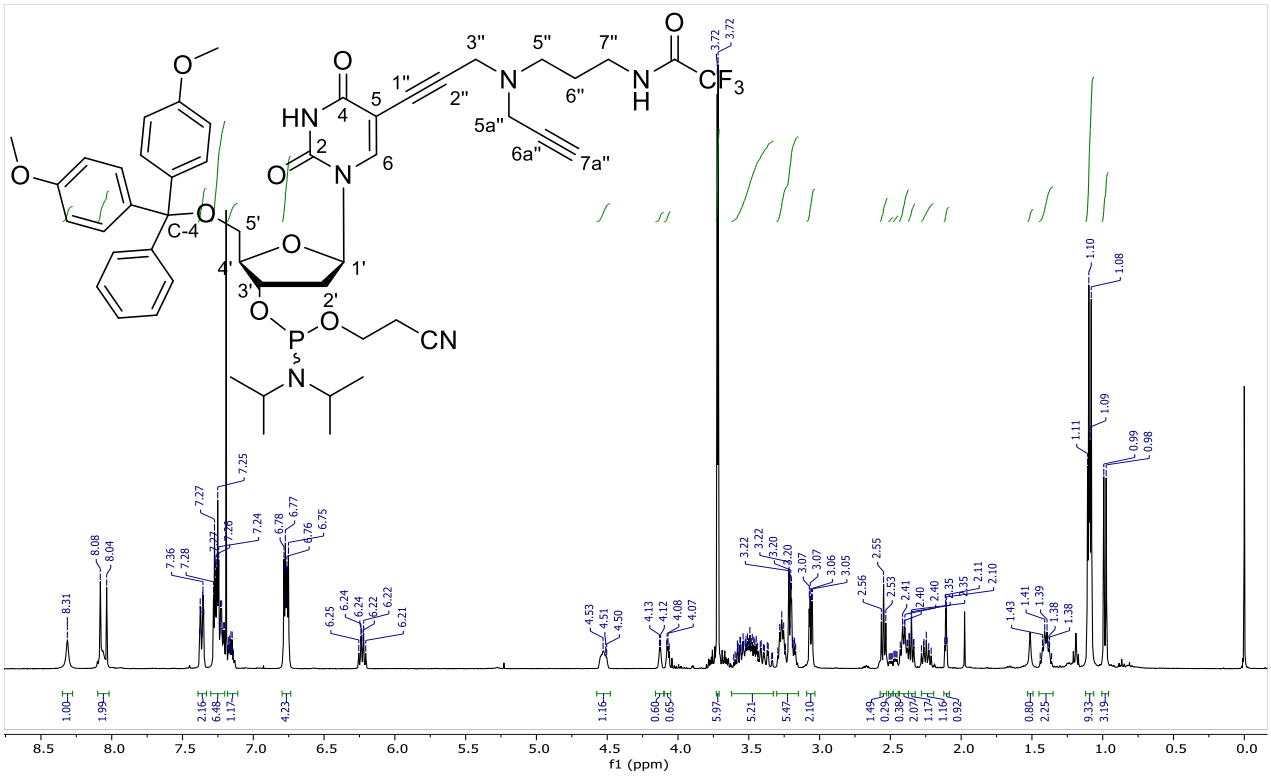


Figure 7.33 ^{1}H NMR $CDCl_3$ spectrum of **32** at 400 MHz

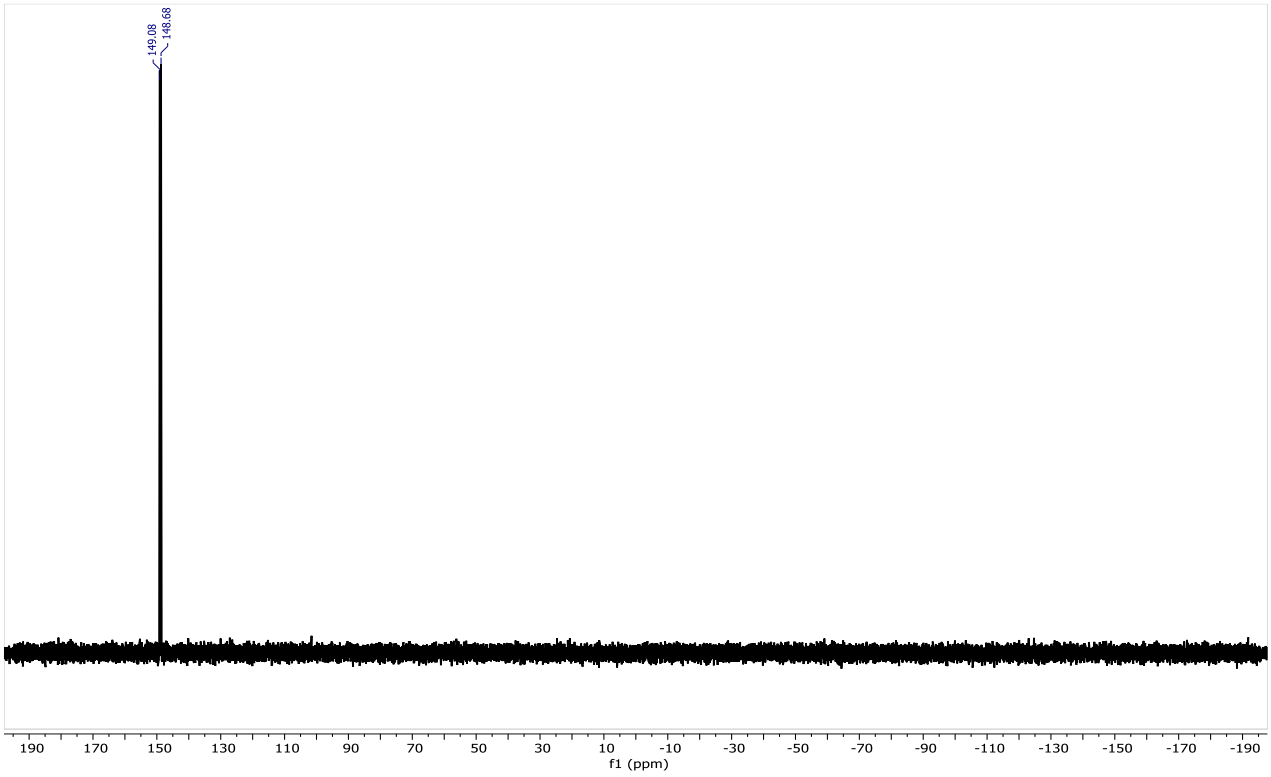


Figure 7.34 ^{31}P NMR $CDCl_3$ spectrum of **32** at 126 MHz

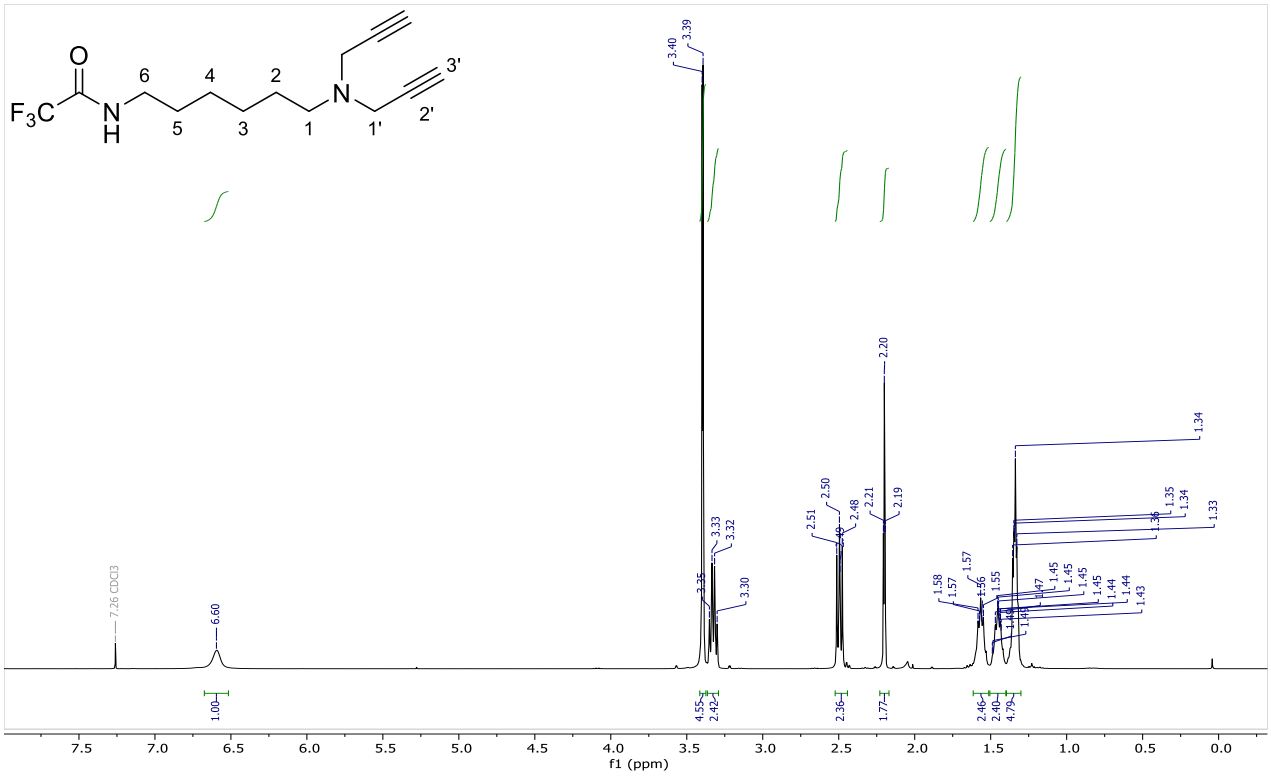


Figure 7.35 ^{1}H NMR $CDCl_3$ spectrum of **35** at 400 MHz

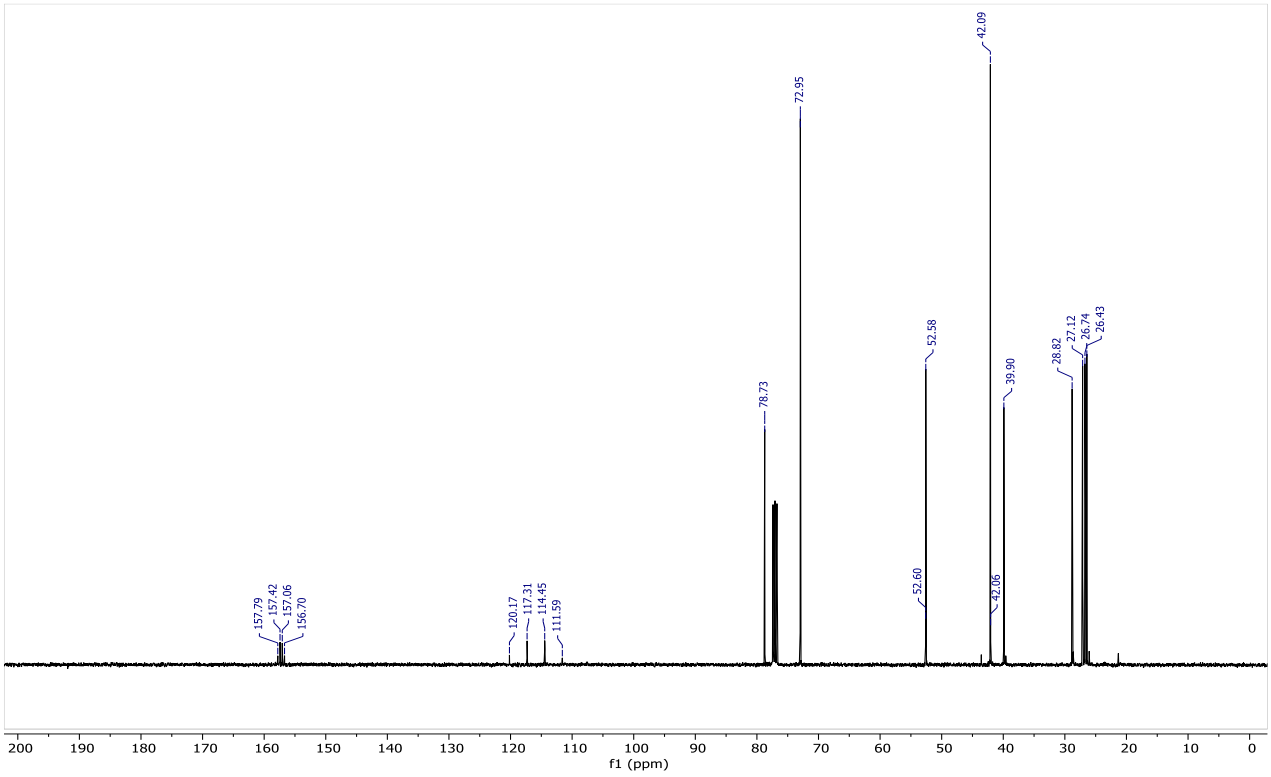


Figure 7.36 ^{13}C NMR $CDCl_3$ spectrum of **35** at 101 MHz

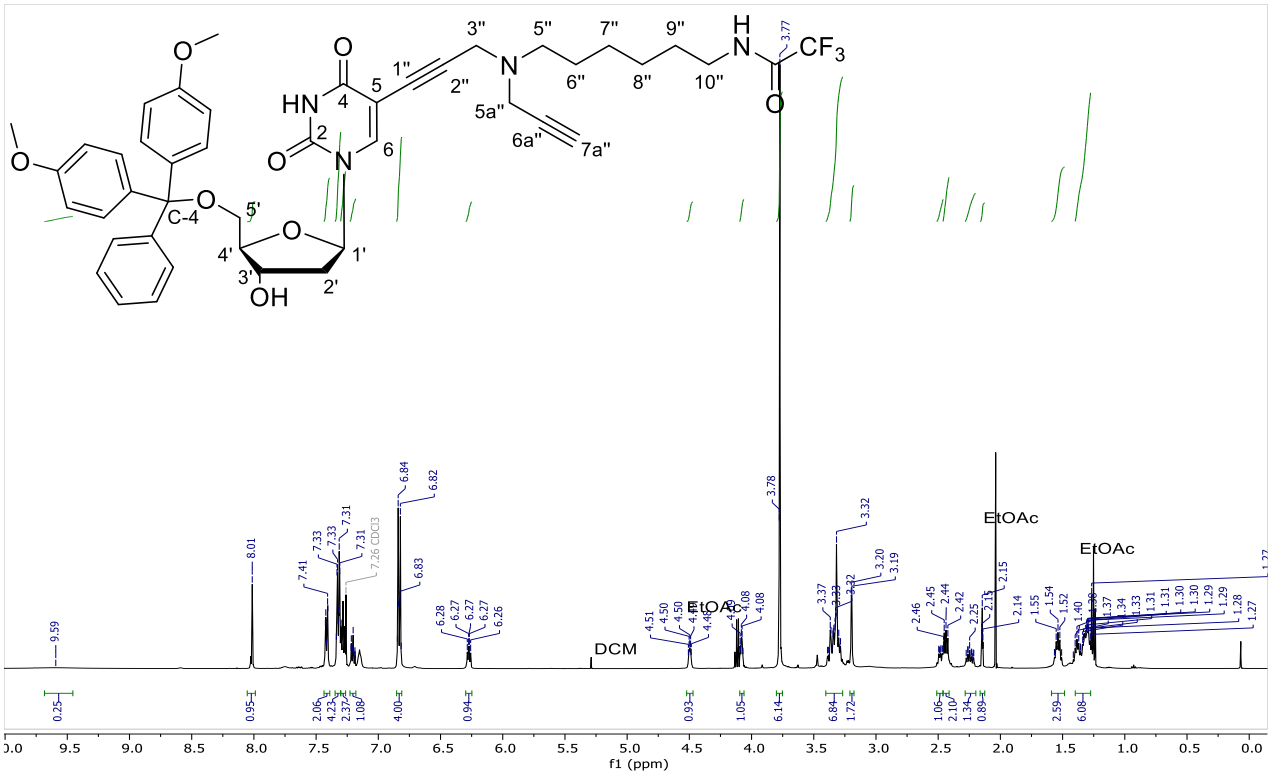


Figure 7.37 ^{1}H NMR $CDCl_3$ spectrum of **36** at 500 MHz

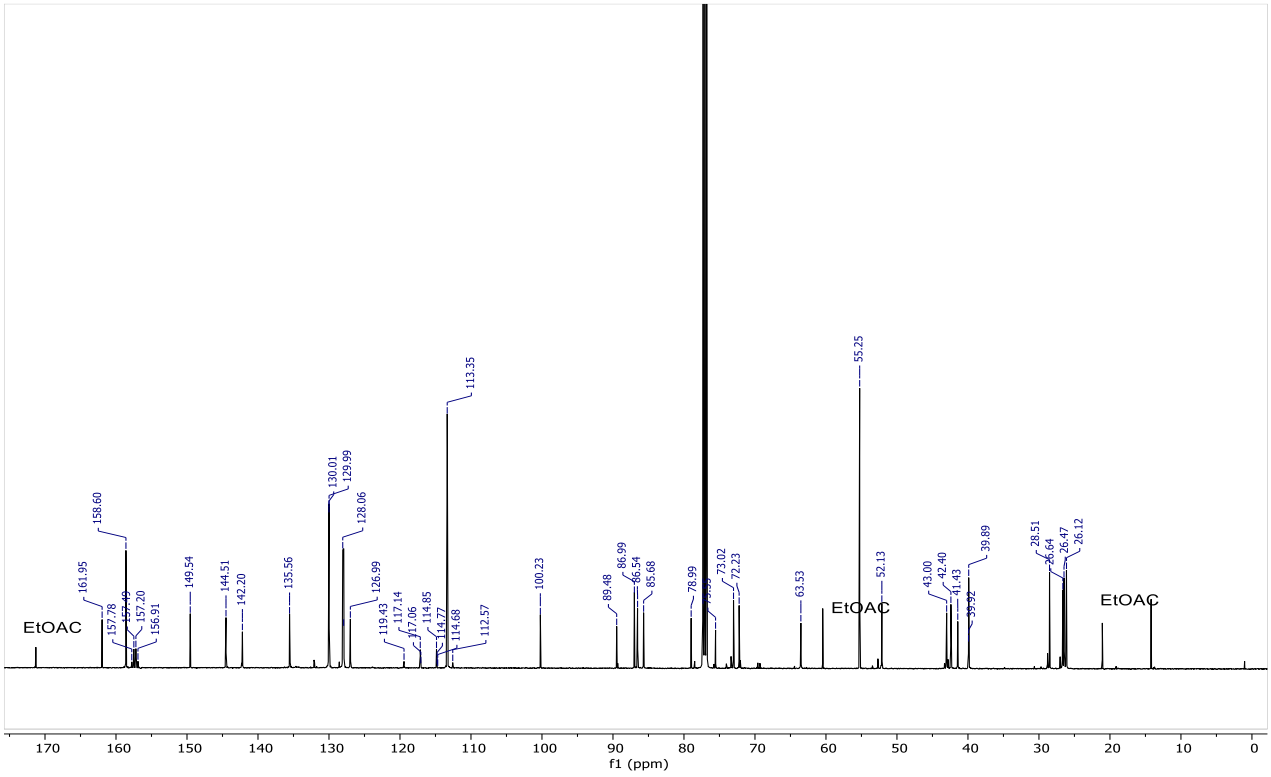


Figure 7.38 ^{13}C NMR $CDCl_3$ spectrum of **36** at 126 MHz

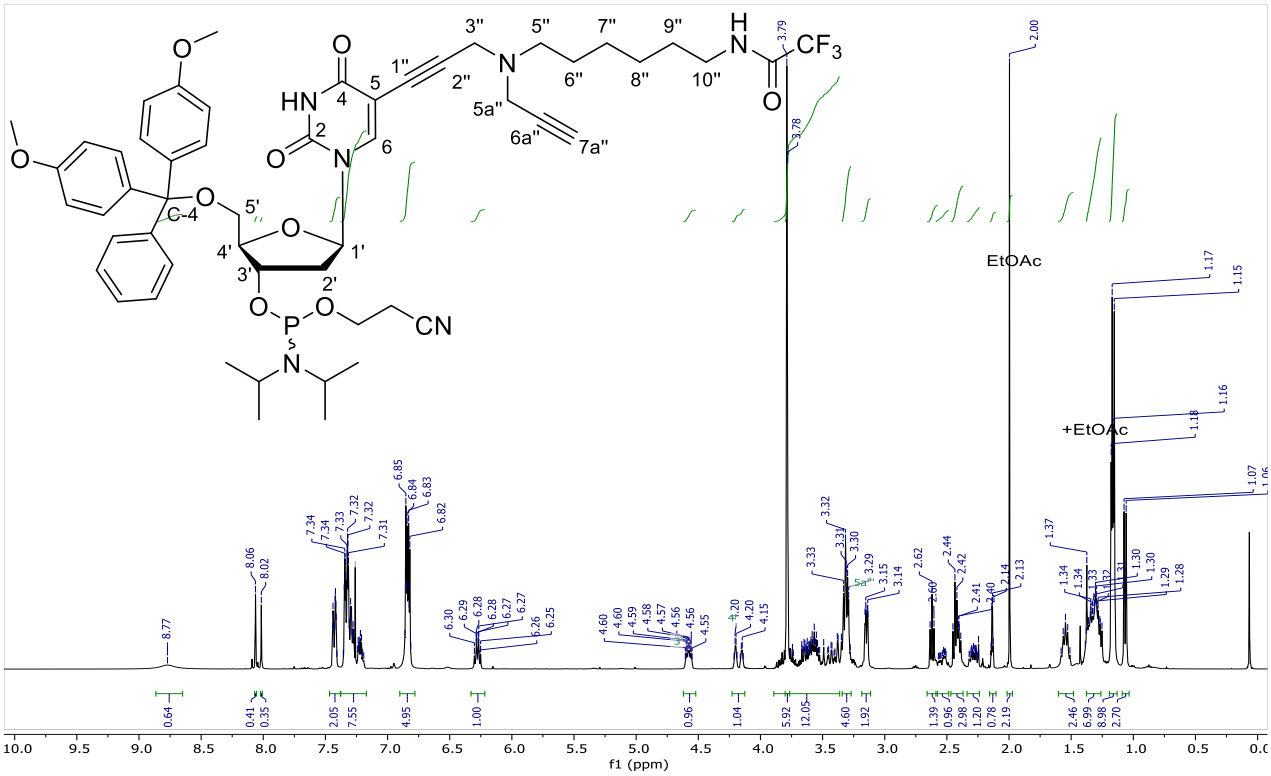


Figure 7.39 ^{1}H NMR $CDCl_3$ spectrum of **37** at 400 MHz

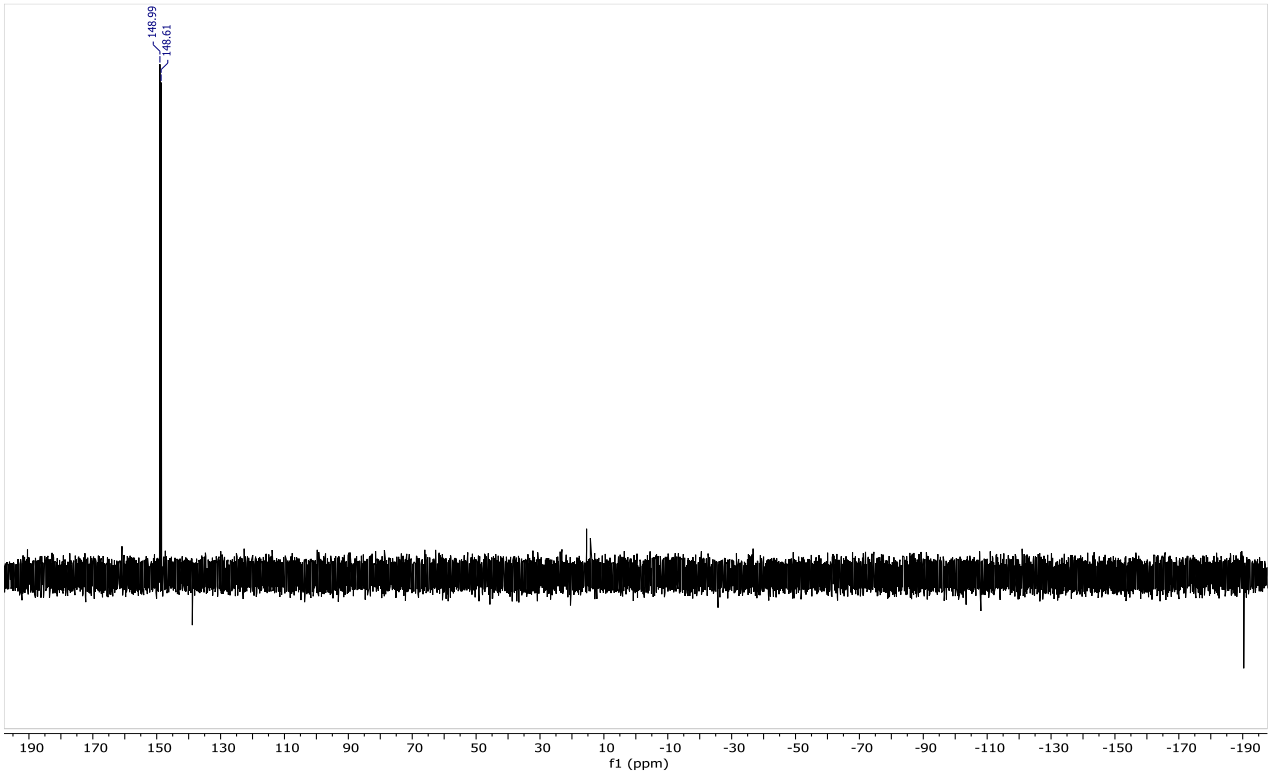


Figure 7.40 ^{31}P NMR $CDCl_3$ spectrum of **37** at 126 MHz

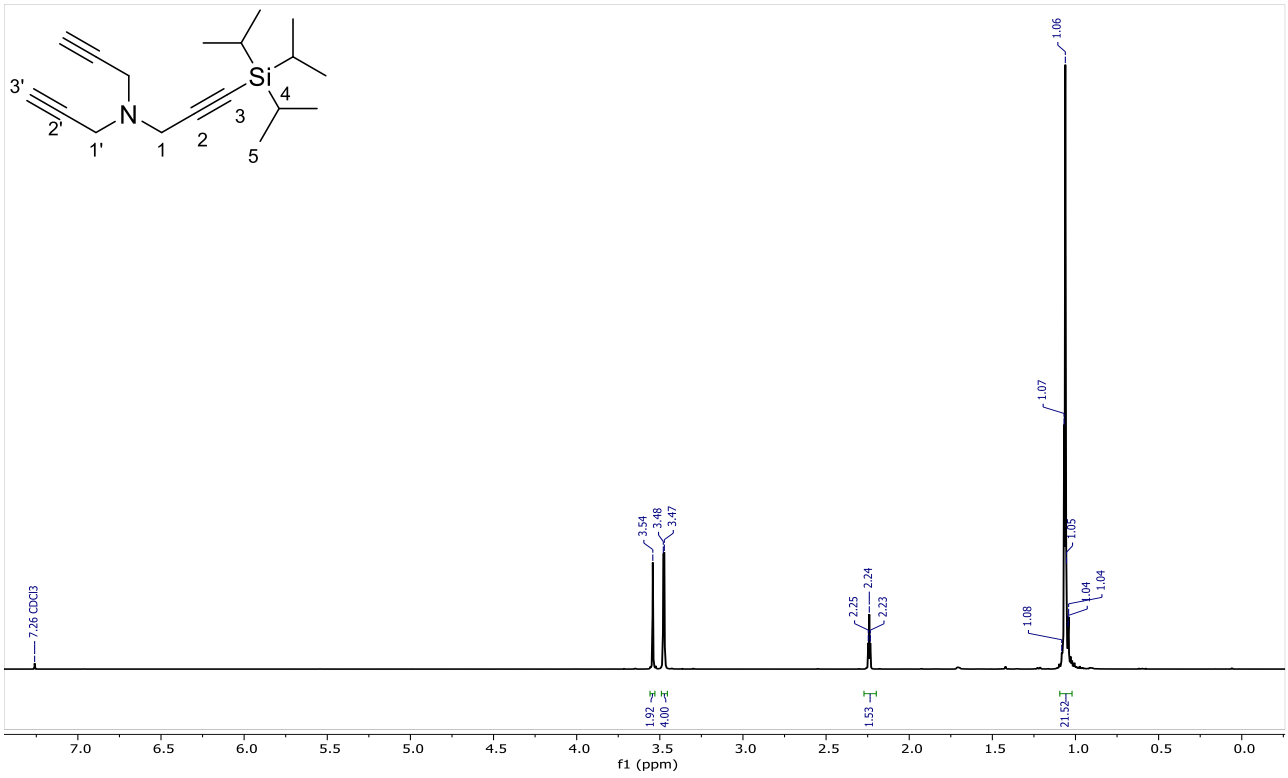


Figure 7.41 ^{1}H NMR $CDCl_3$ spectrum of **38** at 400 MHz

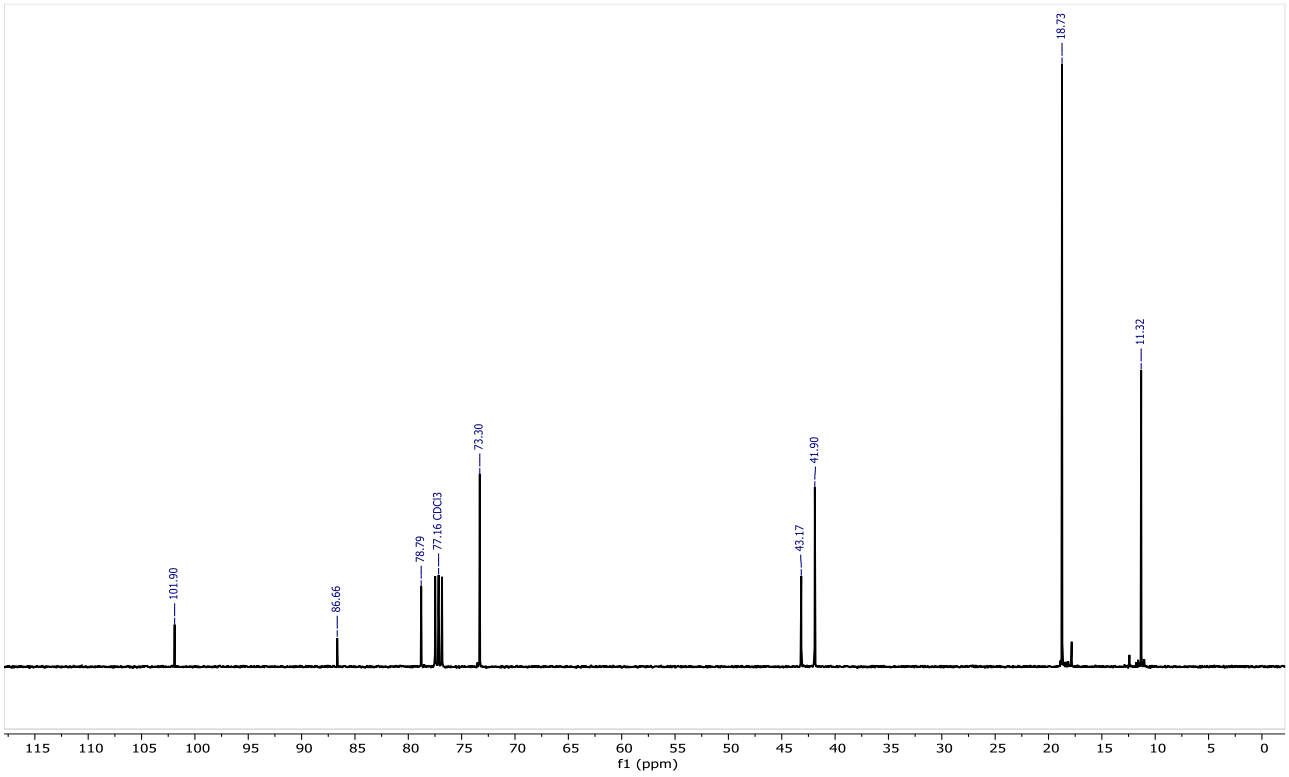


Figure 7.42 ^{13}C NMR $CDCl_3$ spectrum of **38** at 101 MHz

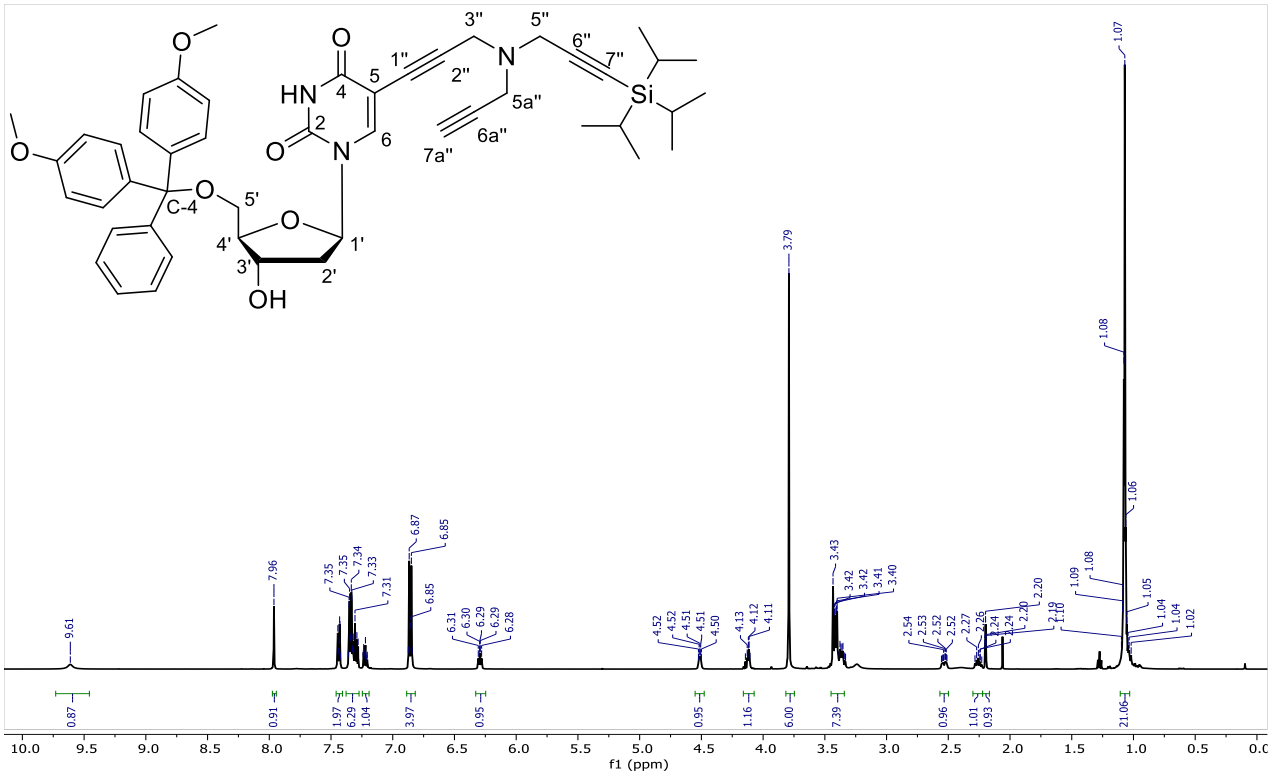


Figure 7.43 ^{1}H NMR $CDCl_3$ spectrum of **39** at 500 MHz

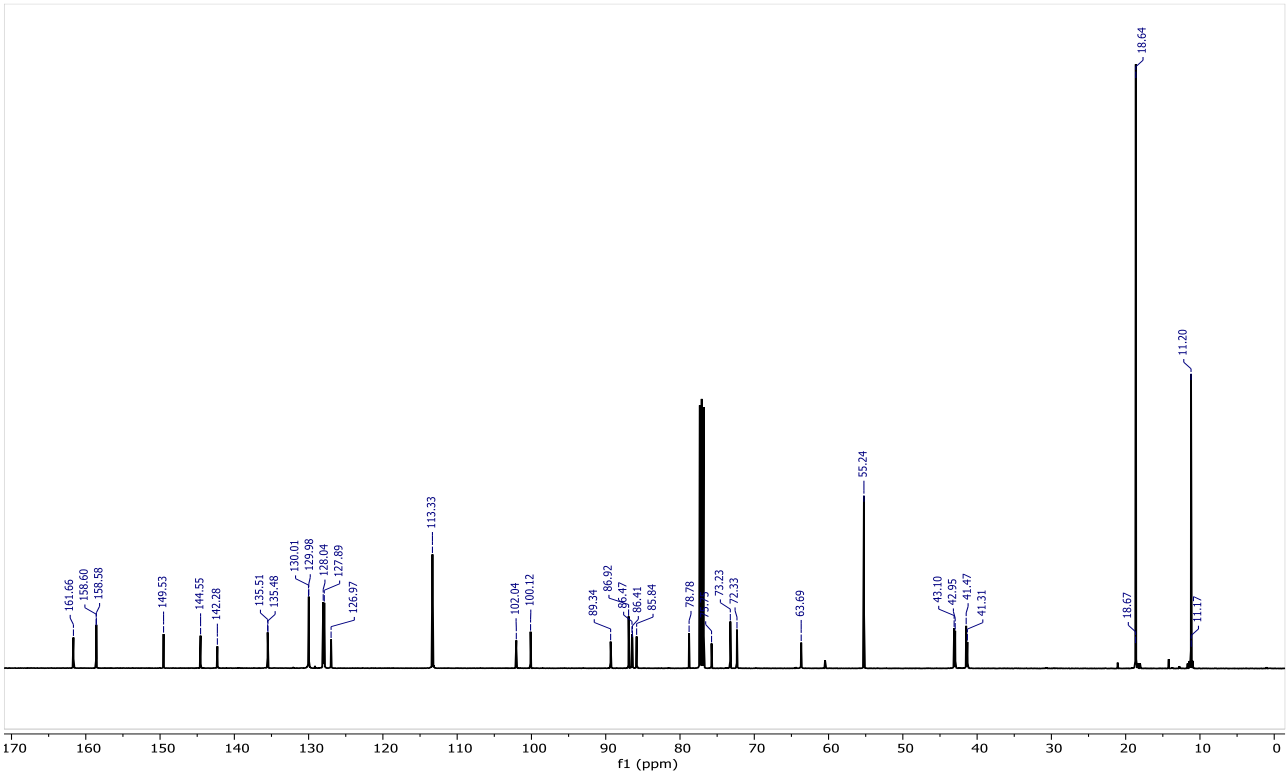


Figure 7.44 ^{13}C NMR $CDCl_3$ spectrum of **39** at 126 MHz

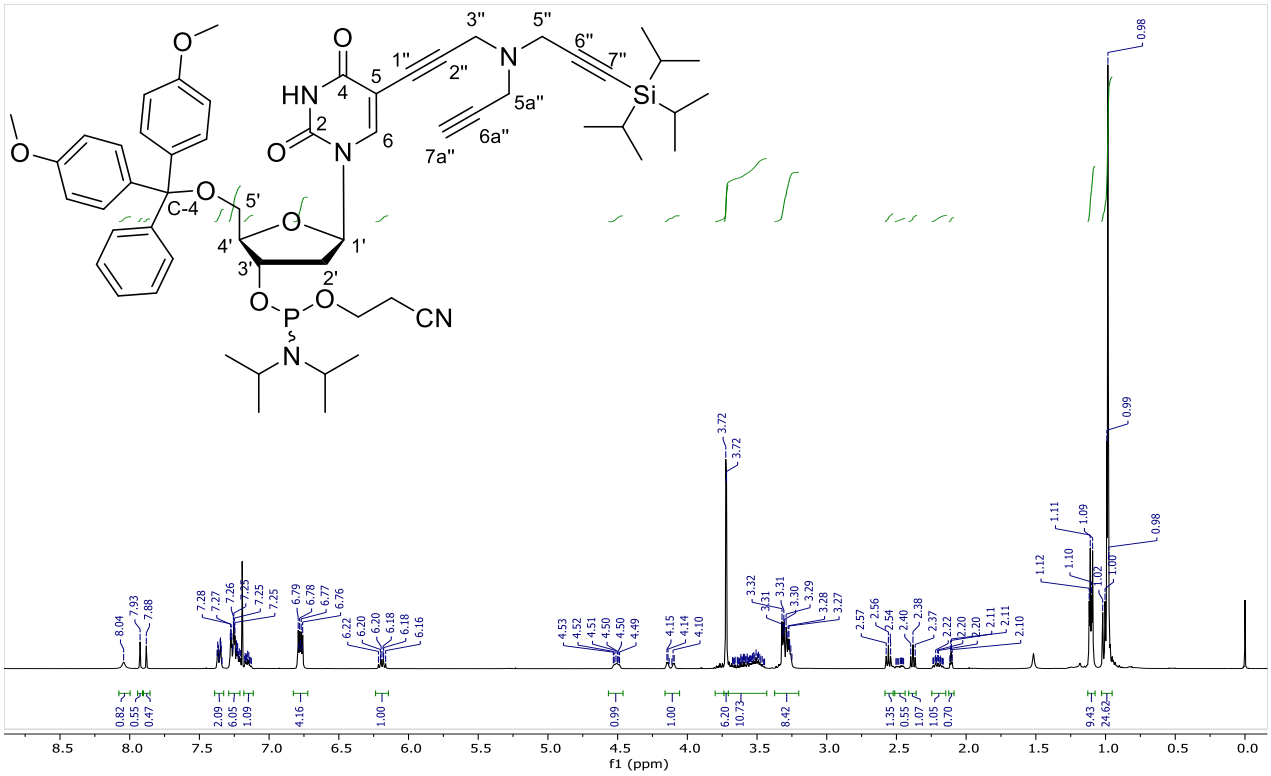


Figure 7.45 ^{1}H NMR $CDCl_3$ spectrum of **40** at 400 MHz

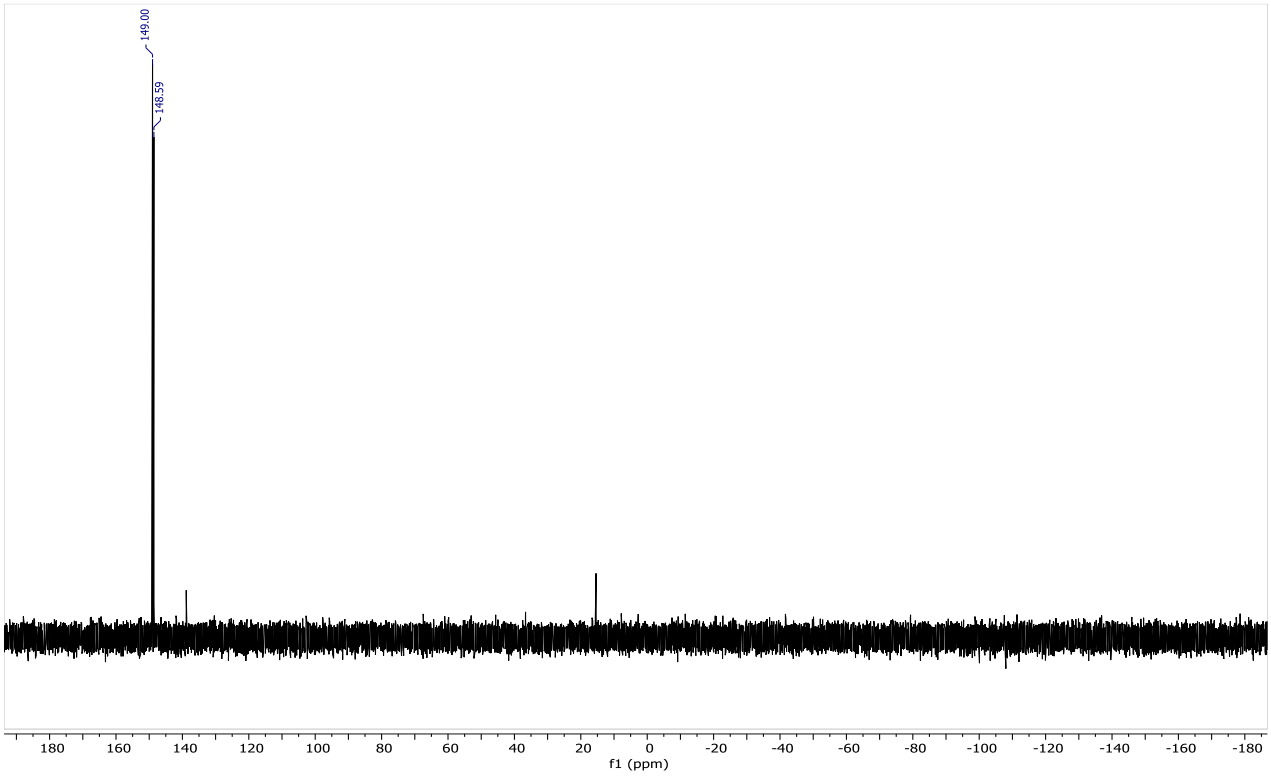


Figure 7.46 ^{31}P NMR $CDCl_3$ spectrum of **40** at 162 MHz

References

(1) Blackburn, G. M.; Gait, M. J.; Loakes, D.; Williams, D. M. *Nucleic Acids in Chemistry and Biology*; 2006.

(2) Watson, J. D.; Crick, F. H. Molecular Structure of Nucleic Acids; a Structure for Deoxyribose Nucleic Acid. *Nature* **1953**, *171*, 737–738.

(3) Chargaff, E. Structure and Function of Nucleic Acids as Cell Constituents. *Fed. Proc.* **1951**, *10* (3), 654—659.

(4) Zamenhof, S.; Shettles, L. B.; Chargaff, E. Human Desoxypentose Nucleic Acid. *Nature* **1950**, *165*, 756–757.

(5) Franklin, E. R.; Gosling, R. G. Evidence for 2-Chain Helix in Crystalline Structure of Sodium Deoxyribonucleate. *Nature* **1953**, *172* (4369), 156–157.

(6) Franklin, R. E.; Gosling, R. G. Molecular Configuration in Sodium Thymonucleate. *Nature* **1953**, *171* (4356), 740–741.

(7) Wilkins, M. H. F.; Stokes, A. R.; Wilson, H. . Molecular Structure of Deoxypentose Nucleic Acids. *Nature* **1953**, *171*, 738–740.

(8) Yakovchuk, P.; Protozanova, E.; Frank-Kamenetskii, M. D. Base-Stacking and Base-Pairing Contributions into Thermal Stability of the DNA Double Helix. *Nucleic Acids Res.* **2006**, *34* (2), 564–574.

(9) Ageno, M.; Dore, E.; Frontali, C. The Alkaline Denaturation of DNA. *Biophys. J.* **1969**, *9* (11), 1281–1311.

(10) Wing, R.; Drew, H.; Takano, T.; Broka, C.; Tanaka, S.; Itakura, K.; Dickerson, R. E. Crystal Structure Analysis of a Complete Turn of B-DNA. *Nature* **1980**, *287* (5784), 755–758.

(11) Dickerson, R. E.; Drew, H. R.; Conner, B. N.; Wing, R. M.; Fratini, A. V; Kopka, M. L. The Anatomy of A- , Bo- , and Z-DNA. *Science (80-.).* **1982**, *216*, 475–485.

(12) Ivanov, V. I.; Krylov, D. Y. A-DNA in Solution as Studied by Diverse Approaches. *Methods Enzymol.* **1992**, *211* (C), 111–127.

(13) Dock-Bregeon, A. C.; Chevrier, B.; Podjarny, A.; Johnson, J.; de Bear, J. S.; Gough, G. R.; Gilham, P. T.; Moras, D. Crystallographic Structure of an RNA Helix: [U(UA)6A]2. *J. Mol. Biol.* **1989**, *209* (3), 459–474.

(14) Al-Obeidi, F.; Okonya, J. F.; Austin, R. E.; Bond, D. R. Using a Noncovalent Protection Strategy to Enhance Solid-Phase Synthesis. *Methods Mol. Biol.* **2002**, No. 201, 3–14.

(15) Merrifield, R. B. Automated Synthesis of Peptides. *Science (80-.).* **1965**, *150* (3693), 178–185.

(16) Merrified, R. Solid-Phase Peptide Synthesis. *Adv. Enzym. Relat. Areas Mol. Biol.* **1969**, *32*, 221–296.

(17) Merrifield, R. B. Solid-Phase Peptide Synthesis. III. An Improved Synthesis of Bradykinin. *Biochemistry* **1964**, *3* (9), 1385–1390.

(18) Merrifield, R. B. Solid Phase Peptide Synthesis. I. The Synthesis of a Tetrapeptide. *J. Am. Chem. Soc.* **1963**, *85* (14), 2149–2154.

(19) Wang, J. C.; Jacobsen, J. H.; Saucier, J. M. Rapid Synthesis of Oligodeoxyribonucleotides: A New Solid-Phase Method. *Nucleic Acids Res.* **1977**, *4* (5), 1419–1427.

(20) Beaucage, S. L.; Caruthers, M. H. Deoxynucleoside Phosphoramidites-A New Class of Key Intermediates for Deoxypolynucleotide Synthesis. *Tetrahedron Lett.* **1981**, *22* (20), 1859–1862.

(21) Letsinger, R. L.; Mahadevan, V. Oligonucleotide Synthesis on a Polymer Support. *J. Am. Chem. Soc.* **1965**, *87* (15), 3526–3527.

(22) Matteucci, M. D.; Caruthers, M. H. Synthesis of Deoxyoligonucleotides on a Polymer Support. *J. Am. Chem. Soc.* **1981**, *103* (11), 3185–3191.

(23) Sinha, N. D. Biernat, J. McManus , J. Koster, H. Polymer Support Oligonudeotide Synthesis XVII: Use of B-Yanoethyl-N,N-Dialkylamino-/N- Morpholino Phosphoramidite of Deoxynudeosides for the Synthesis of DNA Fragments Simplifying Deprotection and Isolation of the Final Product. *Nucleic Acids Res* **1984**, *12* (11), 4539–4557.

(24) McBride, L. J. Caruthers, L. An Investigation of Several Deoxynucleoside Phosphoramidites Useful for Synthetizing Deoxyoligonucleotides. *Tetrahedron Lett.* **1981**, *3* (September), 245–248.

(25) Sojka, B.; Piunno, P. A. E.; Wust, C. C.; Krull, U. J. A Novel Phosphoramidite Method for Automated Synthesis of Oligonucleotides on Glass Supports for Biosensor Development. *Appl. Biochem. Biotechnol. - Part A Enzym. Eng. Biotechnol.* **2000**, *89* (1), 85–103.

(26) Dörper, T.; Winnacker, E. L. Improvements in the Phosphoramidite Procedure for the Synthesis of Oligodeoxyribonucleotides. *Nucleic Acids Res.* **1983**, *11* (9), 2575–2584.

(27) Sonveaux, E. The Organic Chemistry Underlying DNA Synthesis. *Bioorg. Chem.* **1986**, *14* (3), 274–325.

(28) Gillet, L. C. J.; Alzeer, J.; Schärer, O. D. Site-Specific Incorporation of N-(Deoxyguanosin-8-Yl)-2-Acetylaminofluorene (DG-AAF) into Oligonucleotides Using Modified "ultra-Mild" DNA Synthesis. *Nucleic Acids Res.* **2005**, *33* (6), 1961–1969.

(29) Wright, P.; Lloyd, D.; Rapp, W.; Andrus, A. Large Scale Synthesis of Oligonucleotides via Phosphoramidite Nucleosides and a High-Loaded Polystyrene Support. *Tetrahedron Lett.* **1993**, *34* (21), 3373–3376.

(30) Ogilviet, K. K.; Sadana, K. L.; Thompson, E. A.; Quilliam, M. A.; Westmore, J. B. The Use of Silyl Groups in Protecting the Hydroxyl Functions of Ribonucleoside. *Tetrahedron Lett.* **1974**, No. 33, 2861–2863.

(31) Sporat, B. S. *Oligonuclotide Synthesis: Methods and Applications: Chapter 2*; 2005.

(32) R. Welz, S. M. 5-(Benzylmercapto)-1H-Tetrazole as Activator for 2'-O-TBDMS Phosphoramidite Building Blocks in RNA Synthesis. **2002**, *43*, 795–797.

(33) Dellinger, D. J.; Timár, Z.; Myerson, J.; Sierzchala, A. B.; Turner, J.; Ferreira, F.; Kupihár, Z.; Dellinger, G.; Hill, K. W.; Powell, J. A.; et al. Streamlined Process for the Chemical Synthesis of RNA Using 2′-O-Thionocarbamate-Protected Nucleoside Phosphoramidites in the Solid Phase. *J. Am. Chem. Soc.* **2011**, *133* (30), 11540–11556.

(34) Meldal, M. P.; Meldal, M.; Tornøe, C. W. Cu-Catalyzed Azide − Alkyne Cycloaddition Cu-Catalyzed Azide - Alkyne Cycloaddition. *Chem. Rev* **2017**, *108* (8), 2952–3015.

(35) Tornøe, C. W.; Christensen, C.; Meldal, M. Peptidotriazoles on Solid Phase: [1,2,3]-Triazoles by Regiospecific Copper(I)-Catalyzed 1,3-Dipolar Cycloadditions of Terminal Alkynes to Azides. *J. Org. Chem.* **2002**, *67* (9), 3057–3064.

(36) Kolb, H. C.; Finn, M. G.; Sharpless, K. B. Click Chemistry: Diverse Chemical Function from

a Few Good Reactions. *Angew. Chemie - Int. Ed.* **2001**, *40* (11), 2004–2021.

(37) Appukkuttan, P.; Dehaen, W.; Fokin, V. V.; Van Der Eycken, E. A Microwave-Assisted Click Chemistry Synthesis of 1,4-Disubstituted 1,2,3-Triazoles via a Copper(I)-Catalyzed Three-Component Reaction. *Org. Lett.* **2004**, *6* (23), 4223–4225.

(38) Himo, F.; Lovell, T.; Hilgraf, R.; Rostovtsev, V. V.; Noodleman, L.; Sharpless, K. B.; Fokin, V. V. Copper(I)-Catalyzed Synthesis of Azoles. DFT Study Predicts Unprecedented Reactivity and Intermediates. *J. Am. Chem. Soc.* **2005**, *127* (1), 210–216.

(39) Hänni, K. D.; Leigh, D. A. The Application of CuAAC "click" Chemistry to Catenane and Rotaxane Synthesis. *Chem. Soc. Rev.* **2010**, *39* (4), 1240–1251.

(40) Struthers, H.; Mindt, T. L.; Schibli, R. Metal Chelating Systems Synthesized Using the Copper(I) Catalyzed Azide-Alkyne Cycloaddition. *Dalt. Trans.* **2010**, *39* (3), 675–696.

(41) Totobenazara, J.; Burke, A. J. New Click-Chemistry Methods for 1,2,3-Triazoles Synthesis: Recent Advances and Applications. *Tetrahedron Lett.* **2015**, *56* (22), 2853–2859.

(42) Bundy, B. C.; Swartz, J. R. Site-Specific Incorporation of p-Propargyloxyphenylalanine in a Cell-Free Environment for Direct Protein-Protein Click Conjugation. *Bioconjug. Chem.* **2010**, *21* (2), 255–263.

(43) Worrell, B. T.; Malik, J. A.; Fokin, V. V. Direct Evidence of a Dinuclear Copper Intermediate in Cu(I)-Catalyzed Azide-Alkyne Cycloadditions. *Science (80-.).* **2010**, *340*, 457–461.

(44) Chan, T. R.; Hilgraf, R.; Sharpless, K. B.; Fokin, V. V. Polytriazoles as Copper(I)-Stabilizing Ligands in Catalysis. *Org. Lett.* **2004**, *6* (17), 2853–2855.

(45) Kumar, R.; El-Sagheer, A.; Tumpane, J.; Lincoln, P.; Wilhelmsson, L. M.; Brown, T. Template-Directed Oligonucleotide Strand Ligation, Covalent Intramolecular DNA Circularization and Catenation Using Click Chemistry. *J. Am. Chem. Soc.* **2007**, *129* (21), 6859–6864.

(46) Shelbourne, M.; Chen, X.; Brown, T.; El-Sagheer, A. H. Fast Copper-Free Click DNA Ligation by the Ring-Strain Promoted Alkyne-Azide Cycloaddition Reaction. *Chem. Commun.* **2011**, *47* (22), 6257–6259.

(47) Kricka, L. J. Stains, Labels and Detection Strategies for Nucleic Acids Assays. *Ann. Clin. Biochem.* **2002**, *39* (2), 114–129.

(48) Sahl, S. J.; Hell, S. W.; Jakobs, S. Fluorescence Nanoscopy in Cell Biology. *Nat. Rev. Mol. Cell Biol.* **2017**, *18* (11), 685–701.

(49) Illien, F.; Rodriguez, N.; Amoura, M.; Joliot, A.; Pallerla, M.; Cribier, S.; Burlina, F.; Sagan, S. Quantitative Fluorescence Spectroscopy and Flow Cytometry Analyses of Cell-Penetrating Peptides Internalization Pathways: Optimization, Pitfalls, Comparison with Mass Spectrometry Quantification. *Sci. Rep.* **2016**, *6* (November), 1–13.

(50) Cui, C.; Shu, W.; Li, P. Fluorescence in Situ Hybridization: Cell-Based Genetic Diagnostic and Research Applications. *Front. Cell Dev. Biol.* **2016**, *4* (SEP), 1–11.

(51) Mullah, B.; Andrus, A. Automated Synthesis of Double Dye-Labeled Oligonucleotides Using Tetramethylrhodamine (TAMRA) Solid Supports. *Science (80-.).* **1997**, *38* (33), 5751–5754.

(52) Hall, L. M.; Gerowska, M.; Brown, T. A Highly Fluorescent DNA Toolkit : Synthesis and Properties of Oligonucleotides Containing New Cy3 , Cy5 and Cy3B Monomers. **2012**,

40 (14), 1–10.

(53) Bijapur, J.; Bergqvist, S.; Brown, T.; Keppler, M. D.; Fox, K. R. 5-(1-Propargylamino)-2'-Deoxyuridine (UP): A Novel Thymidine Analogue for Generating DNA Triplexes with Increased Stability. *Nucleic Acids Res.* **1999**, *27* (8), 1802–1809.

(54) Cuenoud, B.; Casset, F.; Hüsken, D.; Natt, F.; Wolf, R. M.; Altmann, K.-H.; Martin, P.; Moser, H. E. Dual Recognition of Double-Stranded DNA by 2'-Aminoethoxy-Modified Oligonucleotides. *Angew. Chemie Int. Ed.* **1998**, *37* (9), 1288–1291.

(55) Richardson, J. A.; Gerowska, M.; Shelbourne, M.; French, D.; Brown, T. Six-Colour HyBeacon Probes for Multiplex Genetic Analysis. *ChemBioChem* **2010**, *11* (18), 2530–2533.

(56) Brown, T.; Pritchard, C. E.; Turner, G.; Salisbury, S. A. A New Base-Stable Linker for Solid-Phase Oligonucleotide Synthesis. *J. Chem. Soc. Chem. Commun.* **1989**, No. 14, 891–893.

(57) Sheehan, J. C.; Hess, G. P. A New Method of Forming Peptide Bonds. *J. Am. Chem. Soc.* **1955**, *77* (4), 1067–1068.

(58) Carpino, L. A. 1-Hydroxy-7-Azabenzotriazole. An Efficient Peptide Coupling Additive. *J. Am. Chem. Soc.* **1993**, *115* (10), 4397–4398.

(59) Coste, J.; Le-Nguyen, D.; Castro, B. PyBOP®: A New Peptide Coupling Reagent Devoid of Toxic by-Product. *Tetrahedron Lett.* **1990**, *31* (2), 205–208.

(60) Ghosh, S. S.; Kao, P. M.; McCue, A. W.; Chappelle, H. L. Use of Maleimide-Thiol Coupling Chemistry for Efficient Syntheses of Oligonucleotide-Enzyme Conjugate Hybridization Probes. *Bioconjug. Chem.* **1990**, *1* (1), 71–76.

(61) Chrisey, L. A.; Lee, G. U.; Ferrall, C. E. O. Covalent Attachment of Synthetic DNA to Self-Assembled Monolayer Films. **1996**, *24* (15), 3031–3039.

(62) Seela, F.; Sirivolu, V. R. Nucleosides and Oligonucleotides with Diynyl Side Chains: The Huisgen-Sharpless Cycloaddition "Click Reaction" Performed on Dna and Their Constituents. *Nucleosides, Nucleotides and Nucleic Acids* **2007**, *26* (6–7), 597–601.

(63) Sivakumar, K.; Xie, F.; Cash, B. M.; Long, S.; Barnhill, H. N.; Wang, Q. A Fluorogenic 1,3-Dipolar Cycloaddition Reaction of 3-Azidocoumarins and Acetylenes. *Org. Lett.* **2004**, *6* (24), 4603–4606.

(64) Staudinger, H.; Meyer, J. Über Neue Organische Phosphorverbindungen III. Phosphinmethylenderivate Und Phosphinimine. *Helv. Chim. Acta* **1919**, *2* (1), 635–646.

(65) Gololobov, Y. G.; Kasukhin, L. F. Recent Advances in the Staudinger Reaction. *Tetrahedron* **1992**, *48* (8), 1353–1406.

(66) Gololobov, Y. G.; Zhmurova, I. N.; Kasukhin, L. F. Sixty Years of Staudinger. *Tetrahedron* **1981**, *37* (102), 437.

(67) Tian, W. Q.; Wang, Y. A. Mechanisms of Staudinger Reactions within Density Functional Theory. *J. Org. Chem.* **2004**, *69* (13), 4299–4308.

(68) El-Sagheer, A. H.; Brown, T. Synthesis and Polymerase Chain Reaction Amplification of DNA Strands Containing an Unnatural Triazole Linkage. *J. Am. Chem. Soc.* **2009**, *131* (11), 3958–3964.

(69) Polushin, N. N.; Smirnov, I. P.; Verentchikov, A. N.; Coull, J. M. Synthesis of Oligonucleotides Containing 2'-Azido-and 2'-Amino-2'-Deoxyuridine Using Phosphotriester Chemistry. *Tetrahedron Lett.* **1996**, *37* (19), 3227–3230.

(70) Wada, T.; Mochizuki, A.; Higashiya, S.; Tsuruoka, H.; Kawahara, S. I.; Ishikawa, M.; Sekine, M. Synthesis and Properties of 2-Azidodeoxyadenosine and Its Incorporation into Oligodeoxynucleotides. *Tetrahedron Lett.* **2001**, *42* (52), 9215–9219.

(71) Kiviniemi, A.; Virta, P.; Lönnberg, H. Utilization of Intrachain 4′-C-Azidomethylthymidine for Preparation of Oligodeoxyribonucleotide Conjugates by Click Chemistry in Solution and on a Solid Support. *Bioconjug. Chem.* **2008**, *19* (8), 1726–1734.

(72) Fomich, M. A.; Kvach, M. V.; Navakouski, M. J.; Weise, C.; Baranovsky, A. V.; Korshun, V. A.; Shmanai, V. V. Azide Phosphoramidite in Direct Synthesis of Azide-Modified Oligonucleotides. *Org. Lett.* **2014**, *16* (17), 4590–4593.

(73) Kočalka, P.; El-Sagheer, A. H.; Brown, T. Rapid and Efficient DNA Strand Cross-Linking by Click Chemistry. *ChemBioChem* **2008**, *9* (8), 1280–1285.

(74) El-Sagheer, A. H.; Brown, T. Efficient RNA Synthesis by in Vitro Transcription of a Triazole-Modified DNA Template. *Chem. Commun.* **2011**, *47* (44), 12057–12058.

(75) Lietard, J.; Meyer, A.; Vasseur, J. J.; Morvan, F. An Efficient Reagent for 5′-Azido Oligonucleotide Synthesis. *Tetrahedron Lett.* **2007**, *48* (50), 8795–8798.

(76) Rao, H.; Tanpure, A. A.; Sawant, A. A.; Srivatsan, S. G. Enzymatic Incorporation of an Azide-Modified UTP Analog into Oligoribonucleotides for Post-Transcriptional Chemical Functionalization. *Nat. Protoc.* **2012**, *7* (6), 1097–1112.

(77) Goddard-Borger, E. D.; Stick, R. V. An Efficient, Inexpensive, and Shelf-Stable Diazotransfer Reagent: Imidazole-1-Sulfonyl Azide Hydrochloride. *Org. Lett.* **2007**, *9* (19), 3797–3800.

(78) Stevens, M. Y.; Sawant, R. T.; Odell, L. R. Synthesis of Sulfonyl Azides via Diazotransfer Using an Imidazole-1-Sulfonyl Azide Salt: Scope and 15N NMR Labeling Experiments. *J. Org. Chem.* **2014**, *79* (11), 4826–4831.

(79) Lartia, R.; Murat, P.; Dumy, P.; Defrancq, E. Versatile Introduction of Azido Moiety into Oligonucleotides through Diazo Transfer Reaction. *Org. Lett.* **2011**, *13* (20), 5672–5675.

(80) Michael, K. Characterization of Electronic Transitions in Complex Molecules. *Discuss. Faraday Soc.* **1950**, No. c, 14.

(81) Lakowicz, J. R. *Principles of Fluorescence Spectroscopy. Third Edition*; 2006.

(82) Vladimir, D. V. *Fluorescent Energy Transfer Nucleic Acid Probes*; 2006.

(83) Didenko, V. V. DNA Probes Using Fluoresence Resonance Energy Transfer. *Biotechniques* **2001**, *31* (5), 1106–1121.

(84) Dale, R. E.; Eisinger, J.; Blumberg, W. E. The Orientational Freedom of Molecular Probes. The Orientation Factor in Intramolecular Energy Transfer. *Biophys. J.* **1979**, *26* (2), 161–193.

(85) Lewis, F. D.; Zhang, L.; Zuo, X. Orientation Control of Fluorescence Resonance Energy Transfer Using DNA as a Helical Scaffold. *J. Am. Chem. Soc.* **2005**, *127* (28), 10002–10003.

(86) Iqbal, A.; Arslan, S.; Okumus, B.; Wilson, T. J.; Giraud, G.; Norman, D. G.; Ha, T.; Lilley, D. M. J. Orientation Dependence in Fluorescent Energy Transfer between Cy3 and Cy5 Terminally Attached to Double-Stranded Nucleic Acids. *Proc. Natl. Acad. Sci.* **2008**, *105* (32), 11176–11181.

(87) Kwok, P. Methods for Genotyping Single Nuclotide Polymorphism. *Annu. Rev.*

Genomics Hum. Genet. **2001**, No. 2, 235–258.

(88) Ranasinghe, R. T.; Brown, T. Fluorescence Based Strategies for Genetic Analysis. *Chem. Commun.* **2005**, No. 44, 5487–5502.

(89) Fan, J. B.; Gunderson, K. L.; Bibikova, M.; Yeakley, J. M.; Chen, J.; Wickham Garcia, E.; Lebruska, L. L.; Laurent, M.; Shen, R.; Barker, D. Illumina Universal Bead Arrays. *Methods Enzymol.* **2006**, *410* (06), 57–73.

(90) Bao, G.; Rhee, W. J.; Tsourkas, A. Fluorescent Probes for Live-Cell RNA Detection. *Annu. Rev. Biomed. Eng.* **2009**, *11* (1), 25–47.

(91) Tyagi, S.; Kramer, F. R. Molecular Beacon Probes That Fluoresce on Hybridiztion. *Nat. Publ. Gr.* **1996**, *14* (3), 303–308.

(92) Tyagi, S.; Bratu, D. P.; Kramer, F. R. Multicolor Molecular Beacons for Allele Discrimination. *Nat. Biotechnol.* **1996**, No. 16, 49–53.

(93) French, D. J.; Archard, C. L.; Andersen, M. T.; McDowell, D. G. Ultra-Rapid DNA Analysis Using HyBeacon Probes and Direct PCR Amplification from Saliva. *Mol. Cell. Probes* **2002**, *16* (5), 319–326.

(94) French, D. J.; Archard, C. L.; Brown, T.; McDowell, D. G. HyBeacon™ Probes: A New Tool for DNA Sequence Detection and Allele Discrimination. *Mol. Cell. Probes* **2001**, *15* (6), 363–374.

(95) Hövelmann, F.; Bethge, L.; Seitz, O. Single Labeled DNA FIT Probes for Avoiding False-Positive Signaling in the Detection of DNA/RNA in QPCR or Cell Media. *ChemBioChem* **2012**, *13* (14), 2072–2081.

(96) Molenaar, C.; Wiesmeijer, K.; Verwoerd, N. P.; Khazen, S.; Eils, R.; Tanke, H. J.; Dirks, R. W. Visualizing Telomere Dynamics in Living Mammalian Cells Using PNA Probes. *EMBO J.* **2003**, *22* (24), 6631–6641.

(97) Boutorine, A. S.; Novopashina, D. S.; Krasheninina, O. A.; Nozeret, K.; Venyaminova, A. G. *Fluorescent Probes for Nucleic Acid Visualization in Fixed and Live Cells*; 2013; Vol. 18.

(98) Frickmann, H.; Zautner, A. E.; Moter, A.; Kikhney, J.; Hagen, R. M.; Stender, H.; Poppert, S. Fluorescence in Situ Hybridization (FISH) in the Microbiological Diagnostic Routine Laboratory: A Review. *Crit. Rev. Microbiol.* **2017**, *43* (3), 263–293.

(99) Svanvik, N.; Westman, G.; Wang, D.; Kubista, M. Light-up Probes: Thiazole Orange-Conjugated Peptide Nucleic Acid for Detection of Target Nucleic Acid in Homogeneous Solution. *Anal. Biochem.* **2000**, *281* (1), 26–35.

(100) Okamoto, A. ECHO Probes: A Concept of Fluorescence Control for Practical Nucleic Acid Sensing. *Chem. Soc. Rev.* **2011**, *40* (12), 5815–5828.

(101) Hövelmann, F.; Seitz, O. DNA Stains as Surrogate Nucleobases in Fluorogenic Hybridization Probes. *Acc. Chem. Res.* **2016**, *49* (4), 714–723.

(102) Sato, T.; Sato, Y.; Nishizawa, S. Triplex-Forming Peptide Nucleic Acid Probe Having Thiazole Orange as a Base Surrogate for Fluorescence Sensing of Double-Stranded RNA. *J. Am. Chem. Soc.* **2016**, No. 138, 9397–9400.

(103) Lu, Y. J.; Deng, Q.; Hou, J. Q.; Hu, D. P.; Wang, Z. Y.; Zhang, K.; Luyt, L. G.; Wong, W. L.; Chow, C. F. Molecular Engineering of Thiazole Orange Dye: Change of Fluorescent Signaling from Universal to Specific upon Binding with Nucleic Acids in Bioassay. *ACS Chem. Biol.* **2016**, *11* (4), 1019–1029.

(104) Lubitz, I.; Zikich, D.; Kotlyar, A. Specific High-Affinity Binding of Thiazole Orange to Triplex and g-Quadruplex DNA. *Biochemistry* **2010**, *49* (17), 3567–3574.

(105) Isacsson, J.; Westman, G. Solid-Phase Synthesis of Asymmetric Cyanine Dyes. *Tetrahedron Lett.* **2001**, *42* (18), 3207–3210.

(106) Nygren, J.; Svanvik, N.; Kubista, M.; Institute, L. The Interactions Between the Orange and DNA. **1998**, 39–51.

(107) Rye, H. S.; Yue, S.; Wemmer, D. E.; Quesada, M. A.; Haugland, R. P.; Mathies, R. A.; Giazer, A. N. Stable Fluorescent Complexes of Double-Stranded DNA with Bis-Intercalating Asymmetric Cyanine Dyes: Properties and Applications. *Nucleic Acids Res* **1992**, *20* (11), 2803–2812.

(108) Spielmann, H. P.; Wemmer, D. E.; Jacobsen, J. P. Solution Structure of a DNA Complex with the Fluorescent Bis-Intercalator TOTO Determined by NMR Spectroscopy. *Biochemistry* **1995**, *34* (27), 8542–8553.

(109) Prodhomme, S.; Demaret, J. P.; Vinogradov, S.; Asseline, U.; Morin-Allory, L.; Vigny, P. A Theoretical and Experimental Study of Two Thiazole Orange Derivatives with Single- and Double-Stranded Oligonucleotides, Polydeoxyribonucleotides and DNA. *J. Photochem. Photobiol. B Biol.* **1999**, *53* (1–3), 60–69.

(110) Kapuscinski, J. Interactions of Nucleic Acids with Fluorescent Dyes: Spectral Properties of Condensed Complexes. *J. Histochem. Cytochem.* **1990**, *38* (9), 1323–1329.

(111) Lartia, R.; Asseline, U. New Cyanine-Oligonucleotide Conjugates: Relationships between Chemical Structures and Properties. *Chem. - A Eur. J.* **2006**, *12* (8), 2270–2281.

(112) Privat, E.; Asseline, U. Synthesis and Binding Properties of Oligo-2'-Deoxyribonucleotides Covalently Linked to a Thiazole Orange Derivative. *Bioconjug. Chem.* **2001**, *12* (5), 757–769.

(113) Privat, E.; Melvin, T.; Merola, F.; Schweizer, G.; Prodhomme, S.; Asseline, U.; Vigny, P. Fluorescent Properties of Oligonucleotide-Conjugated Thiazole Orange Probes. *Photochem Photobiol* **2002**, *75* (3), 201–210.

(114) Ikeda, S.; Okamoto, A. Hybridization-Sensitive on-off DNA Probe: Application of the Exciton Coupling Effect to Effective Fluorescence Quenching. *Chem. - An Asian J.* **2008**, *3* (6), 958–968.

(115) Ikeda, S.; Kubota, T.; Yuki, M.; Okamoto, A. Exciton-Controlled Hybridization-Sensitive Fluorescent Probes: Multicolor Detection of Nucleic Acids. *Angew. Chemie - Int. Ed.* **2009**, *48* (35), 6480–6484.

(116) Sugizaki, K.; Okamoto, A. ECHO-LNA Conjugates: Hybridization-Sensitive Fluorescence and Its Application to Fluorescent Detection of Various RNA Strands. *Bioconjug. Chem.* **2010**, *21* (12), 2276–2281.

(117) Ikeda, S.; Yuki, M.; Yanagisawa, H.; Okamoto, A. Doubly Thiazole Orange-Labeled Cytidine for Functional Expansion of a Hybridization-Sensitive Probe. *Tetrahedron Lett.* **2009**, *50* (51), 7191–7195.

(118) Qiu, J.; Wilson, A.; El-Sagheer, A. H.; Brown, T. Combination Probes with Intercalating Anchors and Proximal Fluorophores for DNA and RNA Detection. *Nucleic Acids Res.* **2016**, *44* (17), 1–12.

(119) Steinmeyer, J.; Walter, H. K.; Bichelberger, M. A.; Schneider, V.; Kubař, T.; Rönicke, F.; Olshausen, B.; Nienhaus, K.; Nienhaus, G. U.; Schepers, U.; et al. "siRNA Traffic Lights": Arabino-Configured 2'-Anchors for Fluorescent Dyes Are Key for Dual Color Readout in

Cell Imaging. *Org. Biomol. Chem.* **2018**, *16* (20), 3726–3731.

(120) Wang, X.; Krull, U. J. Synthesis and Fluorescence Studies of Thiazole Orange Tethered onto Oligonucleotide: Development of a Self-Contained DNA Biosensor on a Fiber Optic Surface. *Bioorganic Med. Chem. Lett.* **2005**, *15* (6), 1725–1729.

(121) Kubota, T.; Ikeda, S.; Yanagisawa, H.; Yuki, M.; Okamoto, A. Hybridization-Sensitive Fluorescent Probe for Long-Term Monitoring of Intracellular RNA. *Bioconjug. Chem.* **2009**, *20* (6), 1256–1261.

(122) Kubota, T.; Ikeda, S.; Yanagisawa, H.; Yuki, M.; Okamoto, A. Hybridization-Sensitive Fluorescent Probe for Long-Term Monitoring of Intracellular RNA. *Bioconjug. Chem.* **2009**, *20* (6), 1256–1261.

(123) Lartia, R.; Asseline, U. New Cyanine-Oligonucleotide Conjugates: Relationships between Chemical Structures and Properties. *Chem. - A Eur. J.* **2006**, *12* (8), 2270–2281.

(124) Berndl, S.; Wagenknecht, H. A. Fluorescent Color Readout of DNA Hybridization with Thiazole Orange as Anartificial DNA Base. *Angew. Chemie - Int. Ed.* **2009**, *48* (13), 2418–2421.

(125) Menacher, F.; Rubner, M.; Berndl, S.; Wagenknecht, H.; Uni, V. Thiazole Orange and Cy3 : Improvement of Fluorescent DNA Probes with Use of Short Range Electron Transfer. *J. Org. Chem.* **2008**, *73*, 4263–4266.

(126) Wlttung, P.; Nlelsenh, P. E.; Buchardtt, O.; Egholm, M.; Norden, B. DNA-like Double Helix Formed by Peptide Nucleic Acid. *Nature* **1994**, *368*, 561–563.

(127) Köhler, O.; Jarikote, D. V.; Seitz, O. Forced Intercalation Probes (FIT Probes): Thiazole Orange as a Fluorescent Base in Peptide Nucleic Acids for Homogeneous Single-Nucleotide-Polymorphism Detection. *ChemBioChem* **2005**, *6* (1), 69–77.

(128) Kummer, S.; Knoll, A.; Socher, E.; Bethge, L.; Herrmann, A.; Seitz, O. Fluorescence Imaging of Influenza H1N1 MRNA in Living Infected Cells Using Single-Chromophore FIT-PNA. *Angew. Chemie - Int. Ed.* **2011**, *50* (8), 1931–1934.

(129) Bethge, L.; Singh, I.; Seitz, O. Designed Thiazole Orange Nucleotides for the Synthesis of Single Labelled Oligonucleotides That Fluoresce upon Matched Hybridization. *Org. Biomol. Chem.* **2010**, *8* (10), 2439–2448.

(130) Hövelmann, F.; Gaspar, I.; Ephrussi, A.; Seitz, O. Brightness Enhanced DNA FIT-Probes for Wash-Free RNA Imaging in Tissue. *J. Am. Chem. Soc.* **2013**, *135* (50), 19025–19032.

(131) Hara, Y.; Fujii, T.; Kashida, H.; Sekiguchi, K.; Liang, X.; Niwa, K.; Takase, T.; Yoshida, Y.; Asanuma, H. Coherent Quenching of a Fluorophore for the Design of a Highly Sensitive In-Stem Molecular Beacon. *Angew. Chemie - Int. Ed.* **2010**, *49* (32), 5502–5506.

(132) Koehler, O.; Seitz, O. Thiazole Orange as Fluorescent Universal Base in Peptide Nucleic Acids. *ChemInform* **2004**, *35* (12), 2938–2939.

(133) Bethge, L.; Singh, I.; Seitz, O. Designed Thiazole Orange Nucleotides for the Synthesis of Single Labelled Oligonucleotides That Fluoresce upon Matched Hybridization. *Org. Biomol. Chem.* **2010**, *8* (10), 2439–2448.

(134) Hövelmann, F.; Gaspar, I.; Loibl, S.; Ermilov, E. A.; Röder, B.; Wengel, J.; Ephrussi, A.; Seitz, O. Brightness through Local Constraint--LNA-Enhanced FIT Hybridization Probes for in Vivo Ribonucleotide Particle Tracking. *Angew. Chem. Int. Ed. Engl.* **2014**, *53* (42), 11370–11375.

(135) Hövelmann, F.; Gaspar, I.; Chamiolo, J.; Kasper, M.; Steffen, J.; Ephrussi, A.; Seitz, O.

LNA-Enhanced DNA FIT-Probes for Multicolour RNA Imaging. *Chem. Sci.* **2016**, *7* (1), 128–135.

(136) Bethge, L.; Jarikote, D. V.; Seitz, O. New Cyanine Dyes as Base Surrogates in PNA: Forced Intercalation Probes (FIT-Probes) for Homogeneous SNP Detection. *Bioorg. Med. Chem.* **2008**, *16* (1), 114–125.

(137) Escude, C., Sun, J.-S. *DNA Major Groove Binders: Triple Helix-Forming Oligonucleotides, Triple Helix-Specific DNA Ligands and Cleaving Agents. In DNA Binders and Related Subjects,*; Springer: Berlin, 2005.

(138) Dai, J.; Carver, M.; Yang, D. Polymorphism of Human Telomeric Quadruplex Structures. *Biochimie* **2008**, *90* (8), 1172–1183.

(139) Oganesian, L.; Bryan, T. M. Physiological Relevance of Telomeric G-Quadruplex Formation: A Potential Drug Target. *BioEssays* **2007**, *29* (2), 155–165.

(140) Monchaud, D.; Allain, C.; Teulade-Fichou, M. P. Thiazole Orange: A Useful Probe for Fluorescence Sensing of G-Quadruplex-Ligand Interactions. *Nucleosides, Nucleotides and Nucleic Acids* **2007**, *26* (10–12), 1585–1588.

(141) Walsh, S.; El-Sagheer, A. H.; Brown, T. Fluorogenic Thiazole Orange TOTFO Probes Stabilise Parallel DNA Triplexes at PH 7 and Above. *Chem. Sci.* **2018**, *9* (39), 7681–7687.

(142) Kloosterman, W. P.; Wienholds, E.; de Bruijn, E.; Kauppinen, S.; Plasterk, R. H. A. In Situ Detection of MiRNAs in Animal Embryos Using LNA-Modified Oligonucleotide Probes. *Nat. Methods* **2006**, *3* (1), 27–29.

(143) Peng, X. H.; Cao, Z. H.; Xia, J. T.; Carlson, G. W.; Lewis, M. M.; Wood, W. C.; Yang, L. Real-Time Detection of Gene Expression in Cancer Cells Using Molecular Beacon Imaging: New Strategies for Cancer Research. *Cancer Res.* **2005**, *65* (5), 1909–1917.

(144) Nitin, N.; Santangelo, P. J.; Kim, G.; Nie, S.; Bao, G. Peptide-Linked Molecular Beacons for Efficient Delivery and Rapid MRNA Detection in Living Cells. *Nucleic Acids Res.* **2004**, *32* (6), 1–8.

(145) Orjalo, A.; Johansson, H. E.; Ruth, J. L. Stellaris Fluorescence in Situ Hybridization (FISH) Probes: A Powerful Tool for MRNA Detection. *Nat. Methods* **2011**, *8* (10), i–ii.

(146) Ratan, Z. A.; Zaman, S. Bin; Mehta, V.; Haidere, M. F.; Runa, N. J.; Akter, N. Application of Fluorescence In Situ Hybridization (FISH) Technique for the Detection of Genetic Aberration in Medical Science. *Cureus* **2017**, *9* (6).

(147) Talagrand-Reboul, E.; Latif-Eugenín, F.; Beaz-Hidalgo, R.; Colston, S.; Figueras, M. J.; Graf, J.; Jumas-Bilak, E.; Lamy, B. Genome-Driven Evaluation and Redesign of PCR Tools for Improving the Detection of Virulence-Associated Genes in Aeromonads. *PLoS One* **2018**, *13* (8), 1–17.

(148) Klimkowski, P.; Ornellas, S. De; Singleton, D.; El-sagheer, A. H.; Brown, T. Design of Thiazole Orange Oligonucleotide Probes for Detection of DNA and RNA by Fluorescence and Duplex Melting. *Org. Biomol. Chem.* **2019**, *17*, 5943–5950.

(149) Qiu, J.; Wilson, A.; El-Sagheer, A. H.; Brown, T. Combination Probes with Intercalating Anchors and Proximal Fluorophores for DNA and RNA Detection. *Nucleic Acids Res.* **2016**, *44* (17), 1–12.

(150) Weigert, R.; Porat-Shliom, N.; Amornphimoltham, P. Imaging Cell Biology in Live Animals: Ready for Prime Time. *J. Cell Biol.* **2013**, *201* (7), 969–979.

(151) Chen, A. K.; Behlke, M. A.; Tsourkas, A. Avoiding False-Positive Signals with Nuclease-

Vulnerable Molecular Beacons in Single Living Cells. *Nucleic Acids Res.* **2007**, *35* (16).

(152) Okamoto, A. ECHO Probes: A Concept of Fluorescence Control for Practical Nucleic Acid Sensing. *Chem. Soc. Rev.* **2011**, *40* (12), 5815–5828.

(153) Booth, J.; Brown, T.; Vadhia, S. J.; Lack, O.; Cummins, W. J.; Trent, J. O.; Lane, A. N. Determining the Origin of the Stabilization of DNA by 5-Aminopropynylation of Pyrimidines. *Biochemistry* **2005**, *44* (12), 4710–4719.

(154) Gyi, J. I.; Gao, D.; Conn, G. L.; Trent, J. O.; Brown, T.; Lane, A. The Solution Structure of a DNA·RNA Duplex Containing 5-Propynyl U and C; Comparison with 5-Me Modifications. *Nucleic Acids Res.* **2003**, *31* (10), 2683–2693.

(155) Blommers, M. J. J.; Natt, F.; Jahnke, W.; Cuenoud, B. Dual Recognition of Double-Stranded DNA by 2'-Aminoethoxy-Modified Oligonucleotides: The Solution Structure of an Intramolecular Triplex Obtained by NMR Spectroscopy. *Biochemistry* **1998**, *37* (51), 17714–17725.

(156) Luis A, M.; Lita, C.; Roger A., J.; Kenneth J., B. Calorymetric and Spectroscopic Investigation of the Helix-to-Coil Transition of the Self-Complementary Deoxyribonuclotide ATGCAT. *Biophsical Chem.* **1981**, *13*, 141–149.

(157) Carreon, J. R.; Mahon, K. P.; Kelley, S. O. Thiazole Orange−Peptide Conjugates: Sensitivity of DNA Binding to Chemical Structure. *Org. Lett.* **2004**, *6* (4), 517–519.

(158) Svanvik, N.; Westman, G.; Wang, D.; Kubista, M. Light-up Probes: Thiazole Orange-Conjugated Peptide Nucleic Acid for Detection of Target Nucleic Acid in Homogeneous Solution. *Anal. Biochem.* **2000**, *281* (1), 26–35.

(159) Xia, Y.; Zhang, R.; Wang, Z.; Tian, J.; Chen, X. Recent Advances in High-Performance Fluorescent and Bioluminescent RNA Imaging Probes. *Chem. Soc. Rev.* **2017**, *46* (10), 2824–2843.

(160) Gaspar, I.; Hövelmann, F.; Chamiolo, J.; Ephrussi, A.; Seitz, O. Quantitative MRNA Imaging with Dual Channel QFIT Probes to Monitor Distribution and Degree of Hybridization. *ACS Chem. Biol.* **2018**, *13* (3), 742–749.

(161) Bunkenborg, J.; Gadjev, N. I.; Deligeorgiev, T.; Jacobsen, J. P. Concerted Intercalation and Minor Groove Recognition of DNA by a Homodimeric Thiazole Orange Dye. *Bioconjug Chem* **2000**, *11* (6), 861–867.

(162) Blommers, M. J. J.; Natt, F.; Jahnke, W.; Cuenoud, B. Dual Recognition of Double-Stranded DNA by 2'-Aminoethoxy-Modified Oligonucleotides: The Solution Structure of an Intramolecular Triplex Obtained by NMR Spectroscopy. *Biochemistry* **1998**, *37* (51), 17714–17725.

(163) Sindbert, S.; Kalinin, S.; Nguyen, H.; Kienzler, A.; Clima, L.; Bannwarth, W.; Appel, B.; Muller, S.; Seidel, C. A. Accurate Distance Determination of Nucleic Acids via Forster Resonance Energy Transfer: Implications of Dye Linker Length and Rigidity. *J Am Chem Soc* **2011**, *133* (8), 2463–2480.

(164) Jarikote, D. V.; Köhler, O.; Socher, E.; Seitz, O. Divergent and Linear Solid-Phase Synthesis of PNA Containing Thiazole Orange as Artificial Base. *European J. Org. Chem.* **2005**, No. 15, 3187–3195.

(165) Ikeda, S.; Kubota, T.; Kino, K.; Okamoto, A. Sequence Dependence of Fluorescence Emission and Quenching of Doubly Thiazole Orange Labeled DNA: Effective Design of a Hybridization-Sensitive Probe. *Bioconjug. Chem.* **2008**, *19* (8), 1719–1725.

(166) Mujumdar, R. B.; Ernst, L. A.; Mujumdar, S. R.; Lewis, C. J.; Waggoner, A. S. Cyanine Dye

Labeling Reagents: Sulfoindocyanine Succinimidyl Esters. *Bioconjug Chem* **1993**, *4* (2), 105–111.

(167) Olaf, K.; Venkatrao, J. D.; Oliver, S. Forced Intercalation Probes (FIT Probes): Thiazole Orange as a Fluorescent Base in Peptide Nucleic Acids for Homogeneous Single-Nucleotide-Polymorphism Detection. *ChemBioChem* **2005**, *6* (1), 69–77.

(168) Kimura, Y.; Hanami, T.; Tanaka, Y.; de Hoon, M. J. L.; Soma, T.; Harbers, M.; Lezhava, A.; Hayashizaki, Y.; Usui, K. Effect of Thiazole Orange Doubly Labeled Thymidine on DNA Duplex Formation. *Biochemistry* **2012**, *51* (31), 6056–6067.

(169) Kirchner, J. Data Analysis Toolkit #5: Uncertainty Analysis and Error seismo.berkeley.edu/~kirchner/eps_120/Toolkits/Toolkit_05.pdf (accessed Dec 1, 2019).

(170) Jarikote, D. V.; Krebs, N.; Tannert, S.; Röder, B.; Seitz, O. Exploring Base-Pair-Specific Optical Properties of the DNA Stain Thiazole Orange. **2007**, *13* (1), 300–310.

(171) Woo, J.; Meyer, R. B.; Gamper, H. B. G/C-Modified Oligodeoxynucleotides with Selective Complementarity: Synthesis and Hybridization Properties. *Nucleic Acids Res.* **1996**, *24* (13), 2470–2475.

(172) Fisher, T. L.; Terhorst, T.; Cao, X. D.; Wagner, R. W. Intracellular Disposition and Metabolism of Fluorescently-Labeled Unmodified and Modified Oligonucleotides Microinjected into Mammalian-Cells. *Nucleic Acids Res.* **1993**, *21* (16), 3857–3865.

(173) Ando, T. A Nuclease Specific for Heat-Denatured DNA Isolated from a Product of Aspergillus Oryzae. *BBA Sect. Nucleic Acids Protein Synth.* **1966**, *114* (1), 158–168.

(174) Wiegand, R. C.; Godson, G. N.; Radding, C. M. Of the S , Nuclease from Aspergillus. **1975**, *250* (22), 8848–8855.

(175) Kushner, S. R.; Nagaishi, H.; Templin, A.; Clark, A. J. Genetic Recombination in Escherichia Coli: The Role of Exonuclease I. *Proc. Natl. Acad. Sci.* **2006**, *68* (4), 824–827.

(176) Blommers, M. J. J.; Pieles, U.; De Mesmaeker, A. An Approach to the Structure Determination of Nucleic Acid Analogues Hybridized to RNA. NMR Studies of a Duplex between 2'-OMe RNA and an Oligonucleotide Containing a Single Amide Backbone Modification. *Nucleic Acids Res.* **1994**, *22* (20), 4187–4194.

(177) Sugizaki, K.; Okamoto, A. ECHO-LNA Conjugates: Hybridization-Sensitive Fluorescence and Its Application to Fluorescent Detection of Various RNA Strands. *Bioconjug. Chem.* **2010**, *21* (12), 2276–2281.

(178) Brouwer, A. M. Standards for Photoluminescence Quantum Yield Measurements in Solution (IUPAC Technical Report). *Pure Appl. Chem.* **2011**, *83* (12), 2213.

(179) Hövelmann, F.; Gaspar, I.; Chamiolo, J.; Kasper, M.; Steffen, J.; Ephrussi, a.; Seitz, O. LNA-Enhanced DNA FIT-Probes for Multicolour RNA Imaging. *Chem. Sci.* **2016**, 128–135.

(180) Kubota, T.; Ikeda, S.; Yanagisawa, H.; Yuki, M.; Okamoto, A. Hybridization-Sensitive Fluorescent Probe for Long-Term Monitoring of Intracellular RNA. *Bioconjug. Chem.* **2009**, *20* (6), 1256–1261.

(181) Curtis Johnson, W. Circular Dichromism and the Conformational Analysis of Biomolecules; Fasman, G. D., Ed.; Springer Science+Buisness Media, LLC, 1996; pp 433–468.

(182) Sonar, M. V.; Wampole, M. E.; Jin, Y. Y.; Chen, C. P.; Thakur, M. L.; Wickstrom, E.

Fluorescence Detection of KRAS2 MRNA Hybridization in Lung Cancer Cells with PNA-Peptides Containing an Internal Thiazole Orange. *Bioconjug. Chem.* **2014**, *25* (9), 1697–1708.

(183) Kam, Y.; Rubinstein, A.; Naik, S.; Djavsarov, I.; Halle, D.; Ariel, I.; Gure, A. O.; Stojadinovic, A.; Pan, H. G.; Tsivin, V.; et al. Detection of a Long Non-Coding RNA (CCAT1) in Living Cells and Human Adenocarcinoma of Colon Tissues Using FIT-PNA Molecular Beacons. *Cancer Lett.* **2014**, *352* (1), 90–96.

(184) Torres, A. G.; Fabani, M. M.; Vigorito, E.; Williams, D.; Al-Obaidi, N.; Wojciechowski, F.; Hudson, R. H. E.; Seitz, O.; Gait, M. J. Chemical Structure Requirements and Cellular Targeting of MicroRNA-122 by Peptide Nucleic Acids Anti-MiRs. *Nucleic Acids Res.* **2012**, *40* (5), 2152–2167.

(185) Hövelmann, F.; Bethge, L.; Seitz, O. Single Labeled DNA FIT Probes for Avoiding False-Positive Signaling in the Detection of DNA/RNA in QPCR or Cell Media. *ChemBioChem* **2012**, *13* (14), 2072–2081.

(186) Bethge, L.; Singh, I.; Seitz, O. Designed Thiazole Orange Nucleotides for the Synthesis of Single Labelled Oligonucleotides That Fluoresce upon Matched Hybridization. *Org. Biomol. Chem.* **2010**, *8* (10), 2439–2448.

(187) Murayama, K.; Kashida, H.; Asanuma, H. Acyclic L-Threoninol Nucleic Acid L-ATNA) with Suitable Structural Rigidity Cross-Pairs with DNA and RNA. *Chem. Commun.* **2015**, *51* (30), 6500–6503.

(188) Asanuma, H.; Takarada, T.; Yoshida, T.; Tamaru, D.; Liang, X.; Komiyama, M. Enantioselective Incorporation of Azobenzenes into Oligodeoxyribonucleotide for Effective Photoregulation of Duplex Formation. *Angew. Chemie - Int. Ed.* **2001**, *40* (14), 2671–2673.

(189) Kamiya, Y.; Ito, A.; Ito, H.; Urushihara, M.; Takai, J.; Fujii, T.; Liang, X.; Kashida, H.; Asanuma, H. Selective Labeling of Mature RISC Using a SiRNA Carrying Fluorophore–Quencher Pair. *Chem. Sci.* **2013**, *4* (10), 4016–4021.

(190) Shi, Y.; Machida, K.; Kuzuya, A.; Komiyama, M. Design of Phosphoramidite Monomer for Optimal Incorporation of Functional Intercalator to Main Chain of Oligonucleotide. *Bioconjug. Chem.* **2005**, *16* (2), 306–311.

(191) Carreon, J. R.; Mahon, K. P.; Kelley, S. O. Thiazole Orange-Peptide Conjugates: Sensitivity of DNA Binding to Chemical Structure. *Org. Lett.* **2004**, *6* (4), 517–519.

(192) Tatay, S.; Gavina, P.; Coronado, E.; Palomares, E. Optical Mercury Sensing Using a Benzothiazolium Hemicyanine Dye. *Org. Lett.* **2006**, *8* (17), 3857–3860.

(193) Bethge, L.; Jarikote, D. V.; Seitz, O. New Cyanine Dyes as Base Surrogates in PNA: Forced Intercalation Probes (FIT-Probes) for Homogeneous SNP Detection. *Bioorganic Med. Chem.* **2008**, *16* (1), 114–125.

(194) Liu, K.; Wen, Y.; Shi, T.; Li, Y.; Li, F.; Zhao, Y. L.; Huang, C.; Yi, T. DNA Gated Photochromism and Fluorescent Switch in a Thiazole Orange Modified Diarylethene. *Chem. Commun.* **2014**, *50* (65), 9141–9144.

(195) Zhan, W. H.; Barnhill, H. N.; Sivakumar, K.; Tian, H.; Wang, Q. Synthesis of Hemicyanine Dyes for “click” Bioconjugation. *Tetrahedron Lett.* **2005**, *46* (10), 1691–1695.

(196) Ditmangklo, B.; Boonlua, C.; Suparpprom, C.; Vilaivan, T. Reductive Alkylation and Sequential Reductive Alkylation-Click Chemistry for on-Solid-Support Modification of Pyrrolidinyl Peptide Nucleic Acid. *Bioconjug. Chem.* **2013**, *24* (4), 614–625.

(197) Gahtory, D.; Murtola, M.; Smulders, M. M. J.; Wennekes, T.; Zuilhof, H.; Strömberg, R.; Albada, B. Facile Functionalization of Peptide Nucleic Acids (PNAs) for Antisense and Single Nucleotide Polymorphism Detection. *Org. Biomol. Chem.* **2017**, *15* (32), 6710–6714.

(198) El-Sagheer, A. H.; Brown, T. Click Chemistry with DNA. *Chem. Soc. Rev.* **2010**, *39* (4), 1388–1405.

(199) Gramlich, P. M. E.; Warncke, S.; Gierlich, J.; Carell, T. Click-Click-Click: Single to Triple Modification of DNA. *Angew. Chemie - Int. Ed.* **2008**, *47* (18), 3442–3444.

(200) Jawalekar, A. M.; Meeuwenoord, N.; Cremers, J. G. O.; Overkleeft, H. S.; Van Der Marel, G. A.; Rutjes, F. P. J. T.; Van Delft, F. L. Conjugation of Nucleosides and Oligonucleotides by [3+2] Cycloaddition. *J. Org. Chem.* **2008**, *73* (1), 287–290.

(201) Jawalekar, A. M.; Malik, S.; Verkade, J. M. M.; Gibson, B.; Barta, N. S.; Hodges, J. C.; Rowan, A.; Van Delft, F. L. Oligonucleotide Tagging for Copper-Free Click Conjugation. *Molecules* **2013**, *18* (7), 7346–7363.

(202) Jacobsen, M. F.; Ravnsbaek, J. B.; Gothelf, K. V. Small Molecule Induced Control in Duplex and Triplex DNA-Directed Chemical Reactionst. *Org. Biomol. Chem.* **2010**, *8* (1), 50–52.

(203) Franzini, R. M.; Kool, E. T. Two Successive Reactions on a DNA Template: A Strategy for Improving Background Fluorescence and Specificity in Nucleic Acid Detection. *Chem. - A Eur. J.* **2011**, *17* (7), 2168–2175.

(204) Li, G.; Liu, Y.; Yu, X.; Li, X. Multivalent Photoaffinity Probe for Labeling Small Molecule Binding Proteins. *Bioconjug. Chem.* **2014**, *25* (6), 1172–1180.

(205) Sylvers, L. A.; Wower, J. Nucleic Acid-Incorporated Azidonucleotides: Probes for Studying the Interaction of RNA or DNA with Proteins and Other Nucleic Acids. *Bioconjug. Chem.* **1993**, *4* (6), 411–418.

(206) Murayama, K.; Asanuma, H. Effect of Methyl Group on Acyclic Serinol Scaffold for Tethering Dyes on the DNA Duplex Stability. *ChemBioChem* **2017**, *18* (1), 142–149.

(207) Socher, E.; Knoll, A.; Seitz, O. Dual Fluorophore PNA FIT-Probes - Extremely Responsive and Bright Hybridization Probes for the Sensitive Detection of DNA and RNA. *Org. Biomol. Chem.* **2012**, *10* (36), 7363–7371.

(208) Fang, G. M.; Chamiolo, J.; Kankowski, S.; Hövelmann, F.; Friedrich, D.; Löwer, A.; Meier, J. C.; Seitz, O. A Bright FIT-PNA Hybridization Probe for the Hybridization State Specific Analysis of a C → U RNA Edit: Via FRET in a Binary System. *Chem. Sci.* **2018**, *9* (21), 4794–4800.

(209) Holzhauser, C.; Liebl, R.; Goepferich, A.; Wagenknecht, H. A.; Breunig, M. RNA "Traffic Lights": An Analytical Tool to Monitor SiRNA Integrity. *ACS Chem. Biol.* **2013**, *8* (5), 890–894.

(210) Ikeda, S.; Kubota, T.; Wang, D. O.; Yanagisawa, H.; Yuki, M.; Okamoto, A. Emission Control by Binary Energy Transfer Processes on Oligouridine. *Org. Biomol. Chem.* **2011**, *9* (19), 6598–6603.

(211) Hudson, R. H. E.; Ghorbani-Choghamarani, A. Selective Fluorometric Detection of Guanosine-Containing Sequences by 6-Phenylpyrrolocytidine in DNA. *Synlett* **2007**, No. 6, 870–873.

(212) Chinchilla, R.; Nájera, C. The Sonogashira Reaction: A Booming Methodology in Synthetic Organic Chemistry. *Chem. Rev.* **2007**, *107* (3), 874–922.

(213) ATTO-TEC. Fluorescent Labels and Dyes catalogue www.atto-tec.com/fileadmin/user_upload/Katalog_Flyer_Support/Catalogue_2009_2010.pdf (accessed Jul 10, 2019).

(214) GeneLink. ATTO647N oligo modification www.genelink.com/newsite/products/MODPDFFILES/26-6980.pdf (accessed Jul 10, 2019).

(215) Kellett, A.; Molphy, Z.; Slator, C.; McKee, V.; Farrell, N. P. Molecular Methods for Assessment of Non-Covalent Metallodrug-DNA Interactions. *Chem. Soc. Rev.* **2019**, *48* (4), 971–988.

(216) Agarwala, A.; Jones, P.; Nambi, V. The Role of Antisense Oligonucleotide Therapy in Patients with Familial Hypercholesterolemia: Risks, Benefits, and Management Recommendations. *Curr. Atheroscler. Rep.* **2015**, *17* (1), 1–8.

(217) Derakhshan, S. M.; Khaniani, M. S. Restoration of Correct Splicing in IVSI-110 Mutation of β-Globin Gene with Antisense Oligonucleotides: Implications and Applications in Functional Assay Development. *Iran. J. Basic Med. Sci.* **2017**, *20* (6), 700–707.

(218) Jarvis, T. S.; Smith, B. D. Macrocycle Threading Using Solvatochromic Squaraine Dyes. *Supramol. Chem.* **2019**, *31* (3), 140–149.

(219) Fei, X.; Li, R.; Lin, D.; Gu, Y.; Yu, L. Spectra, Stability and Labeling of a Novel Carbazole Derivative as a Fluorescent Turn-on DNA Probe. *J. Fluoresc.* **2015**, *25* (5), 1251–1258.

(220) Sato, T.; Sato, Y.; Nishizawa, S. Optimization of the Alkyl Linker of TO Base Surrogate in Triplex- Forming PNA for Enhanced Binding to Double-Stranded RNA. **2017**, 4079–4088.

(221) J. Xia , C. Nie, J.Qjan, Y. Zhao, W. Zhao. Preparation of Novel Nucleic Acid Dye for Polyacrylamide Gel Electrophoresis, CN106008495 (A), 2016.

(222) Gu, K.; Bi, L.; Zhao, M.; Wang, C.; Dolan, C.; Kao, M. C.; Tok, J. B. H.; Peng, S. Stereoselective Synthesis and Anti-Inflammatory Activities of 6- and 7-Membered Dioxacycloalkanes. *Bioorganic Med. Chem.* **2006**, *14* (5), 1339–1347.

(223) Keller, T. H.; Haner, R.; Research, P. Synthesis and Hybridization Properties of Oligonucleotides. **1993**, *21* (19), 17–23.

(224) Kumar, V.; Kesavan, V.; Gothelf, K. V. Highly Stable Triple Helix Formation by Homopyrimidine (L)-Acyclic Threoninol Nucleic Acids with Single Stranded DNA and RNA. *Org. Biomol. Chem.* **2015**, *13* (8), 2366–2374.

(225) Ferreira, R.; Aviñó, A.; Mazzini, S.; Eritja, R. Synthesis, DNA-Binding and Antiproliferative Properties of Acridine and 5-Methylacridine Derivatives. **2012**, 7067–7082.

(226) Milelli, A.; Marchetti, C.; Greco, M. L.; Moraca, F.; Costa, G.; Turrini, E.; Catanzaro, E.; Betari, N.; Calcabrini, C.; Sissi, C.; et al. Naphthalene Diimide-Polyamine Hybrids as Antiproliferative Agents: Focus on the Architecture of the Polyamine Chains. *Eur. J. Med. Chem.* **2017**, *128*, 107–122.

(227) Franzini, R. M.; Kool, E. T. Efficient Nucleic Acid Detection by Templated Reductive Quencher Release. *J. Am. Chem. Soc.* **2009**, *131* (44), 16021–16023.

(228) Noe, C. R.; Winkler, J.; Urban, E.; Gilbert, M.; Haberhauer, G.; Brunar, H. Zwitterionic Oligonucleotides: A Study on Binding Properties of 2'-O-Aminohexyl Modifications. *Nucleosides, Nucleotides and Nucleic Acids* **2005**, *24* (8), 1167–1185.

(229) Santiago, J. V.; Burtoloso, A. C. B. Rapid Synthesis of Bicyclic N-Heterocyclic Cores from N-Terminal α,β-Unsaturated Diazoketones. *European J. Org. Chem.* **2018**, No. 22, 2822–2830.

(230) Southwick, P. L.; Ernst, L. A.; Tauriello, E. W.; Parker, S. R.; Mujumdar, R. B.; Mujumdar, S. R.; Clever, H. A.; Waggoner, A. S. Cyanine Dye Labeling Reagents—Carboxymethylindocyanine Succinimidyl Esters. *Cytometry* **1990**, *11* (3), 418–430.